JOURNAL OF RESEARCH

OF THE U.S. GEOLOGICAL SURVEY

NOVEMBER–DECEMBER 1973
VOLUME 1, NUMBER 6

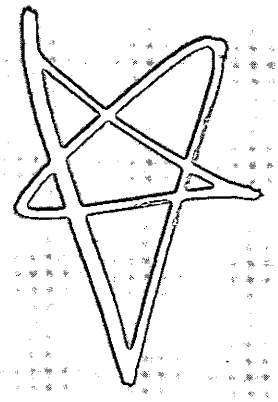

Scientific notes and summaries of investigations in geology, hydrology, and related fields

U.S. DEPARTMENT OF THE INTERIOR

UNITED STATES DEPARTMENT OF THE INTERIOR

ROGERS C. B. MORTON, Secretary

GEOLOGICAL SURVEY

V. E. McKelvey, Director

For sale by the Superintendent of Documents, U.S. Government Printing Office, Washington, D.C., 20402. Order by SD Catalog No. JRGS. Annual subscription rate, effective July 1, 1973, $15.50 (plus $3.75 for foreign mailing). Single copy $2.75. Make checks or money orders payable to the Superintendent of Documents.

Send all subscription inquiries and address changes to the Superintendent of Documents at the above address.

Purchase orders should not be sent to the U.S. Geological Survey library.

Library of Congress Card No. 72-600241

The Journal of Research consists of six issues a year (January-February, March-April, May-June, July-August, September-October, November-December) published in Washington, D.C., by the U.S. Geological Survey. It contains papers by members of the Geological Survey on geologic, hydrologic, topographic, and other scientific and technical subjects.

The Journal supersedes the short-papers chapters (B, C, and D) of the former Geological Survey Research ("Annual Review") series of professional papers. The synopsis chapter (A) of the former Geological Survey Research series will be published as a separate professional paper each year.

Correspondence and inquiries concerning the Journal (other than subscription inquiries and address changes) should be directed to the Managing Editor, Journal of Research, Publications Division, U.S. Geological Survey, Washington, D.C. 20244.

Papers for the Journal should be submitted through regular Division publication channels.

The Secretary of the Interior has determined that the publication of this periodical is necessary in the transaction of the public business required by law of this Department. Use of funds for printing this periodical has been approved by the Director of the Office of Management and Budget through February 11, 1975.

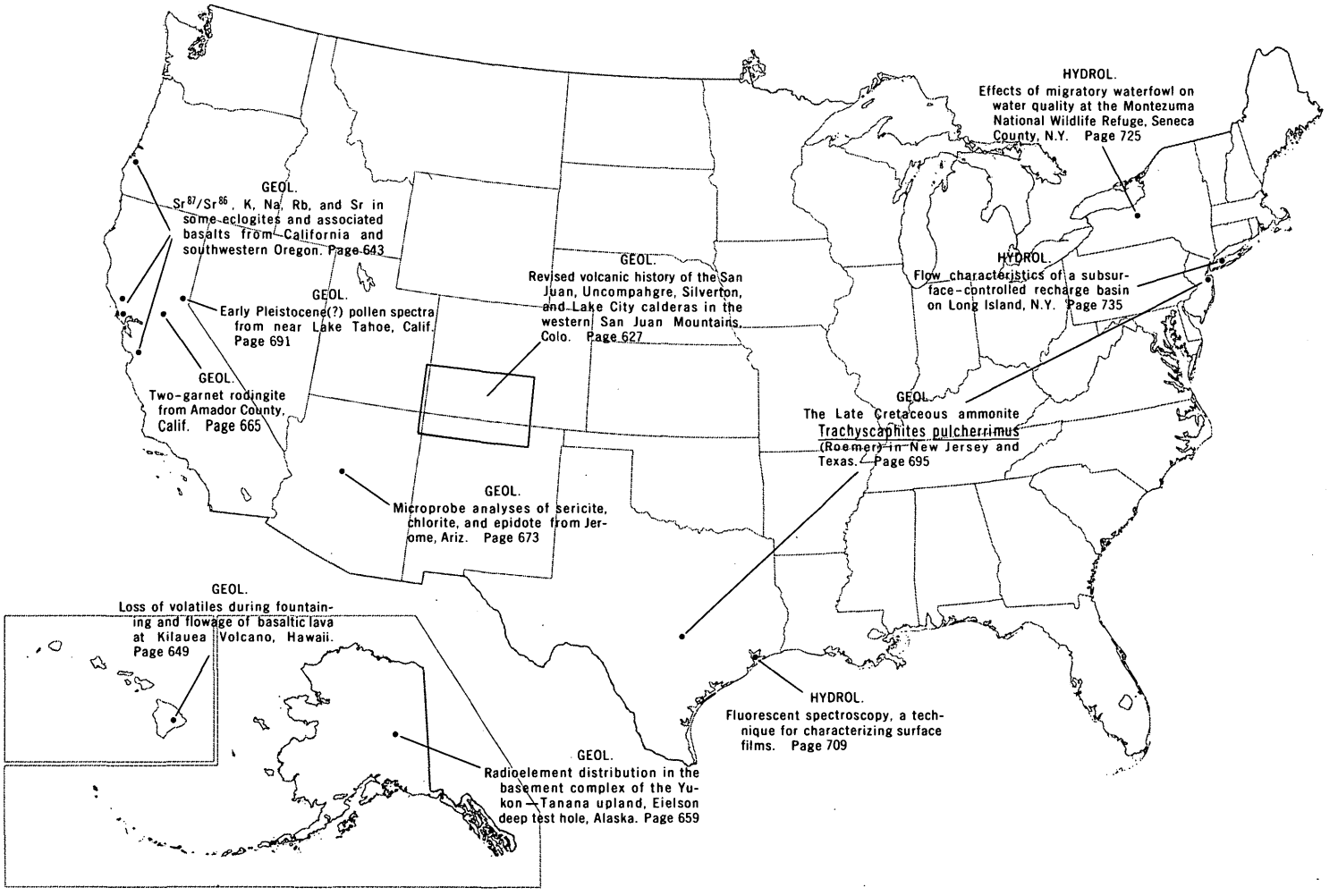

GEOGRAPHIC INDEX TO ARTICLES

[See Contents for articles concerning areas outside the United States and articles without geographic orientation]

JOURNAL OF RESEARCH

of the

U.S. Geological Survey

Vol. 1 No. 6 Nov.-Dec. 1973

CONTENTS

ABBREVIATIONS AND SYMBOLS

[Singular and plural forms for abbreviations of units of measure are the same]

A	angstrom units
A^3	cubic angstroms
a-c	alternating current
amp	amperes
atm	atmosphere
bbl	barrels
B.C.	Before Christ
B.P.	Before Present
c	crystalline state
C_x	molal concentration (of substance x)
cal	calories
cfs	cubic feet per second
Ci	Curies
cm	centimeters
cm^2	square centimeters
cm^3	cubic centimeters
cpm	counts per minute
cu ft	cubic feet
cu mi	cubic miles
d-c	direct current
emu	electromagnetic units
eV	electron volts
fpm	feet per minute
ft	feet
ft^3	cubic feet
g	grams
gal	gallons
gpd	gallons per day
gpm	gallons per minute
hr	hours
Hz	hertz (cycles per second)
in.	inches
kb	kilobars
kg	kilograms
km	kilometers
km^2	square kilometers
km^3	cubic kilometers
kV	kilovolts
l	liters
lb	pounds
ln	logarithm (natural)
m	meters
m^2	square meters
m^3	cubic meters
m	molal (concentration)
M	molar (concentration)
ma	milliamperes
me	milliequivalents
MeV	million electron volts
mg	milligrams
mgd	million gallons per day
mi^2	square miles
min	minutes
ml	milliliters
mm	millimeters
mol	moles
mr	milliroentgens
mV	millivolts
m.y.	million years
μ	microns
μ^2	square microns
μcal	microcalories
μg	micrograms
μm	micrometers
μmho	micromhos
n	neutrons
N	normal
ng	nanograms
nm	nanometers
Oe	oersteds
pCi	picocuries
P.d.t.	Pacific daylight time
pH	pH (measure of hydrogen) ion activity)
ppb	parts per billion
ppm	parts per million
psi	pounds per square inch
rad	radiometric
RaeU	radium equivalent uranium
rpm	revolutions per minute
sec	seconds
sq ft	square feet
sq mi	square miles
v	volts
wt	weight
yr	years

Jour. Research U.S. Geol. Survey
Vol. 1, No. 6, Nov.-Dec. 1973, p. 627–642

REVISED VOLCANIC HISTORY OF THE SAN JUAN, UNCOMPAHGRE, SILVERTON, AND LAKE CITY CALDERAS IN THE WESTERN SAN JUAN MOUNTAINS, COLORADO

By PETER W. LIPMAN, THOMAS A. STEVEN; ROBERT G. LUEDKE;
and WILBUR S. BURBANK, Denver, Colo.;
Washington, D.C.; and Exeter, N.H.

Abstract.—The sequence of mid-Cenozoic volcanic events in the western San Juan Mountains is closely analogous to that elsewhere in the San Juan volcanic field. The Lake Fork, Picayune, and San Juan Formations were erupted from a cluster of central volcanoes from 35 to 30 m.y. ago, when dominant activity shifted to more silicic ash-flow eruptions with accompanying caldera collapses. The Uncompahgre and San Juan calderas, each about 20 km across, formed mainly from eruption of the 28-m.y.-old Sapinero Mesa Tuff. Collapse occurred concurrently with eruption, and intracaldera tuffs accumulated to a thickness of more than 700 m. Both calderas were resurgently domed together; the northeast-trending Eureka graben formed along the distended crest of that dome. The Uncompahgre caldera was then flooded by several 27- to 28-m.y.-old ash-flow sheets from easterly sources, and also by one apparently erupted from the Silverton caldera nested within the older San Juan caldera. The Lake City caldera, located within the older Uncompahgre caldera, formed about 22.5 m.y. ago in response to eruption of the Sunshine Peak Tuff.

The western San Juan Mountains are one of the major mineralized areas in the Rocky Mountain region, with about one-half billion dollars total metal production in the last 100 years (Burbank and Luedke, 1968), and the geology of this region has been studied intensively for many years. Geologic folios by Whitman Cross and his associates at the turn of the century (Cross and Purington, 1899; Cross and others, 1905, 1907) were among the first studies anywhere to determine detailed stratigraphic relations in propylitically and hydrothermally altered Tertiary volcanic rocks. These stratigraphic relations were later amplified by Larsen and Cross (1956) and subsequently modified by Luedke and Burbank (1963). Nevertheless, the stratigraphic interpretations established by the earlier workers have been generally accepted with only minor changes to the present (table 1).

Since 1930 Wilbur S. Burbank and several associates have made detailed structural studies of many of the mineralized areas; among the early noteworthy results of this work have been recognition of two ring-fault-bounded collapse features, called the Silverton and Lake City calderas (Burbank, 1933, 1938, 1941, 1947a, 1947b, 1951), and later recognition that these two structures were nested within a larger older volcanic collapse area, called the San Juan volcanic depression (Luedke and Burbank, 1963, 1968; Burbank and Luedke, 1969).

This paper reports preliminary results of recent regional studies in the San Juan Mountains (fig. 1) (Steven and others, 1973a) and detailed studies in the Lake City area by Lipman and Steven and in the Silverton area by Luedke and Burbank, which require major revisions in interpretations of the volcanic stratigraphy and related caldera-collapse structures. These revisions in turn provide plausible answers to several long-recognized stratigraphic and structural problems of the western region. In particular, the San Juan volcanic depression, rather than being a single large oval collapse structure, consists of two intersecting smaller subcircular calderas. Also, all rock units of the Silverton Volcanic Group (table 1), previously interpreted as a genetically related assemblage of lavas and tuffs that accumulated within the concurrently subsiding San Juan depression (Luedke and Burbank, 1968; Burbank and Luedke, 1969), are generally correlative with other named volcanic formations nearby in the volcanic field that were previously considered to be either older or younger than the units of the Silverton Group. Further revisions of the volcanic stratigraphy and caldera structures are likely by the time our studies are complete.

ROCK UNITS

Tertiary volcanic rocks in the western San Juan Mountains rest unconformably on pre-Tertiary nonvolcanic rocks ranging in age from Precambrian to Cretaceous. The volcanic stratigraphy is most conveniently described in terms of two suites: (1) an older suite, largely Oligocene in age, of intermediate-composition lavas and associated more silicic differentiates, including voluminous ash-flow tuffs of quartz latite and low-silica rhyolite, and (2) a younger bimodal suite of mafic and very silicic rocks of Miocene and possibly younger age. These two suites appear to have fundamental significance, both regionally in the San Juan volcanic field (Lipman and

Table 1.—*Nomenclature of Tertiary volcanic rocks in the western San Juan Mountains*

[K-Ar ages in parentheses are from Lipman, Steven, and Mehnert (1970) and from this report. Asterisk (*) indicates unit previously assigned to the Silverton Volcanic Group]

SILVERTON QUADRANGLE Cross, Howe, and Ransome (1905)	EUREKA DISTRICT Burbank and Luedke (1969)	LAKE CITY AND SILVERTON AREAS This report		
		ASH-FLOW SHEETS	LAVA FLOWS AND BRECCIAS	
Potosi volcanic series	Potosi Volcanic Group: Sunshine Peak Rhyolite	Sunshine Peak Tuff (22.5 m.y.)	Basalts of the Hinsdale Formation (18.0-18.4 m.y.) Quartz latites of Red and Grassy Mountains (22.7 m.y.)	Late (Miocene) bimodal volcanics
	Potosi Volcanic Group: Gilpin Peak[1] Tuff, GP$_6$	Sapinero Mesa Tuff (includes Eureka Member*)	Quartz latite of Rambouillet Park	Oligocene ash-flow sequence and related lavas
	Potosi Volcanic Group: Gilpin Peak[1] Tuff, GP$_5$	Dillon Mesa Tuff		
	Potosi Volcanic Group: Gilpin Peak[1] Tuff, GP$_3$	Blue Mesa Tuff	Volcanics of Uncompahgre Peak	
	Potosi Volcanic Group: Gilpin Peak[1] Tuff, GP$_1$	Rat Creek Tuff (> 26.5 m.y.) Wason Park Tuff Carpenter Ridge Tuff Crystal Lake Tuff Fish Canyon Tuff = welded tuff of the Henson Fm.* (Burbank and Luedke, 1964) = American Flat Latite (Cross and others, 1907). (27.8 m.y.) Ute Ridge Tuff (28.4 m.y.)	Local lavas Henson* and Burns* Formations ≅Carson volcano of the Sheep Mountain Formation (Larsen and Cross, 1956) Local lavas and breccias	
Silverton volcanic series: Pyroxene andesite	Silverton Volcanic Group: Henson Formation			
Silverton volcanic series: Burns latite	Silverton Volcanic Group: Burns Formation			
Silverton volcanic series: Eureka rhyolite	Silverton Volcanic Group: Eureka Tuff			
Silverton volcanic series: Picayune andesite	Silverton Volcanic Group: Picayune Formation			
San Juan tuff	San Juan Formation		San Juan ≅ Picayune* ≅ Lake Fork Fms.: [clastic facies] [vent facies] [vent facies] (32.1 m.y.)	Early (Oligocene) intermediate-composition lavas and breccias

[1] Correlations between ash-flow sheets in the Lake City area and subunits of the Gilpin Peak Tuff mapped by Luedke and Burbank (1963) and by Burbank and Luedke (1964, 1966)

others, 1970) and widely in Cenozoic volcanic rocks of the Western United States (Christiansen and Lipman, 1972).

The Oligocene volcanic suite in the western San Juan area is discussed in terms of six progressively younger groups, as follows: (1) Early intermediate-composition lavas, breccias, and intrusives, (2) lower ash-flow sheets from sources to the southeast, (3) the Sapinero Mesa Tuff (and its Eureka Member) that formed by ash-flow eruptions from the San Juan and Uncompahgre calderas, (4) lower lavas and sediments (including the Burns and Henson Formations) that accumulated within the San Juan and Uncompahgre calderas shortly after collapse, (5) upper ash-flow sheets, mostly erupted from

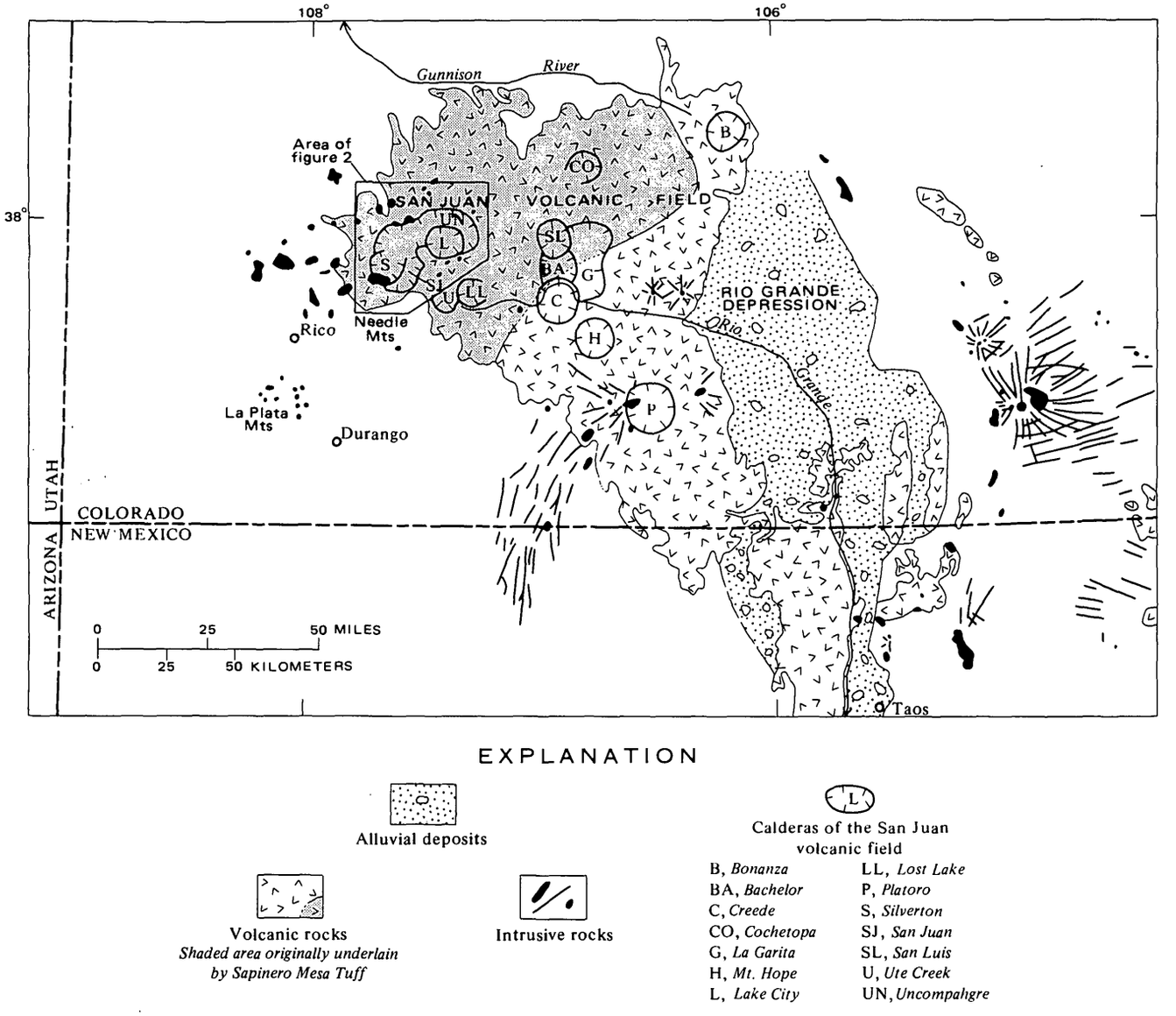

Figure 1.–Index map, showing location of the San Juan volcanic field, calderas of the San Juan Mountains, and generalized distribution of the Sapinero Mesa Tuff (and its Eureka Member) erupted from the San Juan and Uncompahgre calderas. In part modified from Cohee (1961).

sources to the east but including one–the Crystal Lake Tuff, a new name in this report–presumably erupted from the Silverton caldera, and (6) upper lavas and related intrusives that accumulated around margins of the San Juan, Uncompahgre, and Silverton calderas.

Divisions of the Miocene bimodal suite in the western San Juan area are (1) the rhyolitic Sunshine Peak Tuff erupted from the Lake City caldera, (2) silicic postcollapse lavas and intrusives of the Lake City caldera, and (3) regional mafic lavas of the Hinsdale Formation.

Pre-Tertiary Rocks

Pre-Tertiary rocks are exposed within the map area (fig. 2) south of the San Juan caldera on the north flank of the Needle Mountains, north of the San Juan caldera in the Uncompahgre River valley, and between the San Juan and Uncompahgre calderas. The last area, which consists largely of Precambrian granite, provides the main evidence that the San Juan and Uncompahgre calderas are separate structures. Precambrian gneiss of the Irving Formation and overlying Paleozoic sedimentary rocks are the major pre-Tertiary rock types in the area south of the San Juan caldera. In the Uncompahgre valley, Precambrian metasedimentary rocks of the Uncompahgre Formation are exposed below Paleozoic and Mesozoic sedimentary rocks, all of which are intruded by porphyritic granodiorite of Late Cretaceous or early Tertiary age.

Early Intermediate-Composition Lavas and Breccias

The oldest mid-Tertiary volcanic rocks in the western San Juan Mountains are lava flows, flow breccias, and mudflow breccias and conglomerates of predominantly intermediate compositions—calc-alkalic andesite, rhyodacite, and mafic quartz latite. These were erupted from numerous central volcanoes between 35 and 30 m.y. ago (Lipman and others, 1970; Luedke and Burbank, 1968). In the area considered here (fig. 2), early intermediate centers have been recognized near Larson Creek, at the head of the Cimarron River, at Matterhorn Peak, and near Carson Camp, and one or more are believed to have existed in the area north of Silverton.

Diverse formational names have been assigned to different parts of these generally equivalent early intermediate lavas and breccias. In the western San Juan region, the San Juan, Lake Fork, and Picayune Formations (table 1) represent local accumulations within a laterally intertonguing assemblage of lavas and breccias. Only two radiometric ages—32.1 m.y. for a flow breccia from the San Juan Formation (Lipman and others, 1970, table 2, no. 7) and 31.4 m.y. for a lava flow from the Lake Fork Formation (H. H. Mehnert, written commun., 1972)—are thus far available from these units, and their age range is not known.

The widespread San Juan Formation consists mainly of mudflow deposits and less voluminous associated water-laid volcaniclastic sedimentary rocks that originated as alluvial aprons around the vent-facies accumulations of the central volcanoes. Lava flows that interfinger with these volcaniclastic rocks have been mapped as part of the San Juan Formation in several areas; numerous such lava flows north of the Uncompahgre caldera were mismapped as sills in the Ouray folio (Cross and others, 1907), but these flows were later recognized and included in the San Juan Formation (Luedke and Burbank, 1963; Luedke, 1972). Flows also interfinger with the volcaniclastic rocks of the San Juan Formation northwest and southwest of the San Juan caldera (Burbank and Luedke, 1968, p. 17).

The Lake Fork Formation, as mapped by Larsen and Cross (1956, pl. 1), consists of vent-facies accumulations (lavas, flow breccias, and explosion breccias) from at least two central volcanoes, one of which is marked by the cluster of intrusions near Larson Creek about 5 km north of Lake City (fig. 2); the other, about 10 km farther northeast, was described by Larsen and Cross (1956, p. 67–68). The Lake Fork was considered by Larsen and Cross (1956, p. 64, 69) to underlie the San Juan Formation, but our recent mapping north of Lake City indicates that rocks mapped by Larsen and Cross as Lake Fork interfinger with mudflow breccias that they mapped as San Juan Formation; a similar interpretation has been inferred previously by Olson, Hedlund, and Hansen (1968, p. C8), Burbank and Luedke (1969, p. 17), and by Lipman, Steven, and Mehnert (1970, p. 2331).

The Picayune Formation consists mainly of intermediate-composition lava flows and flow breccias that previously have been considered the lowermost unit of the Silverton Volcanic Group (table 1). These rocks were believed to have accumulated mostly within the San Juan volcanic depression during early stages of its development, and to overlie the San Juan Formation unconformably (Luedke and Burbank, 1968; Burbank and Luedke, 1969).

We now interpret these lavas as downfaulted vent-facies accumulations forming the cores of early central volcanoes that were sources of the mudflow breccias in the San Juan Formation.

Apparently the areas that caved away into the San Juan and Uncompahgre calderas were near-source volcanic highlands, probably clusters of central volcanoes prior to collapse, inasmuch as lava flows interfingering with volcaniclastic rocks of the San Juan Formation increase in abundance toward the areas of the calderas (Burbank and Luedke, 1969, p. 17). Also, younger regional ash-flow sheets change from coalesced uniform sheets to local valley-filling deposits and then wedge out toward areas underlain by these vent-facies rocks. Because lavas of the Picayune Formation within the San Juan and Uncompahgre calderas occupy the same stratigraphic position—immediately below the intracaldera Eureka Member of the Sapinero Mesa Tuff—as do the other early intermediate lavas below outflow Sapinero Mesa Tuff beyond the caldera walls, they are logically considered offset parts of the same near-source accumulations.

Lower Ash-Flow Sheets

In the western San Juan area, three regionally widespread ash-flow sheets overlie the early intermediate rocks and underlie the Sapinero Mesa Tuff that resulted from the culminating eruptions of the San Juan and Uncompahgre calderas. The lower two sheets, the Ute Ridge and Blue Mesa Tuffs, were erupted from a caldera source southeast of the map area, but the overlying Dillon Mesa Tuff is uncertainly interpreted as an early eruption from the Uncompahgre caldera (table 2). Regional mapping has demonstrated that these three ash-flow sheets are correlative with units of the Gilpin Peak Tuff, as subdivided in the area west of the Silverton caldera (Burbank and Luedke, 1964, 1966).

Ute Ridge Tuff

The Ute Ridge Tuff is a new name, here applied to the lowermost widespread ash-flow sheet in the western San Juan Mountains. This unit has previously been referred to informally as the tuff of Ute Ridge (Steven and others, 1973a), and as the tuff from Storm King Mountain near the northern limit of its extent where it has been dated—somewhat discordantly—as 28.4 m.y. old (Lipman and others, 1970, table 3, no. 10). The Ute Ridge Tuff is named for excellent exposures on the lower slopes of Ute Ridge; this designated type area is about 5 km southeast of the map area (fig. 2) in the Rio Grande Pyramid 7½-minute quadrangle. The Ute Ridge Tuff is

typically a densely welded red-brown phenocryst-rich quartz latite that contains 30–40 percent phenocrysts of plagioclase, sanidine, biotite, and augite. The Ute Ridge is a multiple-flow ash-flow sheet that displays well-developed compound cooling in the type area. At Ute Ridge it is as much as 200 m thick, but its thickness is rather variable owing to irregular underlying topography. It has been traced as far north as Storm King Mountain 33 km north of Ouray, southeast as far as south-flowing Weminuche Creek 36 km southeast of Silverton (Steven and others, 1973a), and it is present as small erosional remnants on high ridges west of the San Juan caldera where it has been mapped as unit 1 of the Gilpin Peak Tuff (Burbank and Luedke, 1964, 1966). The Ute Ridge appears originally to have covered an area in excess of 6,000 km^2 and had an initial volume of at least 300 km^3. The Ute Ridge Tuff probably was erupted from the Ute Creek caldera (fig. 1), now largely buried.

Blue Mesa Tuff

The Blue Mesa Tuff (Olson and others, 1968) is a relatively phenocryst-poor low-silica rhyolite that widely overlies the Ute Ridge Tuff in the western San Juan Mountains. It generally contains about 5 percent phenocrysts of sanidine and plagioclase in subequal amounts, biotite, and sparse augite; locally, near its inferred source from the Lost Lakes caldera (fig. 1), it is weakly compositionally zoned upward into a more phenocryst-rich and less-silicic tuff. The Blue Mesa, typically densely welded and pale red brown, has a black basal vitrophyre and a well-developed light-gray upper vapor-phase zone. In detail, it varies widely in welding and crystallization characteristics, especially where deposited on irregular surfaces. The Blue Mesa Tuff closely resembles several overlying phenocryst-poor rhyolites of the ash-flow sequence, especially parts of the Sapinero Mesa, Crystal Lake, and Carpenter Ridge Tuffs, and relations in some discontinuously exposed or structurally complex areas are confusing. The Blue Mesa has been mapped as unit 3 of the Gilpin Peak Tuff west of the San Juan caldera (Burbank and Luedke, 1964, 1966). In the type locality the Blue Mesa is about 75 m thick (Olson and others, 1968), but it is as much as 300 m thick on Ute Ridge and Pole Creek Mountain (Steven and others, 1973a) near its probable source at the Lost Lake caldera. The initial areal extent and volume of the Blue Mesa Tuff must have been as great or slightly greater than that of the Ute Ridge Tuff (table 2).

Dillon Mesa Tuff

The Dillon Mesa Tuff (Olson and others, 1968) is a relatively thin ash-flow sheet of red-brown phenocryst-poor rhyolite. The Dillon Mesa seems to be generally similar in phenocryst mineralogy to the underlying Blue Mesa and overlying Sapinero Mesa Tuffs, but in places it is distinguished by abundant small flakes of biotite. Although the Dillon Mesa Tuff is locally as much as 60 m thick and is densely welded in its interior, the unit is more commonly only 5–10 m thick and weakly welded throughout. It is as much as 50 m thick in the Potosi Peak-Gilpin Peak area, but it thins rapidly to the southwest (Burbank and Luedke, 1964, 1966). Southeast of the San Juan caldera this unit is as much as 20 m thick in the Pole Creek Mountain quadrangle, but it is much thinner and present only locally south of the Rio Grande or east of Pole Creek Mountain. Despite its relative thinness, the Dillon Mesa was deposited over a large area in the northwestern San Juan Mountains. The original distribution of the Dillon Mesa Tuff is incompletely known, and this tuff may have been removed by erosion over sizable areas, but it seems to have been most widespread north of the Uncompahgre caldera, where it has been traced north beyond the Gunnison River (Hansen, 1971). Several features of the Dillon Mesa, not detailed here, but including its northerly distribution, suggest that its eruption may have been related to inception of the Uncompahgre caldera. Northwest of the San Juan caldera the Dillon Mesa Tuff has been mapped as unit 5 of the Gilpin Peak Tuff. Initial volume of the Dillon Mesa is uncertain but may have been about 50–100 km^3.

Sapinero Mesa Tuff and Its Eureka Member

The most significant stratigraphic and structural reinterpretations of our recent work have resulted from recognition that the Eureka Tuff within the San Juan and Uncompahgre calderas is the intracaldera accumulation of the regionally widespread Sapinero Mesa Tuff (Olson and others, 1968). West of the San Juan caldera, the Sapinero Mesa Tuff has been mapped as unit 6 of the Gilpin Peak Tuff (Burbank and Luedke, 1964, 1966). To conform to the pattern of nomenclature that has been applied to similar stratigraphic situations elsewhere in the San Juan Mountains (Steven and others, 1973b), we propose that the formational name of the widespread outflow rocks, the Sapinero Mesa Tuff, be retained for the whole ash-flow sheet, and that the name Eureka Member of the Sapinero Mesa Tuff be applied to the same thick intracaldera assemblage of rocks previously called Eureka Rhyolite or Eureka Tuff (table 1).

The Sapinero Mesa Tuff is one of the great ash-flow sheets of the San Juan volcanic field; erosional remnants occur over an area of at least 15,000 km^2, and represent an original volume estimated in excess of 1,000 km^3. These values probably are too low, as the distribution of present erosional remnants suggests that the sheet formerly extended farther to the west (fig. 1).

The outflow Sapinero Mesa Tuff is a phenocryst-poor rhyolitic welded tuff, containing about 5 percent phenocrysts of sanidine and plagioclase in subequal amounts, biotite, and minor augite. Although compound cooling is locally evident, in most sections the Sapinero Mesa displays a simple welding-crystallization zonation—a conspicuous black vitrophyre at the base, a densely welded devitrified red-brown interior, and a light-gray upper zone of vapor-phase crystallization. Near the Uncompahgre and San Juan calderas, pumice fragments in the

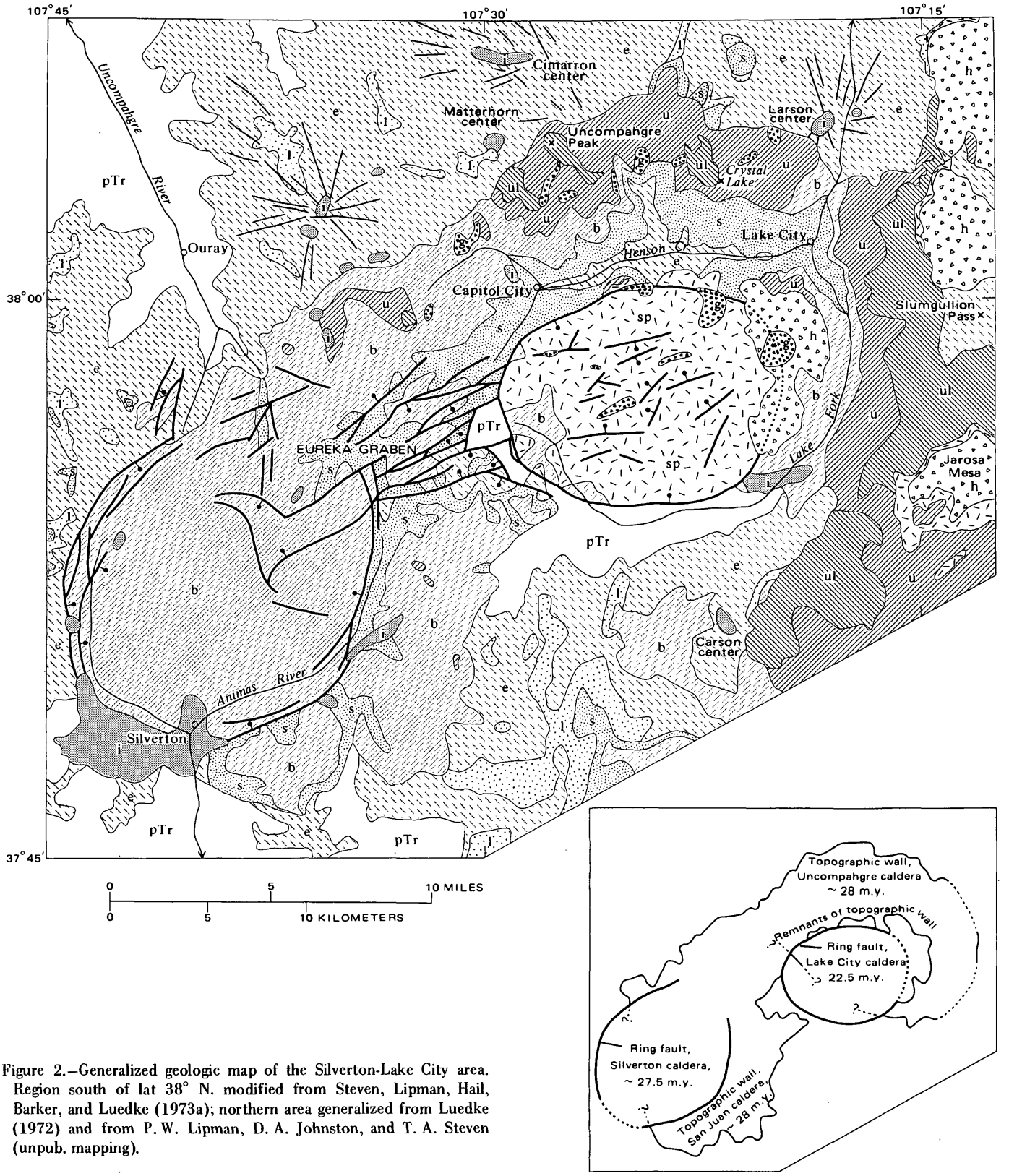

Figure 2.—Generalized geologic map of the Silverton-Lake City area. Region south of lat 38° N. modified from Steven, Lipman, Hail, Barker, and Luedke (1973a); northern area generalized from Luedke (1972) and from P. W. Lipman, D. A. Johnston, and T. A. Steven (unpub. mapping).

CORRELATION OF MAP UNITS

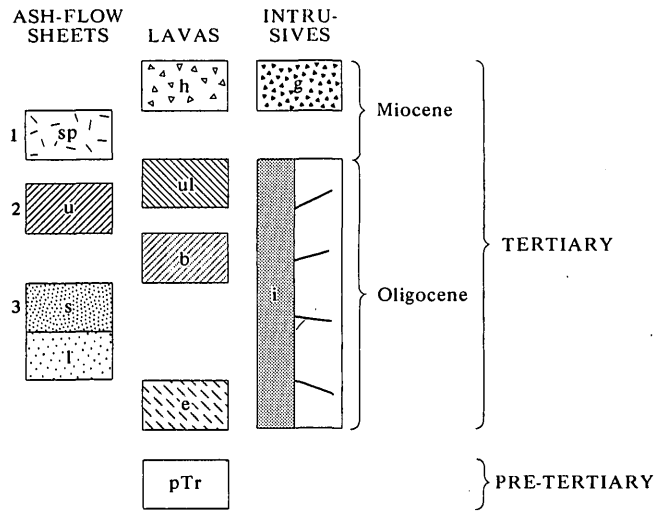

1 Time of collapse of Lake City caldera
2 Time of collapse of Silverton caldera
3 Time of collapse of San Juan and Uncompahgre calderas

DESCRIPTION OF MAP UNITS

ASH-FLOW SHEETS

Sunshine Peak Tuff (Miocene)

Upper ash-flow sheets (Oligocene) – Fish Canyon, Crystal Lake, Carpenter Ridge, Wason Park, and Rat Creek Tuffs

Sapinero Mesa (and Eureka Member) Tuff (Oligocene)

Lower ash-flow sheets (Oligocene) – Dillon Mesa, Blue Mesa, and Ute Ridge Tuffs

LAVAS

Quartz latitic lavas of Lake City caldera and basaltic lavas of the Hinsdale Formation (Miocene)

Upper lavas around margins of Uncompahgre caldera (Oligocene)

Lower caldera lavas and volcaniclastic rocks (Oligocene)–Henson and Burns Formations

Early intermediate-composition lavas and breccias (Oligocene)

INTRUSIVES

Rhyolite and granite intrusives of Lake City caldera (Miocene)

Intermediate-composition intrusives (Oligocene) – Mainly monzonite

Dike

PRE-TERTIARY ROCKS

CONTACT

FAULT – Dotted where covered; bar and ball on downthrown side

Figure 2.

interior of the sheet are elongate and lineate, owing to extreme welding and flowage, and irregularly shaped gas cavities are as much as 0.5 m across. Lineations become obscure outward from the source and are absent near the margins of the sheet. Gas cavities diminish in size away from the source, although they remain characteristic, and near the margin of the sheet a zone of small round lithophysae is commonly well developed in the interior of the unit. Xenoliths are generally sparse, but small fragments of andesitic flow rock are somewhat more abundant near the San Juan and Uncompahgre calderas.

The intracaldera Eureka Member of the Sapinero Mesa Tuff is more variable than the outflow sheet, both in modal composition and in welding-crystallization zonation. The nature of these variations is poorly understood at present because of limited exposures, local deformation, and extensive alteration in most places. The Eureka is typically moderately to strongly propylitized greenish-gray densely welded tuff, but where least altered west of Lake City, the cooling zonation alternates from red-brown densely welded tuff to light-gray less welded tuff. No glassy tuffs have survived, but a spectacular spherulitic zone locally present near the base probably indicates former presence of a glassy zone at this horizon. Upper parts of the Eureka Member are commonly very densely welded and strikingly lineate, and in the Lake City area they closely resemble nearby outflow Sapinero Mesa Tuff. The same phenocryst phases occur in the Eureka Member as in the outflow sheet, but they are generally somewhat more abundant, typically 5–10 percent. Within and near the San Juan caldera, the phenocryst content of the Eureka Member increases upward to as much as 20–30 percent. This change may indicate that the last material erupted was somewhat more mafic, but this relation has not yet been studied in detail. The Eureka generally contains abundant lithic fragments of intermediate-composition lava and locally contains blocks of granite or quartzite that reflect the subvolcanic basement, but the amount of such detritus is locally variable. Some zones of the Eureka contain as much as 10–20 percent rock fragments, and in places included masses of landslide breccia are as much as 50 m thick. The amount of lithic material decreases markedly near the top of the Eureka Member in the Lake City area.

The thickness of the outflow Sapinero Mesa sheet averages about 50 m and is about 100 m at maximum, whereas the intracaldera Eureka Member is at least 700 m thick in places, and its base is only locally exposed. This disparity in thickness between the intracaldera and outflow tuff is interpreted to indicate subsidence of the San Juan and Uncompahgre calderas concurrently with eruption of the Sapinero Mesa. Significantly, owing in part to a difference in stratigraphic interpretation, no major outflow sheet equivalent to the Eureka was recognized previously (Luedke and Burbank, 1968, p. 194).

Thick local intracaldera accumulations characterize many calderas in the San Juan volcanic field (Steven and Ratté,

Table 2.—*Major ash-flow sheets of the western San Juan Mountains*

Tuff unit	Caldera source	Phenocryst content and composition	Estimated initial volume (km^3)	Remanent magnetic polarity[1]	K-Ar age (m.y.)[2]
Sunshine Peak	Lake City	Crystal-rich rhyolite	200–300	?	22.5
Rat Creek	San Luis	Crystal-rich quartz latite	700–800	+	>26.4
Wason Park	Creede area	Crystal-rich rhyolite	200–300	–	<26.7
Carpenter Ridge	Bachelor	Crystal-poor rhyolite	1,200–1,500	–	>26.7
Crystal Lake	Silverton	do	25–50	–	.....
Fish Canyon	La Garita	Crystal-rich quartz latite	3,000+	+	27.8
Sapinero Mesa	San Juan and Uncompahgre	Crystal-poor rhyolite	1,000+	–	.....
Dillon Mesa	Uncompahgre(?)	do	50–100	–	.....
Blue Mesa	Lost Lakes	do	400+	–	.....
Ute Ridge	Ute Creek	Crystal-rich quartz latite	300+	–	28.4

[1] +, normal magnetic polarity; –, reverse magnetic polarity; ?, undetermined.
[2] From Lipman, Steven, and Mehnert (1970) and H. H. Mehnert (written commun., 1971).

1965; Lipman and Steven, 1970; Steven and others, 1973a), and every thick intracaldera accumulation studied so far is demonstrably equivalent to a large widespread ash-flow sheet. Generally, such ash-flow sheets are not continuous across the walls of their source caldera, and equivalencies can be demonstrated only indirectly. Time relations are especially significant, as the intracaldera accumulations may differ markedly from the outflow sheets in appearance and composition owing to variations in welding, crystallization, alteration, and sorting of phenocrysts and lithic fragments.

Contemporaneity of intracaldera Eureka Member and outflow accumulations of the Sapinero Mesa Tuff can be demonstrated precisely for the Uncompahgre caldera; less direct evidence indicates the same timing for the San Juan caldera. The outflow Sapinero Mesa Tuff forms a nearly continuous sheet for about 40 km to the north of the Uncompahgre caldera, where it overlies the Blue Mesa Tuff and is overlain by Fish Canyon Tuff. At the topographic wall of the caldera, about 10 km northwest of Lake City (fig. 2), the outflow Sapinero Mesa is truncated and unconformably overlapped by the younger caldera-filling ash-flow units—the Fish Canyon, Crystal Lake, Carpenter Ridge, and Rat Creek Tuffs—that overlie the thick ponded Eureka Member within the Uncompahgre caldera. Thus, these geologic relations indicate that the outflow Sapinero Mesa can be no younger than the Uncompahgre caldera and the intracaldera Eureka no older; the caldera must have collapsed during or shortly after the emplacement of the outflow Sapinero Mesa. The Eureka cannot be older than the Sapinero Mesa, as was previously thought.

Similar unconformable relations occur on the southeast side of the San Juan caldera, at Sheep Mountain, about 13 km east of Silverton (fig. 2); there, lavas of the Burns and Henson Formations overlie Eureka within the caldera and lap out unconformably against Ute Ridge and Blue Mesa Tuffs at the caldera wall, indicating that the San Juan caldera must be younger than these tuffs. In this area the Sapinero Mesa Tuff is not present at the caldera wall, but it overlies Blue Mesa Tuff a few kilometers to the east. The San Juan caldera therefore subsided after the Blue Mesa Tuff was emplaced and before the Burns and Henson Formations accumulated, and thus within the same time interval that the Sapinero Mesa Tuff was emplaced.

Similarly, near Richmond Pass, 10 km south of Ouray on the northwest side of the San Juan caldera (Burbank and Luedke, 1964) rocks of the Henson Formation were deposited unconformably against steep slopes of the caldera wall. Here, the wall consists of an intertonguing sequence of early intermediate vent-facies lavas and volcaniclastic breccias (including rocks originally mapped as San Juan, Picayune, and Burns Formations) overlain nearly conformably by the Blue Mesa and Sapinero Mesa Tuffs (equivalent to units 3 and 6 of the Gilpin Peak Tuff). Caldera subsidence here clearly preceded the Henson eruptions but was no older than emplacement of Sapinero Mesa Tuff. A few kilometers to the northeast near Engineer Pass, 9 km southeast of Ouray, Fish Canyon Tuff confined within the San Juan caldera overlies lavas of the Burns and Henson Formations, again bracketing the time of the formation of the San Juan caldera to the interval between eruption of the Sapinero Mesa and Fish Canyon Tuffs.

All currently known geologic evidence thus indicates that both the Uncompahgre and San Juan calderas formed during the interval that the Sapinero Mesa Tuff was emplaced. This timing, as well as certain features of the distribution and lithologic variation of the Sapinero Mesa Tuff, discussed more fully in a later section, suggests to us that the eruption of this ash-flow sheet led to virtually simultaneous subsidence of the two calderas, although the Uncompahgre caldera may have begun to subside during eruption of the earlier Dillon Mesa Tuff, as mentioned previously.

Lower Caldera Lavas and Volcaniclastic Rocks

Lavas and volcanic sedimentary rocks that accumulated within and around the margins of the San Juan and Uncompahgre calderas shortly after collapse intervene between the Eureka Member of the Sapinero Mesa Tuff and the Fish Canyon Tuff. In the San Juan caldera these lavas and volcanic sedimentary rocks have been divided into the Burns and Henson Formations. The Burns Formation is a heterogeneous assemblage of rhyodacitic to quartz latitic lavas and breccias,

generally containing biotite or hornblende phenocrysts, and minor tuffs and rhyolitic lavas, whereas the Henson Formation includes more abundant sedimentary rocks in association with more mafic andesites and rhyodacites, commonly characterized by pyroxene phenocrysts (Luedke and Burbank, 1963; Burbank and Luedke, 1969). These distinctions are not recognized within the Uncompahgre caldera, and probably reflect the local sequence within the San Juan caldera rather than having regional significance.

Thick intermediate-composition lavas and breccias overlying the San Juan Formation generally west of the San Juan caldera have previously been mapped as Burns Formation (Burbank and Luedke, 1964, 1966). Pending further study, these rocks are tentatively reinterpreted as parts of the early intermediate sequence because they are overlain by the Ute Ridge, Blue Mesa, and Sapinero Mesa Tuffs (units 1, 3, and 6 of the Gilpin Peak Tuff). Thin ash-flow tuffs below these lavas, previously mapped as Eureka Tuff, are now tentatively considered as local ash-flow deposits within the early intermediate sequence.

The lower lava and volcaniclastic sequence within the Uncompahgre caldera is highly variable both vertically and laterally. North of Lake City, this sequence consists mainly of fine-grained buff to gray tuffaceous sandstone and shale, representing a shallow-water deltaic or lake environment. South of Lake City the main constituents are thick lava flows, varying from sparsely porphyritic dark-gray andesite or rhyodacite to light-gray flow-laminated quartz latite or rhyolite. West of Lake City dark-gray andesitic or rhyodacitic lavas, containing conspicuous large tabular plagioclase phenocrysts, are intricately interlayered with greenish-gray andesitic sandstone.

East and southeast of the San Juan caldera and south of the Uncompahgre caldera a sequence of intermediate-composition mud-flow breccias and local interlayered lavas, described as the Carson volcano of the Sheep Mountain Formation (Larsen and Cross, 1956, p. 126–128), are bounded stratigraphically by the underlying Sapinero Mesa Tuff and overlying Fish Canyon Tuff. These predominantly volcaniclastic rocks are thus in the same stratigraphic position as the Burns and Henson Formations within the San Juan caldera and related lower lavas in the Uncompahgre caldera (table 1), and we regard the Carson rocks as a largely clastic apron, peripheral to the lower lava centers.

The lower lavas and volcaniclastic rocks vary widely in thickness within the calderas, owing to irregularities on the underlying floor and to variations in thickness around different volcanic centers. The rocks are as much as 500–600 m thick locally within both the Uncompahgre and San Juan calderas, and they wedge sharply against buried topography and adjacent caldera walls.

Upper Ash-Flow Sheets

Several ash-flow sheets, including the Fish Canyon, Carpenter Ridge, Wason Park, and Rat Creek Tuffs, flowed into the western San Juan area from caldera sources farther east. These units provide age control on the late evolution of the San Juan and Uncompahgre calderas. The Crystal Lake Tuff, which occurs locally between the Fish Canyon and Carpenter Ridge Tuffs, appears to have been erupted from the Silverton caldera nested within the San Juan caldera.

Fish Canyon Tuff

Positive identification of the Fish Canyon Tuff (Olson and others, 1968) within the Uncompahgre and San Juan calderas is one of the key pieces of evidence on which our stratigraphic reinterpretations are based, as this unit occurs widely above the Sapinero Mesa Tuff and below the Carpenter Ridge Tuff, both within and outside these calderas. The Fish Canyon is the most petrographically distinctive ash-flow sheet in the San Juan volcanic field: it is a gray phenocryst-rich quartz latite, containing 30–50 percent phenocrysts of plagioclase, sanidine, quartz, biotite, hornblende, and accessory sphene. No other major ash-flow sheet in the field contains hornblende rather than augite as the second mafic constituent after biotite. Quartz phenocrysts constitute 1–3 percent of the rock, whereas they are very rare or absent in other quartz latitic tuffs of the field. This quartz is also distinctive in that it occurs as rounded pellets, as large as 5 mm in diameter, that are riddled with wormy glass inclusions due to resorption. Finally, the abundant accessory sphene is unique.

The Fish Canyon Tuff is the most widespread (at least 15,000 km^2) and voluminous (more than 3,000 km^3) ash-flow sheet in the volcanic field. It was erupted about 27.8 m.y. ago (Steven and others, 1967; Lipman and others, 1970) from the large La Garita caldera (fig. 1). Near the Uncompahgre and San Juan calderas (fig. 2) the Fish Canyon underlies almost all the area shown as "upper ash-flow sheets." East and southeast of Lake City the Fish Canyon lies on intracaldera lavas and volcanic sandstones; northwest of Lake City it rests directly on the Eureka Member of the Sapinero Mesa Tuff; and southeast of Ouray, within the northern part of the San Juan caldera, it rests on Burns and Henson lavas. In general, the Fish Canyon Tuff within the Uncompahgre and San Juan calderas was previously mapped as American Flat Latite (Cross and others, 1907) and in part as "welded tuff of the Henson Formation" (Luedke and Burbank, 1961, 1963; Luedke, 1972).

Crystal Lake Tuff

A phenocryst-poor low-silica rhyolite ash-flow sheet lies between the Fish Canyon and overlying Carpenter Ridge Tuffs in the northern moat of the Uncompahgre caldera and also in the upper Rio Grande drainage southeast of Silverton (Steven and others, 1973a). This unit is present at Crystal Lake, about 5 km northwest of Lake City (fig. 2), and is especially well exposed on Crystal Peak just to the west; it is here named the Crystal Lake Tuff. At Crystal Peak, here designated the type area, the Crystal Lake Tuff is about 50 m thick and consists of

a black basal vitrophyre, densely welded red-brown tuff in its interior, and an upper zone of vapor-phase crystallization. The lithology of the Crystal Lake Tuff closely resembles parts of other phenocryst-poor rhyolitic tuffs of the area (Blue Mesa, Sapinero Mesa, and Carpenter Ridge), and, were it not for the intervening distinctive Fish Canyon Tuff, these similar rhyolitic units could be difficult to distinguish and map consistently.

The Crystal Lake Tuff contains about 5 percent phenocrysts of sanidine and plagioclase in subequal amounts, accompanied by biotite and minor augite. Where thick and densely welded, it commonly contains highly compacted light-gray lineate pumice lenses as much as 0.5 m in length, but where the sheet is relatively thin near its margins, it is only weakly welded and contains abundant small angular fragments of intermediate-composition lava.

The Crystal Lake Tuff is thickest and most densely welded in the northern moat of the Uncompahgre caldera where it ponded to a thickness of about 200 m, but it is absent farther east in this moat, where its spread was blocked near Lake City by high parts of the resurgent dome. The Crystal Lake has been recognized outside the San Juan and Uncompahgre calderas only as a single east-trending lobe, covering an area of about 150 km^2, in the upper Rio Grande drainage. This outflow accumulation of Crystal Lake Tuff is thinner and contains fewer lithic fragments and smaller pumice lenses than that within the Uncompahgre caldera. Its distribution suggests that the Crystal Lake originated from within the San Juan caldera and flowed mainly northeast through a low divide into the Uncompahgre caldera and southeast across the San Juan caldera wall into the upper Rio Grande area. This interpretation is favored by the presence within the San Juan caldera of the structural boundary (ring fractures) of a younger caldera—the Silverton caldera—that subsided after accumulation of the Burns and Henson Formations. Maps and cross sections of the Silverton caldera (Varnes, 1963; Burbank and Luedke, 1964, 1969) indicate that this late subsidence has displacements ranging from as much as 500–700 m along the western and southern ring fractures to near zero at the northeast side. The Crystal Lake Tuff is the only sizable upper ash-flow sheet without a recognized source elsewhere in the volcanic field, and conversely the Silverton caldera is a likely source area without a related ash-flow sheet; we therefore suggest that eruption of the Crystal Lake resulted in formation of the Silverton caldera.

The Crystal Lake Tuff was erupted about 27.0–27.5 m.y. ago, as it is underlain by the 27.8-m.y.-old Fish Canyon Tuff and is overlain by the Carpenter Ridge Tuff, which in turn is overlain in the Creede area by the 26.8-m.y.-old Mammoth Mountain Tuff (table 2; Lipman and others, 1970).

The original extent of the Crystal Lake Tuff is uncertain, because it could have overflowed the San Juan caldera to the west but since have been completely removed by erosion. The original volume of the lobes in the upper Rio Grande drainage and within the Uncompahgre caldera must have been on the order of 25–50 km^3.

Carpenter Ridge Tuff

The Carpenter Ridge Tuff (Olson and others, 1968) is a voluminous ash-flow sheet of phenocryst-poor low-silica rhyolite that was erupted from the Bachelor caldera (fig. 1) in the central San Juan Mountains (Steven and others, 1973b). It crops out continuously around the eastern and northern moat areas of the Uncompahgre caldera, where it overlies the Fish Canyon and Crystal Lake Tuffs. The Carpenter Ridge is as much as 40 m thick northeast of Lake City, but even where relatively thin, it characteristically consists of a black basal vitrophyre, a densely welded red-brown central zone, and an upper light-gray vapor-phase zone. In comparison with the underlying Crystal Lake Tuff, pumice fragments in the Carpenter Ridge are smaller and less densely welded, and they lack linear structure. The phenocryst constituents and proportions are similar to those of the Crystal Lake, Blue Mesa, and Sapinero Mesa Tuffs: about 5 percent of plagioclase and sanidine in subequal amounts, biotite, and very sparse augite.

Wason Park Tuff

The Wason Park Tuff is a phenocryst-rich low-silica rhyolite erupted from the Creede area (Ratté and Steven, 1967). It occurs locally along the southeast rim of the Uncompahgre caldera and within adjacent parts of the caldera moat where it rests on the Carpenter Ridge Tuff and is overlain by rhyodacite and quartz latite of the upper lava sequence.

Rat Creek Tuff

Phenocryst-rich quartz latitic ash-flow tuff, tentatively identified as the Rat Creek Tuff (Steven and Ratté, 1965), forms a major unit within the northern and eastern moat areas of the Uncompahgre caldera. The Rat Creek Tuff was erupted from the San Luis caldera in the north-central part of the San Juan volcanic field (fig. 1). In the Uncompahgre caldera area, this tuff typically is light tan to light gray, nonwelded to partly welded, and contains 25–40 percent phenocrysts of plagioclase, biotite, and augite, and minor sanidine and quartz. As many as three petrologically indistinguishable cooling units, with an aggregate thickness of 200 m, fill a paleovalley northwest of Lake City. Southeast of Lake City, similar tuff forms a single cooling unit as much as 60 m thick interlayered within a local lava sequence (see following section). The age of the Rat Creek Tuff is greater than 26.4 m.y. and less than 26.8 m.y., as indicated by relations farther east to rocks erupted from the Creede caldera (Steven and others, 1967; Lipman and others, 1970).

Upper Lavas Around Margins of Uncompahgre Caldera

The upper caldera lavas accumulated principally within and around the margins of the Uncompahgre caldera. They are a heterogeneous assemblage of flows, breccias, and relatively minor sedimentary rocks that are interlayered at one place or

another between every unit of the upper ash-flow sequence. Two of the accumulations are major: (1) at Uncompahgre Peak a succession at least 450 m thick of thick plagioclase-biotite-augite quartz latite flows, and minor interlayered sparsely porphyritic rhyodacite, occurs between the Carpenter Ridge and Rat Creek Tuffs, and (2) on the east rim of the Uncompahgre caldera a sequence as much as 250 m thick of slightly more silicic quartz latites and rhyodacites overlies the Rat Creek Tuff. In addition, andesitic sandstone 30 m in maximum thickness occurs locally between the Fish Canyon and Crystal Lake Tuffs northwest of Lake City, and several andesitic lava flows containing large tabular plagioclase phenocrysts are present in places between the Crystal Lake and Carpenter Ridge Tuffs. Southeast of Lake City, the Wason Park Tuff wedges out into a sequence of rhyodacitic flows as much as 350 m thick between the Carpenter Ridge and Rat Creek Tuffs.

Source vents have been located for only a few of these flows, but most seem to represent continued marginal eruptions related to the late evolution of the Uncompahgre caldera. One major center of this age is exposed in the Capitol City-Matterhorn Peak area, where the upper ash-flow sheets and upper lava sequence are cut by monzonitic plugs and altered by related hydrothermal activity.

Sunshine Peak Tuff

The Sunshine Peak Tuff, the youngest major ash-flow sheet of the San Juan volcanic field, is a distinctive rock characterized by 76 percent or more SiO_2 (Larsen and Cross, 1956, table 21, No. 58), abundant quartz phenocrysts, very sodic alkali feldspar phenocrysts, and a lack of plagioclase phenocrysts. The origin of the Sunshine Peak Tuff as an ash-flow deposit related to subsidence of the Lake City caldera was recognized recently (Luedke and Burbank, 1968), but the age and petrogenetic associations of this tuff unit have remained uncertain.

As originally mapped, the Sunshine Peak Tuff was shown confined to the interior of the Lake City caldera where it is 1 km or more thick; no equivalent outflow sheet was recognized outside the caldera (Larsen and Cross, 1956, pl. 1). Larsen and Cross, uncertain of the stratigraphic position of the Sunshine Peak, tentatively placed it between the Silverton and Potosi Volcanic Groups. Luedke and Burbank (1963) later included the Sunshine Peak Tuff within their redefined Potosi Group, on the basis that the Sunshine Peak was interbedded with and equivalent to Potosi rocks, as then interpreted, southeast of Lake City.

More recently, Lipman, Steven, and Mehnert (1970, p. 2344) postulated that the intracaldera Sunshine Peak might correlate with a young rhyolite welded tuff—previously included in the Hinsdale Formation (Larsen and Cross, 1956, p. 193–194) which is preserved beneath capping basalt flows at Jarosa Mesa (Steven, 1967; Steven and others, 1967) and as nearby erosional remnants over a 40-km arc around the high rim south and east of the Lake City caldera. This inference, which was originally based on distribution and petrologic similarity, has been confirmed by more detailed mapping in the Lake City area and by additional K-Ar radiometric determinations. Biotite and alkali feldspar from intracaldera Sunshine Peak Tuff and a similar mineral pair from an overlying silicic intracaldera lava flow are both highly accordant, and the difference between the averaged Sunshine Peak age, 22.5 m.y., and that of the overlying lava flow, 22.7 m.y., is within analytical uncertainty (H. H. Mehnert and others, 1973). These ages are also in excellent agreement with feldspar ages from the outflow tuff at Jarosa Mesa, 22.0 and 22.9 m.y. (Steven and others, 1967).

The thick intracaldera Sunshine Peak Tuff typically shows compound cooling with numerous light-gray partly welded zones separating dark-gray more densely welded rocks. Andesitic lithic fragments are abundant, as are interlayered lenses of andesitic landslide breccia as much as 100 m thick. Lower parts of the intracaldera tuff are pervasively propylitically altered, and large areas are hydrothermally altered, especially near granite porphyry plugs. The intracaldera tuff has been resurgently domed and dips outward 10°–15° in all directions from the center of the caldera. Northeast-trending faults clearly define an apical graben at the crest of the dome (fig. 2).

In contrast to the intracaldera facies, the outflow sheet is rarely more than 50 m thick, is incipiently to only partly welded, and contains few lithic fragments. The original extent of the outflow sheet is uncertain; it now is preserved only where capped by resistant basalt flows of the Hinsdale Formation.

The original volume of the Sunshine Peak Tuff is rather uncertain because so much of the outflow sheet has been eroded. The volume of the intracaldera accumulation, calculated as 125–150 km^3, is believed reliable, but the total volume, stated as 200–300 km^3 (table 2), is only an estimate based largely on analogy with other San Juan calderas where the outflow sheets are at least as voluminous as the intracaldera accumulations.

Lavas and Intrusions of the Lake City Caldera

After subsidence, the core of the Lake City caldera was flooded by coarsely porphyritic (sanidine-plagioclase-biotite) quartz latitic lavas and intruded by granite porphyry. North of the structural boundary of the caldera, a northeast-trending chain of rhyolite porphyry plugs, dikes, and sills (fig. 2) that petrologically resemble the Sunshine Peak Tuff probably were emplaced late in the Lake City caldera cycle. The outflow Sunshine Peak Tuff on the high mesas east of the caldera is overlain by thick heterogeneous lava domes that vary from porphyritic rhyolite to sparsely porphyritic dark andesite, and by thinner flows of uniform alkalic olivine basalt. Both these rock types previously have been mapped as Hinsdale Formation (Larsen and Cross, 1956, pl. 1). A sequence of at least 15 basalt flows on the high mesas northeast of Lake City have

yielded K-Ar ages (H. H. Mehnert and others, 1973) of 18.0 m.y. (top flow) and 18.4 m.y. (low flow); one of the porphyritic lava domes appears to wedge out between this basalt sequence and the underlying Sunshine Peak Tuff. We consider that in a general way these mafic rocks, together with the rhyolitic rocks of Lake City caldera, constitute a bimodal mafic-silicic association similar to that widespread elsewhere in upper Cenozoic volcanic rocks of the Western United States (Christiansen and Lipman, 1972).

Recommended Changes in Stratigraphic Nomenclature

We suggest that the terms Silverton Volcanic Group, Potosi Volcanic Group, and Gilpin Peak Tuff be abandoned as formal geologic names. The assemblage of rocks represented by each of these names includes several unrelated major volcanic units that now are believed to correlate with other named formations grouped differently elsewhere in the San Juan volcanic field (table 1).

All units of the Silverton Volcanic Group appear to correlate with older or younger formations nearby in the volcanic field. The intermediate-composition Picayune Formation is believed generally equivalent to the Lake Fork Formation and other unnamed vent-facies accumulations of lavas and breccias that intertongue with volcaniclastic rocks of the San Juan Formation. The rhyolitic Eureka Tuff is the intracaldera equivalent of outflow Sapinero Mesa Tuff and is included with the Sapinero Mesa as a member. The Burns and Henson Formations, as postcollapse accumulations of lavas, breccias, and sediments within the San Juan caldera, are in part correlative with similar lavas and breccias of the Carson center of the Sheep Mountain Formation, as used by Larsen and Cross (1956, p. 126–128). A quartz latitic welded tuff (Luedke and Burbank, 1961) interbedded within the late moat fill of the San Juan and Uncompahgre calderas, and formerly included in the redefined Henson Formation (Luedke and Burbank, 1963; Burbank and Luedke, 1969, p. 12–14), is a distal part of the Fish Canyon Tuff—the largest ash-flow sheet in the San Juan field. In the absence of a close genetic association between these varied units, the formal group classification is now superfluous, and nomenclature of the different units should be established on an individual basis.

The Potosi Volcanic Group, as redefined (Luedke and Burbank, 1963), contained only two formations—the Gilpin Peak Tuff and the Sunshine Peak (Rhyolite) Tuff. The Gilpin Peak Tuff consists largely of four ash-flow sheets that are only a part of the general Oligocene ash-flow sequence of the San Juan volcanic field. The Sunshine Peak Tuff, on the other hand, is now known to be much younger and to be petrogenetically related to the Miocene-Pliocene bimodal volcanic suite (Hinsdale Formation) long recognized to overlie the Potosi Group (Larsen and Cross, 1956, p. 193–194; Luedke and Burbank, 1968, table 1). As originally defined, the Potosi Group included all the Oligocene ash-flow sequence, as well as some early intermediate-composition rocks (Conejos Formation) of the eastern San Juan Mountains (Larsen and Cross, 1956). The Potosi Volcanic Group has thus outlived its usefulness as a meaningful assemblage of rocks, and nomenclature of the different component units is best established on the basis of regional correlations.

The major units of the Gilpin Peak Tuff correlate with at least four major ash-flow sheets that have been separately named in adjacent parts of the volcanic field (Ute Ridge, Blue Mesa, Dillon Mesa, and Sapinero Mesa Tuffs) and that were erupted from at least three separate unrelated caldera centers (Ute Creek, Lost Lake, and San Juan-Uncompahgre). Considering that each of these four sheets previously has been given formational rank elsewhere in the San Juan volcanic field, we believe that the term Gilpin Peak Tuff now lacks utility as a formal stratigraphic name.

EVOLUTION OF THE CALDERAS

The Uncompahgre and San Juan calderas developed as a closely interrelated pair and are therefore described together; the slightly younger Silverton caldera, although an integral part of this earlier history, is considered separately. The Lake City caldera formed more than 5 m.y. later, and its evolution is likewise considered separately.

Uncompahgre and San Juan Calderas

Prior to the ash-flow eruptions and related collapse of the San Juan and Uncompahgre calderas, the western San Juan region was a volcanic highland consisting of a cluster of central volcanoes surrounded by an alluvial plain of outwash debris. The near-source vent-facies rocks consist of the Picayune Formation, Lake Fork Formation, and unnamed similar lavas and breccias around local centers. The volcanoes were dissected as they grew, broad valleys were eroded in their flanks, and the intervening basins and outer flanks were mantled by volcanic detritus represented by the San Juan Formation. These rocks accumulated largely in early and middle Oligocene time, between 35 and 30 m.y. ago. Between 29 and 28 m.y. ago, the flanks of these volcanoes were partly buried by ash-flow deposits comprising the Ute Ridge and Blue Mesa Tuffs, erupted from caldera sources to the southeast. These ash-flow sheets formed discontinuous valley-filling lobes near the central volcanoes and coalesced downslope into widespread continuous sheets.

Eruption of the Dillon Mesa Tuff, that overlies the Blue Mesa Tuff, may have led to initial collapse at the Uncompahgre caldera site. The inferred 50–100 km^3 initial volume of the Dillon Mesa (table 2), though relatively small, would seemingly have been sufficient to permit subsidence of the source area (by analogy with size-volume relations of other calderas: Smith, 1960, fig. 3), and the northerly distribution of this unit makes the Uncompahgre caldera area a plausible source. This relation is inferential, however, and we know of no direct evidence supporting it.

The eruptions that deposited the Sapinero Mesa Tuff about 28 m.y. ago were more than an order of magnitude larger than those of the Dillon Mesa (table 2), and the resulting ash flows spread as much as 90 km to the northeast of the Uncompahgre caldera, as well as sizable distances in other directions (fig. 1). Both San Juan and Uncompahgre calderas are filled by 500–700 m of the intracaldera Eureka Member of the Sapinero Mesa Tuff, indicating that both calderas existed as deep depressions before the Sapinero Mesa eruptions were completed. Abundant lithic fragments and lenses of landslide breccia within the Eureka Member in both calderas indicate that their walls were oversteepened and caving during Sapinero Mesa eruptions, and the landslide material is especially abundant and coarse within the San Juan caldera.

Seemingly, therefore, both calderas were actively subsiding during eruption of the Sapinero Mesa Tuff, with the San Juan caldera being somewhat more active than the Uncompahgre caldera. Conceivably the Sapinero Mesa Tuff was erupted largely from the San Juan caldera, and the Eureka Member in the Uncompahgre caldera accumulated within an earlier basin, related to Dillon Mesa eruptions, that was undergoing slight additional subsidence. However, we favor an interpretation that the Sapinero Mesa Tuff emanated from both calderas, for three reasons. First, the Sapinero Mesa Tuff is abruptly truncated at the Uncompahgre caldera walls, indicating major subsidence during and after its eruption. Also, extension of the Sapinero Mesa ash flows so far to the northeast (fig. 1) would have been unlikely if the Uncompahgre caldera had formed a deep intervening depression. Both the Uncompahgre and San Juan calderas were resurgently domed together after the Sapinero Mesa activity ceased, indicating that the active magma chamber that supplied this tuff underlay both calderas at shallow levels. Finally, the Sapinero Mesa Tuff is among the largest ash-flow sheets in the San Juan field, and we believe that its eruption should have resulted in collapse of a larger caldera than one formed by eruption of the much smaller Dillon Mesa Tuff (table 2).

The virtually simultaneous collapse of two calderas as a result of the Sapinero Mesa eruptions, if a valid interpretation, represents an unusual geometry for caldera formation. We can only speculate that eruption of the Sapinero Mesa was from an irregularly shaped body of shallow magma, elongate to the northeast in plan, that had two separate cupolas at its roof.

The rib of Precambrian rocks separating the San Juan and Uncompahgre calderas was an unsolved problem in earlier interpretations that related eruption of the Eureka Member to the formation of a single large collapse structure, the San Juan volcanic depression (Luedke and Burbank, 1968; Burbank and Luedke, 1969, p. 17). Our recent detailed mapping has shown that these rocks constitute an unsubsided remnant of the regional Needle Mountains-Uncompahgre structural high (Kelly, 1957). The rib developed as a prominent feature only when the Sapinero Mesa eruptions caused the adjacent San Juan and Uncompahgre calderas to collapse. The early intermediate-composition lavas and breccias covered a broad surface of low relief on Precambrian and older sedimentary rocks, and the volcaniclastic beds interlayered with the lavas and breccias contain only minor detritus of Precambrian rocks. In contrast, the Eureka Member and overlying caldera-fill lavas and sediments were deposited against the Precambrian rocks on slopes of the caldera wall as steep as 60°, and Precambrian detritus is abundant both within the Eureka ash-flow tuffs and in the clastic parts of the overlying lavas and sediments. In one place, a monolithologic landslide breccia within the Eureka Member consists of Precambrian fragments as much as 10 m across, and at several localities the Eureka overlies fossil talus of Precambrian rocks at the caldera walls.

An especially interesting feature of the evolution of the San Juan and Uncompahgre calderas was their joint resurgence to form a large elliptical dome, as much as 15 km wide and at least 30 km long, with a well-developed apical graben (the Eureka graben) clearly evident in the area between the two calderas. Previously described resurgent calderas mostly have domes nested centrally within the collapsed area, such as at Valles (New Mexico), Creede (Colorado), and Timber Mountain (Nevada) calderas (Smith and Bailey, 1968), and the development of the large resurgent dome across both the San Juan and Uncompahgre calderas appeared to support the earlier concept of a large single "San Juan volcanic depression" (Luedke and Burbank, 1968; Burbank and Luedke, 1969). Complex geometric relations between caldera collapse and resurgence exist in other volcanic areas, however: two discrete resurgent domes are nested within the single large Yellowstone caldera in Wyoming (U.S. Geological Survey, 1972) and resurgence of the San Luis caldera in the San Juan field (fig. 1) was asymmetrical to the area of collapse (Steven and Lipman, unpub. data).

The geometry of the joint resurgence of the San Juan and Uncompahgre calderas is imperfectly known, because large parts of the resurgent dome have been covered by late caldera-fill rocks or have caved away as a result of the late collapses that formed the Silverton and Lake City calderas. Nevertheless, several features indicate that this resurgence produced a low-amplitude broad structure: (1) Most of the Eureka Member within these calderas is topographically lower than the outflow Sapinero Mesa Tuff, in contrast with many other well-studied resurgent calderas in which the intracaldera tuff stands higher on the resurgent dome than the general level of the outflow sheet (Smith and Bailey, 1968). (2) The Eureka Member in the Lake City area has dips only slightly steeper than overlying units of the caldera-fill sequence, mostly 20° or less, and a sizable component of this dip is due to later regional northeasterly tilting. (3) The intricate system of fractures and veins radiating from the collapsed areas, especially around the northwest and southeast sides of the San Juan caldera (Burbank and Luedke, 1969, pl. 1), indicate resurgence of an area larger than that which collapsed. The general confinement of mineralized veins in the Lake City area to the moat area of the Uncompahgre caldera suggests that the area of resurgence may have been more restricted in the

northeast part of the twin caldera system.

The joint resurgent doming of the San Juan and Uncompahgre calderas began shortly after collapse, before accumulation of the lower lavas and sediments (Burns and Henson Formations), as indicated by the unconformable onlap of these caldera-fill rocks against tilted Eureka Member in the area between the two calderas (Luedke and Burbank, 1968, p. 194, fig. 9). Resurgence continued during accumulation of the thick sequence of lavas, sediments, and ash-flow tuffs within the San Juan and Uncompahgre calderas. The lavas and sediments of the Burns and Henson Formations, the initial part of this sequence, are intensely faulted along the distended crest of the dome in the Eureka graben zone. General resurgence of the two calderas together probably continued during accumulation of the middle part of the caldera-fill sequence, which consists mainly of ash-flow sheets (Fish Canyon, Carpenter Ridge, and so forth), as this ash-flow sequence dips northeast and east away from the core of the Uncompahgre caldera nearly as steeply as the underlying Eureka Tuff.

Late postcaldera lavas intertongue with and overlie the upper ash-flow sheets and probably accumulated about 27.5–26.5 m.y. ago. These rocks are preserved mainly around the north and east sides of the Uncompahgre caldera, where they overflowed the eastern caldera wall to spread at least 5–10 km farther to the east. In these areas they are as much as 300–400 m thick. The original extent of these lavas to the south and west may have been considerably greater, but they have been largely removed by erosion.

The total subsidence of the Uncompahgre and San Juan calderas is difficult to establish, because the base of the intracaldera Eureka Member is exposed only locally within the calderas, probably on relatively high parts of the caldera floor. A minimum value of 1.5–2 km is indicated by the 500–700 m thickness of the exposed Eureka, plus the 800–1,200 m thickness of overlying caldera-fill lavas, sediments, and ash-flow tuffs.

Silverton Caldera

The relatively small-volume Crystal Lake Tuff, one of the upper ash-flow sheets, apparently originated from within the San Juan caldera about 27.5–27.0 m.y. ago, and probably is related to subsidence of the Silverton caldera along ring fractures that offset the Burns and Henson Formations. This late subsidence, which in part may have reactivated earlier formed ring fractures, tilted the intracaldera rocks asymmetrically in "trapdoor" style. Maximum displacement was at the south end of the Silverton caldera, whereas little displacement appears to have taken place at the north end (fig. 2) (Burbank, 1951, p. 291). Local late resurgence has been postulated within the Silverton caldera (Luedke and Burbank, 1968; Burbank and Luedke, 1969), after the collapse probably related to eruption of the Crystal Lake Tuff, but any such late resurgence is difficult to distinguish from the earlier general doming of the two larger calderas together.

Lake City Caldera

After about a 4-m.y. period of greatly reduced volcanic activity in the western San Juan Mountains, ash-flow eruptions that produced the Sunshine Peak Tuff began about 22.5 m.y. ago in the Lake City area. Outflow Sunshine Peak Tuff must have been deposited widely in the region, although only small erosional remnants have survived. Concurrently with these eruptions, an elliptical block about 12 to 15 km across, nested within the southern part of the older Uncompahgre caldera, began to subside to form the Lake City caldera. Late eruptions of the Sunshine Peak accumulated to a thickness of as much as 1 km within the concurrently subsiding caldera, and great landslide avalanches caved off the caldera wall to spread across the caldera floor and to intertongue with the accumulating ash flows.

The ring fault along which this collapse occurred is continuously exposed for about 300° of arc around the caldera; it is nearly everywhere a single fault, typically marked by only a few feet of gouge and minor hydrothermally altered rock. It is exposed over topographic relief of as much as 600 m, and is everywhere steep, with dips varying from near vertical to about 75° inward. It is gradually being recognized that steep inward dips characterize the bounding faults of many calderas (Reynolds, 1956; Taubeneck, 1967).

Shortly after the ash-flow eruptions ceased, lava flows and domes of viscous silicic quartz latite, fed largely from vents along the ring fault, accumulated around the margins of the caldera floor. These lavas tend to overlie the Sunshine Peak Tuff conformably and dip quite steeply in places. They may largely predate resurgent doming, although the effects of doming on them are difficult to separate reliably from primary dips of the flows. An east-northeast-trending line of rhyolite intrusives was emplaced in the moat area of the older Uncompahgre caldera, north of the Lake City caldera. Compositionally these rocks closely resemble the Sunshine Peak Tuff and probably were emplaced during the same period of magmatism. Their place in the detailed sequence of events related to development of the Lake City caldera is not known, however.

Resurgence of the Lake City caldera produced a simple dome characterized by outward dips of 20°–25° on its flanks and a northeast-trending apical graben over its distended crest. The trend of this graben clearly reflects reactivation of the trends of the earlier Eureka graben system related to resurgence of the Uncompahgre and San Juan calderas. Most of the mapped faults of the Lake City resurgent structure have relatively small displacements (10–50 m) and some seem to be little more than cracks that localized weak hydrothermal alteration. The floor of the caldera is exposed on its southwest side, and the resurgence appears to have been somewhat

asymmetrical, with maximum uplift in this area. Resurgence clearly resulted from upward movement of magma which crystallized as a shallow stock of granite porphyry.

Gently dipping upper contacts of the granite porphyry are exposed at bottoms of several deep erosional valleys within the Lake City caldera core, and the most intensely altered rock within the resurgent dome occurs around margins of the granite porphyry. Parts of the northern ring fault are occupied by a discontinuous stubby ring dike, which broadens and becomes coarser grained downward. Geometric relations revealed in exposures within the core indicate that the top of the granite porphyry crystallized within 1 km of the surface of the resurgent dome.

Most of the original topographic wall of the Lake City caldera has been eroded, and only a few small remnants are preserved southeast of Lake City. The present valleys of Henson Creek and the upper Lake Fork of the Gunnison River, that define a striking elliptical drainage pattern just outside the structural boundary of the Lake City caldera (fig. 2), are not directly controlled by any major fault structures. They more likely developed in the topographically low moat of the Lake City caldera and were subsequently superimposed onto older rocks outside the subsided block.

After development of the Lake City caldera, the only major late Cenozoic volcanism in the western San Juan Mountains was outpouring of thin flows of alkalic olivine basalt of the Hinsdale Formation. Only a few such erosional remnants are preserved, but these flows must formerly have been much more extensive. Locally intertongued with the flows of olivine basalt are more heterogeneous lava domes that vary in composition from basalt to rhyolite and seem to be mix lavas. Together with the rhyolites of the Lake City caldera, these basalts and mix lavas constitute a major part of the Miocene-Pliocene bimodal mafic-silicic volcanic association of the San Juan Mountains (Lipman and others, 1970). This association contrasts strikingly with the older ash-flow sheets of the San Juan field, which are Oligocene in age and belong to the older intermediate-composition volcanic association. These contrasting associations seem to have fundamental significance both in the San Juan field and widely in Cenozoic volcanic rocks of the Western United States (Christiansen and Lipman, 1972).

ECONOMIC CONSIDERATIONS

Any thorough stratigraphic and structural reinterpretation of an area affects other aspects of the geology, and in an area as intensely mineralized as the western San Juans the implications for economic geology are major. In this preliminary paper only the place and time of mineralization with respect to the caldera cycles are summarized. Burbank (1930, 1940, 1947a), Burbank and Luedke (1968), and Luedke and Burbank (1962) have demonstrated two major epochs of mineralization in the San Juan Mountains: (1) a Late Cretaceous-early Tertiary (Laramide) epoch related to intrusive centers at Ouray and, possibly, at Rico and in the La Plata Mountains, and (2) a middle to late Tertiary epoch related to the San Juan volcanic field. These major epochs still are completely valid, but the younger epoch can be subdivided into several stages, rather than just a single stage related to emplacement of postvolcanism intrusives in and around the calderas.

Elsewhere we have found that mineralization related to the different ash-flow calderas in the San Juan field occurred mostly late in the local cycle, during and spatially associated with postsubsidence magmatic activity. This activity typically emplaced lavas and intrusives along ring fractures and outward-extending radial fractures of the calderas, and was related in time and space to the mineralization. These generalizations seem valid for the individual calderas in the western San Juan Mountains, but the multiple caldera cycles resulted in several periods of mineralization.

In the Lake City area, where an exceptionally complete stratigraphic succession allows determination of detailed age relations, at least three distinct stages of mid-Tertiary mineralization can be related to different local environments of deposition. Cores of four early intermediate-composition precollapse volcanoes around the periphery of the Uncompahgre caldera are altered and mineralized, with minor ore production from one. In addition, the caldera fill in the Uncompahgre caldera is cut by monzonitic intrusives and is locally hydrothermally altered. Many associated fractures were filled by quartz-sulfide veins that have supplied most of the production from this area. The altered rocks and veins are locally truncated by the Lake City caldera wall and clearly are older than this caldera. Finally, some ring-fracture intrusives and lavas around the Lake City caldera are intensely altered, and many of the distensional fractures within the resurgent core are altered and some contain metalliferous veins.

The younger volcanic formations are absent in the highly mineralized and productive Silverton caldera area, and the relative ages of mineralization in different areas have not yet been established. The generally similar paragenesis of most of the veins has been interpreted as resulting from deposition during a single major stage of mineralization (Burbank and Luedke, 1968, 1969). However, Burbank and Luedke also noted that the veins were recurrently opened and filled with vein materials of contrasting compositions. The possibility of multistage deposition resulting in superposition of mineralization of several ages along the same fractures has never been ruled out, and remains a fascinating problem for future study.

REFERENCES CITED

Burbank, W. S., 1930, Revision of the geologic structure and stratigraphy in the Ouray district of Colorado, and its bearing on ore deposition: Colorado Sci. Soc. Proc., v. 12, no. 6, p. 151–232.

—— 1933, Vein systems of Arrastre Basin and regional geologic structure in the Silverton and Telluride quadrangles, Colorado: Colorado Sci. Soc. Proc., v. 13, no. 5, p. 135–214.

—— 1938, Silverton caldera, San Juan County, Colo. [abs.]: Washington Acad. Sci. Jour., v. 28, no. 9, p. 417–418.

—— 1940, Structural control of ore deposition in the Uncompahgre district, Ouray County, Colorado: U.S. Geol. Survey Bull. 906-E, p. 189–265.

—— 1941, Structural control of ore deposition in the Red Mountains, Sneffels, and Telluride districts of the San Juan Mountains, Colorado: Colorado Sci. Soc. Proc., v. 14, no. 5, p. 141–261.

—— 1947a, General features [of San Juan region], *in* Vanderwilt, J. W., ed., Mineral resources of Colorado: Colorado Mineral Resources Board, p. 396–408.

—— 1947b, Lake City area, Hinsdale County, *in* Vanderwilt, J. W., ed., Mineral resources of Colorado: Colorado Mineral Resources Board, p. 439–443.

—— 1951, The Sunnyside, Ross Basin, and Bonita fault systems and their associated ore deposits, San Juan County, Colorado: Colorado Sci. Soc. Proc., v. 13, no. 5, p. 285–304.

Burbank, W. S., and Luedke, R. G., 1964, Geology of the Ironton quadrangle, Colorado: U.S. Geol. Survey Geol. Quad. Map GQ-291.

—— 1966, Geologic map of the Telluride quadrangle, southwestern Colorado: U.S. Geol. Survey Geol. Quad. Map GQ-504.

—— 1968, Geology and ore deposits of the western San Juan Mountains, Colorado, *in* Ore deposits of the United States, 1933–1967 (Graton-Sales Volume), V. 1: New York, Am. Inst. Mining, Metall. and Petroleum Engineers, p. 714–733.

—— 1969, Geology and ore deposits of the Eureka and adjoining districts, San Juan Mountains, Colorado: U.S. Geol. Survey Prof. Paper 535, 73 p.

Christiansen, R. L., and Lipman, P. W., 1972, Cenozoic volcanism and plate-tectonic evolution of the Western United States, II. Late Cenozoic: Royal Soc. London Philos. Trans., v. 271, p. 249–284.

Cohee, G. V., chm., 1961, Tectonic map of the United States–exclusive of Alaska and Hawaii: U.S. Geol. Survey and Am. Assoc. Petroleum Geologists [1962].

Cross, Whitman, Howe, Ernest, and Irving, J. D., 1907, Description of the Ouray quadrangle [Colorado]: U.S. Geol. Survey Geol. Atlas, Folio 153.

Cross, Whitman, Howe, Ernest, and Ransome, F. L., 1905, Description of the Silverton quadrangle [Colorado]: U.S. Geol. Survey Geol. Atlas, Folio 120.

Cross, Whitman, and Purington, C. W., 1899, Description of the Telluride quadrangle [Colorado]: U.S. Geol. Survey Geol. Atlas, Folio 57.

Hansen, W. R., 1971, Geologic map of the Black Canyon of the Gunnison River and vicinity, western Colorado: U.S. Geol. Survey Misc. Geol. Inv. Map I-584.

Kelley, V. C., 1957, General geology and tectonics of the western San Juan Mountains, Colorado, *in* New Mexico Geol. Soc., Guidebook, 8th Field Conf., Sept. 1957: p. 154–162.

Larsen, E. S., Jr., and Cross, Whitman, 1956, Geology and petrology of the San Juan region, southwestern Colorado: U.S. Geol. Survey Prof. Paper 258, 303 p.

Lipman, P. W., and Steven, T. A., 1970, Reconnaissance geology and economic significance of the Platoro caldera, southeastern San Juan Mountains, Colorado, *in* Geological Survey Research 1970: U.S. Geol. Survey Prof. Paper 700-C, p. C19–C29.

Lipman, P. W., Steven, T. A., and Mehnert, H. H., 1970, Volcanic history of the San Juan Mountains, Colorado, as indicated by potassium-argon dating: Geol. Soc. America Bull., v. 81, p. 2329–2352.

Luedke, R. G., 1972, Geologic map of the Wetterhorn Peak quadrangle, Ouray and Hinsdale Counties, Colorado: U.S. Geol. Survey Geol. Quad. Map GQ-1011.

Luedke, R. G., and Burbank, W. S., 1961, Central vent ash-flow eruption, western San Juan Mountains, Colorado: Art. 326 *in* U.S. Geol. Survey Prof. Paper 424-D, p. D94–D96.

—— 1962, Geology of the Ouray quadrangle, southwestern Colorado: U.S. Geol. Survey Geol. Quad. Map GQ-152.

—— 1963, Tertiary volcanic stratigraphy in the western San Juan Mountains, Colorado: Art. 70 *in* U.S. Geol. Survey Prof. Paper 474-C, p. C39–C44.

—— 1968, Volcanism and cauldron development in the western San Juan Mountains, Colorado, *in* Epis, R. G., ed., Cenozoic volcanism in the southern Rocky Mountains: Colorado School Mines Quart., v. 63, no. 3, p. 175–208.

Mehnert, H. H., Lipman, P. W., and Steven, T. A., 1973, Age of the Lake City caldera and related Sunshine Peak Tuff, western San Juan Mountains, Colorado: Isochron West, no. 6, p. 31–33.

Olson, J. C., Hedlund, D. C., and Hansen, W. R., 1968, Tertiary volcanic stratigraphy in the Powderhorn-Black Canyon region, Gunnison and Montrose Counties, Colorado: U.S. Geol. Survey Bull. 1251-C, p. C1–C29.

Ratté, J. C., and Steven, T. A., 1967, Ash flows and related volcanic rocks associated with the Creede caldera, San Juan Mountains, Colorado: U.S. Geol. Survey Prof. Paper 524-H, 58 p.

Reynolds, D. L., 1956, Calderas and ring-complexes: Verh. K. Ned. Geol.-mijnb. Genoot., Geol. Ser., v. 16, p. 355-379.

Smith, R. L., 1960, Ash flows: Geol. Soc. America Bull., v. 71, p. 795–842.

Smith, R. L., and Bailey, R. A., 1968, Resurgent cauldrons, *in* Studies in volcanology–A memoir in honor of Howel Williams: Geol. Soc. America Mem. 116, p. 613–662.

Steven, T. A., 1967, Geologic map of the Bristol Head quadrangle, Mineral and Hinsdale Counties, Colorado: U.S. Geol. Survey Geol. Quad. Map GQ-631.

Steven, T. A., Lipman, P. W., Hail, W. J., Jr., Barker, Fred, and Luedke, R. G., 1973a, Geologic map of the Durango quadrangle, southwestern Colorado: U.S. Geol. Survey Misc. Geol. Inv. Map I-764. (In press.)

Steven, T. A., Lipman, P. W., and Olson, J. C., 1973b, Ash flow stratigraphy and caldera structures in the San Juan volcanic field, southwestern Colorado, *in* Cohee, G. V., and Wright, W. B., Changes in stratigraphic nomenclature by the U.S. Geological Survey, 1973: U.S. Geol. Survey Bull. 1394-A. (In press.)

Steven, T. A., Mehnert, H. H., and Obradovich, J. D., 1967, Age of volcanic activity in the San Juan Mountains, Colorado, *in* Geological Survey Research 1967: U.S. Geol. Survey Prof. Paper 575-D, p. D47-D55.

Steven, T. A., and Ratté, J. C., 1965, Geology and structural control of ore deposition of the Creede district, San Juan Mountains, Colorado: U.S. Geol. Survey Prof. Paper 487, 87 p.

Taubeneck, W. H., 1967, Notes on the Glen Coe cauldron subsidence, Argyllshire, Scotland: Geol. Soc. America Bull., v. 78, p. 1295–1316.

U.S. Geological Survey, 1972, Geologic map of Yellowstone National Park: U.S. Geol. Survey Misc. Geol. Inv. Map I-711.

Varnes, D. J., 1963, Geology and ore deposits of the South Silverton Mining Area, San Juan County, Colorado: U.S. Geol. Survey Prof. Paper 378-A, 56 p.

Jour. Research U.S. Geol. Survey
Vol. 1, No. 6, Nov.-Dec. 1973, p. 643–647

Sr^{87}/Sr^{86}, K, Na, Rb, AND Sr IN SOME ECLOGITES AND ASSOCIATED BASALTS FROM CALIFORNIA AND SOUTHWESTERN OREGON

By E. D. GHENT[1], Z. E. PETERMAN, and R. G. COLEMAN,
Menlo Park, Calif., Denver, Colo., Menlo Park, Calif.

Abstract.—Six samples of group C eclogites from California and southwestern Oregon have initial Sr^{87}/Sr^{86} ratios in the range of 0.7028 to 0.7051; Rb contents from less than 1 to 53.4 ppm; and Sr contents from 147 to 270 ppm. These data and major-element compositions suggest that the eclogites were derived from basalts older than but similar in composition to those intercalated with Mesozoic eugeosynclinal sedimentary rocks in California and western Oregon. The isotopic heterogeneity of the eclogites and associated graywackes contrasts with a uniformity of Sr^{87}/Sr^{86} in many younger calc-alkaline volcanic rocks of the circum-Pacific province. Derivation of the younger volcanic rocks from an eclogite-blueschist melange isotopically similar to those investigated here would require isotopic homogenization or integrated partial melting over sufficient volumes so as to reduce these variations in the derived melts.

Eclogites occur in a variety of geologic settings (Coleman and others, 1965) and have apparently crystallized over a range of temperature-load pressure conditions (Coleman and others, 1965; Green and Ringwood, 1967). Eclogites have been divided into three groups by Coleman and others (1965): group A, inclusions in kimberlites and alkali olivine basalts, or as layers in ultramafic rocks; group B, bands or lenses within migmatite gneiss terrains; and group C, bands or lenses within metamorphic rocks of blueschist facies. Several workers have concluded that some eclogites can form stably within the crust under low-water-pressure conditions (Green and Ringwood, 1967; Fry and Fyfe, 1969). Others have suggested that eclogites are produced in the lithosphere during subduction and are the source rocks for andesitic magmas (Ringwood and Green, 1966; Miyashiro, 1972).

Eclogites from California and Oregon occur as isolated blocks within Mesozoic eugeosynclinal rocks. They are thought to have formed from crustal rocks and to have been tectonically transported as part of a serpentinite melange (Coleman and Lanphere, 1971). Most eclogites have a bulk chemistry approximating that of basalts; however, eclogites from California and Oregon are generally richer in normative nepheline and diopside than are associated Mesozoic eugeosynclinal basaltic rocks (Ghent and Coleman, 1973). These authors have tentatively concluded that these compositions resulted from metasomatism of rocks of originally basaltic composition during the process of eclogitization.

This report is concerned with samples whose bulk chemistry, mineralogy, K-Ar ages, and field occurrences have been described elsewhere (Coleman and others, 1965; Coleman and Lanphere, 1971; Ghent and Coleman, 1973). Sr isotopes have been of value in placing constraints on and providing clues for choosing between petrogenetic models of mafic igneous rocks (see Faure and Powell, 1972). This study of Sr^{87}/Sr^{86}, and Rb and Sr contents of group C eclogites (Coleman and others, 1965) from Oregon and California was undertaken for comparison with similar data on associated Mesozoic mafic volcanic rocks, modern oceanic basalts, and andesites. Data for Mesozoic eugeosynclinal basalts and graywackes from California and Oregon have been reported by Coleman (1972) and by Sinha and Davis (1971). Few other data of this sort have been published for eclogites (Steuber and Murthy, 1966; Allsopp and others, 1969; Compston and Lovering, 1969). The analyses reported by Allsopp and others (1969) are of group A and group B eclogites, whereas the analyses by Compston and Lovering (1969) are of group A eclogites only. According to these workers, considerable amounts of Rb and radiogenic Sr are concentrated in "matrix materials" and these elements may have been introduced during the transport of the eclogites in the pipes.

Acknowledgments.—We are indebted to W. G. Ernst, University of California at Los Angeles, for giving us the analyzed powders of the metabasalts from Pacheco Pass; to W. P. Doering for the XRF Rb and Sr analyses; and to R. A. Hildreth and W. T. Henderson for the Sr isotopic measurements. Marvin Lanphere and Miles Silberman kindly reviewed the manuscript and their comments are greatly appreciated. The work was done while Ghent was at Menlo Park, Calif., on leave from the University of Calgary.

[1] University of Calgary, Calgary, Alberta, Canada.

Table 1.—*Analytical data*

[Na_2O and K_2O data for eclogites from Coleman and others (1965) and Ghent and Coleman (1973); Na_2O and K_2O data for metabasalts from Ernst and others (1970)]

Sample No.	Na_2O (wt percent)	K_2O (wt percent)	Rb (ppm)	Sr_t (ppm)	Rb/Sr	K/Rb	$(Sr^{87}/Sr^{86})_t$[1]	$(Sr^{87}/Sr^{86})_o$[2]	Locality and source of descriptive data
Eclogite samples									
62-RGC-58.....	4.3	0.04	<1	270	0.004	>330	0.7037	0.7037	Ward Creek, Sonoma County, Calif. (Coleman and others, 1965).
100-RGC-58.....	3.1	.22	7.4	189	.039	250	.7053	.7051	Tiburon Peninsula, Marin County, Calif. (Coleman and others, 1965).
102-RGC-58.....	4.4	.20	8.4	147	.057	200	.7042	.7039	Junction School, Sonoma County, Calif. (Coleman and others, 1965).
113-RGC-58.....	3.4	.18	3.5	164	.021	430	.7037	.7035	Occidental Quarry, Sonoma County, Calif. (Coleman and others, 1965).
207-RGC-58.....	5.1	.40	18.9	139	.136	180	.7036	.7028	Valley Ford, Sonoma County, Calif. (Coleman and others, 1965).
95-69-1.....	4.29	1.20	53.4	232	.230	190	.7049	.7035	Waterman Ranch, Coos County, Oreg. (Ghent and Coleman, 1973).
Metabasalt samples									
X-72.....	2.70	0.31	6.6	105	0.063	390	0.7052	0.7048	Pacheco Pass area, California (Ernst and others, 1970).
X-81.....	3.68	.28	2.0	110	.018	1,160	.7048	.7047	Do.

[1] Measured Sr^{87}/Sr^{86} ratio. Data for Eimer and Amend standard yield an average Sr^{87}/Sr^{86} value of 0.7080.
[2] Initial Sr^{87}/Sr^{86} ratio calculated on age corrections of 150 m.y. for the eclogites and 140 m.y. for the metabasalts.

ISOTOPIC AND TRACE-ELEMENT RESULTS

Sr^{87}/Sr^{86} ratios, alkalis, and Sr contents of six eclogite samples from California and Oregon and of two basalt samples from California are presented in table 1. On a conventional isochron diagram (fig. 1), Sr^{87}/Sr^{86} values of the eclogites, except for one sample, are higher than those of ocean ridge basalts from the Juan de Fuca and Gordo Rises, and are in the range of values shown for the ophiolite suite from Cyprus, basalts from the Colebrooke Schist, and two basalts from the Franciscan Formation of the Pacheco Pass area (for mineralogy and bulk chemistry of these, see Ernst and others, 1970). Other basalts from the Franciscan Formation have significantly higher Sr^{87}/Sr^{86} values which Sinha and Davis (1971) attributed to reaction with sea water.

Rb and Sr contents of the eclogites are compared with those of basalts on figure 2. Sr in the eclogites shows less variation than in basalts from the Franciscan Formation and Colebrooke Schist and generally ranges between the values for the average ocean-ridge tholeiite and low-potassium tholeitte given by Hart

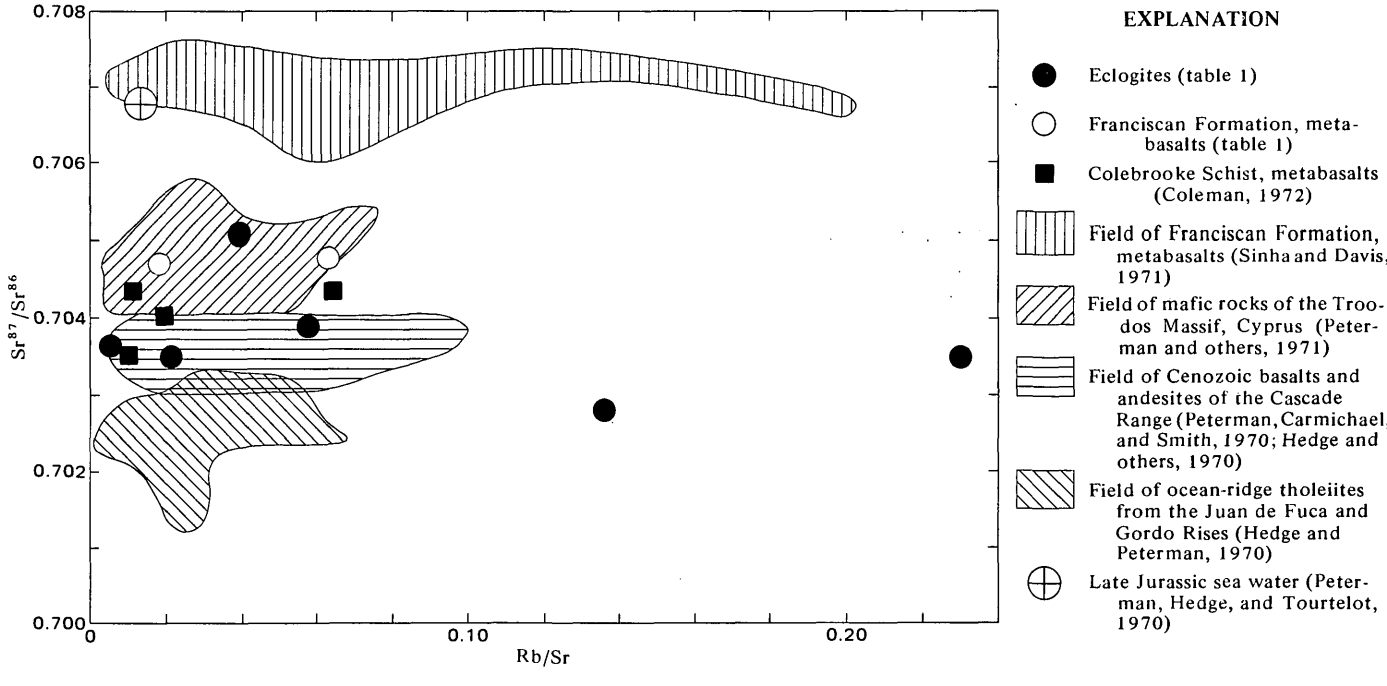

Figure 1.—Sr^{87}/Sr^{86} versus Rb/Sr diagram.

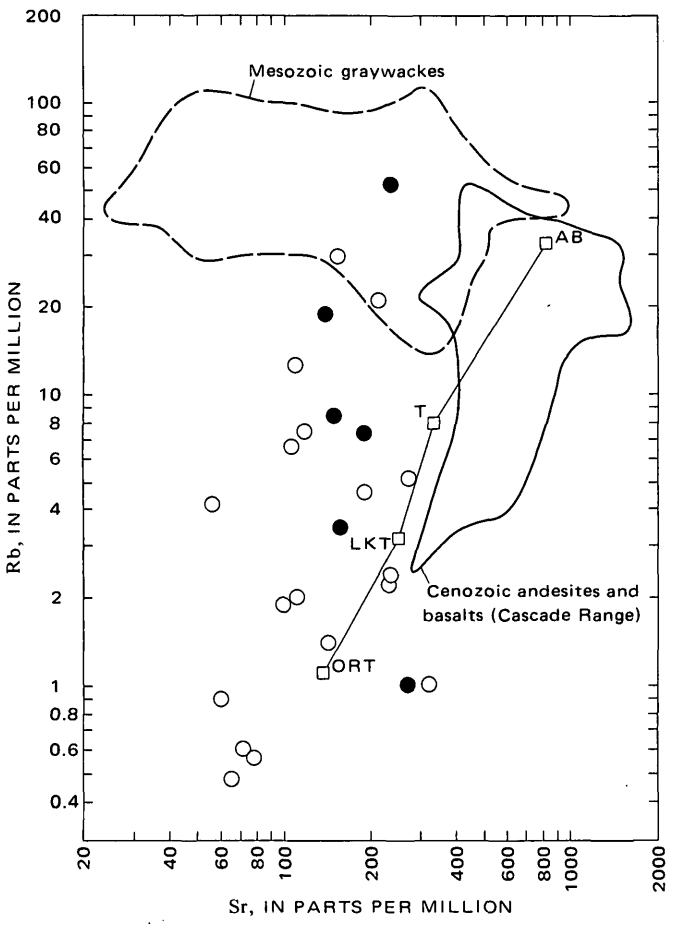

Figure 2.—Plot of Rb and Sr contents. Solid dots are eclogites (table 1); open circles are basalts from the Franciscan Formation (Sinha and Davis, 1971; table 1) and from the Colebrooke Schist (Coleman, 1972); and squares are averages of basalt types from Hart and others (1970). ORT, ocean-ridge tholeiites; LKT, low-potassium tholeiites; T, tholeiites; and AB, alkali basalts. Data defining field of Cascade andesites and basalts are from Hedge and others (1970) and Peterman, Carmichael, and Smith (1970). Data for graywackes are from Peterman and others (1967), Coleman (1972), and Peterman (unpub. data).

and others (1970). Rb shows much greater variation than Sr in the eclogites and ranges from less than 1 to 53 ppm. It should be noted that the average Rb and Sr contents for ocean-ridge tholeiites were obtained from data on the freshest material obtainable (Hart and others, 1970), and if all available data are considered, these elements show nearly as much variation as in the eclogites (see Ewart and Bryan, 1972, fig. 7).

The present Sr isotopic character, and major- and trace-element chemistry have undoubtedly been influenced by modification during eclogitization and possibly by alteration prior to this higher grade metamorphism. The initial Sr^{87}/Sr^{86} ratios calculated in table 1 should represent the isotopic composition of Sr at the time of eclogitization. As a result of a high phengite content, the Oregon eclogite has a high Rb content and high Rb/Sr ratio, yet the calculated initial Sr^{87}/Sr^{86} ratio is not anomalous with respect to the others. The lack of correlation between Sr^{87}/Sr^{86} and Rb content suggests that isotopically anomalous Sr was not introduced along with the alkalis. The possibility of alteration of the parent basalts prior to eclogitization is difficult to evaluate from these data alone. Trace-element (Hart, 1969) and isotopic (Hart, 1972) modification of submarine basalts as a result of interaction with sea water is well documented. Perhaps alteration of this type affected the parent basalts before they were subjected to eclogite metamorphism, and the Sr^{87}/Sr^{86} ratios were increased during this initial stage of alteration. The high Na contents of the eclogites may reflect an early-stage spilitization (Coleman and others, 1965; Ghent and Coleman, 1973). The migration of alkalis in pillow lavas is a well-documented phenomenon (for example, Bailey and others, 1964).

The most likely precursors of the eclogites are ocean-ridge tholeiites or eugeosynclinal basalts similar to those intercalated with the Mesozoic eugeosynclinal sediments. Coleman and others (1965) and Ghent and Coleman (1973) favor the latter source for the eclogites. Cann (1970) considers Ti to be one of the elements in basalts for which the original concentration is least affected by later alteration, and according to his data Ti ranges from 3,200 to 11,100 ppm in ocean-floor basalts, with most of the samples containing between 5,000 and 10,000 ppm. The eclogites contain between 8,400 and 19,000 ppm Ti (Coleman and others, 1965; Ghent and Coleman, 1973) and hence overlap but exceed the Ti range for ocean-floor basalts on the high side. The eugeosynclinal basalts from California and Oregon exhibit a range in Ti similar to that of the eclogites (Ernst and others, 1970; Coleman, 1972). In this respect, the eugeosynclinal rocks do not correspond to any of the volcanic series alleged by Jakeš and White (1972) to represent a continuum of igneous rock series in the island-arc domain. Younger compositional analogs of these eugeosynclinal basalts may be the tholeiites of the Eocene Siletz River Volcanics of western Oregon. These were erupted along the continental margin in evolving eugeosynclines but have chemical similarities to oceanic submarine basalts (Snavely and others, 1968).

GEOLOGIC IMPLICATIONS

A few clues provided by the present study, and much information from previous detailed investigations (Coleman and others, 1965; Coleman and Lanphere, 1971; Ghent and Coleman, 1973) lead to the following comments concerning the implications of the eclogite data:

1. Rb and Sr contents in the precursors of the eclogites were probably modified at the time of eclogitization and possibly during an earlier stage of alteration such as might result from interaction with sea water. Sr^{87}/Sr^{86} values may also have been changed during this earlier alteration. In the Late Jurassic, ocean waters contained Sr with a Sr^{87}/Sr^{86} value of 0.70675 (Peterman, Hedge, and Tourtelot, 1970) and this provides an upper limit for Sr^{87}/Sr^{86} values which could be produced by sea-water interaction on basalts (fig. 1). All

the eclogites have Sr^{87}/Sr^{86} values lower than that of Jurassic sea water; accordingly, if exchange did occur, it was variable and far from complete. Whether or not the basalt precursors underwent alteration prior to metamorphism, the initial Sr^{87}/Sr^{86} values (table 1) should be the isotopic composition of Sr at the time of eclogitization, provided that the rocks have been closed systems in Rb and Sr since that time. Tectonic transport of the eclogites in an ultramafic milieu should not have significantly modified the Rb and Sr contents because of the extremely low concentrations of these elements in the serpentinites.

2. Because of the chemical changes attendant with eclogitization, comparison of the compositions of the eclogites and unaltered basalts is difficult. Nevertheless, previous studies and the present data suggest that eugeosynclinal basalts compositionally similar to, but older than, those now exposed in the lower grade Mesozoic deposits of California and Oregon could have been the precursors of the eclogites.

3. Whatever the compositions of the parent basalts, these eclogites may represent material whose passage down a subduction zone and conversion to high-grade metamorphic rocks was somehow aborted by tectonic transport to the surface (Ernst, 1970). If this model is correct, the present data can be used to reconstruct the isotopic and chemical nature of subducted material composed of eclogite and associated rocks. From the limited data reported here, we can conclude that the eclogites are characteristically variable in Sr^{87}/Sr^{86} ratios (0.7028 to 0.7051) and Rb and Sr contents (figs. 1, 2). Associated metagraywackes show comparable variation in these parameters; Mesozoic graywackes of California and Oregon have initial Sr^{87}/Sr^{86} ratios in the range of 0.7030 to 0.7081 (Peterman and others, 1967; Coleman, 1972) and a wide range in Rb and Sr contents (fig. 2).

Without implying an actual genetic relationship, we can compare the isotopic and trace-element characteristics of the eclogite-graywacke association with those of the younger circum-Pacific calc-alkaline volcanic rocks. Obviously, if these volcanics are derived from a subducted plate, that plate is much younger than the rocks we are discussing. Most calc-alkaline volcanic rocks of the circum-Pacific province are characterized by a remarkably narrow range in Sr^{87}/Sr^{86} values of 0.7030 to 0.7040 (Hedge and Peterman, 1969). Andesites and basalts of the Cascades exemplify this limited range in Sr^{87}/Sr^{86} (fig. 1) but show much variation in Rb and Sr contents (fig. 2). To produce isotopically uniform magmas from a heterogeneous source composed of eclogite and graywacke would require either isotopic homogenization or partial melting to be integrated over sufficient volume so as to average out the isotopic variations. Isotopic homogenization among such diverse rock compositions is not supported by available data on high-grade, even granulite-facies, metamorphic rocks. Integrated partial melting of the degree necessary to reduce the isotopic variations to the required narrow range would also tend to smooth out the primary variations in Rb and Sr contents as well as in major elements. Thus it would be difficult to obtain a primary basalt melt with the compositional characteristics observed in the erupted lavas from a graywacke-eclogite mixture. In considering a similar mixed source for basalts and andesites of the Cascade Range, Hedge and others (1970) concluded that the sedimentary component would have to be minor in order to satisfy the limitation imposed by the Sr isotopic data.

At present, the degrees of freedom are many and the constraints are few. These data on eclogites merely provide some additional boundary conditions which should be considered in models postulating fusion of eclogites to produce calc-alkaline rocks.

REFERENCES CITED

Allsopp, H. L., Nicolaysen, L. O., and Hahn-Weinheimer, P., 1969, Rb/K ratios and Sr-isotopic compositions of minerals in eclogitic and peridotitic rocks: Earth and Planetary Sci. Letters, v. 5, p. 231–244.

Bailey, E. H., Irwin, W. P., and Jones, D. L., 1964, Franciscan and related rocks and their significance in the geology of western California: California Div. Mines Bull. 183, 176 p.

Cann, J. R., 1970, Rb, Sr, Y, Zr and Nb in some ocean floor basaltic rocks: Earth and Planetary Sci. Letters, v. 10, p. 7–11.

Coleman, R. G., 1972, The Colebrooke Schist of southwestern Oregon and its relation to the tectonic evolution of the region: U.S. Geol. Survey Bull. 1339, 61 p.

Coleman, R. G., and Lanphere, M. A., 1971, Distribution and age of high-grade blueschists, associated eclogites and amphibolites from Oregon and California: Geol. Soc. America Bull., v. 82, p. 2397–2412.

Coleman, R. G., Lee, D. E., Beatty, L. B., and Brannock, W. W., 1965, Eclogites and eclogites–their differences and similarities: Geol. Soc. America Bull., v. 76, p. 483–508.

Compston, W., and Lovering, J. R., 1969, The strontium isotope geochemistry of granulitic and eclogitic inclusions from the basic pipes at Delegate, eastern Australia: Geochim. et Cosmochim. Acta, v. 33, p. 691–699.

Ernst, W. G., 1970, Tectonic contact between the Franciscan melange and the Great Valley Sequence–crustal expression of a late Mesozoic Benioff zone: Jour. Geophys. Research, v. 75, p. 886–901.

Ernst, W. G., Seki, Y., Onuki, H., and Gilbert, M. C., 1970, Comparative study of low-grade metamorphism in the California Coast Ranges and the outer metamorphic belt of Japan: Geol. Soc. America Mem. 124, 270 p.

Ewart, A., and Bryan, W. B., 1972, Petrography and geochemistry of the igneous rocks from Eua, Tongan Islands: Geol. Soc. America Bull., v. 83, p. 3281–3298.

Faure, G., and Powell, J. L., 1972, Strontium isotope geochemistry: New York, Springer-Verlag, 188 p.

Fry, N., and Fyfe, W. S., 1969, Eclogites and water pressure: Contr. Mineralogy and Petrology, v. 24, p. 1–6.

Ghent, E. D., and Coleman, R. G., 1973, Eclogites from southwestern Oregon: Geol. Soc. America Bull. v. 84, p. 2471–2488.

Green, D. H., and Ringwood, A. E., 1967, An experimental investigation of the gabbro to eclogite transformation and its petrological implications: Geochim. et Cosmochim. Acta, v. 31, p. 767–833.

Hart, S. R., 1969, K, Rb, Cs contents and K/Rb, K/Cs ratios of fresh and altered submarine basalts: Earth and Planetary Sci. Letters, v. 6, p. 295–303.

——1972, Sr isotopic composition of the oceanic crust: Carnegie Inst. Washington Yearbook 71, p. 288–290.

Hart, S. R., Brooks, C., Krogh, T. W., Davis, G. L., and Nava, D., 1970, Ancient and modern volcanic rocks—a trace element model: Earth and Planetary Sci. Letters, v. 10, p. 17–28.

Hedge, C. E., Hildreth, R. A., and Henderson, W. T., 1970, Strontium isotopes in some Cenozoic lavas from Oregon and Washington: Earth and Planetary Sci. Letters, v. 8, p. 434–438.

Hedge, C. E., and Peterman, Z. E., 1969, Sr^{87}/Sr^{86} of Circum-Pacific andesites: Geol. Soc. America Abs. with Programs for 1969, pt. 7, p. 96.

——1970, The strontium isotopic composition of basalts from the Gordo and Juan de Fuca Rises, northeastern Pacific Ocean: Contr. Mineralogy and Petrology, v. 27, p. 114–120.

Jakeš, P., and White, A. J. R., 1972, Major and trace element abundances in volcanic rocks of orogenic areas: Geol. Soc. America Bull., v. 83, p. 29–40.

Miyashiro, A., 1972, Metamorphism and related magmatism in plate tectonics: Am. Jour. Sci., v. 272, p. 629–656.

Peterman, Z. E., Carmichael, I. S. E., and Smith, A. L., 1970, Sr^{87}/Sr^{86} ratios in Quaternary lavas of the Cascade Range, northern California: Geol. Soc. America Bull., v. 81, p. 311–318.

Peterman, Z. E., Coleman, R. G., and Hildreth, R. A., 1971, Sr^{87}/Sr^{86} in mafic rocks of the Troodos Massif, Cyprus, *in* Geological Survey Research 1971: U.S. Geol. Survey Prof. Paper 750-D, p. D157–D161.

Peterman, Z. E., Hedge, C. E., Coleman, R. G., and Snavely, P. D., Jr., 1967, Sr^{87}/Sr^{86} ratios in some eugeosynclinal sedimentary rocks and their bearing on the origin of granitic magma in orogenic belts: Earth and Planetary Sci. Letters, v. 2, p. 433–439.

Peterman, Z. E., Hedge, C. E., and Tourtelot, H. A., 1970, Isotopic composition of strontium in sea water throughout Phanerozoic time: Geochim. et Cosmochim. Acta, v. 34, p. 105–120.

Ringwood, A. E., and Green, D. H., 1966, An experimental investigation of the gabbro to eclogite transformation and some geophysical implications: Tectonophysics, v. 3, p. 383–427.

Sinha, A. K., and Davis, T. E., 1971, Geochemistry of Franciscan volcanic and sedimentary rocks from California: Carnegie Inst. Washington Yearbook 69, p. 394–397.

Snavely, P. D., Jr., MacLeod, N. S., and Wagner, H. C., 1968, Tholeiitic and alkalic basalts of the Eocene Siletz River Volcanics, Oregon Coast Range: Am. Jour. Sci., v. 266, p. 454–481.

Steuber, A. M., and Murthy, V. R., 1966, Strontium isotope and alkali element abundances in ultramafic rocks: Geochim. et Cosmochim. Acta, v. 30, p. 1243–1259.

Jour. Research U.S. Geol. Survey
Vol. 1, No. 6, Nov.-Dec. 1973, p. 649–658

LOSS OF VOLATILES DURING FOUNTAINING AND FLOWAGE OF BASALTIC LAVA AT KILAUEA VOLCANO, HAWAII

By DONALD A. SWANSON and BRENT P. FABBI, Menlo Park, Calif.

Abstract.—The amount of water and sulfur in pumice erupted during periods of vigorous activity during the 1969–71 Mauna Ulu eruption varied inversely with fountain height because of degassing during the fountaining. The pumice lost about 0.05 wt percent water and 0.003 wt percent sulfur during fountaining to heights of 400–540 m. Analyses suggest that the initial volatile content of Mauna Ulu lava was greater immediately preceding periods of high fountaining than during weak activity between those periods or after the last high fountains on December 30, 1969. Water and sulfur were systematically depleted during nearly isothermal flowage in lava tubes. Rapidly quenched samples of dipped melt show losses of about 0.03–0.04 wt percent water and 0.007–0.008 wt percent sulfur during flowage for several hours through a distance of 12 km. Glassy skins on cooled pahoehoe flows contain about 0.002–0.003 wt percent less sulfur than quenched melt at comparable distances from the vent, because of continued degassing under natural cooling conditions. Chlorine shows similar but less well defined trends. Pumice erupted in high fountains becomes more strongly oxidized than the parent magma, because of mixing with air while still at high temperatures.

The sudden reduction in confining pressure causes basaltic lava to degas as it erupts and flows away from the vent. Large fume clouds accompanying high lava fountains are clear evidence of degassing. Subtle but conclusive evidence of continued degassing during subsequent flowage away from the vent is provided by the observed downslope decrease in (1) the amount of fume emitted from the flowing lava, (2) the number of bubbles on the surface of the flowing lava and vesicularity of the solidified flow, and (3) the fluidity at nearly constant temperature. Swanson elaborates on this evidence of degassing during the 1969–71 Mauna Ulu eruption of Kilauea in another paper (1973). In general, the degree of degassing is important in governing the structures and textures of all solidified flows, whether subaerial (Swanson, 1973) or subaqueous (Jones, 1969; Moore, 1970a).

Chemical analysis of the volatile content of glassy, quickly chilled samples collected at various stages during an eruption is one way to measure the degree of degassing. If the quench is rapid enough, the volatile content of the resulting glass is nearly the same as that dissolved in the liquid lava at the site of collection. If not so rapid, gases are lost to a degree dependent on the rate of cooling.

We have examined the content of water, sulfur, and chlorine in many fresh, rapidly quenched samples of pumice, spatter, and flow material from the 1969–71 Mauna Ulu eruption. The rate of volatile loss is dependent in part on height of fountaining and distance of flowage, that is, on the length of time at which the sample was held at about 1 atm pressure and at magmatic temperature. The data also suggest that the lava which fountained to great heights contained more volatiles before eruption than that which erupted during weak activity or flowed out of the vent without spattering. Pumice ejected to heights of 100 m or more became more highly oxidized than the parent magma, presumably from extended contact with air at high temperatures.

Basaltic magma, if saturated, probably contains at least 0.5 wt percent water and 0.08 wt percent sulfur at confining pressures equivalent to those in Kilauea's shallow (1–3 km depth) reservoir system (Moore, 1970b; Moore and Fabbi, 1971). The distribution of these and other volatiles in the parent magma before and during the 1969–71 Mauna Ulu eruption is not known. Possibly volatiles were enriched in lower pressure (shallower depth) parts of the reservoir system owing to diffusion before eruption. Such possible enrichment cannot be evaluated in this study, however, as all analyzed samples contain only 20 percent or less of the presumed original volatile content owing to the dominance of the eruptive and flowage degassing processes. Our computed rates of volatile loss during fountaining probably are minimum rates, because we assume, for the purpose of this paper, a uniform distribution of volatiles in the magma immediately before eruption and no diffusion of volatiles into the magma from the reservoir wallrock.

Many uncertainties were involved in collecting the suite of samples examined in this paper, as is true of most collections obtained under dynamic, at times dangerous, conditions. Such uncertainties make some of the interpretations tentative. This is particularly true of samples of pumice from high fountains. One cannot possibly know the preeruption volatile history of such samples, exactly what processes take place during the time the pumice is in the fountain, and the precise trajectory of the pumice as it falls to the ground. These and other uncertainties can drastically affect the volatile content of the

samples in unpredictable ways. We believe that much of the scatter in our data, especially for high fountains, is caused by such uncertainties. Furthermore, many of the changes that we examine are small and close to the analytical uncertainty. We have interpreted the results simply and find them to be reasonably consistent but emphasize the possibilities of alternative interpretations.

The fountain data, though less reliable than the flowage data, are discussed first because of the temporal sequence of the degassing processes.

Acknowledgments.—Swanson is responsible for the field observations and collection of samples; Fabbi made the sulfur and chlorine analyses. They share the interpretations. W. A. Duffield and T. L. Wright reviewed the manuscript and improved it greatly, and R. L. Christiansen and R. I. Tilling suggested stimulating alternative interpretations. We thank D. W. Peterson for help in collecting samples; E. L. Brandt, E. E. Engleman, G. O. Riddle, and V. C. Smith for the water and fluorine analyses under the direction of L. C. Peck; R. T. Okamura for the specific gravity determinations; and J. G. Moore for helpful discussion.

ANALYTICAL PROCEDURE AND EVALUATION

Sixty-two samples were analyzed for sulfur and chlorine by X-ray fluorescence using the techniques, equipment, and standards described in papers by Fabbi and Moore (1970), Moore and Fabbi (1971), and Fabbi and Espos (1972). Two pellets were analyzed for each element. The precision of the analyses is estimated to be ±0.0010 wt percent for both sulfur and chlorine. The estimated accuracy is ±0.0050 wt percent for sulfur and ±0.0020 wt percent for chlorine. Samples were analyzed for sulfur and chlorine in three batches at different times, and the results are consistent within and between batches.

Standard wet chemical analyses of 26 samples were made in the laboratories of the U.S. Geological Survey, using the methods of L. C. Peck (1964). The constituents pertinent to this study are given in table 1. Samples were submitted for analysis in four batches, for the most part in time-sequential order. Several specimens from early in the eruption were submitted in a late batch, however, and each batch contained samples of both vigorous and weak activity. Two analysts were

Table 1.—*Volatile content of completely analyzed Mauna Ulu pumice, spatter, and flow material*

[All values in weight percent. Except where noted, analyst is E. E. Engleman or V. C. Smith, U.S. Geological Survey, under the direction of L. C. Peck]

Field No.	H_2O+	H_2O-	Total H_2O	MgO	CO_2	[1] Cl	F	[1] S	Oxidation ratio[2]	Distance from Mauna Ulu (km)	Fountain height (m)	Date of activity
Vigorous fountaining												
DAS691-3	0.04	0.03	0.07	9.14	0.01	0.0106	0.04	0.0195	9.8	.....	40	May 24, 1969
693-2	.07	.00	.07	9.54	.02	.0085	.04	.017	11.0	.....	100	June 13, 1969
694-5	.06	.00	.06	10.72	.02	.0088	.03	.0165	12.0	.....	220	June 26, 1969
695-1	.04	.02	.06	12.18	.01	.0072	.03	.0155	10.3	.....	350	July 15, 1969
697-1	.04	.01	.05	13.72	.03	.0095	.04	.0165	10.4	.....	300	Aug. 6, 1969
698-1	.00	.03	.03	8.97	.02	.0087	.04	.016	12.6	.....	400	Aug. 22, 1969
699-1	.00	.03	.03	9.54	.02	.0093	.04	.021	15.9	.....	540	Sept. 6, 1969
6911-1	.01	.01	.02	9.00	.01	.0079	.04	.018	11.4	.....	300	Oct. 20, 1969
6912-5	.01	.00	.01	14.45	.01	.0079	.03	.014	10.2	.....	390	Dec. 30, 1969
Weak fountaining												
DAS6956-5	0.02	0.00	0.02	9.08	0.02	0.0079	0.04	0.0125	9.4	.....	<10	July 29, 1969
6978-9	.05	.01	.06	9.10	.02	.0082	.04	.0115	9.1	.....	<10	Aug. 18–19, 1969
691112-38	.05	.01	.06	10.87	.01	.0087	.04	.0215	9.7	.....	<10	Dec. 6, 1969
691112-56	.05	.00	.05	8.82	.01	.0082	.04	.011	8.8	.....	<10	Dec. 29, 1969
701213-2	.03	.02	.05	8.54	.01	.0075	.04	.014	8.8	.....	<10	Jan. 25, 1970
701213-35	.02	.03	.05	10.01	.02	.0066	.03	.013	8.4	.....	<10	May 20–21, 1970
701213-41	.04	.01	.05	9.57	.01	.0068	.04	.018	8.4	.....	<10	May 24, 1970
701213-62	.08	.01	.09	12.02	.02	.0057	.03	.0145	8.9	.....	<10	July 9, 1970
701213-83	.07	.02	.09	10.92	.02	.0061	.03	.0125	8.8	.....	<10	Sept. 3, 1970
701213-115	.05	.02	.07	11.54	.02	.0085	.03	.013	9.3	.....	<10	Dec. 5, 1970
711213-126	.07	.01	.08	11.37	.02	.0093	.03	.013	7.6	.....	<10	Feb. 13, 1971
Lava flows[3]												
DAS711213-127	0.05	0.00	0.05	11.33	0.04	0.0065	0.03	0.012	9.0	0.4	....	Feb. 15, 1971
711213-131A	.06	.03	.09	10.69	.02	.0061	.04	.011	9.5	5.8	....	Apr. 7, 1971
711213-134	.02	.00	.02	8.14	.02	.0061	.03	.0095	10.2	10.0	....	Apr. 12, 1971
711213-134A	.03	.03	.06	11.21	.02	.0051	.03	.0095	9.7	10.0	....	Apr. 12, 1971
711213-136	.03	.03	.06	10.33	.02	.0062	.03	.0065	9.4	12.0	....	Apr. 19, 1971
711213-137	.01	.02	.03	11.96	.01	.0155	.03	.0075	8.9	12.0	....	Apr. 19, 1971

[1] X-ray fluorescence duplicate determinations of Cl and total S by B. P. Fabbi.

[2] $\frac{0.9Fe_2O_3 \times 100}{0.9Fe_2O_3 + FeO}$.

[3] Collected while liquid from flowing lava, except for sample DAS711213-137, which was collected underwater by R. L. Phillips.

also involved, and comparison of all data shows no evidence of analytical bias or drift in the results.

The estimated precision of the MgO analyses is ±0.05 wt percent or better (Wright, 1971, p. 6). Analytical precisions for the volatiles are not known. Water is notoriously difficult to determine with precision by the modified Penfield method; we believe, however, that when a set of water analyses shows distinct trends, these analyses can be reasonably interpreted as reliable. If the trends shown by the water analyses in this paper are valid and are straight-line functions, then the analytical precision for water can be estimated to be about ±0.02 wt percent.

In addition to possible analytical imprecision, the interpretation of water analyses is made difficult by the largely arbitrary division into H_2O+ and H_2O- at 110°C. Most petrologists assume that all H_2O- is contaminant and use only H_2O+ in their studies. Our samples analyzed for water were generally collected while still hot, and always before any rain fell on them. Most of them, however, were stored in a moderately humid environment for weeks to months before analysis. The true value for magmatic water in each sample is probably somewhere between the reported amounts of H_2O+ and total water.

LOSS OF VOLATILES AND OXIDATION DURING FOUNTAINING

Type of eruption

Twelve episodes of vigorous fountaining took place at Mauna Ulu, a new lava shield on Kilauea's east rift, between May 24 and December 30, 1969 (Swanson and others, 1971). Nine of these episodes featured lava fountains 100 m or more high; the maximum measured height was 540 m. Fountains of the other three episodes were 20 to 50 m high.

Beginning in July 1969, weak eruptive activity often took place between the fountaining episodes. This activity usually involved no more than a cyclic rise and fall of the lava column within the main vent, but at times the column reached the lip of the vent and spilled out on the ground surface as flows. Spattering 10 m or less in height sometimes accompanied this weak activity.

Samples

Samples of pumice from the high, vigorous fountains and spatter from the low, weak activity are the basis of the present study (table 1). These samples were, with few exceptions, collected while still warm and before rain fell. All the pumice samples were erupted during, or close to, the time of maximum fountain height. The fountain heights assigned to pumice samples in table 1 are subject to perhaps a 25-percent error because of difficulties in defining the top of a fountain and knowing the trajectory of the pumice fragments. The relative heights are considered reliable.

Most of the lava erupted in high fountains fell to the ground around the vent while still molten, gathered into a pool, and flowed away from the vent area. Only a comparatively small volume of the lava that reached the top of the fountain (itself only a small part of the total volume of erupted lava) was actually blown away as pumice fragments, most of which fell to the ground within 1 km of the vent. Such pumice fragments constitute the samples of high fountains studied in this paper. Typically, this pumice was too hot to touch when it landed but cooled within several minutes to ambient temperature.

Pumice fragments produced by the high fountains are very frothy. Some pieces are incompletely enclosed by a thin, glassy skin similar to that described and pictured by Friedman (1967). Spatter formed during weak activity is less vesicular than the pumice but still has a bulk specific gravity of less than 1. Vesicles are generally larger in the pumice than in the spatter. The larger vesicles and greater vesicularity of the pumice provide visual evidence that it degassed more completely than the spatter, and this conclusion is supported by the volatile contents.

Volatile loss

Compositions of most Kilauea lava with MgO greater than 6.8 percent, including the 1969–71 Mauna Ulu lava (Hawaiian Volcano Observatory, unpub. data), are largely controlled by the content of olivine and hence show straight-line variation when plotted on MgO variation diagrams (Powers, 1955; Wright, 1971; Wright and Fiske, 1971). Constituents not incorporated into olivine, such as volatiles, increase systematically as MgO decreases, if this relation has not been disturbed by other processes. The variation of water and sulfur with MgO, as plotted on figure 1, is not systematic, and chlorine follows a similar pattern. From this we conclude that processes other than simple olivine control have strongly influenced the volatile content.

In order to eliminate the effects of olivine control and facilitate comparison of the data, we have adjusted the analyses to an MgO value of 8 percent, using olivine control lines shown in the variation diagram, and an unpublished control line for chlorine. Each control line was drawn through the scatter of data in the diagram (fig. 1) and projects to 0 percent of the volatile constituent at Fo_{85} (about 45 percent MgO). A more precise method entails drawing a separate control line through each point and determining the appropriate adjustment for that point. As comparison of the two methods shows virtually no difference in the adjusted values, the simpler method was used. The adjusted volatile percentages (fig. 2) are all slightly higher than the unadjusted values but show similar variation trends.

One of the most critical processes affecting the volatile content is high fountaining, as indicated by the inverse relation between fountain heights of 40 m or more and content of water and, to a lesser degree, sulfur (fig. 2). Pumice erupted from low fountains during episodes of vigorous activity (filled

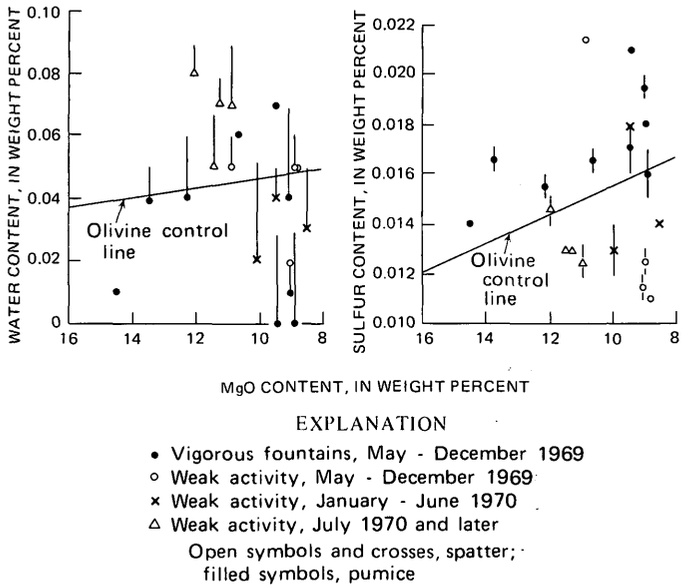

Figure 1.–Relation of water and sulfur to MgO. Symbol for water represents H_2O+, and end of line represents total water. Lines through sulfur symbols are error bars. Olivine control lines project to 0 percent water and sulfur at an olivine composition of Fo_{85}.

circles in fig. 2) contains about 0.07 wt percent total water and 0.020 percent sulfur, whereas that from high fountains contains 0.03 percent or less total water and about 0.016 percent sulfur. (Spatter erupted during weak activity, discussed below, does not follow this trend.) Except for the sample from the highest fountain (sample DAS699-1 in table 1), the inverse variation is reasonably systematic and seemingly above analytical error. We interpret this relation to indicate degassing during fountaining, high fountains allowing more time for degassing than the low ones. Chlorine may decrease from about 0.011 to 0.0085 percent with increased fountain height, but this trend is poorly defined (fig. 2).

The comparatively high content of sulfur and chlorine (checked by reanalysis) in the sample from the highest fountain cannot be adequately explained. The sample differs texturally from all others, as it is reticulite, or thread-lace scoria (Wentworth and Macdonald, 1954, p. 78), a variety of highly vesicular pumice commonly thought to form during exceptionally gassy eruptions. Accordingly, the preeruption contents of sulfur and chlorine may have been unusually high. Alternatively, the reticulite may have provided adsorption traps for sulfur and chlorine present in the fume cloud, either as gases or liquid droplets (Cadle and Frank, 1968).

The volatile content correlates with the type of eruptive activity. Most 1969 spatter samples erupted during weak activity between periods of vigorous fountaining contain less total water and sulfur and possibly less chlorine than do pumice samples from the lowest of the vigorous fountains (fig. 2). One sample[1] (DAS691112-38 in table 1) is a marked

[1] Close examination of this sample shows trace amounts of a sublimate coating many surfaces; this sublimate may be a contaminant in the analysis, explaining the high sulfur value.

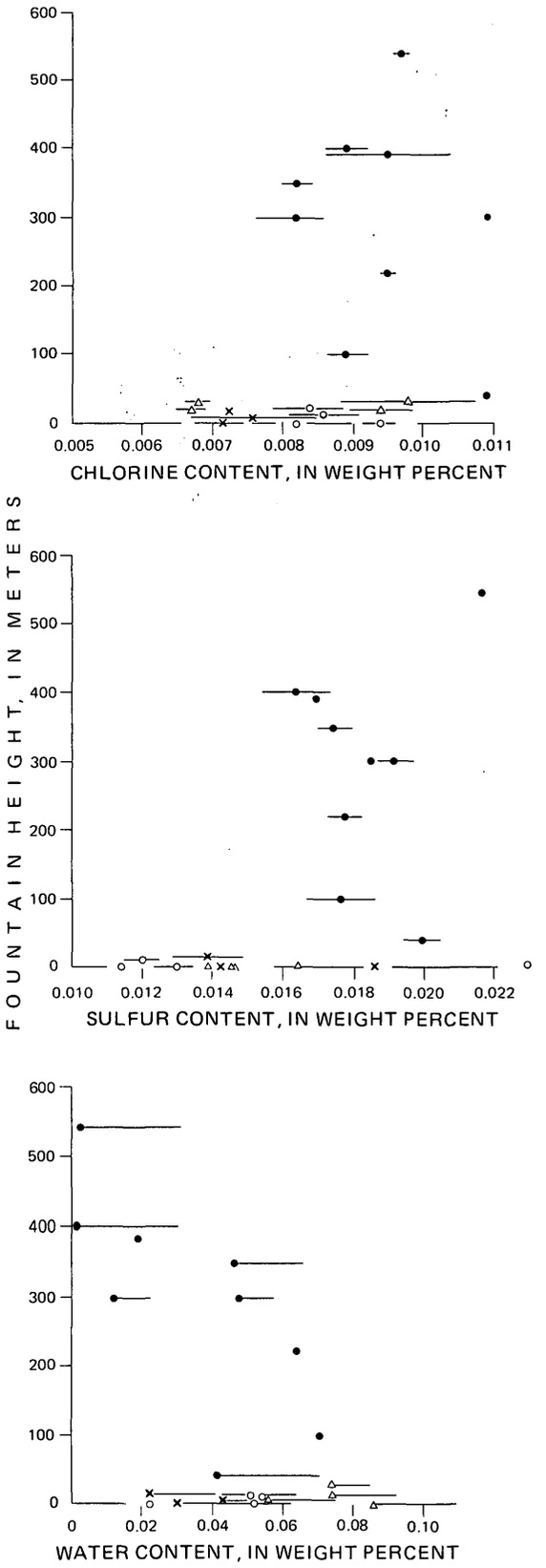

Figure 2.–Relation of water, sulfur, and chlorine to fountain height. Plotted values are adjusted for olivine control. Symbols are the same as in figure 1. Spatter samples plotted at fountain heights of less than 40 m on this and subsequent figures were actually erupted to heights of 10 m or less.

exception for it contains more sulfur than any other analyzed sample; otherwise the relation is quite clear. No other systematic chemical difference (except the degree of oxidation, as described in the next section) was noted between the pumice and spatter samples. The data suggest that the magma contained more dissolved volatiles just before high fountaining than just before weak activity, and this greater volatile content may have been instrumental in driving the fountains to greater heights. If this interpretation is correct, then the preeruption volatile content of the 1969 magma was not strictly constant, and this may account for some of the scatter in figure 2.

Available analyses (table 1) of CO_2 and fluorine show no systematic variations related to fountain height or mode of eruption. The precision of analytical techniques used for their determination probably was not sufficient to detect the small changes expected.

It could be argued that the inverse relation between fountain height and water content can be interpreted as a temporal variation in composition, for magma erupted prior to August 6 contained more water than that erupted between August 22 and December 30 (table 1). This interpretation, however, fails to explain why the three highest fountains of the eruption were produced after August 6, that is, during the time that hypothetically "dry" magma was being erupted. Also, the water content of spatter from weak activity was less before August 6 than after—a relation opposite to that of the high fountaining.

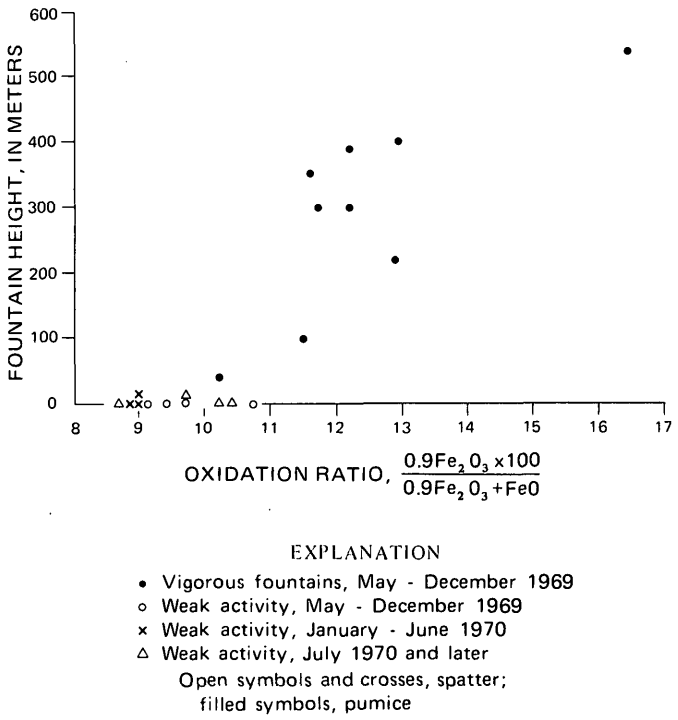

Figure 3.—Relation of oxidation ratio to fountain height. The ratios are adjusted for olivine control, assuming a ratio of 0.9 for olivine and intergrown spinel.

Oxidation

The degree of oxidation of Mauna Ulu pumice and spatter shows a positive correlation with fountain height. The data plotted in figure 3, adjusted for olivine control assuming an oxidation ratio, $\frac{0.9Fe_2O_3 \times 100}{0.9Fe_2O_3 + FeO}$, of 0.9 for combined olivine and spinel (T. L. Wright, written commun., 1972), indicate that pumice from vigorous fountains has an oxidation ratio of 10.4 or more, whereas all other samples except two have ratios of 10.4 or less. Some of the oxidation probably occurred during high-temperature exposure to air, so it is greater in pumice from high fountains.

The average oxidation ratio of the 11 analyses of spatter from weak activity is about 9.5 and may be a reliable value for the 1969–71 Mauna Ulu parent magma under near-surface conditions and adjusted for olivine control.

Change in water content with time

Spatter erupted during the period January through June 1970 contains about the same amount of water as spatter erupted during weak activity in 1969 (table 1; fig. 2). Spatter erupted in July 1970 and later contains more water (about 0.08 as compared with 0.05 wt percent total water). Wet chemical analyses (Hawaiian Volcano Observatory, unpub. data) indicate that several small but significant changes in major-element chemistry other than those caused by olivine control took place sequentially during the eruption, the largest in early July 1970, precisely when the water content also increased. It appears that the new batch of magma differed from that erupted earlier in water content as well as in major oxides. No change in sulfur or chlorine was detected at this time.

Comparison with the 1959 eruption

Friedman (1967) studied the water content of pumice erupted during the 1959 eruption in Kilauea Iki pit crater at Kilauea. He found an overall dependence of water content on the amount of olivine present (olivine control) but recognized deviations that he ascribed to concentration of volatiles at the top of a magma column.

Water content of Kilauea Iki pumice was plotted in relation to approximate fountain heights, which were extrapolated from data in Richter and others (1970) using the time of collection and times and heights of fountains (fig. 4). All the data have been corrected for olivine control (Murata and Richter, 1966; Wright, 1973). The water analyses are in two sets, those using the modified Penfield method (Peck, 1964) and published by Murata and Richter (1966, table 1) and those using a technique involving reaction of H_2O+ vapor with uranium metal by Friedman (1967). The two sets of analyses disagree as to absolute amount, most likely because of the difference in analytical techniques. Both sets, however, show a trend of lower water content with increased fountain height.

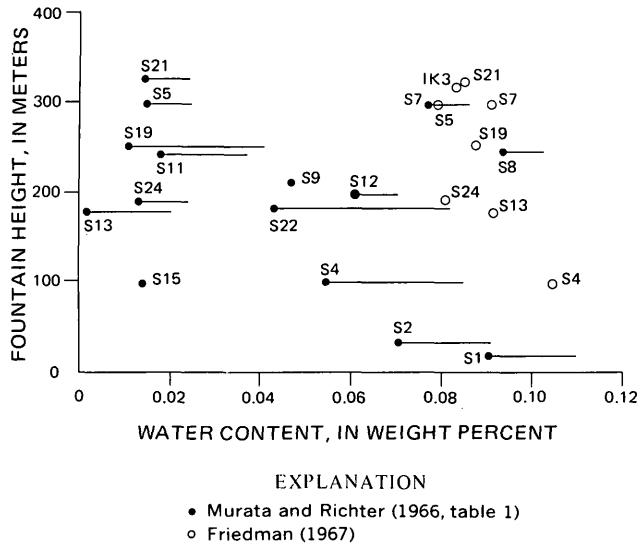

Figure 4.—Relation of water content to fountain height for pumice samples from the 1959 Kilauea eruption. Plotted values are adjusted for olivine control. Symbols for H_2O+ and total water are the same as in figure 1. Sample numbers are those given in Friedman (1967) and Murata and Richter (1966, table 1).

Friedman (1967) considered pumice of the eruption's first phase (Nov. 17–20, 1959) to contain water in amounts greater than predicted from strict olivine control, although only one analysis (S-4) deviated significantly from the olivine control line. He reasonably suggested that this concentration of water was caused by diffusion toward the top of the magma column before the eruption began. The plot of water in relation to fountain height (fig. 4) shows that S-4 was erupted from the lowest fountain of any sampled by Friedman (1967) and so had the best chance of retaining its original water content, whether or not enriched in the parent magma through diffusion. In view of the small number of samples available and the complex controls exerted by olivine content, fountain height, and possible water enrichment before eruption, we feel that no firm conclusions can be drawn concerning the cause of variation in water content of the 1959 pumice.

LOSS OF VOLATILES AND OXIDATION DURING FLOWAGE

Samples

Glassy samples were collected at regular intervals along a complex pahoehoe lava flow erupted in 1971. The flow advanced from Mauna Ulu to the ocean, 12 km to the south. It was chiefly fed through lava tubes (Peterson and Swanson, 1973), which allowed the moving lava to remain hot while permitting continuous degassing. Optical pyrometer measurements indicate that the lava cooled less than 15°C during transport in the tubes, indicating that the degassing took place under nearly isothermal conditions. Swanson gives further information on this complex lava flow in another paper (1973).

All analyzed samples listed in table 2 and plotted in figures 5–7 are of lava erupted between February and May 1971, chiefly during March and April when the flow was most active. Petrographic observations and several major-element chemical analyses suggest that the parent lava remained chemically uniform during the period of collecting.

Six samples of molten lava were obtained by dipping a metal sampling device (usually a rock hammer or a small bucket) into the flowing river free of surface crust. Each sample was quickly withdrawn and quenched in air. Lava collected in this way solidified in a few seconds but did not cool to ambient temperature for several tens of minutes unless broken into small pieces. Complete chemical analyses of five of these

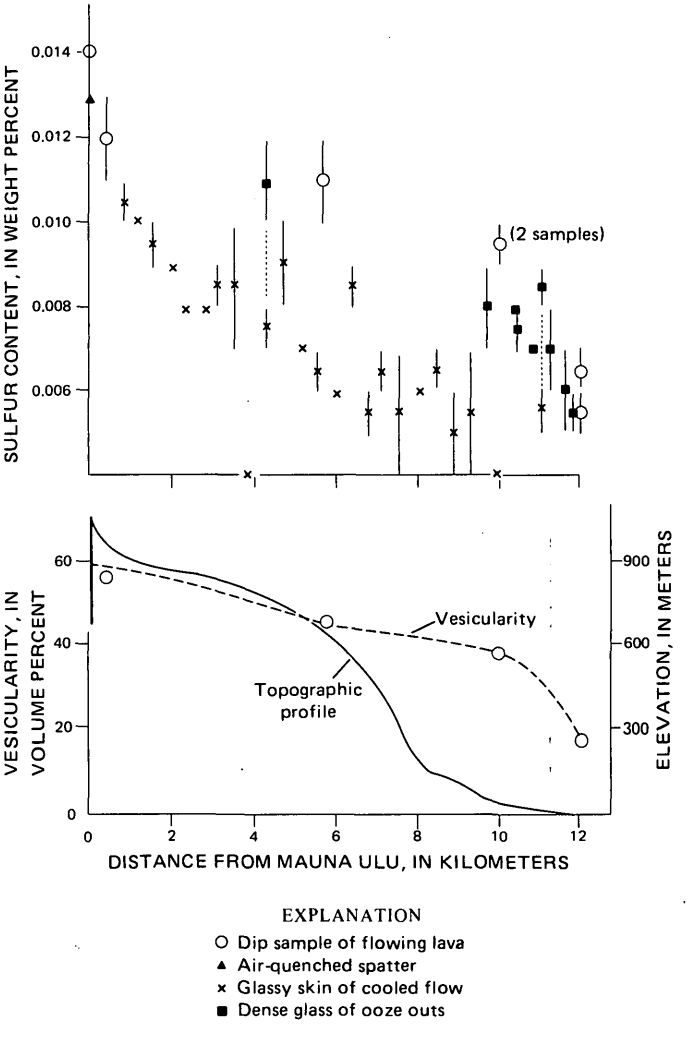

Figure 5.—Relations of sulfur content to distance of flowage, topography, and vesicularity. Lines through sulfur symbols are error bars. Dotted lines connect paired samples 10-10a and 28-28a. Heavy bar between 45- and 70-percent vesicularity indicates range of measured values for spatter. Other vesicularity values were determined on the same samples of dipped melt analyzed for sulfur and chlorine.

Table 2.—*Sulfur, chlorine, and water content of flow material from Mauna Ulu*

[X-ray fluorescence analyses of sulfur and chlorine by B. P. Fabbi. Water analyses by V. C. Smith and E. L. Brandt. All values in weight percent]

Field No.	Sulfur[1]	Chlorine[1]	H_2O+	H_2O-	Type of sample	Distance from vent (km)
DAS711213-126	0.013	0.0093	0.07	0.01	Spatter	0
711213-129	.014	.0061	....	....	Dipped from vent	0
711213-127	.012	.0065	.05	.00	Dipped from flow	.4
1	.0105	.0087	....	....	Glassy skin	.8
2	.010	.0085	....	....	.....do.....	1.2
3	.0095	.0084	....	....	.....do.....	1.5
4	.009	.0081	.00	.00	.....do.....	1.9
5	.008	.0075	....	....	.....do.....	2.3
6	.008	.0074	....	....	.....do.....	2.8
7	.0085	.0067	....	....	.....do.....	3.2
8	.0085	.0062	....	....	.....do.....	3.6
9	<.004	.0060	....	....	.....do.....	4.0
10	.0075	.0062	.03	.00	.....do.....	4.3
10a	.011	.0064	.04	.00	Dense ooze	4.3
11	.009	.0057	....	....	Glassy skin	4.8
12	.007	.0062	....	....	.....do.....	5.2
13	.0065	.0061	....	....	.....do.....	5.6
DAS711213-131A	.011	.0061	.06	.03	Dipped from flow	5.8
14	.006	.0058	....	....	Glassy skin	6.0
15	.0085	.0057	....	....	.....do.....	6.4
16	.0055	.0065	.03	.00	.....do.....	6.8
17	.0065	.0063	....	....	.....do.....	7.1
18	.0055	.0068	....	....	.....do.....	7.6
19	.0060	.0065	....	....	.....do.....	8.0
20	.0065	.0068	.00	.00	.....do.....	8.5
21	.005	.0064	....	....	.....do.....	8.9
22	.0055	.0064	....	....	.....do.....	9.4
23	.008	.0061	....	....	Dense ooze	9.8
24	.004	.0055	....	....	Glassy skin	10.0
DAS711213-134	.0095	.0061	.02	.00	Dipped from flow	10.0
711213-134A	.0095	.0051	.03	.03	.....do.....	10.0
25	.008	.0063	....	....	Dense ooze	10.4
26	.0075	.0056	....	....	.....do.....	10.5
27	.007	.0059	....	....	.....do.....	10.8
28	.0055	.0055	....	....	Glassy skin	11.1
28a	.0085	.0061	....	....	Dense ooze	11.1
29	.007	.0068	....	....	.....do.....	11.3
30	.006	.0061	....	....	.....do.....	11.7
31	.0055	.0062	....	....	.....do.....	11.8
DAS711213-135	.0055	.0053	....	....	Dipped from flow	12.0
711213-136	.0065	.0062	.03	.03	.....do.....	12.0
[2]711213-137	.0075	.0155	.01	.02	Sampled under water	12.0

[1] Average of two determinations on separate pellets.
[2] Not plotted in figures 5 and 6.

samples and of numerous similar samples show no evidence of contamination from the sampler used, except for an oxidized film adjacent to the metal. Some degassing must have taken place during the period of quenching but is thought to have been minor because of the short time involved and the high viscosity of the solidifying lava.

Nine samples are of relatively dense, glassy ooze outs less than 30 cm thick. These ooze outs did not extend farther than a few meters from their point of emergence on the ground surface, usually a crack in a tumulus or the thin roof of a small lava tube. The glassiness, thinness, and small volume of the ooze outs indicate that they must have cooled very rapidly, and the comparatively small number of vesicles suggests that little degassing could have taken place during the rapid cooling.

Twenty-four samples of the chilled glassy skin on solidified and cooled flow units 1 m or more thick were analyzed. This skin, less than 2 mm thick, is so highly vesicular and flaky that winds tend to strip it from the flow in a few days. Special care was taken to avoid collecting skin next to one of the numerous small cracks along which sulfurous deposits were forming. The skin probably cooled to ambient temperatures more slowly than the melt or ooze-out samples because of heat supplied from the body of the flow.

All flow samples contain 95 percent or more glass; most carry less than 2 percent phenocrysts, all olivine. Some samples near the coastline contain small plagioclase microlites in addition to the olivine phenocrysts, reflecting slightly cooler temperatures before quenching.

For comparison, a sample of spatter and one of melt dipped from the vent at Mauna Ulu are included in table 2 and shown on figures 5–7.

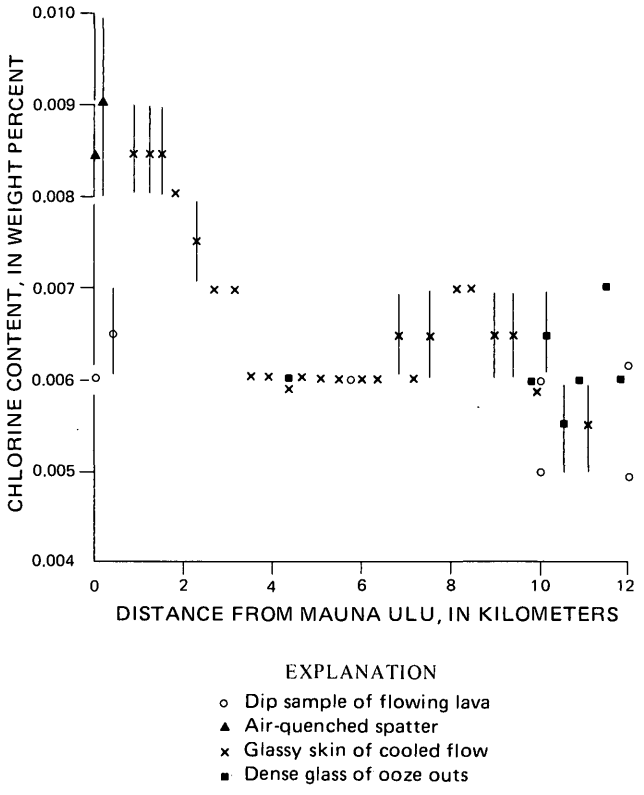

Figure 6.—Relation of chlorine content to distance of flowage. Lines through symbols are error bars.

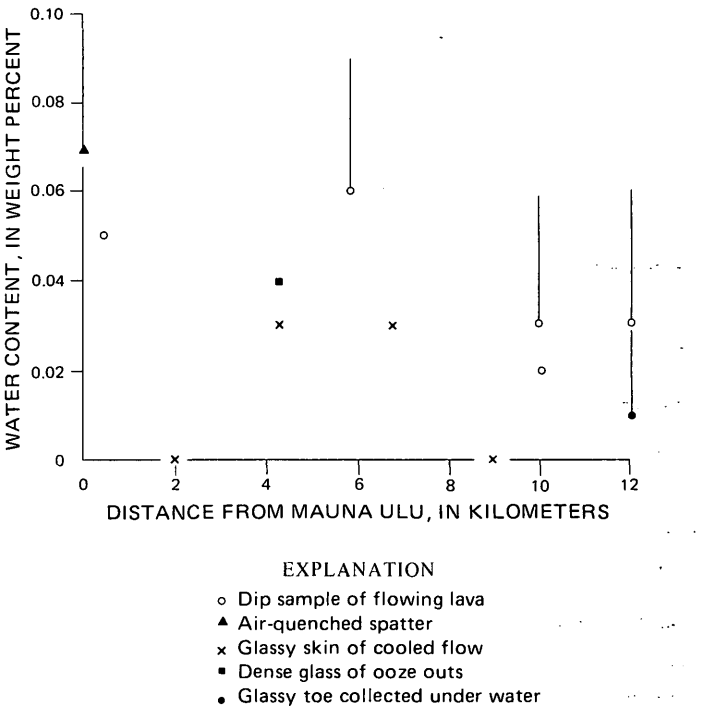

Figure 7.—Relation of water content to distance of flowage. Symbol indicates H_2O+; end of line indicates total water.

Sulfur

Sulfur is lost during flowage, as shown by the data in table 2 and figure 5. Considering only the samples of dipped melt and the air-quenched spatter—the most reliable samples—we note that about 60 percent of the sulfur originally in the lava at the vent was lost during flowage of 12 km. The average rate of loss for the first 10 km of flowage is about 0.001 percent per hour, using an average velocity of flowage of 2.5 km/hr estimated by observation through skylights in the lava tubes. The rate of loss for the last 2 km is not known, for the ground surface flattened greatly (fig. 5) and the lava spread laterally in a complex braided network of tubes where its velocity could not be adequately estimated. The flow velocity must have been considerably slower than for the preceding 10 km, however, because of the much gentler gradient, and this decreased velocity probably accounts for the abrupt loss of sulfur between 10 and 12 km. It seems likely that the rate of sulfur loss remained roughly constant throughout the duration of flowage.

Most of the dense ooze-out samples contain slightly less sulfur than predicted from the melt samples alone, suggesting a small amount of degassing during cooling.

Nearly all samples of glassy skin contain less sulfur than the melt or ooze-out samples collected at the same distance from Mauna Ulu (fig. 5), for the slower cooling of the skin allows more time for degassing. At the calculated rate of 0.001 percent per hour, this degassing must have continued for more than 2 to 4 hours after solidification of the skin, as the skin contains about 0.002 to 0.004 wt percent less sulfur than equivalent melt samples and the rate of degassing would decrease with cooling. Evidence of such prolonged degassing was always present in the field, for walking across a flow only a few hours old was made unpleasant by the SO_2 fumes being evolved.

Two paired sets of samples (10-10a and 28-28a) demonstrate clearly the relation between the sulfur content of skins and ooze outs (table 2; fig. 5). The skins contain 0.0035 and 0.003 wt percent, respectively, less sulfur than the neighboring ooze-outs.

The specific gravities of the samples dipped from melt and of four samples of spatter were determined and converted to percentage vesicularity by use of the curve in Peck, Wright, and Moore (1966, fig. 7, p. 642). A curve through the vesicularity data (fig. 5) has a shape similar to that of the sulfur-loss curve defined by the dip or ooze-out samples.

Chlorine

The amount of chlorine decreases away from the vent less markedly than sulfur (table 2; fig. 6). Melt samples suggest only a slight loss of chlorine, but skin samples show a steady decline in the first 4 km of flowage. Beyond 4 km, the

chlorine content is virtually constant at about 0.006 wt percent and perhaps indicates the residual amount of chlorine that can remain trapped in the silicate framework of the melt. In this regard, none of the 141 samples of Hawaiian lavas analyzed by Iwasaki and Katsura (1964) contain less than 0.006 wt percent total chlorine.

The high chlorine content of samples between 7.5 and 9.5 km from Mauna Ulu may reflect contamination by wet sea breezes, for mist commonly hangs over this area during stormy periods involving south winds.

Other volatiles

Samples of dipped melt and air-quenched spatter suggest a loss of water of about 0.03–0.04 wt percent during flowage of 12 km (fig. 7). Samples of glassy skin show lower water contents consistent with prolonged cooling and degassing. The plotted data are not adjusted for olivine control, because MgO was not analyzed for all samples.

The one sample of lava quenched under several meters of sea water contains no more water than adjacent subaerial samples, suggesting that little if any hydration took place during high-temperature contact of lava and water. Chlorine and possibly sulfur are, however, higher than in nearby subaerial samples (table 2) despite thorough washing in distilled water, suggesting contamination by sea water.

Fluorine and CO_2 (table 1) show no consistent trends.

Oxidation ratios

The oxidation ratios (table 1) of the dipped melt samples do not increase systematically with distance traveled. This conclusion is consistent with field observations, which suggest that little if any atmospheric air entered the tubes during flowage of lava through them. In fact, there was always a very strong outward rush of hot fume at skylights in the roofs of tubes. Further, combustible material thrown into lava in the tubes burned much more slowly than on the ground surface. The tubes apparently acted as high-temperature buffers that maintained an approximately equal degree of oxidation throughout the system.

DISCUSSION

This study suggests that water, sulfur, and chlorine are lost in a systematic, measurable way from basaltic lava during vigorous fountaining and flowage. It extends the work of Moore and Fabbi (1971) to surface processes; and their seven sulfur analyses of Hawaiian pumice, spatter, and subaerially erupted lava flows (1971, table 1, p. 121) are consistent with our conclusions.

Water is lost much faster during vigorous fountaining than during flowage, when about 0.01 wt percent per hour is lost. The rate of loss during fountaining is difficult to estimate precisely, owing to the quality of the data and uncertainties as to how long the pumice fragments from different fountain heights remained airborne. Accepting the data in figure 2 and assuming that typical pumice from high fountains effectively lost water for 15 minutes longer than that from low fountains (probably longer than reasonable), we find that the rate of loss during fountaining is about 0.2 wt percent per hour, 20 times that during flowage. The actual difference is probably greater.

The rates of sulfur loss during vigorous fountaining and flowage differ greatly. The rate of loss during flowage is about 0.001 wt percent per hour, whereas that during fountaining (assuming a 15 minute longer duration of gas loss) is about 0.016 wt percent per hour, 16 times that during flowage. Again, the actual difference is probably greater.

The marked reduction in confining pressure during eruption and the subsequent breakage of rapidly formed vesicles (Muenow, 1973) must account for the rapid loss of volatiles during fountaining. During the 1969–71 Mauna Ulu eruption, magma was apparently stored at depths of 1 to 3 km (Hawaiian Volcano Observatory, unpub. data), where, if saturated, it probably contained at least 0.5 wt percent water and 0.08 wt percent sulfur (Moore, 1970b; Moore and Fabbi, 1971). Within a few minutes, as judged by the interval between the onset of seismic tremor and initial eruptive activity, this magma surged upward and reached the surface, reducing the confining pressure by about 250 to 750 bars. During this rapid rise the magma lost about 0.4 wt percent water and 0.06 wt percent sulfur, roughly 80 percent of its original water and sulfur content. With high fountaining, about 0.05 wt percent water and 0.004 wt percent sulfur were lost in addition. With flowage after fountaining or immediately upon eruption, still more volatiles were lost. These values, though necessarily approximate, demonstrate the importance of the eruptive process in determining the volatile content of the solidified lava.

The measured amounts of volatiles lost during fountaining are probably maximum values for they were obtained from pumice fragments blown far from the fountains and consequently subjected to prolonged degassing. The pumice that fell directly to the base of the fountain, where it pooled before flowing away, had less time to degas, so the volatile content of quenched glass from a near-vent flow fed by such pumice would probably be somewhat higher than our measured values.

The ratio of water lost to sulfur lost, H_2O/S, was similar during fountaining and flowage, about 12.5 for fountaining and 10 for flowage. These values are about twice the 5.7 found by Moore and Fabbi (1971) for intratelluric degassing. This difference is reasonable, as sulfur is thought to be less soluble in basaltic magma than water at confining pressures of several hundred bars (Moore and Calk, 1971) and so would be lost more rapidly than water during the early high-pressure stage of vesiculation. The ratio H_2O/S of magmatic gases lost should therefore be higher for surface degassing than for intratelluric degassing.

Sigvaldason and Elísson (1968) found that the ratio of SO_2 to water and other volatile components in volcanic gases from

Surtsey increased with advanced degassing; consequently, the S/H_2O ratio left in the residual glass should decrease. Our samples do not show this, probably because most of their degassing was at high temperatures (1,150°C or more), whereas the Surtsey gases were collected from lava in the process of cooling and thus show temperature-dependent chemical variation.

The results of this study, like those on volcanic gas at Surtsey (Sigvaldason and Elísson, 1968; Árnason and Sigurgeirsson, 1968; Björnsson, 1968), demonstrate the need for great care in selecting samples for studies of volatile contents or degree of oxidation. The effect of surface processes on both degassing and oxidation can be large and rather unexpected. For example, pumice fragments from high fountains, a common type of material used in petrologic studies, are apt to be depleted in volatiles and more highly oxidized than spatter or dipped-melt samples obtained at the vent. On the other hand, the glassy skins of tube-fed pahoehoe may preserve original oxidation ratios despite long distances of travel, whereas surface flows may become more highly oxidized after flowing only short distances from the vent (Hawaiian Volcano Observatory, unpub. data). In general, spatter at the vent would be expected to preserve original volatiles and degree of oxidation better than any other type of material.

The data for demonstrating degassing during flowage show far better internal consistency than those from the fountains. This may well reflect critical differences in the two environments. Flowage through lava tubes takes place nearly isothermally and with minimal, if any, oxidation. Fountaining, especially that higher than a few meters, involves highly oxidizing and variable thermal conditions and rapid transient effects. Aside from single samples of fountain pumice being questionable representatives of such physiochemical disequilibrium, the differences in tube versus fountain environments may cause fundamental differences in patterns of degassing, involving rates, reactions, secondary effects, and other parameters. These possibilities can best be resolved by careful sampling of high fountains, a very difficult and dangerous task.

The pattern of volatile loss, especially sulfur, with longer distance of flowage should characterize all lava flows and may be an important tool in locating source areas and inferring the direction of advance of prehistoric flows. For such a study, care should be taken to compare only those samples whose posteruption histories are similar.

REFERENCES CITED

Arnason, Bragi, and Sigurgeirsson, Thorbjörn, 1968, Deuterium content of water vapour and hydrogen in volcanic gas at Surtsey, Iceland: Geochim. et Cosmochim. Acta, v. 32, p. 807–813.

Björnsson, Sveinbjörn, 1968, Radon and water in volcanic gas at Surtsey, Iceland: Geochim. et Cosmochim. Acta, v. 32, p. 815–821.

Cadle, R. D., and Frank, E. R., 1968, Particles in the fume from the 1967 Kilauea eruption: Jour. Geophys. Research, v. 73, p. 4780–4783.

Fabbi, B. P., and Espos, L. F., 1972, X-ray fluorescence determination of chlorine in standard silicate rocks: Appl. Spectroscopy, v. 26, p. 293–295.

Fabbi, B. P., and Moore, W. J., 1970, Rapid X-ray fluorescence determination of sulfur in mineralized rocks from the Bingham mining district, Utah: Appl. Spectroscopy, v. 24, p. 426–428.

Friedman, Irving, 1967, Water and deuterium in pumice from the 1959–60 eruption of Kilauea Volcano, Hawaii, *in* Geological Survey Research 1967: U.S. Geol. Survey Prof. Paper 575-B, p. B120–B127.

Iwasaki, Bunji, and Katsura, Takashi, 1964, The chlorine content of Hawaiian lavas: Chem. Soc. Japan. Bull., v. 37, p. 1827–1833.

Jones, J. G., 1969, Pillow lavas as depth indicators: Am. Jour. Sci., v. 267, p. 181–195.

Moore, J. G., 1970a, Pillow lava in a historic lava flow from Hualalai Volcano, Hawaii: Jour. Geology, v. 78, p. 239–243.

——1970b, Water content of basalt erupted on the ocean floor: Contr. Mineralogy and Petrology, v. 28, p. 272–279.

Moore, J. G., and Calk, L., 1971, Sulfide spherules in vesicles of dredged pillow basalt: Am. Mineralogist, v. 56, p. 476–488.

Moore, J. G., and Fabbi, B. P., 1971, An estimate of the juvenile sulfur content of basalt: Contr. Mineralogy and Petrology, v. 33, p. 118–127.

Muenow, D. W., 1973, High temperature mass spectrometric gas-release studies of Hawaiian volcanic glass—Pele's Tears: Geochim. et Cosmochim. Acta, v. 37, no. 6, p. 1551–1561.

Murata, K. J., and Richter, D. H., 1966, Chemistry of the lavas of the 1959–60 eruption of Kilauea Volcano, Hawaii: U.S. Geol. Survey Prof. Paper 537-A, 26 p.

Peck, D. L., Wright, T. L., and Moore, J. G., 1966, Crystallization of tholeiitic basalt in Alae lava lake, Hawaii: Bull. Volcanol., v. 29, p. 629–656.

Peck, L. C., 1964, Systematic analysis of silicates: U.S. Geol. Survey Bull. 1170, 89 p.

Peterson, D. W., and Swanson, D. A., 1973, Observed formation of lava tubes during 1970–71 at Kilauea Volcano, Hawaii: Studies in Speleology, v. 2, pt. 6. (In press.)

Powers, H. A., 1955, Composition and origin of basaltic magma of the Hawaiian Islands: Geochim. et Cosmochim. Acta, v. 7, p. 77–107.

Richter, D. H., Eaton, J. P., Murata, K. J., Ault, W. U., and Krivoy, H. L., 1970, Chronological narrative of the 1959–60 eruption of Kilauea Volcano, Hawaii: U.S. Geol. Survey Prof. Paper 537-E, 73 p.

Sigvaldason, G. E., and Elísson, Gunnlaugur, 1968, Collection and analysis of volcanic gases at Surtsey, Iceland: Geochim. et Cosmochim. Acta, v. 32, p. 797–805.

Swanson, D. A., 1973, Pahoehoe flows from the 1969–1971 Mauna Ulu eruption, Kilauea Volcano, Hawaii: Geol. Soc. America Bull., v. 84, p. 615–626.

Swanson, D. A., Jackson, D. B., Duffield, W. A., and Peterson, D. W., 1971, Mauna Ulu eruption, Kilauea Volcano: Geotimes, v. 16, p. 12–16.

Wentworth, C. K., and Macdonald, G. A., 1954, Structures and forms of basaltic rocks in Hawaii: U.S. Geol. Survey Bull. 994, 98 p.

Wright, T. L., 1971, Chemistry of Kilauea and Mauna Loa lava in space and time: U.S. Geol. Survey Prof. Paper 735, 40 p.

——1973, Magma mixing as illustrated by the 1959 eruption, Kilauea Volcano, Hawaii: Geol. Soc. American Bull., v. 84, p. 849–858.

Wright, T. L., and Fiske, R. S., 1971, Origin of the differentiated and hybrid lavas of Kilauea Volcano, Hawaii: Jour. Petrology, v. 12, p. 1–65.

Jour. Research U.S. Geol. Survey
Vol. 1, No. 6, Nov.-Dec. 1973, p. 659—663

RADIOELEMENT DISTRIBUTION IN THE BASEMENT COMPLEX OF THE YUKON-TANANA UPLAND, EIELSON DEEP TEST HOLE, ALASKA

By C. M. BUNKER, C. A. BUSH; and R. B. FORBES,
Denver, Colo.; College, Alaska

Abstract.—Uranium, thorium, and potassium contents were determined in 94 samples of drill cuttings from a 9,774-foot-deep exploratory hole drilled entirely in crystalline schists of the basement complex of the Yukon-Tanana Upland. The data indicate two distinctively different rock types and reflect differences in the calcite content of the rock. Zones of anomalously high concentrations of the radioelements probably reflect the effects of the emplacement of the nearby Eielson pluton.

The Eielson deep test hole is about 26 miles east-southeast of Fairbanks, Alaska, and about 8 miles northeast of Eielson Air Force Base (fig. 1). The hole was drilled 9,774 feet from a collar elevation of 1,350 feet above sea level. Cores were obtained at approximately 1,000-foot intervals, and cuttings were collected at 10-foot intervals. Reported here are analyses of the radioelements uranium, thorium, and potassium in 94 samples of the cuttings from 100-foot intervals except those between 2,200 and 2,800 feet, which were unavailable.

The hole is entirely within crystalline schists of the basement complex of the Yukon-Tanana Upland, and it provides an unusual opportunity for geologic and geophysical studies of the complex. Measurements of the radioelement concentrations are a part of a series of investigations using various data obtained from the drill hole (Lachenbruch and Bunker, 1971; Forbes and F. R. Weber, unpub. data).

The principal objective of the radioelement analyses was to determine the distribution of the radioelements and that of the associated radiogenic heat through a thick vertical section of schist. The heat production and averages of the radioelement concentrations were reported by Lachenbruch and Bunker (1971). An extensive report that is being prepared by Forbes and F. R. Weber on the geology of the area and the petrology of 11 drill-core samples from the deep test hole, plus two drill-core samples from two nearby preliminary test holes, provides a basis for examining some of the possible causes for variations in the vertical distribution of the radioelements and radiogenic heat.

GEOLOGY AND PETROLOGY

R. B. Forbes and F. R. Weber, during several geologic studies in the general area of the Eielson Air Force Base, examined and analyzed the drill cores recovered from the deep test hole and supplemented these data with less critical examinations of intervening chip samples. According to results of that work, the site of the deep test hole is in a northeast-trending belt of greenschist-facies rocks, which were believed by Mertie (1937) to be of pre-middle Ordovician age. On the basis of limited K-Ar age data, the metamorphism occurred about 140 m.y. ago (Forbes and Weber, unpub. data). Characteristic rock types in the area include calc-mica schist, calc-phyllites, greenschists, phyllitic schists, slates and fine-grained quartzites which appear to be metacherts or siltstones. Where unaffected by superimposed thermal metamorphism, outcrop mineral assemblages are characteristically those of the greenschist facies. The drill-hole site is located on calc-mica schist.

Two granitic plutons, which may be parts of a continuous mass in the subsurface, are present in the greenschist-facies belt. The contact of the Eielson pluton is about 2 miles southeast of the well site; that of the Tors pluton is about 16 miles northeast. Both plutons are surrounded by contact aureoles, as much as a mile wide, which contain rocks recrystallized under temperatures equivalent to those required to produce mineral assemblages of the hornblende or pyroxene hornfels facies. In some areas contact metamorphism was accompanied by pneumatolytic alteration.

The metamorphic mineral assemblages in the section cut by the drill hole indicate that metamorphic grade increases with depth. This increase apparently represents the transition from upper-greenschist facies to lower-amphibolite facies.

The rocks in the drill hole appear to be of sedimentary parentage, with the exception of carbonate-free quartz-poor biotite amphibolites which are more likely derived from the recrystallization of basic igneous rocks. The top 3,195 feet of the section is chiefly composed of calc-mica and calc-greenschists which represent recrystallized impure (argillace-

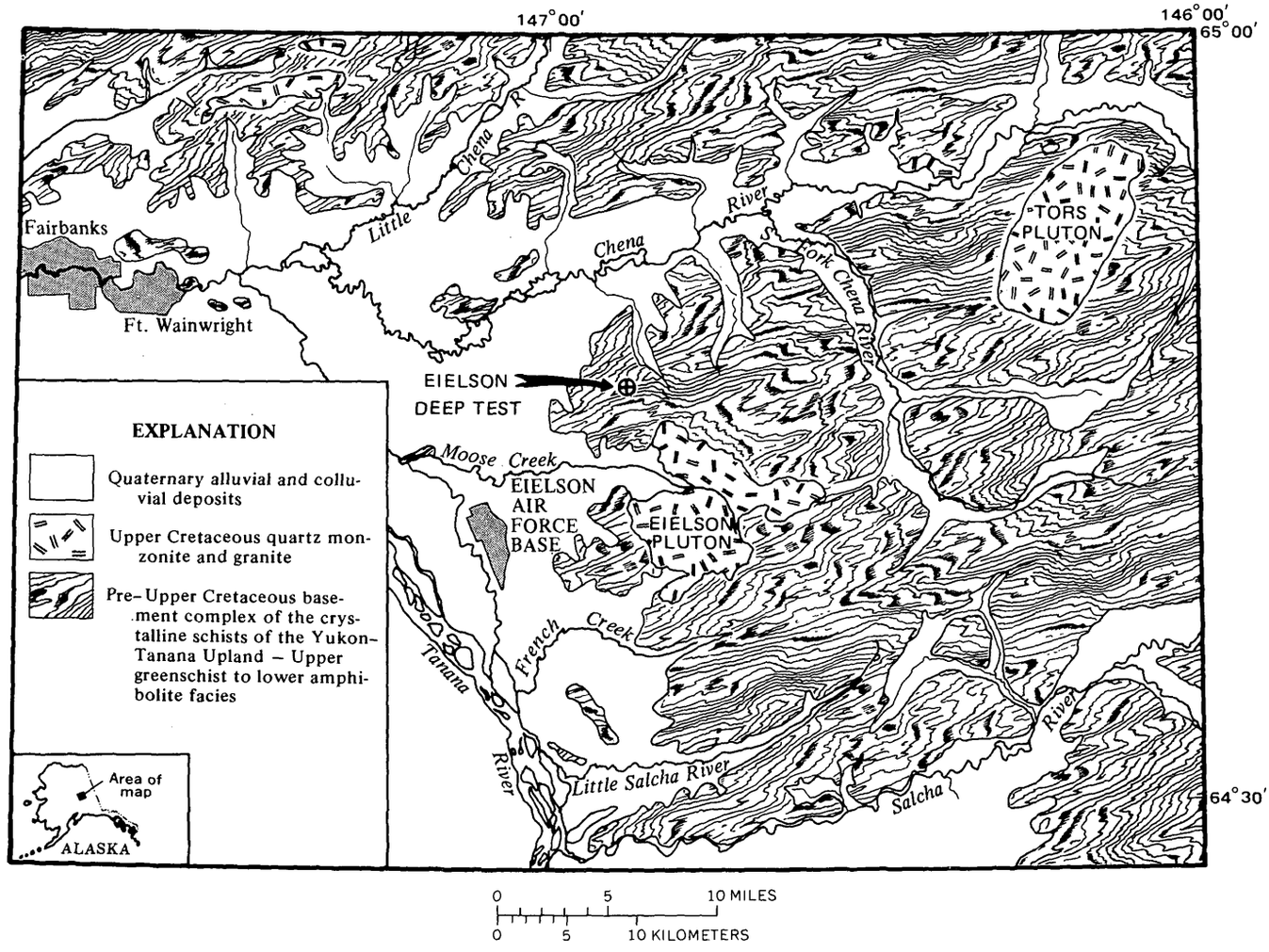

Figure 1.—Generalized geologic map of the Fairbanks district, Alaska, showing location of Eielson deep test hole.

ous) dolomitic limestones and marls. The interval from 4,065 to 9,198 feet contains both calc-magnesium and pelitic schists and sparse layers of micaceous quartzite. The deepest core (from 9,770 ft) is composed of actinolite-bearing calc-mica schists similar to those described from cores taken from the interval 3,193½ to 3,195½ feet.

ANALYTICAL METHOD

The concentrations of the radioelements in the samples were measured by gamma-ray spectrometry. The basic operational procedures and calibration techniques were described by Bunker and Bush (1966, 1967). The spectra were interpreted with the aid of a linear least-squares computer method which matches the spectrum from a sample to a library of radioelement standards and calculates the concentrations of the radioelements in the sample. The computer method is a modification of a program written by Schonfeld (1966).

Uranium concentrations are determined indirectly by measuring the radium daughters to obtain radium equivalent uranium (RaeU) values. Radium equivalent uranium is the amount of uranium, under the assumption of radioactive equilibrium, required to support the amount of daughter products that emit the radioactivity measured in a sample. Throughout the report where "U" and "uranium" are used "radium equivalent uranium" is implicit. Although thorium is also measured from daughter products, disequilibrium is improbable because of short half-lives; therefore, the concentrations are considered to be a direct measurement of parent thorium. Potassium is determined from its K^{40} constituent, which is proportional to the total potassium. The coefficients of variation for the accuracy of the data included in this report (table 1) are about 3 percent for uranium and thorium and 1 percent for potassium when compared to standards analyzed by isotope dilution and flame photometer methods.

RESULTS

The vertical distribution of the radioelement data (table 1, fig. 2) indicates two types of fairly homogeneous rock

Table 1.—*Radioelement concentrations and ratios, and calculated radiogenic heat determined from drill cuttings, Eielson deep test hole, Alaska*

Sample depth (feet)	U (ppm)	Th (ppm)	K (percent)	Heat (μcal/g-yr)	Th/U	U/K×10⁻⁴	Th/K×10⁻⁴
10–20	1.29	9.51	1.69	3.30	7.37	0.76	5.63
100–110	1.32	9.44	1.58	3.28	7.15	.84	5.97
200–210	1.67	10.83	1.67	3.84	6.49	1.00	6.49
300–310	1.79	9.68	1.77	3.72	5.41	1.01	5.47
400–410	2.18	10.93	2.14	4.36	5.01	1.02	5.11
500–510	1.52	8.89	1.57	3.31	5.85	.97	5.66
600–610	1.89	10.65	1.88	4.02	5.63	1.01	5.66
700–710	1.79	6.86	1.96	3.21	3.83	.91	3.50
800–810	2.77	8.47	1.26	4.06	3.06	2.20	6.72
900–910	1.51	10.17	1.96	3.67	6.74	.77	5.19
1,000–1,010	1.06	8.39	1.63	2.89	7.92	.65	5.15
1,310–1,320	1.98	11.61	1.83	4.26	5.86	1.08	6.34
1,400–1,410	1.62	10.97	2.00	3.92	6.77	.81	5.48
1,500–1,510	2.20	14.46	2.21	5.09	6.57	1.00	6.54
1,600–1,610	2.62	13.58	2.03	5.18	5.18	1.29	6.69
1,700–1,710	2.83	14.37	2.34	5.57	5.08	1.21	6.14
1,800–1,810	3.03	13.63	1.73	5.40	4.50	1.75	7.88
1,910–1,920	2.42	11.58	2.00	4.62	4.79	1.21	5.79
2,000–2,010	2.40	12.79	2.52	4.99	5.33	.95	5.08
2,100–2,110	3.61	15.27	2.14	6.27	4.23	1.69	7.14
2,200–2,210	2.02	12.92	1.64	4.50	6.40	1.23	7.88
2,800–2,810	2.07	11.92	2.11	4.46	5.76	.98	5.65
2,900–2,910	2.95	15.45	1.78	5.72	5.24	1.66	8.68
3,000–3,010	1.88	10.85	1.90	4.06	5.77	.99	5.71
3,100–3,110	1.53	4.82	1.29	2.43	3.15	1.19	3.74
3,200–3,210	1.51	6.09	1.30	2.67	4.03	1.16	4.68
3,300–3,310	2.78	12.15	1.99	5.00	4.37	1.40	6.11
3,400–3,410	2.77	12.80	2.01	5.12	4.62	1.38	6.37
3,500–3,510	4.22	16.59	2.62	7.11	3.93	1.61	6.33
3,600–3,610	3.10	13.74	2.19	5.60	4.43	1.42	6.27
3,710–3,720	2.70	14.40	2.01	5.39	5.33	1.34	7.16
3,800–3,810	2.94	14.12	2.40	5.62	4.80	1.22	5.88
3,900–3,910	2.63	13.02	2.20	5.12	4.95	1.20	5.92
4,000–4,010	3.17	13.61	2.57	5.73	4.29	1.23	5.30
4,100–4,110	3.98	38.08	1.62	10.96	9.57	2.46	23.51
4,200–4,210	2.69	11.39	1.43	4.63	4.23	1.88	7.97
4,300–4,310	2.83	12.65	2.04	5.15	4.47	1.39	6.20
4,400–4,410	3.08	14.20	1.87	5.59	4.61	1.65	7.59
4,500–4,510	3.60	17.10	2.48	6.72	4.75	1.45	6.90
4,600–4,610	4.83	20.37	3.55	8.56	4.22	1.36	5.74
4,700–4,710	4.24	13.88	3.02	6.69	3.27	1.40	4.60
4,800–4,810	4.81	19.71	3.14	8.30	4.10	1.53	6.28
4,900–4,910	5.73	23.71	3.77	9.94	4.14	1.52	6.29
5,000–5,010	5.37	21.95	4.19	9.44	4.09	1.28	5.24
5,100–5,110	4.54	18.79	3.73	8.08	4.14	1.22	5.04
5,200–5,210	3.43	15.93	2.82	6.45	4.64	1.22	5.65
5,300–5,310	3.84	16.76	3.06	6.98	4.36	1.25	5.48
5,400–5,410	4.16	18.51	3.34	7.64	4.45	1.25	5.54
5,500–5,510	3.82	16.97	3.66	7.17	4.44	1.04	4.64
5,510–5,520	4.30	17.87	3.45	7.64	4.16	1.25	5.18
5,520–5,530	4.81	20.03	3.62	8.49	4.16	1.33	5.53
5,530–5,540	4.14	18.16	3.10	7.49	4.39	1.34	5.86
5,600–5,610	4.32	18.49	3.06	7.68	4.28	1.41	6.04
5,700–5,710	3.84	17.14	3.00	7.04	4.46	1.28	5.71
5,800–5,810	4.73	18.76	2.97	8.01	3.97	1.59	6.32
5,900–5,910	2.91	12.92	2.50	5.38	4.44	1.16	5.17
6,000–6,010	3.11	14.31	2.72	5.87	4.60	1.14	5.26
6,100–6,110	4.39	17.45	2.93	7.49	3.97	1.50	5.96
6,200–6,210	1.89	9.65	1.72	3.77	5.11	1.10	5.61
6,300–6,310	2.85	16.24	2.16	5.91	5.70	1.32	7.52
6,400–6,410	3.04	16.97	2.26	6.22	5.58	1.35	7.51
6,500–6,510	3.46	13.05	2.93	5.93	3.77	1.18	4.45
6,600–6,610	2.57	10.65	1.86	4.51	4.14	1.38	5.73
6,700–6,710	3.52	16.25	2.75	6.56	4.62	1.28	5.91
6,800–6,810	2.80	15.77	2.75	5.94	5.63	1.02	5.73
6,900–6,910	3.00	14.41	2.59	5.77	4.80	1.16	5.56
7,000–7,010	3.09	15.09	2.32	5.90	4.88	1.33	6.50
7,100–7,110	3.47	16.44	2.93	6.61	4.74	1.18	5.61
7,200–7,210	2.89	12.70	2.20	5.24	4.39	1.31	5.77
7,300–7,310	1.62	7.19	1.10	2.92	4.44	1.47	6.54
7,400–7,410	3.39	14.61	2.45	6.06	4.31	1.38	5.96
7,500–7,510	4.30	17.10	2.33	7.19	3.98	1.85	7.34
7,600–7,610	3.79	16.52	2.41	6.72	4.36	1.57	6.85
7,700–7,710	4.29	20.37	2.99	8.01	4.75	1.43	6.81
7,800–7,810	3.68	17.75	2.92	7.02	4.82	1.26	6.08
7,900–7,910	2.35	11.88	2.10	4.66	5.06	1.12	5.66
8,000–8,010	2.84	12.90	2.54	5.34	4.54	1.12	5.08
8,100–8,110	2.73	14.44	2.62	5.59	5.29	1.04	5.51
8,200–8,210	2.68	14.89	2.21	5.53	5.56	1.21	6.74
8,300–8,310	2.85	13.86	2.57	5.55	4.86	1.11	5.39
8,400–8,410	2.76	13.03	2.24	5.23	4.72	1.23	5.82
8,500–8,510	3.15	14.13	2.48	5.80	4.49	1.27	5.70
8,600–8,610	3.30	16.73	2.78	6.51	5.07	1.19	6.03
8,700–8,710	2.71	13.48	2.33	5.30	4.97	1.16	5.79
8,800–8,810	2.95	14.69	2.55	5.78	4.98	1.16	5.76
8,900–8,910	4.49	18.38	2.75	7.70	4.09	1.63	6.68
9,000–9,010	3.90	16.17	3.40	7.00	4.15	1.15	4.76
9,100–9,110	3.98	19.00	3.20	7.57	4.77	1.24	5.94
9,200–9,210	3.66	16.88	3.08	6.88	4.61	1.19	5.48
9,300–9,310	4.26	17.87	3.03	7.50	4.19	1.41	5.90
9,400–9,410	3.51	15.66	2.78	6.44	4.46	1.26	5.63
9,500–9,510	3.23	14.99	2.39	6.00	4.64	1.35	6.28
9,600–9,610	3.71	13.94	2.12	6.07	3.76	1.75	6.58
9,700–9,710	4.89	15.95	2.54	7.45	3.26	1.93	6.28

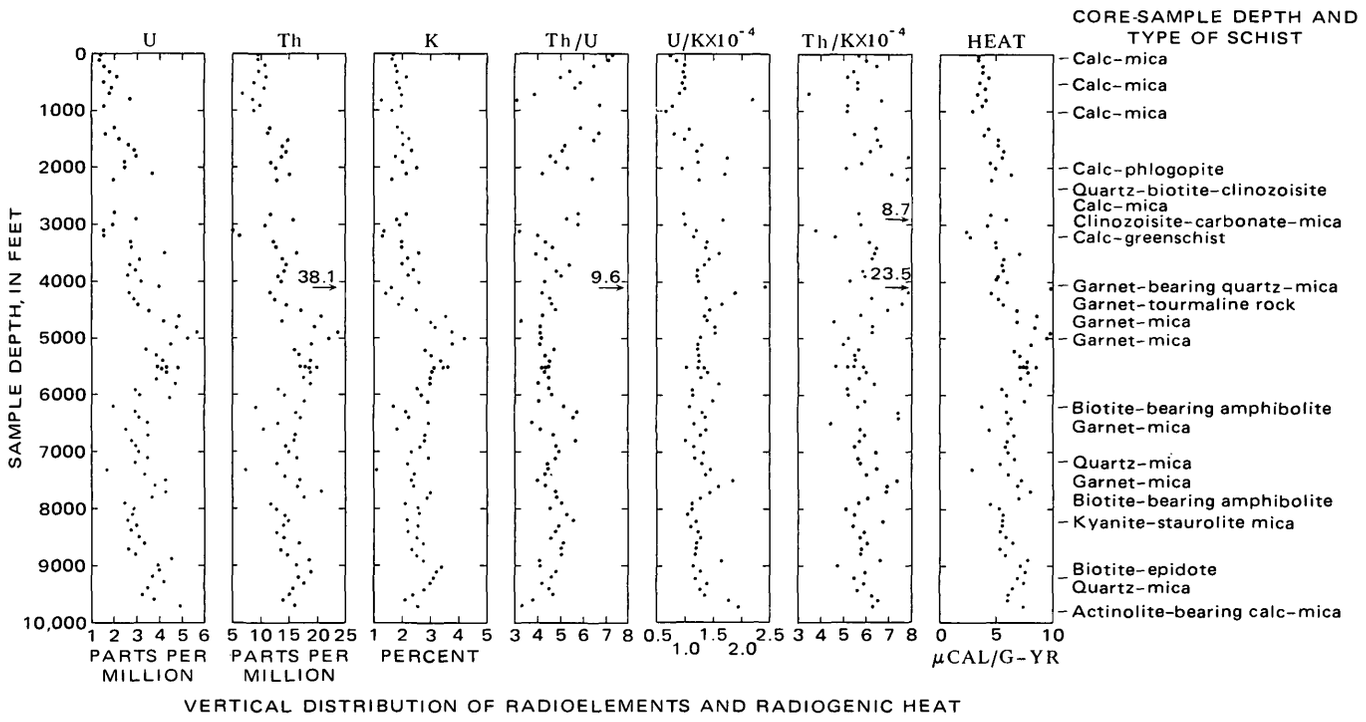

Figure 2.—Vertical distribution of radioelements and radiogenic heat, core-sample depths, and rock types.

separated at a depth of about 3,200 feet. The apparent differences observable on the vertical distribution plots are confirmed in histograms of the data (fig. 3). The data from the two rock types are also statistically different with 95-percent confidence (table 2). The averages of the radioelement concentrations may be abnormally high for both rock types because of the presence of enriched zones.

The calcic rocks, which are predominant above 3,200 feet, contain, in comparison to rocks lower in the section, significantly less uranium and slightly less thorium and potassium, and they have a lower uranium-potassium ratio. Within the calcic rocks, radioelement concentrations increase slightly at about the 1,400-foot depth, which may reflect the location of the contact between the calc-mica schist and the underlying thermally overprinted calc-phlogopite schist. Cores from depth intervals 3,193½–3,195½ and 9,766–9,770 feet are petrologically similar; however, the radioelement data do not reflect this similarity.

Zones of anomalously high concentrations of uranium, thorium, and potassium are present within the section. Parts of the entire section penetrated by the drill hole have probably been affected by thermal metamorphism and alteration associated with the emplacement of the nearby Eielson pluton, which resulted in the enrichment of radioelements to the affected parts of the section. Examples of the enriched zones are depth intervals 4,400–5,800, 7,400–7,800, and 8,900–9,500 feet. The section above 3,200 feet may also be affected by ground water moving through joint systems; the highly variable thorium-uranium ratios suggest differential mobilization of the radioelements and perhaps varying degrees of disequilibrium.

Table 2.—*Averages and standard deviations of data determined for two sections of the Eielson deep test hole*

	Averages and standard deviations[1]	
Section (depth interval, ft)	10–3,210	3,300–9,710
U (ppm)	2.06±0.62	3.52±0.52
Th (ppm)	10.93±2.74	15.96±3.97 (15.63±2.91)
K (percent)	1.84±0.31	2.64±0.58
Th/U	5.50±1.24	4.52±0.49
U/KX10⁻⁴	1.13±0.35 (1.09±0.28)	1.35±0.24 (1.33±0.20)
Th/KX10⁻⁴	5.92±1.17	5.88±0.72
Heat (μcal/g-yr)	4.18±0.98	6.47±1.40 (6.41±1.28)

[1] Values in parentheses exclude samples from depth intervals 800–810 and 4,100–4,110 ft inasmuch as values for those samples differed from the mean by more than three standard deviations.

REFERENCES CITED

Bunker, C. M., and Bush, C. A., 1966, Uranium, thorium, and radium analyses by gamma-ray spectrometry (0.184–0.352 million electron volts), *in* Geological Survey Research 1966: U.S. Geol. Survey Prof. Paper 550-B, p. B176–B181.

—— 1967, A comparison of potassium analyses by gamma-ray spectrometry and other techniques, *in* Geological Survey Research 1967: U.S. Geol. Survey Prof. Paper 575-B, p. B164–B169.

Lachenbruch, A. H., and Bunker, C. M., 1971, Vertical gradients of heat production in the continental crust–[Pt.] 2, Some estimates from bore-hole data: Jour. Geophys. Research, v. 76, no. 17, p. 3852–3860.

Mertie, J. B., Jr., 1937, The Yukon-Tanana region, Alaska: U.S. Geol. Survey Bull. 872, 276 p.

Schonfeld, Ernest, 1966, Alpha M–An improved computer program for determining radioisotopes by least-squares resolution of the gamma-ray spectra: U.S. Natl. Lab., Oak Ridge, Tenn. [Pub.] ORNL 3975, 42 p.

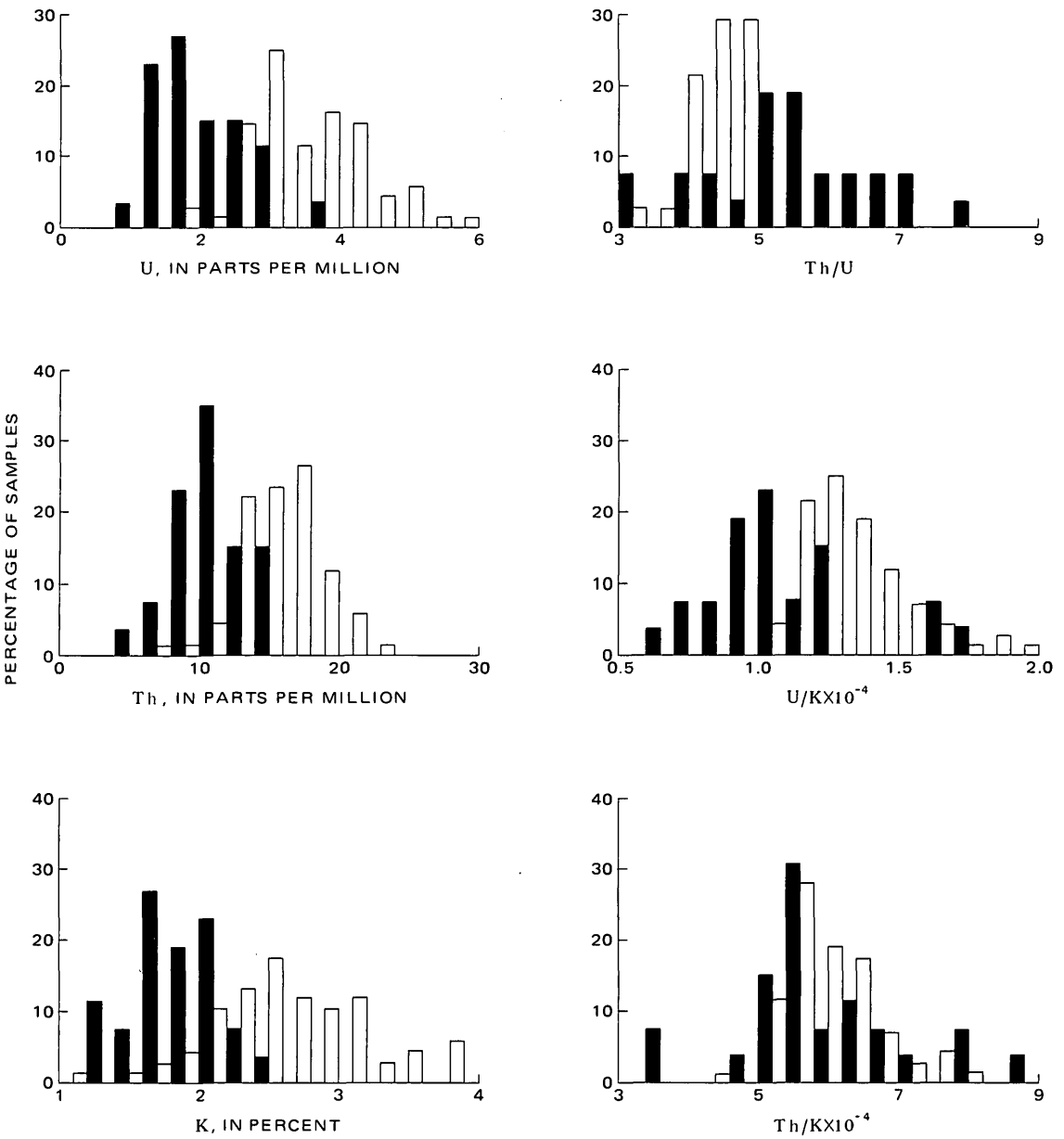

Figure 3.–Frequency distribution of radioelement data. Shaded bars are data from depth interval 10–3,210 feet (26 samples); open bars are from depth interval 3,300–9,710 feet (68 samples).

Jour. Research U.S. Geol. Survey
Vol. 1, No. 6 Nov.-Dec. 1973, p. 665–672

TWO-GARNET RODINGITE FROM AMADOR COUNTY, CALIFORNIA

By W. A. DUFFIELD and M. H. BEESON, Menlo Park, Calif.

Abstract.—Two distinct phases of garnet have been discovered in rodingite from Amador County, Calif. The two garnets are hydrogrossular and (hydro?)grossular-andradite. Only one, generally hydrogrossular, has been reported in rodingites studied by other workers. The rodingite of this study formed from a mafic dike with abundant euhedral plagioclase laths. The hydrogrossular is concentrated within the areas of these laths and is volumetrically about as abundant. The (hydro?)grossular-andradite is concentrated in the groundmass and as incursions into the plagioclase laths. The garnets apparently grew during one general episode of metasomatism, and their spatial distribution and compositions were controlled principally by the unequal distribution of iron and aluminum caused by the presence of plagioclase laths (and mafic minerals?) in the original unaltered dike.

Acknowledgment.—We thank R. G. Coleman and Edward G. Ghent for helpful reviews of the manuscript.

Rodingite of the type locality in New Zealand was reported by Marshall (1911) to consist of grossular and diallage, with or without minor prehnite. Hutton (1943), in a later study, showed that the grossular contained essential water in its formula and proposed a new mineral name, hydrogrossular. Subsequently, many workers (among them, Scott, 1951; Miles, 1950; Frankel, 1959; Bilgrami and Howie, 1960) reported hydrogrossular from rodingite and closely allied rocks.

Because rodingite commonly is extremely fine grained, the separation and study of its constituent minerals are difficult, and chemical analyses of hydrogrossular from such rocks are few. Characteristically, however, rodingite is reported to contain only one garnet—hydrogrossular (see all works cited above).

We have discovered rodingite that contains two garnets, hydrogrossular and (hydro?)grossular-andradite, in roughly equal abundance. All available evidence suggests that both garnets grew simultaneously in one general period of metasomatism and that their compositions simply reflect the unequal distribution of some major elements, principally iron and aluminum, in the original unaltered rock, a mafic dike with abundant plagioclase laths. The hydrogrossular preferentially grew at the sites of the laths.

It seems likely that similar two-garnet rodingite exists elsewhere and that the presence of more than one garnet in such rocks has been overlooked in earlier studies. The garnets of this study are so similar in appearance and properties that they cannot be distinguished in thin section. They were accidentally discovered from X-ray diffractometer analysis.

FIELD OCCURRENCE

Numerous outcrops of rodingite were discovered during a program of detailed mapping in the western foothills of the Sierra Nevada, Amador County, Calif. All lie within serpentinite masses. Most outcrops are concentrated in two relatively small areas (fig. 1), but a more thorough search within the zone of serpentinite probably would lead to more discoveries. The host serpentinite is part of a series of elongate ultramafic

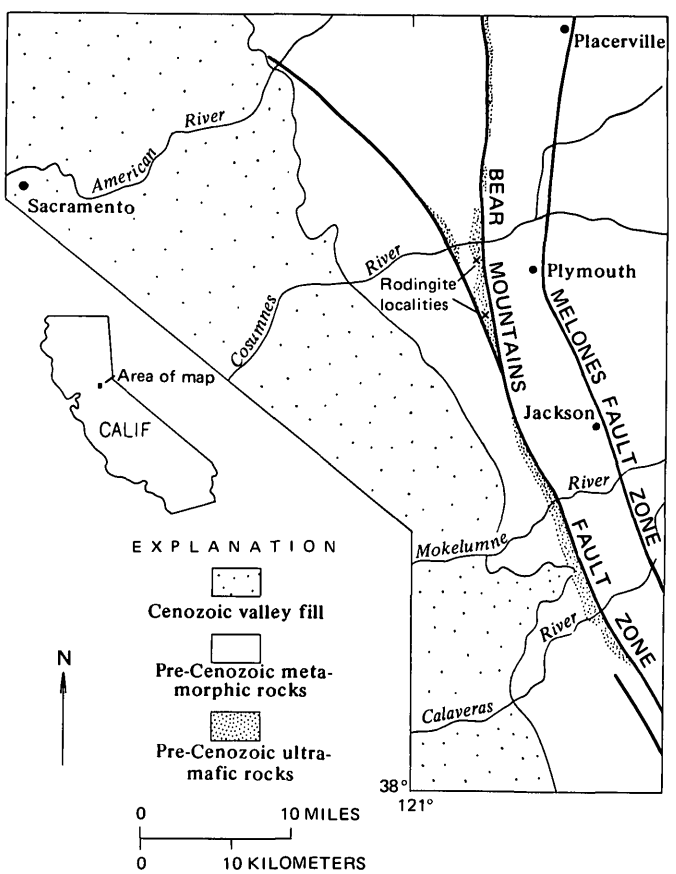

Figure 1.—Areas of ultramafic rocks (stippled) along the Bear Mountains fault zone and the two rodingite localities discussed in the text.

bodies that lie within the Bear Mountains fault zone of Clark (1960, 1964). More recent work by Duffield and Sharp (1973) indicates that the serpentinite is within a melange that possibly marks the locus of a Mesozoic subduction zone.

At both rodingite localities, the host serpentinite is pervasively sheared into pods that range in maximum diameter from several centimeters to nearly a meter. Rodingite occurs as similarly shaped bodies and as steeply dipping dikes. At the northern locality (fig. 1), a dike about 0.5 m thick is traceable along strike for several meters. The contacts of this dike are repeatedly offset several centimeters by a conjugate set of steeply dipping faults that roughly parallel shear planes in adjacent serpentinite. At the southern locality, a single dike is traceable along strike for about 35 m. The thickness there ranges from about 1 m to several centimeters; rare internal slickensided surfaces are evident, but the margins of the dike are not visibly offset. Scattered pods of rodingite, a few meters in maximum dimension, crop out at both localities; they are believed to be faulted fragments of formerly continuous dikes.

The time relations among shearing in serpentinite, emplacement of the dikes, and fault offsets on dikes are not well known, but the presence of isolated pods of rodingite and limited but clear evidence of faulting in the dikes suggest that a single period of pervasive shearing affected both rocks. Some dikes might have been preserved because they were stronger than the serpentinite within which they were enclosed.

We have studied samples of the dike at the southern locality, in the NE¼NW¼ sec. 29, T. 7 N., R. 10 E., about 60 m east of the prominent hilltop that is enclosed by the 820-foot contour on the U.S. Geological Survey topographic map of the Irish Hill 7½-minute quadrangle.

RODINGITE IN HAND SAMPLE AND IN THIN SECTION

In hand sample the rodingite is aphanitic and pale green, with a specific gravity of about 3.26 to 3.31 g/cm^3, averaging 3.30 g/cm^3. The texture of the original dike rock, although not always preserved, is often evident in thin section (figs. 2 and 3). The euhedral outlines of former plagioclase laths as much as 0.3 mm long are still clearly recognizable, and the original rock appears to have been about 50 percent plagioclase by volume. The outline of a single phenocryst of clinopyroxene(?) also has been identified (fig. 3), but judging from the several thin sections studied, such phenocrysts were rare in the original dike rock.

Original mafic dike mineralogy has been obscured by metamorphism. Scattered grains of clinopyroxene (diopside?), chlorite, and vesuvianite form about 10 percent of the rock; isotropic to weakly birefringent garnet accounts for the remaining 90 percent. The minor constituents form small grains (average about 0.1 mm in diameter) between the relict plagioclase laths. Extremely fine grained garnet replaces all plagioclase grains and a substantial amount of the groundmass.

Two distinct phases of garnet are present, although indistinguishable in thin section. Garnet is perfectly pseudomorphous

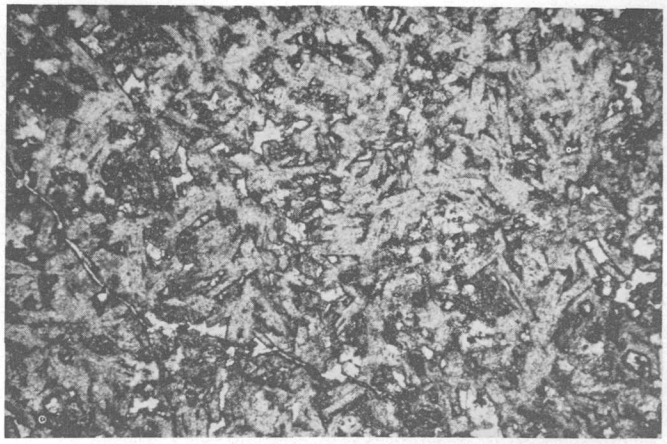

Figure 2.—Photomicrograph of rodingite showing the euhedral outlines of former plagioclase laths. Plane-polarized light.

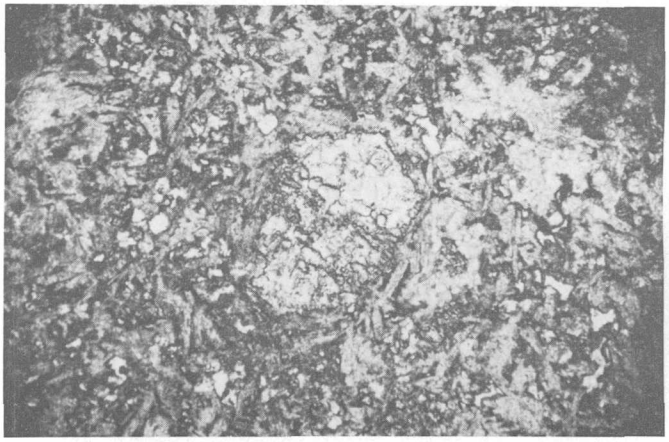

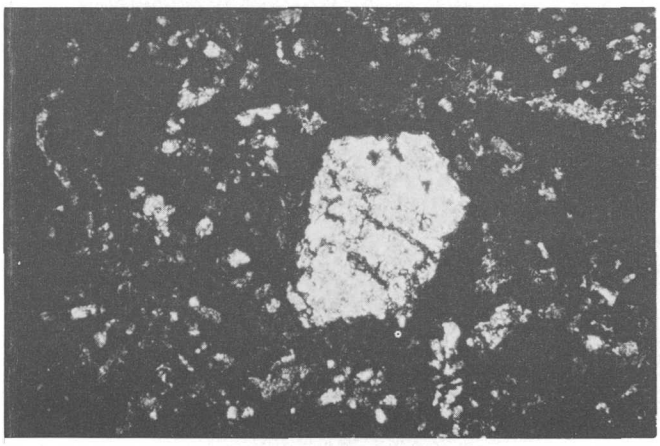

Figure 3.—Photomicrographs of rodingite showing a relict clinopyroxene(?) phenocryst. Note the euhedral outlines of former plagioclase laths. *A*, Plane-polarized light. *B*, Same view as *A*, with crossed nicols. Most of the phenocryst is replaced by chlorite.

after plagioclase laths with no evidence of its characteristic isometric crystal outline, and it forms anhedral masses in the groundmass. All garnet is turbid; the cores of relict plagioclase laths generally are relatively less turbid and tend to be slightly more birefringent than other areas of garnet, perhaps reflecting original compositional zoning in feldspar and original gross compositional contrasts between feldspar and groundmass. Microprobe analysis, discussed later, proves that one garnet phase is indeed concentrated in relict plagioclase laths and that the other is mostly in the groundmass.

METHODS OF STUDY

The presence of two distinct phases of garnet in the rodingite was discovered when X-ray diffractometer studies consistently showed closely spaced doublets for all garnet reflections (fig. 4). Attempts were then made to separate and purify mineral concentrates for further examination, but the extremely fine grain size and nearly identical properties of the two garnets partly frustrated these efforts. Chemical composition of the pure phases was estimated from comparison of chemical analyses of the mineral concentrates, and also from comparison of cell dimensions and refractive indices with determinative curves of Winchell and Winchell (1964). These results were checked by partial microprobe analysis, which also verified the suspected uneven distribution of the two garnets in the rock.

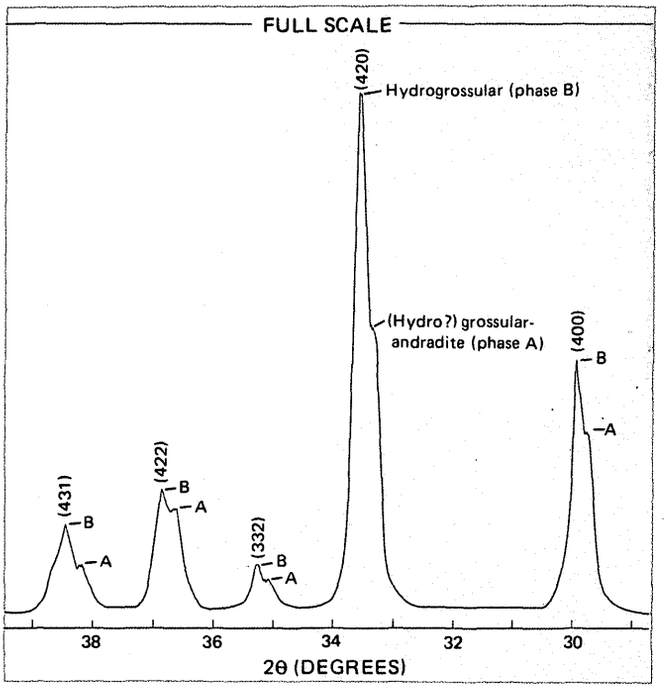

Figure 4.—Tracing of part of an X-ray diffractometer chart of garnets from the rodingite. Note that all reflections are paired and that those of phase A tend to show a slight broadening.

Mineral separation and refractive index

Standard techniques of mineral separation with heavy liquids and a Frantz magnetic separator were used to produce three mixtures (X, Y, and Z) containing different proportions of the garnets. Minerals other than garnet were easily removed from the whole-rock powder, but the two garnets were never successfully separated from one another. Best results were obtained with 320-mesh material that was elutriated to remove the finest dust.

The precise determination of refractive index was impeded by the turbid nature of the grains, but the approximate indices clearly reflect the different compositions of the two garnets and are useful in placing restraints on possible compositions for the pure phases. The refractive index of all grains is between 1.787 and 1.727. At intervals of 0.005 between these extremes, all samples studied contained some grains with indices greater than and some with indices less than all tested liquids, but this continuum was bimodal, with most indices about 1.775 and 1.740. These data suggest possible ranges in the compositions of the two phases, whereas the relatively sharp peaks characteristic of the X-ray diffraction patterns suggest the presence of two fixed compositions. The reason for this discrepancy is not known.

X-ray diffraction study

Several whole-rock powders were X-rayed to determine the size of the unit cell for each garnet. The major reflections are indexed, and unit-cell dimensions are reported in table 1.

Table 1.—*X-ray diffraction data for garnets*

[The conditions of X-ray diffraction were: Cu$K\alpha$ radiation, Ni filter, LiF internal standard. Relative intensities are in arbitrary chart units. The unit-cell edge, a_0, was determined by graphing one-half $\left(\frac{\cos^2\theta}{\sin\theta}+\frac{\cos^2\theta}{\theta}\right)$ versus a_0 for each reflection and projecting a least-squares fit to these data back to the a_0 axis (that is, $\theta = 90$)]

hkl	Phase A (hydro?)grossular-andradite)		Phase B (hydrogrossular)	
	d (A)	*I*	*d* (A)	*I*
400	3.001	63	2.983	48
420	2.683	100	2.667	100
332	2.557	13	2.543	9
422	2.451	35	2.436	24
510	2.353	17	2.338	16
521	2.190	13	2.178	13
611	1.947	17	1.934	18
444	.....	....	1.721	9
640	1.665	17	1.654	18
642	1.602	33	1.594	31
800	1.501	6	1.491	6
840	1.342	6	1.333	6
842	1.310	6	1.301	7
864	.....	....	1.107	5
1042	.....	....	1.089	3
880	.....	....	1.054	3
1222	.....	....	.967	2
a_0	A 12.01		B 11.92	

Splits of the three garnet concentrates, X, Y, and Z, were X-rayed to approximate the relative amounts of the two phases in each sample. Other parameters being equal, such an approximation should be possible by comparison of the heights of paired reflections on the diffractometer charts. That all reflections occur as closely spaced doublets (fig. 4) suggests that the two garnets are similar enough to make such a procedure reasonable. The results of comparing peak heights of the seven major reflections between 28° and 48° 2θ for the three mineral concentrates are given in table 2. Apparently, the most nearly pure sample (Z) is about 30 percent one garnet, hereafter called phase A, and 70 percent phase B. Concentrates X and Y consist of nearly the same proportions of the two phases.

The relative amounts of background radiation (table 2) suggest that phase A is relatively enriched in the source of such radiation. Under the conditions of the X-ray analysis used in this study (see table 2), iron is the most common constituent of silicate rocks that produces background radiation, and as shown in the next section, the mineral concentrate that contains the most phase A also contains the most iron.

Table 2.—*Peak-height analysis of garnet concentrates*

[The relative peak heights were assessed for the seven major reflections between 28° and 48° 2θ. Background radiation was compared from about 6° to 50° 2θ]

hkl	Ratio of peak heights $\left(\frac{\text{phase A}}{\text{phase B + phase A}}\right)$ of garnet concentrates		
	X	Y	Z
400	0.53	0.49	0.34
420	.40	.42	.29
332	.59	.47	.35
422	.54	.49	.33
510	.44	.51	.26
521	.51	.44	.27
611	.47	.44	.26
Average	.50	.47	.30
Standard deviation.	.060	.031	.036
Background radiation.	>Z;=Y	>Z	Least

A relative-peak-height analysis was also completed for X-rayed whole-rock samples and suggests that phase B is slightly more abundant than A, the ratio being about 6:4. This might have been surmised from the approximate modal percentage of relict plagioclase grains (see fig. 2) and the knowledge that one of the garnets appears to have preferentially replaced the feldspar laths. Thus the X-ray diffraction study suggests that an iron-poor garnet accounts for somewhat more than half of the whole rock and is preferentially concentrated in relict plagioclase laths.

Chemical analyses

Chemical analyses were run on one whole-rock sample and on the three garnet concentrates, by use of the rapid-rock-analysis methods of the U.S. Geological Survey (see table 3). The garnets are members of the grossular-andradite solid-solution series with minor amounts of other garnet molecules; one or both of the phases contains water in its formula. The analyses confirm the conclusions about relative iron contents drawn from X-ray diffraction. The sample with the lowest level of background radiation contains the least iron, and total iron varies directly with the amount of phase A in each sample (computed from relative peak heights). To a reasonable first approximation, the two garnets can be assigned to the grossular-$Ca_3Al_2O_6 \cdot 6H_2O$-andradite-$Ca_3Fe_2O_6 \cdot 6H_2O$ system.

Winchell and Winchell (1964, p. 493, fig. 388) presented graphs showing refractive index and length of unit-cell edge in relation to composition for this system. By fitting the unit-cell data and the extreme values of refractive index of this report to the graphs, the approximate limiting compositions of the two garnets can be determined: phase A—47.2 percent grossular, 41.8 andradite, 5.8 $Ca_3Al_2O_6 \cdot 6H_2O$, and 5.2 $Ca_3Fe_2O_6 \cdot 6H_2O$; phase B—86.4 percent grossular, 3.6 andradite, 9.6 $Ca_3Al_2O_6 \cdot 6H_2O$, and 0.4 $Ca_3Fe_2O_6 \cdot 6H_2O$ (all molecular percentages). These are expressed as weight percent of oxides in table 4 and are used to calculate the bulk composition of mixtures (by weight) that correspond to the three garnet concentrates, assuming the relative amounts of the two phases as determined by X-ray analysis.

It is immediately apparent that the garnet compositions calculated from refractive index and unit-cell size show more water (and correspondingly less SiO_2) than those determined by analysis and that the relative degree of hydration for the two phases is not the same as suggested by the laboratory analyses. Similarly, other constituents show some differences between the calculated analyses and the laboratory analyses, but in a gross way the agreement is fairly good. The source of the discrepancies is not known, but many undoubtedly are related to the presence in the analyzed garnets of elements other than those of the pure system assumed for the graphically derived compositions. Titanium, for instance, is known to increase the size of the unit cell when present in andradite (Deer and others, 1962). Magnesium, ferrous iron, and manganese, on the other hand, should tend to decrease the size of the unit cell. It is also possible that relations of the pure system, as depicted in graphs, are not precisely correct. In any event, the graphically derived compositions do suggest that the two minerals are indeed hydrogarnets, although the degree of hydration is not great; this conclusion is consistent with other data.

Microprobe analyses

To test further the accuracy of the indirectly derived compositions of the pure phases A and B, and to identify

Table 3.—*Chemical analyses of samples, in weight percent of oxides*

[Analyses by rapid methods (Shapiro and Brannock, 1956) supplemented by atomic absorption. Because of insufficient sample for a separate determination, H_2O+ in X and Z is assumed to be the loss of weight on ignition]

	1[a]	2[b]	50% phase A 50% phase B	47% phase A 53% phase B	30% phase A 70% phase B
			X	Y	Z
SiO_2	51.45	37.0	36.2	36.2	36.6
Al_2O_3	15.64	14.1	13.0	13.8	16.6
Fe_2O_3	3.91	7.9	11.6	9.9	7.1
FeO	7.93	1.1	.48	.64	.64
MgO	5.90	3.8	1.3	2.0	.57
CaO	9.11	32.1	34.5	34.1	36.2
Na_2O	3.13	.05	.00	.00	.02
K_2O	.98	.08	.05	.05	.03
H_2O+	.....	1.8	1.2	1.2	1.4
H_2O-	.....	.12	.....	.02	.....
TiO_2	1.48	1.0	1.4	1.4	.64
P_2O_5	.26	.20	.14	.19	.13
MnO	.21	.12	.14	.16	.13
CO_2	.....	<.05	.....	<.05	.....

[a]Analysis from Daly (1933). Represents a worldwide average for diabase, based on 90 analyses that are averaged and calculated water-free to total 100 percent.

[b]Analysis of a whole-rock sample of the rodingite of which X, Y, and Z are the three garnet concentrates; relative amounts of the two garnets as determined by the X-ray study.

Table 4.—*Chemical compositions of the garnets, in weight percent of oxides*

[Compositions for phases A and B are calculated from the molecular compositions read from the graphs of Winchell and Winchell (1964). The other three compositions are calculated by mixing phases A and B by the indicated weight percents; compare with analyses X, Y, and Z of table 3]

	Phase A	Phase B	50% phase A 50% phase B	47% phase A 53% phase B	30% phase A 70% phase B
SiO_2	34.2	36.4	35.3	35.4	35.7
Al_2O_3	11.5	22.0	16.8	16.9	18.9
Fe_2O_3	16.0	1.4	8.7	8.3	5.8
CaO	35.8	37.8	36.8	36.8	37.1
H_2O	2.5	2.4	2.5	2.5	2.5
	100.0	100.0	100.1	99.9	100.0

unambiguously any spatial segregation of the phases in the rock, several partial microprobe analyses were made on each garnet using an ARL EXM-SM electron microprobe and natural mineral standards. All data were corrected for drift, background, matrix absorption, characteristic fluorescence, and atomic number effects (Beeson, 1967; Beaman and Isasi, 1970). Quantitative analysis was difficult because of the small size of areas of uniform composition and the low visual contrast between the two garnets. Iron was monitored during all analytical runs as a convenient method of discriminating one garnet from the other; only those analyses that could be reasonably duplicated on different days and samples were retained, and these are summarized in figure 5. The range of microprobe-derived values for the pure phases shown on figure 5 probably is partly due to analytical error and partly to actual ranges in garnet compositions. For example, the data suggest, but do not prove, that the iron-rich garnet that locally occurs within relict plagioclase laths (fig. 6) may be slightly richer in iron and poorer in aluminum and titanium than that replacing glass of the groundmass. Minor broadening of some of the X-ray peaks (fig. 4) also suggests slightly different iron-rich garnets. The approximate composition of the garnet replacing glass in the groundmass (represented by G next to the composition bar in fig. 5) is invariably near the composition determined from cell-edge and index of refraction measurements.

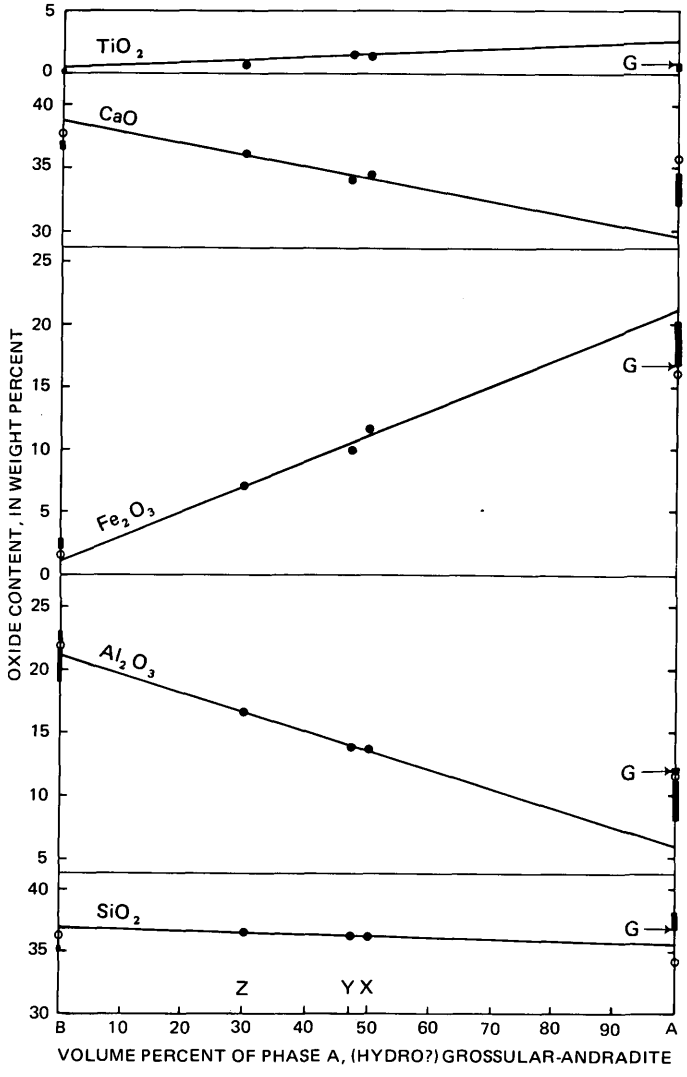

Figure 5.—A summary and comparison of the compositions of the two garnet phases as determined by: (1) fitting the length of cell edge and refractive indices to determinative curves (open circles); (2) extrapolating from the rapid-rock analyses of the three concentrates in which relative amounts of the two phases are known from peak-height studies (intersection of extrapolated lines with end-member lines); and (3) analyzing with a microprobe (range of compositions, shown by solid bars). Microprobe analyses of garnet after groundmass are indicated by G next to the bar, generally a value near that determined by cell edge and indices of refraction. The graph shows that agreement among the three methods is surprisingly good, considering that analysis of such a fine-grained material by these methods is admittedly imprecise.

Beam-scan photos (fig. 6) provide visual evidence that the iron-poor phase is indeed concentrated within relict plagioclase laths and the iron-rich phase in the groundmass; some areas of iron-rich garnet within the plagioclase laths may represent selective replacement of plagioclase cores, possibly controlled by initial zoning in the plagioclase or by fractures along cleavage directions.

SUMMARY

The approximate compositions of the two garnets have been estimated in three independent ways: (1) by fitting the unit-cell dimensions and refractive indices to determinative curves, (2) by projecting visual best-fit lines from the data points of the chemically analyzed two-garnet mineral concentrates X, Y, and Z to end-member compositions, and (3) by partial analysis with a microprobe.

Detailed comparison of the compositions determined by these three methods shows some large differences. We feel that the many difficulties of all types of analysis that we tried preclude selecting one of the three methods as best. Nonetheless, to a first approximation, all methods indicate the presence of grossular for one garnet and a member of the grossular-andradite series for the other garnet. The grossular also contains some water in its formula. The chemical data of table 3 also suggest, but do not prove, the presence of water in the other garnet. It seems likely, however, that both minerals are indeed hydrogarnets, for all evidence indicates that both formed simultaneously under the same conditions.

Structural relations in the field and textural relations in thin section indicate that the recrystallization of the original diabase dike to form rodingite occurred in a volume-for-volume manner. Otherwise, it seems unlikely that both the form of the dike and the diabasic texture would have been so perfectly preserved. It is also apparent, from a comparison of the chemical analyses of the rodingite and the average diabase of Daly (1933), that the original dike rock underwent considerable metasomatism (see table 3). As the exact composition of the unaltered rock is unknown, the details of these changes in bulk chemistry cannot be described, but silicon was clearly removed while calcium was added to the system. Total iron probably changed little, if any, but apparently much original ferrous iron was oxidized to the ferric state.

Other investigators (for example, Bilgrami and Howie, 1960; Coleman, 1967; Barnes and others, 1972) have concluded, on the basis of much more complete field and chemical data, that rodingites form from gabbroic to diabasic rocks contemporaneously with the serpentinization of enclosing or closely associated ultramafic plutons; calcium is freed from the ultramafic plutons as they are serpentinized and is then fixed primarily in hydrogrossular as the mafic rocks are altered to rodingite. This model is thought to apply to the present study; the general requirements for the serpentinization-rodingitization process are satisfied, and there are no known chemical, petrologic, structural, or other features to strain the conditions and explanations of the general model.

The presence of two garnets is unusual. Possibly, the two garnets reflect separate periods of metasomatism differing greatly in composition. This seems unlikely, however, as there is no evidence of metasomatic zoning in the dike. More likely, the dike was subjected to one general period of metasomatism, and the two garnets simply reflect the original distribution of some major elements in the unaltered rock. The relict

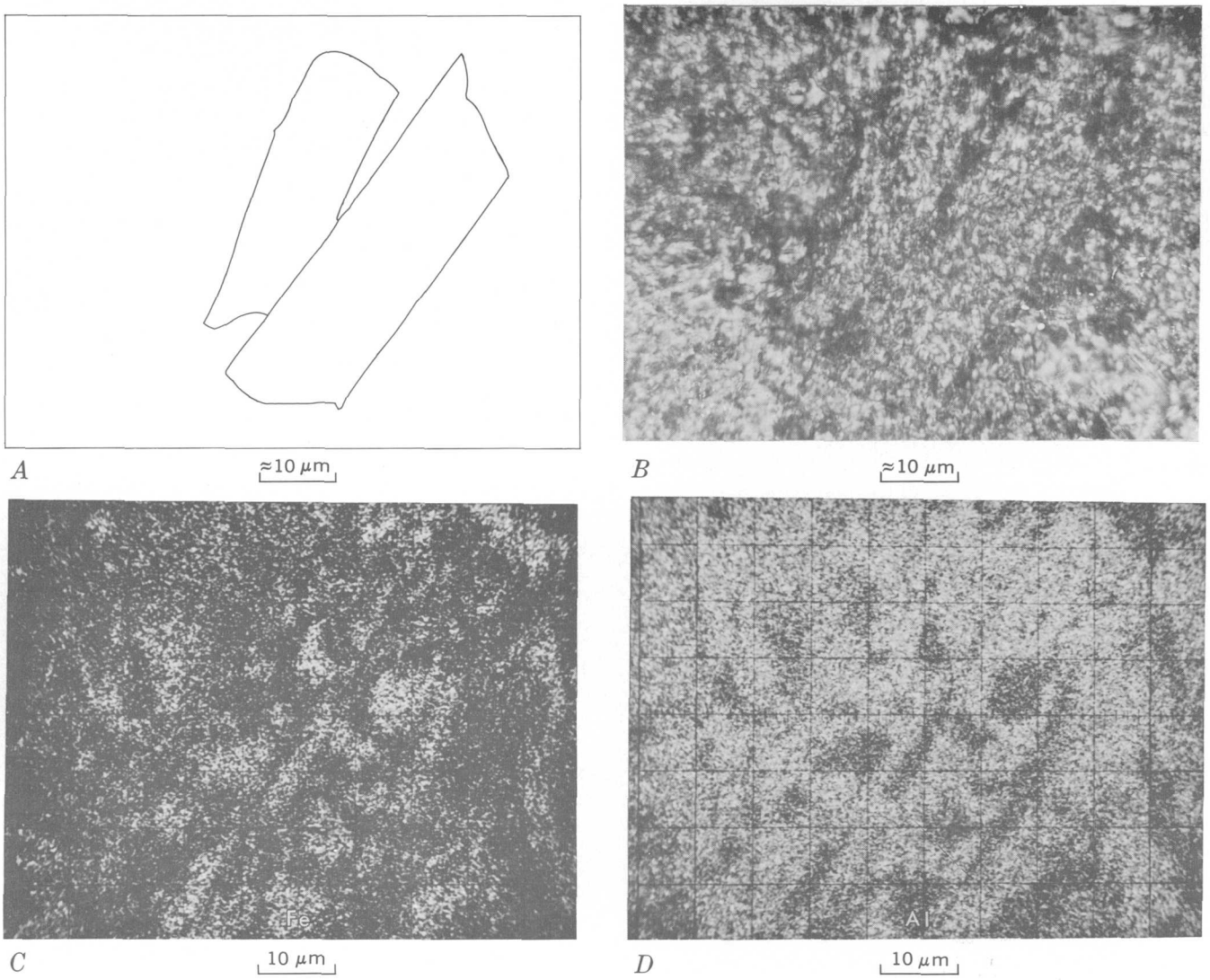

Figure 6.—Images of an area of garnet analyzed with the electron microprobe.

A. Sketch of two adjacent plagioclase laths pseudomorphed by garnet.

B. Photomicrograph of the plagioclase laths sketched in *A*. The laths contrast very little with the groundmass because both the plagioclase and the groundmass have been replaced by garnet.

C. Beam scan showing the iron distribution in approximately the area covered in *A* and *B*. Iron-rich garent occurs as patches within the plagioclase as well as in the groundmass and may reflect an initial zoning in the plagioclase. The outline of the relict plagioclase laths is therefore somewhat obscured in the beam-scan photographs.

D. Beam scan of same area shown in *C*, showing the distribution of aluminum that is antithetic to iron.

porphyritic texture described in an earlier section (see fig. 2) certainly suggests that iron in particular was unequally distributed in the original rock, and the sites where it was relatively depleted (plagioclase laths) are the prefered sites of the iron-poor hydrogarnet. We therefore suggest that the distribution of the two garnets was a direct result of the presence of plagioclase laths in the original rock and that a similar situation may be expected in other occurrences of rodingite that resulted from the metasomatism of plagioclase porphyry and perhaps many multimineralic precursor rocks.

REFERENCES CITED

Barnes, Ivan, Rapp, J. B., O'Neil, J. R., Sheppard, R. A., and Gude, A. J., III, 1972, Metamorphic assemblages and the direction of flow of metamorphic fluids in four instances of serpentinization: Contr. Mineralogy and Petrology, v. 35, p. 263–276.

Beaman, D. R., and Isasi, J. A., 1970, A critical examination of computer programs used in quantitative electron microprobe analysis: Anal. Chemistry, v. 42, no. 13, p. 1540–1568.

Beeson, M. H., 1967, A computer program for processing electron microprobe data: U.S. Geol. Survey open-file rept., 10 p., 31 p. appendix.

Bilgrami S. A., and Howie, R. A., 1960, The mineralogy and petrology of a rodingite dyke, Hindubagh, Pakistan: Am. Mineralogist, v. 45, p. 791–801.

Clark, L. D., 1960, Foothills fault system, western Sierra Nevada, California: Geol. Soc. America Bull., v. 71, p. 483–496.

—— 1964, Stratigraphy and structure of part of the western Sierra Nevada metamorphic belt, California: U.S. Geol. Survey Prof. Paper 410, 70 p. [1965]

Coleman, R. G., 1967, Low-temperature reaction zones and alpine ultramafic rocks of California, Oregon, and Washington: U.S. Geol. Survey Bull. 1247, 49 p.

Daly, R. A., 1933, Igneous rocks and the depths of the Earth: New York, McGraw-Hill Book Co., 508 p.

Deer, W. A., Howie, R. A., and Zussman, J., 1962, Rock-forming minerals: London, Longmans, Green and Co., Ltd., v. 1, 333 p.

Duffield, W. A., and Sharp, R. V., 1973, Geology of the Sierra foothills melange and adjacent areas, Amador County, California: U.S. Geol. Survey Prof. Paper 827 (In press).

Frankel, J. J., 1959, Uvarovite garnet and South African jade (hydrogrossular) from the Bushveld Complex, Transvaal: Am. Mineralogist, v. 44, p. 565–591.

Hutton, C. O., 1943, Hydrogrossular, a new mineral of the garnet-hydrogarnet series: Royal Soc. New Zealand Trans., v. 73, p. 174–180.

Marshall, Patrick, 1911, The geology of the Dun Mountain subdivision, Nelson: New Zealand Geol. Survey Bull., v. 12, p. 29–40.

Miles, K. R., 1950, Garnetized gabbros from the Eulamina district, Mount Margaret Goldfield: Western Australia Geol. Survey Bull. 103, no. 2, p. 108–130.

Scott, Beryl, 1951, A note on the occurrence of intergrowth between diopsidic augite and albite and of hydrogrossular from King Island, Tasmania: Geol. Mag., v. 58, p. 429–431.

Shapiro, Leonard, and Brannock, W. W., 1956, Rapid analysis of silicate rocks: U.S. Geol. Survey Bull. 1036-C, p. 19–56.

Winchell, A. N., and Winchell, H., 1964, Elements of optical mineralogy—Part II, Descriptions of the minerals, 4th ed.: New York, John Wiley and Sons, Inc., 551 p.

Jour. Research U.S. Geol. Survey
Vol. 1, No. 6, Nov.-Dec. 1973, p. 673–678

MICROPROBE ANALYSES OF SERICITE, CHLORITE, AND EPIDOTE FROM JEROME, ARIZONA

By J. THOMAS NASH, Menlo Park, Calif.

Abstract.—Volcanic rocks in the vicinity of the massive sulfide deposits at the United Verde mine, Jerome, Ariz., have been modified in several periods of hydrothermal alteration and greenschist metamorphism. Chlorite, $2M_1$ mica (sericite), and epidote are characteristic alteration products. Microprobe analyses for sericite, chlorite, and epidote are recalculated to structural formulas by the method employing oxygen anion equivalents. The sericite has the general composition of muscovite, but is moderately phengitic, and two samples have 6–12 percent paragonite in solid solution. Most of the chlorite is ripidolite with approximately one-third of the tetrahedral sites filled by aluminum; octahedral aluminum slightly exceeds tetrahedral. Fe:Fe+Mg+Mn ratios range from 0.34 to 0.66; low values are associated with sulfide minerals; higher values occur in a sample peripheral to the massive sulfide deposit. The epidote is a solid solution of 70 percent epidote, 30 percent clinozoisite.

The composition of fine-grained phyllosilicates developed during hydrothermal alteration is critical to the geochemistry of ore deposition, yet there is a paucity of microprobe analyses of these minerals from hydrothermal ore deposits. This paper reports the analyses of mica, chlorite, and epidote from samples taken in and near the massive sulfide deposits at Jerome, Ariz. (fig. 1).

The geology, ore deposits, wallrocks, and alteration at Jerome have been described in detail by Anderson and Creasey (1958) and by Anderson (1968). Wallrocks that contain large amounts of sericite and chlorite have recently been reinterpreted to be submarine pyroclastic tuffs and breccias constituting the Cleopatra Member of the Precambrian Deception Rhyolite (Anderson and Nash, 1972). Sericite that pervades these rocks is probably a hydrothermal alteration product of glassy or pumiceous debris (Anderson and Nash, 1972, fig. 3; fig. 2). Iron-magnesium metasomatism near the massive sulfide deposits has transformed the volcanic rocks to a chlorite-rich rock called "black schist" (Anderson and Creasey, 1958). Later metamorphism produced widespread epidote and other minerals typical of the greenschist facies.

Acknowledgments.—The author wishes to thank C. A. Anderson for introducing him to the geology of the Jerome area and for supplying several samples, and G. K. Czamanske for the microprobe standards and helpful suggestions during analysis. Czamanske and N. J Page offered helpful criticism of the manuscript.

TECHNIQUES FOR ANALYSIS AND CALCULATION

Polished thin sections of 13 selected samples were analyzed on a ARL Model EMX microprobe. Operating parameters were: 15 kilovolts accelerating potential, 0.3 microamperes sample current. LiF, ADP, and RAP crystals were used to analyze for Si, Al, Ti, Fe, Mg, Mn, Ca, K, and Na in sets of three. Beam diameter was close to 1μ. To minimize the effect of volatilization of elements under the electron beam, the beam was moved to a fresh sample area immediately before analysis. Typically, the beam was on a spot less than 15 seconds, of which about 10 seconds was used for analysis. Although X-ray intensities from a single spot, integrated for a few seconds, can yield an "analysis," the author prefers to relocate the beam and repeat counts until at least six data sets can be averaged and count statistics examined. Analyses of sericite and chlorite are for different grains in a microarea of approximately $50\mu^2$. Intensity data were corrected by computer for background, drift, atomic number, and matrix absorption (Beeson, 1967). A biotite standard was used for Si, Al, Ti, K, Fe, and Mg and an amphibole standard for Ca, Mn, and Na, as these standards have well-established uniform compositions. Because far more data were collected than can be reported here, tables of mineral analyses give the data for only one typical microarea of a sample, followed by the maximum standard deviation in any analysis of that sample.

Calculation of mineral formulas is commonly based on summation of anions ($O^{-2}+OH^{-}+F^{-}+Cl^{-}$) to a fixed number, but this technique cannot be used for microprobe analyses because water (H_2O+) and oxidation states of elements such as iron cannot be determined. Because anion analyses are unreliable, some mineralogists calculate formulas by methods that involve only oxygen to balance known cations (Foster, 1960; Borg, 1967; Robinson and others, 1971). The method used here is basically that of Foster (1960, 1962): oxide weight percentages are converted to hydrogen equivalents, then multiplied by a factor to balance the desired number of

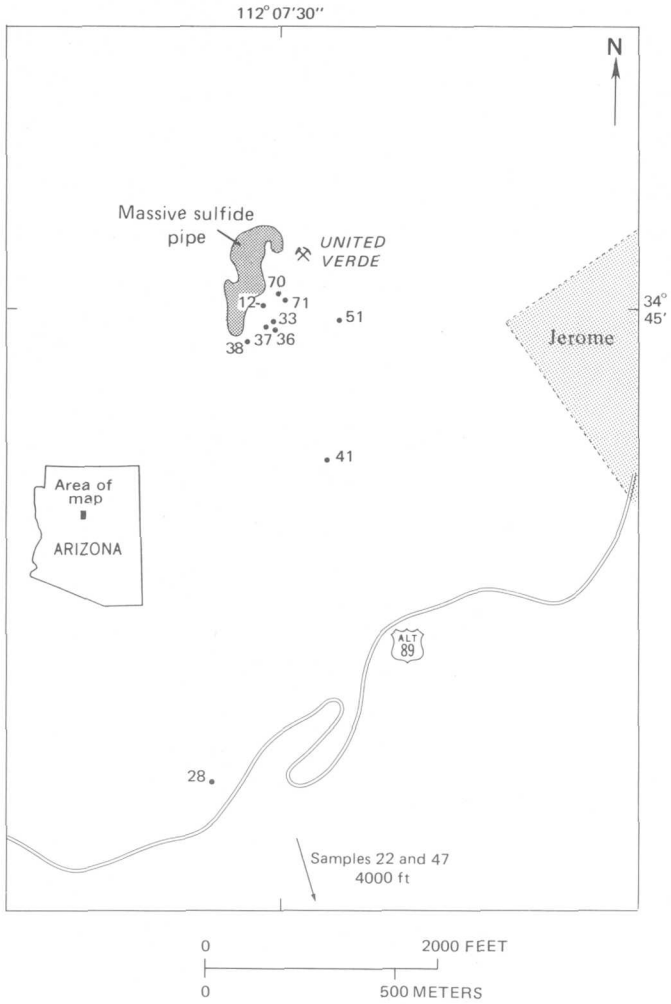

Figure 1.—Location of the United Verde mine and sample localities. Samples 70 and 71 are from the 3,300-foot underground mine level. Outline of the massive sulfide pipe from Anderson and Creasey (1958).

negative charges in the unit cell. For sericite, summation was to 22 oxygens (44 charges), for chlorite to 28 oxygens. For epidote with one OH^- group per cell, calculations were made on the basis of a double cell and 25 oxygens rather than 12½. Computations followed the procedure of Jackson, Stevens, and Bowen (1967) as modified by T. L. Wright.

ANALYSES

Sericite

Four samples of sericite-rich Cleopatra tuff were selected for analysis. The mica in these samples is the $2M_1$ polytype as determined by X-ray diffraction. In samples 28 and 41, it occurs as very fine grained (mostly $<1\mu$) sericite pseudomorphous after fragmented pumice (fig. 2). Sample 51 is similar but has weak foliation; sample 37 is a sandier tuff in

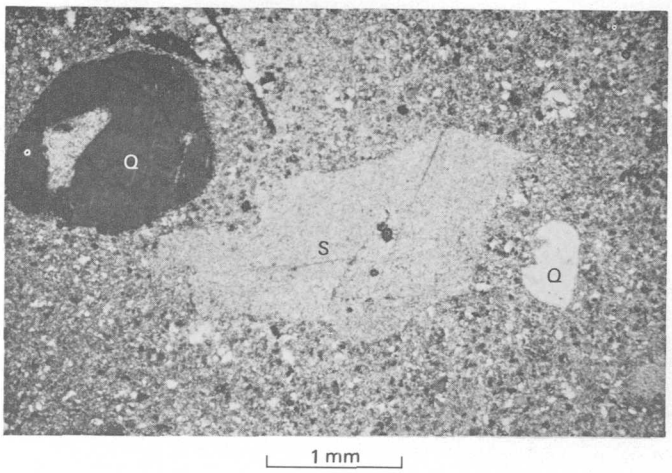

Figure 2.—Photomicrograph of crystal tuff from the Cleopatra Member of the Deception Rhyolite, showing pumice clasts replaced by sericite. S, sericite; Q, quartz. Crossed polarizers, sample 41.

which the fine mica is disseminated throughout the matrix, a relation that probably caused the difficulty in obtaining reproducible analyses. The larger standard deviations reported in table 1 reflect grain-boundary effects and foreign grains that could not be avoided during visual positioning of the beam.

The chemistry of sericite is reckoned in terms of the general structural formula $X_2Y_4Z_8O_{20}(OH)_4$ in which X interlayer cations are large ions such as K^+ and Na^+, Y are medium-size cations such as Al^{+3}, Mg^{+2}, Fe^{+2}, and Mn^{+2} in octahedral positions, and Z are smaller cations such as Si^{+4} and Al^{+3} in tetrahedral positions. The structural calculations (table 1) show that in most analyzed microareas[1] the interlayer alkalies sum to near 1.9, which is not far below the ideal 2.0; hence, the likely H_3O^+ substitution (hydromuscovite) must be relatively small. The Y or octahedral totals are somewhat above the ideal 4.0; this probably reflects the influence of the alkali deficiency on the calculations (which forces a sum of 44 cation charges) rather than any excess of octahedral cations. These subtotals are as good as, or better than, the selected analyses of micas done by conventional wet chemical methods (Deer and others, 1962b, p. 218–220). Because offsetting errors are more apparent and water cannot be determined, the structural calculations are considered by the author to be a more sensitive test of accuracy than weight totals.

From their composition and by X-ray diffraction analysis, it is apparent that these are dioctahedral micas very similar to muscovite. In more detail, substitutions in the octahedral and interlayer positions indicate some variation in phengite and paragonite solid solution. Substitution

[1] Because the crystals analyzed are commonly smaller than the $\approx 1\mu^2$ area excited by the electron beam, we cannot refer to these as mineral grain analyses as we do for analyses of coarser material.

Table 1.—*Microprobe analyses and formulas of sericite from Jerome, Ariz.*

[Analyses by J. T. Nash. A representative analysis is given for each sample, followed by standard deviation which typically is equal to or greater than range in values in microareas of sample. Total iron expressed as FeO. Structural calculations based on 22 oxygens per unit cell.]

Sample No. and (number of analyses)		28(5)		37(3)		41(8)		51(5)	
Chemical analysis (weight percent)									
Analysis No.		28-2	σ	37-2	σ	41-8	σ	51-2	σ
SiO_2		46.3	0.9	46.2	1.5	45.0	1.1	46.4	1.0
Al_2O_3		32.2	.6	35.6	1.0	33.4	.9	36.	.5
TiO_2		.23	.03	.10	.01	.08	.01	.01	.02
MgO		.91	.03	.76	.5	.91	.08	.63	.08
FeO		2.80	.1	.61	.4	3.08	.2	.22	.02
K_2O		10.97	.2	9.68	.6	10.47	.4	7.07	1.
Na_2O		.12	.02	.54	.1	.32	.04	1.60	.3
Total		93.5		93.5		93.3		91.9	
Structural formula									
Si	Z	6.34	8.00	6.21	8.00	6.18	8.00	6.20	8.00
Al_{iv}		1.66		1.79		1.82		1.80	
Al_{vi}	Y	3.54	4.07	3.84	4.07	3.59	4.14	3.87	4.02
Ti		.02		.01		.01		.00	
Mg		.19		.15		.19		.13	
Fe		.32		.07		.35		.02	
K	X	1.91	1.94	1.66	1.80	1.83	1.91	1.67	1.90
Na		.03		.14		.08		.23	

of sodium in the mica of samples 37 and 51 suggests a range of from 12 to 25 percent for the paragonite end member.

Calcium and magnanese were determined in all analyses but are not reported in table 1. Calcium generally was at background levels, although in sample 51, which has low alkali totals and fairly high sodium content, calcium ranged from 0.03 to 0.19 weight percent and may be significant. Manganese consistently ranges from 0.00 to 0.02 weight percent and is presumed to be in the octahedral layer. Titanium ranges from 0.01 to 0.23 percent (table 1) and is presumably in octahedral sites.

Chlorite

Nine samples representing four different occurrences of chlorite were selected for analysis. Samples 22 and 47 are from Mescal Gulch, approximately 2 miles south of the United Verde mine. Chlorite in these rocks occurs as masses and clasts; no sulfides are present. This chlorite possibly formed by hydrothermal alteration during accumulation of the Cleopatra Member (Anderson and Nash, 1972, p. 857). Samples 36, 38, 70, and 71 contain chlorite-quartz-pyrite-chalcopyrite assemblages typical of the United Verde "black schist" ores. Samples 36 and 37 are from a quartz-chalcopyrite stockwork "quartz porphyry" ore (shown in fig. 2*G*, Anderson and Nash, 1972); sample 36 is from a chlorite-rich vein selvage; 37 represents adjacent sericite-rich Cleopatra with traces of incipient chlorite replacing sericite. Samples 12 and 33 are from quartz-carbonate-sulfide veins that cut "black schist" and represent vein-filling or recrystallized chlorite from the "black schist." The chlorite is typically coarse grained (fig. 3), and, except for that in sample 37, is physically well suited for microprobe analysis.

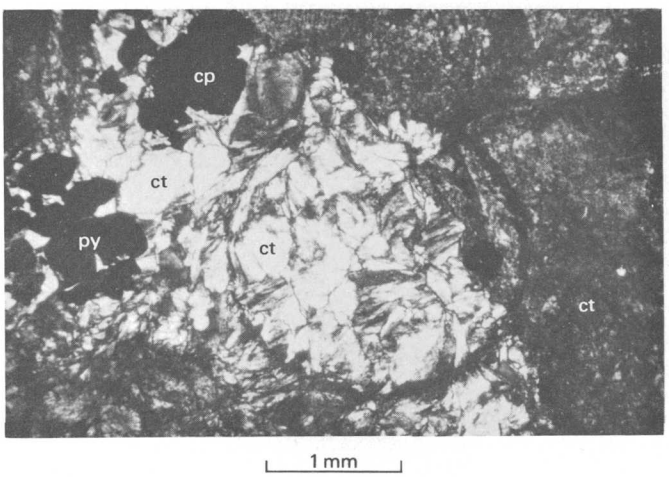

Figure 3.—Photomicrograph of chlorite-rich "black schist" ore. Dark circle is scribed to facilitate location. ct, chlorite; cp, chalcopyrite; py, pyrite. Crossed polarizers, sample 38.

Analytical determinations for most elements were quite consistent in these samples. The variation within microareas was typically similar to the variation between different areas of the same sample and is summarized in table 2. The standard deviations for sample 37 are much higher and reflect intergrown quartz and sericite that could not be entirely avoided. The variation in iron and magnesium for all the samples commonly is relatively higher than for other elements and is considered to reflect real differences within small areas of chlorite. The totals at about 84 weight percent are a few percent lower than expected if one assumes normal H_2O+ content; no reasons for this are known. Much of the deficiency could be accounted for by calculating iron as Fe_2O_3, but there are no geochemical justifications for this. The structural calculations suggest that the analyses are reasonable. Deficiencies in the octahedral position (Y = 11.87, compared with an ideal 12.00) are not large and are not necessarily a reflection of error in the analysis, as R^{+3} ions (Fe^{+3}, Al^{+3}) in octahedral positions in excess of R^{+3} in tetrahedral sites will cause this effect. Calcium, sodium, and titanium were determined but are not included in table 2 because their levels are consistently low. Calcium is consistently at background levels, sodium ranges from 0.00 to 0.04 weight percent, and titanium from 0.01 to 0.06 weight percent.

Chlorite has the general formula $Y_{12}Z_8O_{20}(OH)_{16}$, in which Y and Z cations are Fe, Mg, Mn, and Al and Si and Al, respectively. In ideal chlorites, octahedral Al should equal tetrahedral Al, but this does not obtain for most chlorites because of the presence of ferric iron or vacancies in the octahedral layer (Foster, 1962). In these chlorites octahedral Al is more abundant than tetrahedral, a relation observed by Foster (1962) in about one-third of the analyses studied by her. In such chlorites the extra charges in the octahedral layer can create vacancies in that layer as a result of substituting $2R^{+3}$ for $3R^{+2}$ (Foster, 1962, p. A8). A mechanism of this type apparently obtains in most of the Jerome chlorites because the sums of octahedral cations (Y) range from 11.69 to 11.99 relative to the ideal 12.00. The structural formulas reveal that in all the chlorites the difference between octahedral and tetrahedral Al is very close to twice the apparent deficiencies in the octahedral positions (Y). A ratio of about 3:2 would suggest substitution of Al^{+3} for Mg^{+2} and Fe^{+2}, as noted by Foster (1962). That this ratio is 2:1 rather than 3:2 suggests some other charge and position balance, such as Fe^{+3} for Fe^{+2}, and may be an artifact of calculating iron as FeO.

According to the classification of Foster (1962), most of the chlorite is ripidolite (fig. 4). By the composition-classification plot, figure 4, chlorite compositions are uniform within samples and generally similar for eight of nine samples. Sample 22, from an outlying area, contains the most iron-rich chlorite. The ranges of chlorite compositions in the other samples overlap. With the exception of sample 22 and one for which analysis of chlorite is poor, sample 37, there does not appear to be any correlation of composition with age or geologic occurrence.

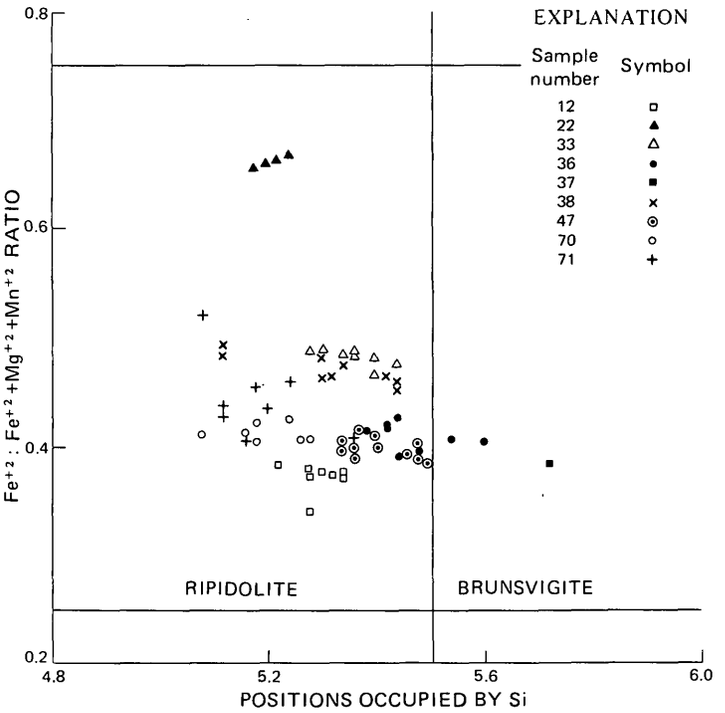

Figure 4.—Composition and classification of 64 chlorite microareas. Classification system is that of Foster (1962).

Optical properties of chlorite were employed to select areas and estimate compositions, but for some types the predictions proved erroneous. The chlorite of most microareas selected was coarse grained, length fast, nearly colorless, with very low birefringence. From these properties the chlorite was expected to have Fe:Fe+Mg ratios of <0.5 (Albee, 1962). This is confirmed by the microprobe analyses (see fig. 4). Crosscutting strands of fine-grained chlorite with anomalous blue birefringence and anticipated Fe:Fe+Mg ratios >0.5 in fact differed slightly in composition from adjacent chlorite. Chlorite in sample 47 has a peculiar circular texture resembling perlitic cracks with radial zones of different color, but these zones did not differ in composition. Green coloration in these chlorites is not simply correlated with Fe:Fe+Mg ratio; for example, chlorite in sample 47 is greener than that in samples with higher ratios.

Epidote

Epidote-group minerals are fairly common in the altered and metamorphosed volcanic rocks; they usually occur as a replacement of plagioclase in crystal tuffs. Conspicuous epidote euhedra in plagioclase were analyzed during the course of chlorite analyses.

Epidote-group minerals have the general formula $X_2Y_3Z_3(O,OH,F)_{13}$. For these analyses X = Ca+Mn, Y = Al+Fe+Ti, and Z = Si. Mg and K determinations were consistently at background levels, and Na was 0.01 percent or less. The analysis of a typical crystal is presented in table 3 along with the structural formula: Iron has been calculated as

Table 2.—*Microprobe analyses and formulas of chlorite from Jerome, Ariz.*

[Microprobe analyses by J. T. Nash. A representative analysis is given for each sample, followed by the standard deviation which is typically equal to or greater than the range in analyses for microareas of the sample. Total iron expressed as FeO. Structural calculations based on 28 oxygens per unit cell]

Sample No. and (number of analyses)	12(8)		22(4)		33(8)		36(8)		37(1)		38(9)		47(10)		70(7)		71(9)	
Chemical analysis (weight percent)																		
Analysis No.	12-8	σ	22-3	σ	33-5	σ	36-3	σ	37-1	σ	28-2	σ	47-6	σ	70-2	σ	71-1	σ
SiO_2	25.1	0.6	22.8	0.6	24.2	0.6	25.3	0.8	28.9	1.6	24.1	0.6	26.2	0.5	24.7	0.4	23.5	0.5
Al_2O_3	22.5	.4	22.1	.4	22.	.4	21.5	.6	24.8	.7	22.4	.6	22.8	.2	23.	.4	23.2	.5
MgO	17.6	.4	8.57	.2	14.1	.5	16.	.5	16.4	.3	14.2	.7	16.5	.4	16.1	.6	14.7	.4
FeO	18.8	.4	30.5	.5	23.8	.6	21.3	.6	18.4	.3	22.4	1.5	19.5	.5	21.4	.6	23.3	.6
MnO	.09	.01	.66	.03	.11	.01	.10	.01	.06	.00	.14	.02	.05	.01	.01	.00	.08	.01
Total	84.1		84.6		84.2		84.2		88.6		83.3		85.0		85.2		84.8	
Structural formula																		
Si	5.33		5.17		5.28		5.44		5.72		5.29		5.49		5.23		5.08	
Al_{iv} Z	2.67	8.00	2.83	8.00	2.72	8.00	2.56	8.00	2.28	8.00	2.71	8.00	2.51	8.00	2.77	8.00	2.92	8.00
Al_{vi}	2.95		3.08		2.94		2.88		3.50		3.07		3.12		2.99		3.00	
Mg	5.56		2.89		4.58		5.12		4.85		4.63		5.15		5.09		4.73	
Fe Y	3.34	11.87	5.77	11.87	4.35	11.89	3.82	11.84	3.04	11.40	4.10	11.83	3.42	11.70	3.79	11.89	4.21	11.95
Mn	.02		.13		.02		.02		.01		.03		.01		.02		.01	

Fe_2O_3 because that form predominates in epidote (Deer and others, 1962a, p. 197–199).

The sums in table 3 are a little low, at 96 percent, as H_2O+ should be about 2 percent. However, the structural calculations show that the ratios of elements are good for the structural positions are close to ideal occupancy. SiO_2 determinations appear to be erroneously high by about 0.6 weight percent, possibly because biotite was used as the Si standard. Presumably, high SiO_2 determinations cause the structural calculations on other elements to be somewhat low. Ferric iron occupies about 0.7 positions, making these crystals approximately 70 percent epidote in the solid solution epidote-clinozoisite.

Table 3.—*Microprobe analysis and formula of epidote from Jerome, Ariz.*

[Analysis by J. T. Nash. Total iron expressed as Fe_2O_3]

Sample No. and (number of analyses)	22(4)		
Chemical analysis (weight percent)			
Analysis No.	22-2		σ
SiO_2	38.0		0.3
Al_2O_3	23.7		.8
Fe_2O_3	11.5		.4
TiO_2	.06		.01
MnO	.25		.03
CaO	22.6		.2
Total	96.1		
Structural formula			
Si	3.05	Z	3.05
Al	2.25		
Fe^{+3}	.70	Y	2.95
Ti	.00		
Mn	.02	X	1.98
Ca	1.96		

DISCUSSION

The internal consistency of the microprobe analyses and the good structural formulas resulting from them suggest that the analyses are credible. Although microprobe analysis of small isolated particles is fraught with difficulties (White, 1964; Page and others, 1968; Eugster and others, 1972), analysis of polished masses of small particles should not and apparently does not result in large errors. Structural formula calculations based on oxygen equivalents are effective for handling the microprobe analyses and put them in a readily usable form.

The moderately phengitic nature of the micas and their paragonite content presumably reflect conditions of greenschist metamorphism; the metamorphic effects are believed to be superimposed on earlier hydrothermal alteration (Anderson and Nash, 1972). The micas differ from typical phengites (Ernst, 1963) by dominance of Fe over Mg. Further, there is no evidence for very large load pressures in this environment (Anderson and Nash, 1972) as for many phengite occurrences. Mica compositions range from 2 to 21 atom percent paragonite solid solution. If these compositions are related to the muscovite-paragonite solvus (Eugster and others, 1972, fig. 9),

temperatures of 200°–560°C are suggested. However, the solvus is not located with certainty (Eugster and others, 1972), and the more sodic analyses may reflect grain-boundary effects from paragonite-rich micas.

The physicochemical controls on the compositions of the chlorites and epidotes are not clear, and there are no pertinent experimental data. The chlorite analyses are in agreement with the generalization of Anderson and Creasey (1958) that chlorite near the massive sulfide deposits is more magnesian in composition than in outlying areas. Ekstrand (1963) found the opposite trend at Chibougamau, Canada, with Fe:Fe+Mg ratios of 0.75 in the sulfide zone. Although iron-magnesium metasomatism is common in massive sulfide deposits, little systematic study has been made of the mafic silicates. Presumably, chemical factors, such as fugacity of CO_2 or sulfur, or $Mg^{+2}:(H^{+})^{2}$ are important in determining mineral stability and composition. At Jerome, chlorites formed at about 235°C and relatively high CO_2 pressures (Anderson and Nash, 1972). Sulfur fugacities cannot be determined with much certainty from the sulfide assemblage, but apparently they did not depress the activity of iron sufficiently to produce highly magnesian chlorites.

REFERENCES CITED

Albee, A. L., 1962, Relationships between the mineral association, chemical composition and physical properties of the chlorite series: Am. Mineralogist, v. 47, nos. 7–8, p. 851–870.

Anderson, C. A., 1968, Metamorphosed Precambrian silicic volcanic rocks in central Arizona, *in* Studies in volcanology–a memoir in honor of Howel Williams: Geol. Soc. America Mem. 116, p. 9–45.

Anderson, C. A., and Creasey, S. C., 1958, Geology and ore deposits of the Jerome area, Yavapai County, Arizona: U.S. Geol. Survey Prof. Paper 308, 185 p.

Anderson, C. A., and Nash, J. T., 1972, Geology of the massive sulfide deposits at Jerome, Arizona–a reinterpretation: Econ. Geology, v. 67 , no. 7, p. 845–863.

Beeson, M. H., 1967, A computer program for processing electron microprobe data: U.S. Geol. Survey open-file report, 41 p.

Borg, I. Y., 1967, On conventional calculations of amphibole formulae from chemical analyses with inaccurate $H_2O(+)$ and F determinations: Mineralog. Mag., v. 36, no. 280, p. 583–590.

Deer, W. A., Howie, R. A., and Zussman, J., 1962a, Ortho and ring silicates, v. 1, *of* Rock-forming minerals: New York, John Wiley and Sons, 333 p.

——1962b, Sheet silicates, v. 3, *of* Rock-forming minerals: New York, John Wiley and Sons, 270 p.

Eckstrand, O. R., 1963, Crystal chemistry of chlorite: Harvard Univ., Cambridge, Mass., Ph. D. thesis, 128 p.

Ernst, W. G., 1963, Significance of phengitic micas from low-grade schists: Am. Mineralogist, v. 48, nos. 11–12, p. 1357–1373.

Eugster, H. P., Albee, A. L., Bence, A. E., Thompson, J. B., and Waldbaum, D. R., 1972, The two-phase region and excess mixing properties of paragonite-muscovite crystalline solutions: Jour. Petrology, v. 13, p. 147–179.

Foster, M. D., 1960, Interpretation of the composition of trioctahedral micas: U.S. Geol. Survey Prof. Paper 354-B, p. 11–49.

——1962, Interpretation of the composition and a classification of the chlorites: U.S. Geol. Survey Prof. Paper 414-A, p. A1–A33.

Jackson, E. D., Stevens, R. E., and Bowen, R. W., 1967, A computer-based procedure for deriving mineral formulas from mineral analyses, *in* Geological Survey Research 1967: U.S. Geol. Survey Prof. Paper 575-C, p. C23–C31.

Page, N. J, Calk, L. C., and Carr, M. H., 1968, Problems of small-particle analysis with the electron microprobe, *in* Geological Survey Research 1968: U.S. Geol. Survey Prof. Paper 600-C, p. C31–C37.

Robinson, P., Ross, M., and Jaffe, H. W., 1971, Composition of the anthophyllite-gedrite series, comparisons of gedrite and hornblende, and the anthophyllite-gedrite solvus: Am. Mineralogist, v. 56, p. 1005–1041.

White, E. W., 1964, Microprobe technique for the analysis of multiphase microcrystalline powders: Am. Mineralogist, v. 49, nos. 1–2, p. 196–197.

Jour. Research U.S. Geol. Survey
Vol. 1, No. 6, Nov.-Dec. 1973, p. 679—680

NOTES ON THE BROMINE PENTAFLUORIDE TECHNIQUE OF OXYGEN EXTRACTION

By IRVING FRIEDMAN and JIM D. GLEASON,
Denver, Colo.

Abstract.—The necessity to use a dry box when loading silicate samples into reaction vessels prior to fluorination is eliminated by the use of a simple loading technique. Data presented show the reproducibility of the fluorination reaction using this technique. Sodium fluoride, when added to saline waters prior to fluorination, improves the precision of the overall technique.

In describing the use of bromine pentafluoride for the extraction of oxygen from minerals for O^{18} analysis, Clayton and Mayeda (1963) suggested that the nickel reaction vessel be opened in a dry box containing air dried by P_2O_5. This precaution was deemed necessary to prevent the uptake of water by the nickel fluoride coating in the reaction vessel and the subsequent release of oxygen from this adsorbed(?) water.

We have found that the dry box is unnecessary if the nickel reaction vessel is first filled with dry nitrogen and the mineral sample quickly introduced into the vessel through a small opening. The amount of water vapor entering the vessel is too small to be measured and too small to affect the O^{18} analysis.

The nickel reaction vessel (¾-in. OD tube) has at its open end a Swagelock fitting and Teflon front ferrules; the fitting terminates in a ¼-inch ID stainless steel tube about 2 inches long (fig. 1). This tube in turn is connected by means of another Swagelock fitting on a Teflon and stainless steel ball valve to the line leading to the reaction manifold (not shown in fig. 1).

The weighed powder sample of approximately 20 mg is placed in a special long-handled spatula (fig. 1). The line from the reaction manifold and the reaction vessel are filled with dry nitrogen at slightly more than atmospheric pressure, the valve on the line above the reaction vessel is closed, the reaction vessel is removed from the line by loosening the Swagelock fitting on the valve, and the sample on the spatula is inserted through the ¼-inch tube into the bottom of the reaction vessel. The reaction vessel is then quickly reattached to the line to the reaction manifold. The reaction vessel is exposed to the atmosphere for no longer than 1 minute, and diffusion of water vapor is minimized by the fact that a ¼-inch opening is exposed to air. The reaction vessel seldom requires cleaning—only after 20 or 30 reactions.

During the past year we repeatedly analyzed a standard quartz sample. Some analyses were made by prefluorinating the reaction tube containing the sample to remove any water contamination, and others were carried out without prefluorination. The 19 prefluorination analyses gave δO^{18} a value of +10.85 with a sigma of $0.16°/_{oo}$. The 38 analyses without prefluorination gave an average value of +10.72 with a sigma of $0.11°/_{oo}$. From this we conclude that contamination by

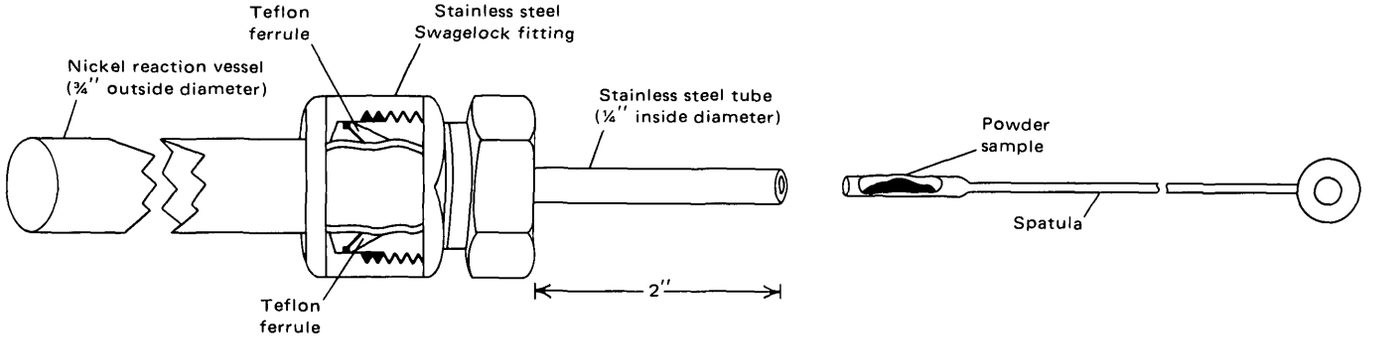

Figure 1.—Sample spatula ready for insertion of sample into reaction vessel through stainless steel tube.

water vapor is negligible during sample introduction without the use of a dry box.

In 1966 O'Neil and Epstein described the use of bromine pentafluoride for the O^{18} analysis of milligram quantities of water. We have confirmed the usefulness of this technique on water samples that are relatively "fresh." For example, replicate samples of snow water were processed and gave precisions of 0.1°/₀₀ (2 sigma). However, if we attempted to use unpurified sea-water samples, the results scattered widely, and, depending upon the technique of introduction of the water into the system, the 2 sigma values were about 2°/₀₀ to 5°/₀₀. The scatter in the data was independent of whether or not the solids that formed by evaporation of the water were heated to above 100°C.

According to Frank Manheim, U.S. Geological Survey, the discrepancy was probably related to the magnesium ions that form hydrates which are stable to temperatures above 400°C. He suggested that sodium fluoride be added to precipitate the magnesium. Accordingly, NaF (10 g/l) dried at 110°C was added to the sea water. Twelve replicate fluorinations of this treated sea water resulted in the data shown in table 1. The data points have a precision of 0.16°/₀₀ (2 sigma).

Table 1.—*Twelve replicate analyses of sea-water sample by fluorination*

[Data in per mil SMOW, Standard Mean Ocean Water]

+0.49	+0.35	+0.26	+0.33	+0.46	+0.44
+.32	+.40	+.32	+.22	+.32	+.36

Average = 0.36±0.16°/₀₀ (2 sigma).

REFERENCES CITED

Clayton, R. N., and Mayeda, T. K., 1963, The use of bromine pentafluoride in the extraction of oxygen from oxides and silicates for isotopic analysis: Geochim. et Cosmochim. Acta, v. 27, no. 1, p. 43–52.

O'Neil, J. R., and Epstein, Samuel, 1966, A method for oxygen isotope analysis of milligram quantities of water and some of its applications: Jour. Geophys. Research, v. 71, no. 20, p. 4955–4961.

Jour. Research U.S. Geol. Survey
Vol. 1, No. 6, Nov.-Dec. 1973, p. 681—685

ATOMIC ABSORPTION SPECTROPHOTOMETRIC DETERMINATION OF MICROGRAM LEVELS OF Co, Ni, Cu, Pb, AND Zn IN SOIL AND SEDIMENT EXTRACTS CONTAINING LARGE AMOUNTS OF Mn AND Fe

By T. T. CHAO and R. F. SANZOLONE, Denver, Colo.

Abstract.—An atomic absorption spectrophotometric method has been developed for the determination of seven metal ions in the hydroxylamine extract of soils and sediments. Mn, Fe, and Zn are directly determined in the aqueous extract upon dilution. Co, Ni, Cu, and Pb in a separate aliquot of the extract are chelated with APDC (ammonium pyrrolidine dithiocarbamate) and extracted into MIBK (methyl isobutyl ketone) before determination. Data are presented to show the quantitative recovery of microgram levels of Co, Ni, Cu, and Pb by APDC-MIBK chelation-extraction from synthetic solutions containing as much as 2,000 μg/ml (micrograms per milliliter) Mn or 50 μg/ml Fe. Recovery of known amounts of the metal ions from sample solutions is equally satisfactory. Reproducible results are obtained by replicate analyses of two sediment samples for the seven metals.

Hydrous manganese and iron oxides are credited with being strong scavenging agents for heavy metal ions (Canney, 1966; Jenne, 1968). Information on heavy metals associated with manganese and iron oxides has been used in mineral exploration (Hawkes and Webb, 1962; Horsnail and others, 1969). Currently used extraction methods for determining metal associations do not differentiate metal ions associated with manganese oxides and those associated with iron oxides. This is mainly because the available methods dissolve both manganese and iron oxides, simultaneously, to varying and significant degrees. An extraction method has recently been developed (Chao, 1972) using a 0.1 *M* hydroxylamine hydrochloride ($NH_2OH \cdot HCl$) solution in 0.01 *M* HNO_3 (pH 2) for the preferential dissolution of manganese oxides. During dissolution of manganese oxides, the associated metal ions and minor proportions of hydrous iron oxides in the sample are brought into solution.

Atomic absorption spectrophotometry, because of its simplicity, selectivity, and sensitivity, has been chosen for the determination of metal ions in the hydroxylamine extract. Preliminary observations have shown that Mn, Fe, and Zn can be determined directly in the aqueous extract after proper dilution to compensate for the high concentrations of Mn and Fe present and for the high sensitivity for Zn. The determination of Co, Ni, Cu, and Pb in the original extract poses analytical problems. Hydroxylamine in the matrix tends to suppress absorption at the resonance lines of the metals, and metal concentrations in the extract are often too low to be analyzed directly by atomic absorption. Several investigators (Allan, 1961; Sprague and Slavin, 1964a, 1964b; Brooks and others, 1967; Burrell, 1967; Fishman and Midgett, 1968) have used APDC (ammonium pyrrolidine dithiocarbamate) -MIBK (methyl isobutyl ketone) chelation-extraction for the determination of one or more of the four metals in various samples. Not only are the metals separated from the matrix solution, but also the sensitivity of the methods is enhanced in the presence of the organic solvent. Since in none of these methods have provisions been made to deal with high concentrations of Mn and Fe relative to those of the metal ions to be determined as found in the hydroxylamine extract of soils and sediments, the major problem was to investigate whether microgram levels of Co, Ni, Cu, and Pb in solutions containing relatively large amounts of Mn and Fe could be determined by APDC-MIBK chelation-extraction and atomic absorption spectrophotometry.

This paper describes a systematic procedure for the determination of Mn, Fe, Zn, Co, Ni, Cu, and Pb in the hydroxylamine extract of soils and sediments. Mn, Fe, and Zn are determined directly in the aqueous extract after dilution. Co, Ni, Cu, and Pb, in a separate aliquot of the extract, are chelated with APDC, extracted into MIBK, and determined by atomic absorption. Data are presented to show the quantitative recovery of known amounts of Co, Ni, Cu, and Pb from solutions containing high concentrations of Mn and Fe which may occur in hydroxylamine extracts of soil and sediment samples.

Acknowledgments.—The authors wish to thank F. C. Canney and G. A. Nowlan for furnishing sediment samples used in the development of the proposed method.

EXPERIMENTAL METHOD

Apparatus

Perkin-Elmer Model 303 atomic absorption spectrophotometer equipped with a Boling burner head and single-element hollow

Table 1.—*Instrument settings for analysis of the seven metals*

[For the analysis of all metals the following settings apply: grating, ultraviolet; air pressure, 30 psi; acetylene pressure, 8 psi; aspiration rate, about 3.8 ml/min]

Element	Wavelength (A)	Slit	Scale expansion	Response	Lamp current (ma)	Air flow	Fuel flow
Mn	2795	3	1	1	20	7.5	6.5
Fe	2483	3	1	1	30	7.5	6.5
Zn	2139	4	5	3	15	7.5	6.5
Cu	3247	4	1	1	15	5.0	2.5
Co	2407	3	5	3	30	5.0	2.5
Ni	2320	3	5	3	25	5.0	2.5
Pb	2833	4	5	3	8	5.0	2.5

cathode lamps. Table 1 shows the instrument settings for the seven metals.

Sorvall SS-3 superspeed centrifuge.

Radiometer pH meter, Model 26, connected to a combination electrode.

Reagents

Extracting solution, 0.1 *M* hydroxylamine hydrochloride ($NH_2OH \cdot HCl$) in 0.01 *M* HNO_3 (pH = 2). Dissolve 6.95 g reagent grade $NH_2OH \cdot HCl$ in demineralized water, add 10 ml 1 *M* HNO_3, and dilute to approximately 900 ml in 1-liter volumetric flask. Adjust the pH of the solution with 1 *M* HNO_3 to 2 and make up to volume.

Whatman filter accelerator, one tablet cut into four.

Ammonium pyrrolidine dithiocarbamate (APDC), 1 percent (w/v). Dissolve 1 g APDC in 100 ml demineralized water. Prepare fresh daily.

Hydrochloric acid, 0.3 *M*. Mix 25 ml concentrated HCl (sp gr 1.19) with demineralized water and dilute to 1 liter.

Hydrochloric acid (1+1). Mix 100 ml concentrated HCl (sp gr 1.19) with equal volume of demineralized water.

Sodium hydroxide, 2.5 *M*. Dissolve 10 g NaOH in demineralized water and dilute to 100 ml.

Methyl isobutyl ketone (MIBK), water-saturated. Saturate 300 ml MIBK with 100 ml demineralized water by shaking vigorously in a 500-ml separatory funnel for 3 minutes. Discard the aqueous layer.

Stock standard solutions of metals. Prepare each stock standard solution from the pure metal so that the solution contains 1 mg metal per milliliter of 1-percent (v/v) concentrated HCl (sp gr 1.19) for Mn, Fe, and Zn, and 1-percent (v/v) concentrated HNO_3 (sp gr 1.42) for Co, Ni, Cu, and Pb.

Working standard solutions of metals. Prepare two series of working standard solutions from stock solutions. One series contains Mn, Fe, and Zn in 1 percent (v/v) concentrated HCl for metal determinations in aqueous solutions after dilution of the soil or sediment extracts. The second series contains Co, Ni, Cu, and Pb in 1-percent (v/v) concentrated HNO_3 for determinations of the metals after chelation with APDC and extraction into MIBK. The concentration of each metal in the two series of mixed standard solutions is presented in table 2.

Table 2.—*Working standard solutions of metals*

Element	Standard 1	2	3	4	5
Series 1—for determinations in aqueous solution (μg/ml)					
Mn	1	2.5	5	7.5	10
Fe	1	2.5	5	7.5	10
Zn	.025	.05	.1	.2	.4
Series 2—for determinations in MIBK (μg/10 ml)					
Co	0.25	0.5	1	2	4
Ni	.25	.5	1	2	4
Cu	2.5	5	10	20	40
Pb	1.5	3	6	12	24

Procedure

Weigh 0.10 to 0.50 g of a finely powdered soil or sediment sample (<100 mesh) along with 0.1 g Whatman filter accelerator into a 29- by 103-mm polypropylene centrifuge tube. Add 25 ml 0.1 *M* hydroxylamine in 0.01 *M* HNO_3 (pH = 2) and equilibrate the contents of the tube on a mechanical shaker for 30 minutes. Then, spin the suspension at 15,000 rpm in a Sorvall SS-3 centrifuge for 10 minutes and decant the supernatant extract into a 50-ml polyethylene bottle. The function of the ashless accelerator is to help pack the sample on the bottom of the tube during centrifugation and to prevent fine particles from dislodging upon decantation of the clear extract.

Transfer 5 ml of the extract and 1 ml HCl (1+1) into a 50-ml volumetric flask and dilute to volume. This solution is used for the determination of Mn, Fe, and Zn.

For the determination of Co, Ni, Cu, and Pb, transfer 10 ml of the extract into a 25 - by 150-mm glass culture tube. Add 10 ml demineralized water and adjust the pH of the solution with a pH meter to 2.5 to 2.7 by addition of 2.5 *M* NaOH and 0.3 *M* HCl, using a tube vibrator to aid mixing. Pipet 1 ml 1-percent APDC into the tube and adjust the pH to 2.8. Add 10 ml MIBK and shake vigorously for 1 minute. Allow the organic and aqueous phases to separate. Aspirate the upper organic layer into the flame to obtain the absorption readings for Co, Ni, Cu, and Pb. For establishing calibration curves, mix 10 ml of each of the working standard solutions (series 2 in table 2) with 10 ml of the hydroxylamine extracting solution and treat identically as for the sample extracts.

Analyze duplicate blanks with each batch of samples for correction of possible impurities present in the reagents.

RESULTS AND DISCUSSION

Calibration curves

Calibration curves for the seven metals are shown in figures 1 and 2. Linear or nearly linear relationship exists between the concentration of a given metal and its absorbance. With a 0.50-g sample taken for analysis, the range of concentrations of the seven metals that can be determined by the procedure outlined is: Mn and Fe, 500–5,000 ppm; Zn and Cu, 10–200 ppm; Co and Ni, 1–20 ppm; and Pb, 5–120 ppm. Concentrations above this range may be determined either by reducing the sample weight or by further diluting the aqueous extract with demineralized water and the organic extract with MIBK. By this technique, a wide range of concentrations of the seven

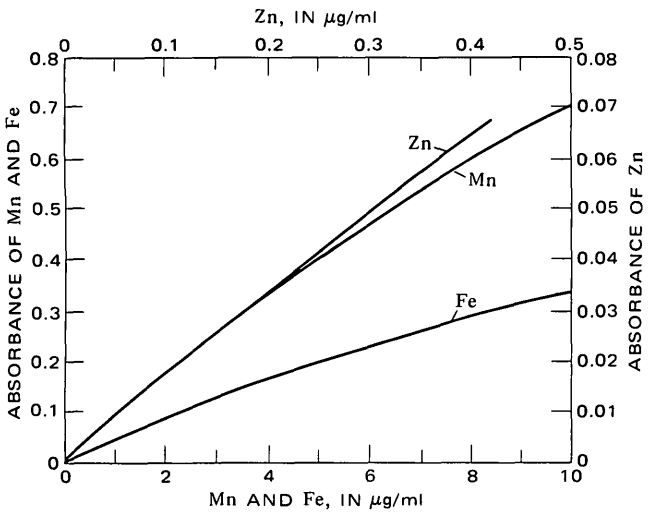

Figure 1.—Calibration curves for Mn, Fe, and Zn.

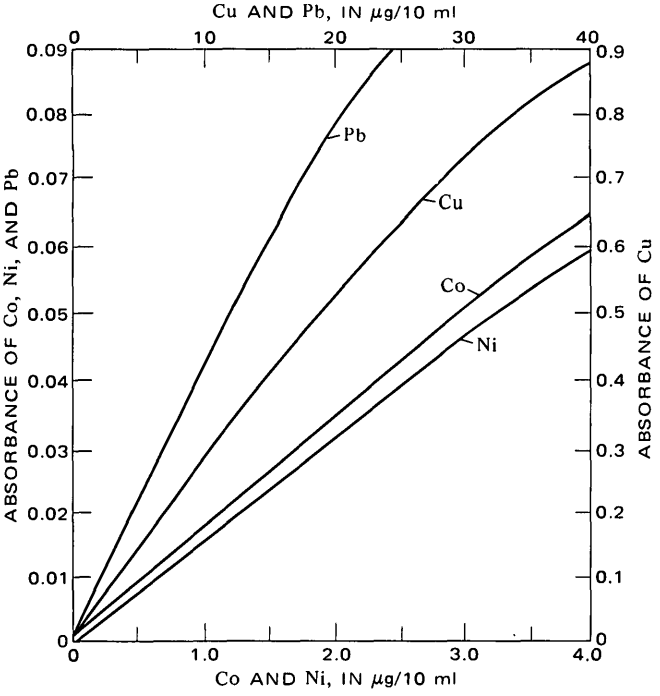

Figure 2.—Calibration curves for Co, Ni, Cu, and Pb.

metals present in background as well as mineralized samples can be covered.

The effect of Mn and Fe on Co, Ni, Cu, and Pb determinations

Analyses of more than 100 sediment samples collected from various mineralized areas show that in the hydroxylamine extract the concentration of Mn ranges from several tens to a few thousands of micrograms per milliliter and that of Fe generally ranges from 5 to 20 μg/ml, although occasionally some may range from 40 to 50 μg/ml. In order to adopt the APDC-MIBK chelate-extraction method for the determination of Co, Ni, Cu, and Pb in the hydroxylamine extract, it was essential to test whether such concentrations of Mn and Fe could interfere with the determination of microgram levels of the four metals.

Solutions were prepared containing known amounts of Co, Ni, Cu, and Pb, and of either Mn or Fe, and the same concentration of the hydroxylamine extracting solution as the sample extract. These solutions were analyzed for the metals according to the procedure just described. Recovery of the four metals in the presence of different amounts of Mn and Fe is shown in tables 3, 4, and 5. Table 3 presents data indicating no interference of 6,000 to 20,000 μg Mn (in 10 ml) with the determinations of 1 μg Co and Ni, and 5 μg Cu and Pb. Table 4

Table 3.—*Recovery of* Co, Ni, Cu, *and* Pb *from 10-ml solutions containing 0 to 20,000* μg Mn *(average of duplicates)*

Mn in 10-ml solution (μg)	Recovery (μg)			
	Co	Ni	Cu	Pb
0	1.0	1.0	5.0	5.0
6,000	1.0	1.0	5.2	5.0
10,000	1.0	1.0	5.0	5.1
16,000	1.0	1.0	5.1	5.0
20,000	1.0	1.0	5.0	5.1

Table 4.—*Recovery of* Co, Ni, Cu, *and* Pb *from 10-ml solutions containing 10,000* μg Mn *(average of four replicates)*

Element	Present (μg)	Recovered (μg)	Standard deviation (μg)	Relative standard deviation (percent)
Co	0.5	0.5	0.015	3.0
	2.0	2.1	.045	2.3
Ni	.5	.5	.027	5.4
	2.0	2.0	.046	2.3
Cu	5.0	5.2	.24	4.8
	20.0	20.2	.27	1.4
Pb	3.0	3.0	.033	1.1
	12.0	12.2	.27	2.3

shows the results of recovery of two levels of each of the four metals in the presence of a constant amount of Mn (10,000 μg in 10-ml solution) with calculated relative standard deviations for replicate analyses. Iron in amounts ranging from 50 to 500 μg in 10 ml of solution does not seem to influence the recovery of 0.5 μg Co, 1.0 μg Ni, 5.0 μg Cu, and 1.0 μg Pb as evidenced in table 5. Data on the recovery of known amounts of Co, Ni, Cu, and Pb added to hydroxylamine extracts of two sediment samples are presented in table 6.

A turbidity has been observed at the interface between the MIBK and aqueous phases with Mn concentrations greater than 10,000 μg in 10 ml solution. Presumably, this turbidity may be caused by formation of the unstable Mn-APDC complex (Mansell, 1965; Yanagisawa and others, 1968; Jenne and Ball, 1972); however, it has not interfered with the determination of any of the four metals.

Table 5.—*Recovery of* Co, Ni, Cu, *and* Pb *from 10-ml solutions containing 0 to 500 μg* Fe *(average of duplicates)*

Fe in 10-ml solution (μg)	Recovery (μg)			
	Co	Ni	Cu	Pb
0	0.5	1.0	5.0	1.0
50	.5	1.0	5.0	1.0
100	.5	1.0	4.9	...
200	.5	1.0	4.9	1.0
300	.5	1.0	5.0	...
400	.5	1.0	5.0	1.1
500	.5	1.0	5.2	.9

Table 6.—*Recovery of* Co, Ni, Cu, *and* Pb *from 10 ml of two sample solutions (hydroxylamine extracts) containing varying amounts of* Mn *and* Fe *(average of triplicates)*

Sample solution No.		Mn	Fe	Co	Ni	Cu	Pb
1	Present (μg/10 ml)	6,000	290	4.7	1.9	21.4	9.6
	Added (μg)			.7	.7	6.0	3.6
	Recovered (μg)			.7	.6	5.8	3.4
2	Present (μg/10 ml)	1,270	433	3.8	1.7	14.4	3.5
	Added (μg)			.7	.7	6.0	3.6
	Recovered (μg)			.6	.6	6.2	3.4

Two sediment samples (lab. Nos. 603305 and 613051) with distinctly different contents of hydroxylamine-extractable Mn and Fe were analyzed following the described procedure (table 7). Relative standard deviations range from 0.6 to 5.9 percent, excluding the Cu determination for sample 603305 which contains Cu at a very low concentration of 1.3 ppm.

Thus, the procedure as outlined is capable of recovering known amounts of Co, Ni, Cu, and Pb from both synthetic and sample solutions containing large amounts of Mn or Fe, and it provides reproducible results of analysis for the seven metals.

Sample size

The dissolution of manganese oxides from soil or sediment samples by acidified hydroxylamine hydrochloride is accomplished mainly through reduction; therefore, there is a limit to the amount of manganese oxides that can be brought into solution. When the reducing capacity of a fixed volume of the hydroxylamine solution is reached, no more manganese oxides will be dissolved. This statement was proved in the present investigation by experiments on the dissolution of a sample of manganese oxides containing 46.4 percent Mn and 0.4 percent Fe. There was a nearly proportional increase in Mn in the hydroxylamine extract with sample size ranging from 0.10 to 0.30 g, beyond which the dissolution of Mn leveled off to a constant value with further increments of sample size. The break of the manganese dissolution curve occurred at a manganese concentration of about 2,500 μg/ml in the extract. If 10 ml of the extract is taken for the APDC-MIBK chelation-extraction, this would mean that microgram levels of Co, Ni, Cu, and Pb can be determined in the presence of 25,000 μg Mn. The dissolution of Fe, on the other hand, decreased continuously with increasing sample size. At a sample weight of 1.00 g, no Fe was detected in the hydroxylamine extract.

Table 7.—*Eight replicate analyses of seven metals extracted from two sediment samples by 0.1* M *hydroxylamine hydrochloride in 0.01* M HNO_3 *(pH = 2)*

Sample No.	Mn	Fe	Zn	Co	Ni	Cu	Pb
603305:							
Average (ppm).	15,400	2,315	153.4	47.8	6.8	1.3	100.6
Relative standard deviation (percent).	.6	2.4	3.6	3.8	5.9	15.4	4.4
613051:							
Average (ppm).	3,733	693	122.8	38.7	8.1	19.8	55.9
Relative standard deviation (percent).	4.3	2.1	4.2	5.2	4.9	3.5	2.3

On the basis of the preceding discussion, no more than 20,000 μg Mn should be present in the 10-ml aliquot of the extract taken for analysis. This amount corresponds to 10 percent hydroxylamine-extractable Mn in the sample, assuming a sample weight of 0.50 g. Soil or sediment samples, except those containing high-manganese ferromanganese nodules or concretions, contain less than 10 percent hydroxylamine-extractable Mn. For those samples that contain more than 10 percent hydroxylamine-extractable manganese, the sample weight should be reduced accordingly.

REFERENCES CITED

Allan J. E., 1961, The determination of copper by atomic absorption spectrophotometry: Spectrochim. Acta, v. 17, p. 459–466.

Brooks, R. R., Presley, B. J., and Kaplan, I. R., 1967, APDC-MIBK extraction system for the determination of trace-elements in saline waters by atomic absorption spectrophotometry: Talanta, v. 14, p. 809–816.

Burrell, D. C., 1967, Trace elements in marine waters by atomic absorption spectrophotometry: Anal. Chim. Acta, v. 38, p. 447–455.

Canney, F. C., 1966, Hydrous manganese-iron oxide scavenging—Its effect on stream sediment survey [abs.]: Canada Geol. Survey Paper 66-54, p. 11–12.

Chao, T. T., 1972, Selective dissolution of manganese oxides from soils and sediments with acidified hydroxylamine hydrochloride: Soil Sci. Soc. America Proc., v. 36, p. 764–768.

Fishman, M. J., and Midgett, M. R., 1968, Extraction techniques for the determination of cobalt, nickel, and lead in fresh water by atomic absorption, [Chap.] 12 *in* Trace inorganics in water—A symposium: Am. Chem. Soc. Adv. Chemistry Ser. 73, p. 230–235.

Hawkes, H. E., and Webb, J. S., 1962, Geochemistry in mineral exploration: New York and Evanston, Harper and Row Publishers, 415 p.

Horsnail, R. F., Nichol, I., and Webb, J. S., 1969, Influence of variations in secondary environment on the metal content of drainage sediments: Colorado School Mines Quart., v. 64, no. 1, p. 307–322.

Jenne, E. A., 1968, Controls on Mn, Fe, Co, Ni, Cu, and Zn concentrations in soils and water—The significant role of hydrous Mn and Fe oxides, [Chap. 2] *in* Trace inorganics in waters—A symposium: Am. Chem. Soc. Adv. Chemistry Ser. 73, p. 337–339.

Jenne, E. A., and Ball, J. W., 1972, Time stability of aqueous APDC and its manganese and nickel complexes in MIBK: Atomic Absorption Newsletter, v. 11, no. 4, p. 90–91.

Mansell, R. E., 1965, Notes on the extraction of manganese with chelating agents and MIBK: Atomic Absorption Newsletter, v. 4, no. 5, p. 276–277.

Sprague, Sabina, and Slavin, Walter, 1964a, Determination of very small amounts of copper and lead in KCl by organic extraction and atomic absorption spectrophotometry: Atomic Absorption Newsletter, no. 20, p. 11–15.

——1964b, The determination of nickel in urine by atomic absorption spectrophotometry—Preliminary study: Atomic Absorption Newsletter, v. 3, no. 11, p. 160–164.

Yanagisawa, Masaaki, Suzuki, Masami, and Tukeuchi, Tsugio, 1968, Extraction of manganese dithiocarbamate complexes for atomic absorption spectrophotometry: Anal. Chim. Acta, v. 43, p. 500–502.

Jour. Research U.S. Geol. Survey
Vol. 1, No. 6, Nov.-Dec. 1973, p. 687–689

ARCHAEOCYCAS AND PHASMATOCYCAS—NEW GENERA OF PERMIAN CYCADS

By SERGIUS H. MAMAY, Washington, D.C.

Abstract.—The generic names *Archaeocycas* and *Phasmatocycas* are introduced for two previously announced but unnamed new genera of Early Permian plants; these taxa are regarded as early stages in the cycadean lineage. The names are formalized with diagnoses, illustrations, and type designations.

BACKGROUND

In a previous article (Mamay, 1969) I gave preliminary descriptions of two new genera of fossil plants on the basis of fertile organs from Lower Permian rocks of Texas and Kansas. These structures were, and are, regarded as evidence of Paleozoic origin of the cycads. Hypothetical evolutionary implications of the plants were discussed briefly, but new names were not introduced. The taxa were referred to only as "new genus A" and "new genus B." A formalized nomenclature, complete descriptions, and pertinent discussions were deferred.

The 1969 article was subsequently discussed in at least two publications by other authors. Delevoryas and Hope (1971) briefly mentioned the new fossils and some of my interpretations. Sporne (1971) also commented on the Permian fossils, duplicating some of my illustrations and pointing out the nomenclatural limbo of the material. In discussing these fossils relative to early angiosperm evolution, however, Sporne added credence to my cautiously qualified hypothesis involving derivation of a carpellike organ from new genus B, and attributed to me a claim of discovery (Sporne, 1971, p. 14: "Fig. 18. The origin of the carpel, according to Mamay * * * .") that I had neither expressed nor intended at the time of publication of the Science article. Thus, in these days of intensified search for the origins of angiospermy, the Texas fossils may become the subject of debate among theoretical plant morphologists.

In recognition of the possibly controversial future of these fossils, and in deference to inquiries as to their nomenclatural status, it seems appropriate to apply formal names at this time. This renders it possible for "new genus A" and "new genus B" to be discussed henceforth with benefit of legitimate names.

SYSTEMATIC DESCRIPTIONS

Order CYCADALES

Genus ARCHAEOCYCAS Mamay, n. gen.

New genus B. Mamay, 1969, Science, v. 164, no. 3877, p. 295–296, fig. 1.

Generic diagnosis.—Bilaterally symmetrical fertile appendage (megasporophyll) with broad midrib; several pairs of apparently sessile, closely appressed ovules borne in two lateral rows on surface of reduced basal part of lamina; ovules closely invested by lamina, each ovule with a small circular scar of attachment to lamina near midrib. Distal part of appendage expanded as flattened, sterile foliar blade.

Type species: Archaeocycas whitei Mamay, n. sp.

Figure 1*a–c*

Specific diagnosis.—Megasporophylls cuneiform, ovate, or lanceolate, 1.7 to 2.3 cm long, with greatest widths of 1.0 cm. Midribs straight, flat, faintly marked with closely set, parallel striations; midrib widths uniform or increasing distally from 1.0 to 1.3 mm at the bases, to 3.0 mm at distal termini of fertile areas; midribs flaring out conspicuously or becoming obscure in distal laminar parts of megasporophylls; sides of midribs more or less concavely scalloped through appression with ovule bases.

Proximal fertile area 1.2 to 1.6 cm long, 3.0 to 5.0 mm wide at base, nearly uniform in width or increasing distally to width of 9.0 mm. Ovules produced in opposite pairs, 4 to 6 ovules in each row. Ovules oblong, oblanceolate, rhombic or rhomboidal, tightly appressed with each other, obliquely directed forward at broad angles to the rachis. Basalmost ovules proportionately shorter, broader than distal ones; ovules 1.5 to 3 mm long (measured along lines of appression between contiguous ovules), 1.5 to 3.0 mm wide (measured along outer free margins and along lines of appression with the rachis), reaching 5 mm in greatest (diagonal) dimension. Ovules each with a small circular shallow depression or attachment scar, 0.7 to 1.0 mm in diameter, uniformly placed on the upper surfaces of ovules near the center of area of ovular appression with the midrib. Upper (adaxial) surfaces of

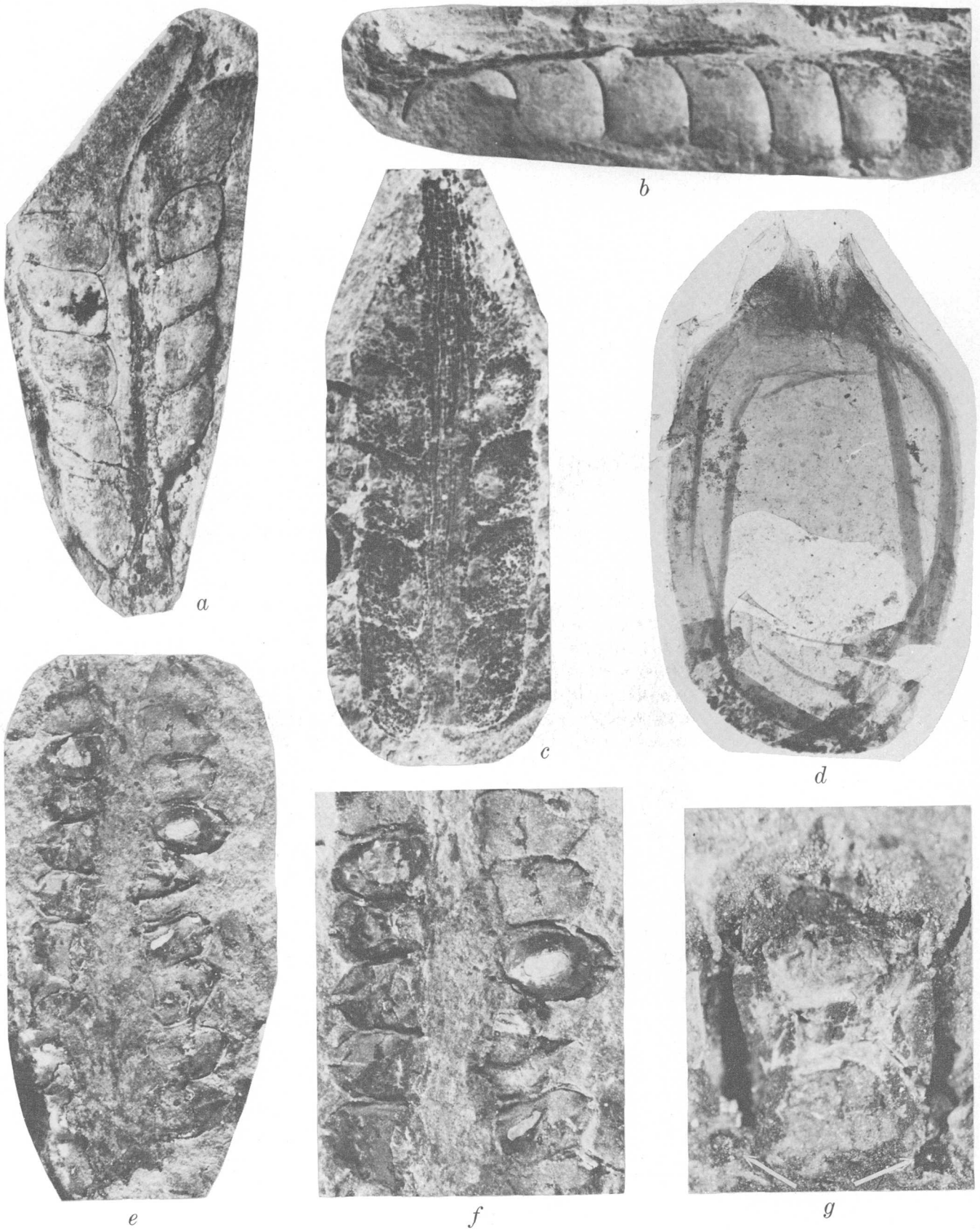

Figure 1.

ovules closely invested by foliar lamina; extent of lamina over lower (abaxial) ovular surfaces unknown; laminar investment of ovules showing fine closely spaced parallel striations perpendicular to midrib.

Megasporophylls abruptly modified into sterile laminar structures immediately distal to uppermost pair of ovules and contiguous with ovules; extent, venation, and margination of distal laminae obscure.

Holotype.—USGS 8877-1 (fig. 1*a*).

Occurrences.—USGS localities 8877, 8959 (Belle Plains Formation, Lower Permian, Baylor County, Tex.).

Derivation of names.—Generic name refers to the antiquity of the genus; specific name acknowledges David White's discovery of the holotype and other specimens.

Genus PHASMATOCYCAS Mamay, n. gen.

New genus A. Mamay, 1969, Science, v. 164, no. 3877, p. 295–296, fig. 1.

Generic diagnosis.—Fertile axis with two lateral rows of sessile broadly attached gymnospermous ovules; ovules simple, with blunt funnel-shaped micropyles, two distinct cuticular layers and a thick megaspore membrane; laminar tissue unknown, interseminal appendages lacking.

Type species: Phasmatocycas kansana Mamay, n. sp.

Figure 1*d–g*

Specific diagnosis.—Axial fragment 2.5 cm long, relatively stout, from 2.5 to 4.0 mm wide, rather abruptly broader at (?)basal end of specimen; surface of axis with obscure narrow longitudinal striations, lacking other characteristic markings.

Bilateral arrangement of ovules symmetrical, with no evidence of ovules between lateral rows. Ovules inserted alternately to suboppositely, extending virtually perpendicularly to axis, closely arranged so as to juxtapose against but not overlap each other. Ovules 2.8 to 4.0 mm long, 2.0 to 2.6 mm wide, ovate to oblong, broadly attached with point of attachment to axis nearly as long as greatest width of ovule; ovular apices blunt, some specimens with a shallow apical cleft or notch.

Cuticular envelopes slightly smaller than impressions of ovules, lacking ornamentation; cuticles apparently complete except for micropylar openings; apices of cuticles gradually decreasing in diameter, without marked constriction, terminating in micropylar openings from 0.2 to 0.5 mm wide; specialized chalazal features absent. Outer cuticle very thin, diaphanous, with elongate cells reaching 20 by 80 μ in dimensions, parallel to long axis of ovule. Inner cuticle apparently thicker and separate from outer; cells thick-walled, walls abruptly increasing in thickness toward the micropylar area; cells in micropylar area virtually isodiametric, averaging 10 μ in diameter. Megaspore membrane nearly filling cavity within cuticles; membrane dense, lacking ornamentation.

Small (0.25–0.33 mm in diameter) spherical sessile bodies with resinlike luster regularly alternating with ovules in each row, one such body partly imbedded in axial tissue at point between and approximately level with bases of two adjacent ovules.

Holotype.—USGS 8869-1 (figs. 1*d–g*).

Occurrence.—USGS locality 8869 (Wellington Formation, Lower Permian, Dickinson County, Kans.).

Derivation of names.—*Phasmatocycas* derives from the Greek "phasma" (apparition; phantom) and the modern generic name *Cycas; kansana* refers to geographic source of material.

Figure 1.—*Archaeocycas* and *Phasmatocycas*, new genera of Permian cycads.

a–c. *Archaeocycas whitei* Mamay, n. sp. *a*, Ventral view of holotype (USGS 8877-1), × 6; *b*, lateral view of sporophyll, dark spots near midrib representing points of ovule attachment (USGS 8877-2), × 6; *c*, ventral view of sporophyll, showing circular points of ovular attachment on either side of midrib (USGS 8959-1), × 6.

d–g. *Phasmatocycas kansana* Mamay, n. sp. *d*, Macerated cuticular system of seed removed from holotype, × 30; *e*, holotype (USGS 8869-1), × 4; *f*, more enlarged part of holotype, × 6; *g*, single seed on holotype, arrows indicating resinoid globules at either side of seed base, × 21.

REFERENCES CITED

Delevoryas, Theodore, and Hope, R. C., 1971, A new Triassic cycad and its phyletic implications: Postilla, no. 150, p. 1–21, figs. 1–12.

Mamay, S. H., 1969, Cycads: Fossil evidence of late Paleozoic origin: Science, v. 164, no. 3877, p. 295–296, fig. 1.

Sporne, K. R., 1971, The mysterious origin of flowering plants: London, Oxford Univ. Press, 16 p., 21 figs.

Jour. Research U.S. Geol. Survey
Vol. 1, No. 6, Nov.-Dec. 1973, p. 691–693

EARLY PLEISTOCENE(?) POLLEN SPECTRA FROM NEAR LAKE TAHOE, CALIFORNIA

By DAVID P. ADAM, Menlo Park, Calif.

Abstract.—Fossil pollen was recovered at Tahoe City, Calif., from beneath a 1.9-m.y.-old volcanic flow. Pollen counts of four fossil samples are compared with soil-surface pollen samples from the Sierra Nevada. The presence of *Picea* (spruce) pollen in the fossil samples suggests that summer drought conditions in the central Sierra Nevada were less severe prior to 1.9 m.y. ago than they are now.

Fossil pollen has been recovered from beneath a 1.9-m.y.-old olivine latite flow (Dalrymple, 1964; Birkeland, 1963) near the outlet of Lake Tahoe, Calif. The site (fig. 1), in a gravel quarry on the north side of the Truckee River about 0.7 km west of the Lake Tahoe dam is at an elevation of about 1,900 m in a mixed coniferous forest (*Pinus* spp., *Abies* spp., and *Libocedrus decurrens* Torr. predominate). The area now has a Mediterranean climate; summers are dry (fig. 2; see also Storer and Usinger, 1963; Russell, 1947).

The fossil pollen was recovered from a bed of clayey silt. Although the strata dip about 10°–15° SE., the fine grain size and the visible organic detritus in the pollen-bearing stratum suggest that it was laid down nearly horizontally in standing water. The fossiliferous unit, which is less than a meter thick, is conformably overlain by about 15 m of crossbedded sand, gravel, and cobbles. These sediments were probably deposited by a river flowing into the Tahoe Basin from the north, or they may have been deposited by the Truckee River in a local pond created by a lava dam.

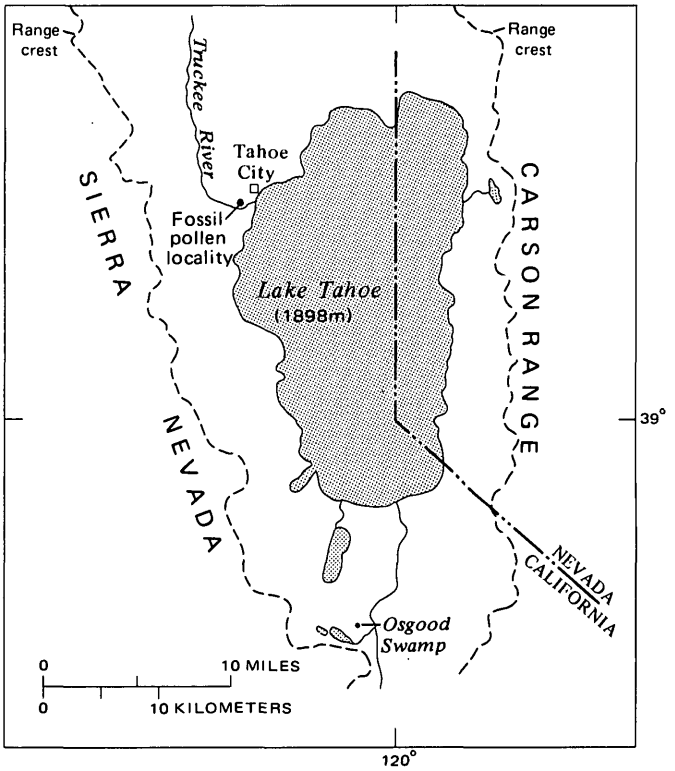

Figure 1.—Map of Lake Tahoe and vicinity, California and Nevada, showing the fossil pollen locality and Osgood Swamp. The crests of the Sierra Nevada and the Carson Range provide a rough outline of the Tahoe graben.

PROCEDURES

One soil-surface pollen sample was collected from the vicinity of the fossil samples by pooling 20 pinches of dirt from an area about 50 m square. Because of the high frequencies of *Pinus* pollen, all samples were counted using double fixed sums (Mehringer and Haynes, 1965; Adam, 1967). Two hundred grains of all pollen were counted for each sample, and this count was used to estimate the frequency of pine pollen. The second sum consisted of 100 nonpine pollen grains for all samples, except for fossil sample 2, in which 200 nonpine grains were counted. A total of some 1,686 fossil and 383 modern pollen grains was counted by this procedure. The results are presented in table 1; the frequencies for all types except pine are expressed as percentages of the second sum.

DISCUSSION

The fossil counts were compared with the soil-surface pollen sample from the site and also with transects of soil-surface pollen samples across the Sierra Nevada (Adam, 1967, figs. 3 and 4). The fossil samples most strongly resemble surface samples from about 300 m lower on the western slope of the Sierra, but with one important exception: the second sums of the fossil samples contain between 6 and 11 percent *Picea*

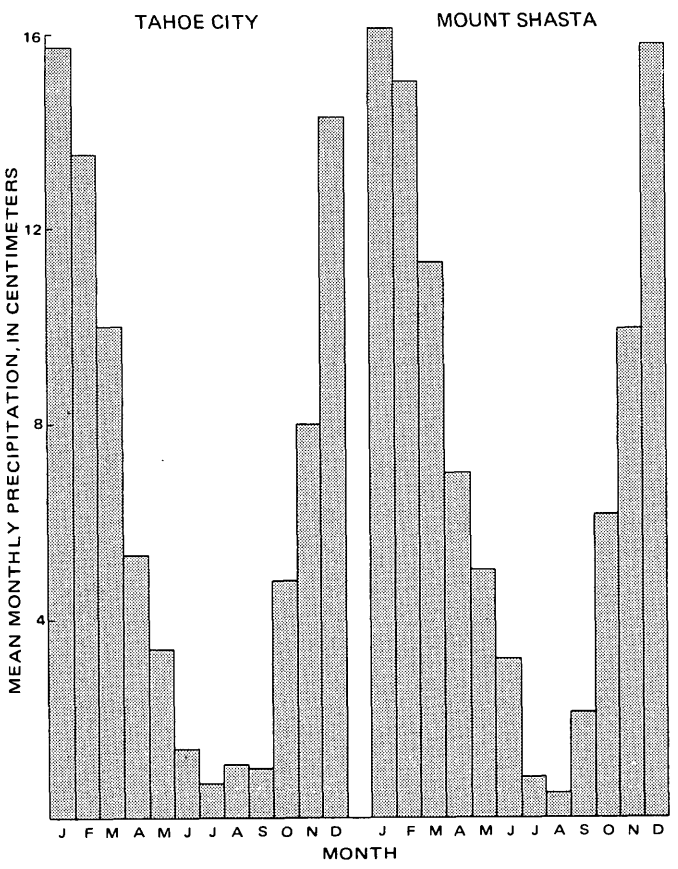

Figure 2.—Mean monthly precipitation, in centimeters, for Tahoe City and Mount Shasta, Calif. (Shasta City). Data from U.S. Weather Bureau California climatic summary.

Table 1.—*Counts of modern and fossil pollen grains from Tahoe City, Calif.*

[TCT includes Taxodiaceae, Cupressaceae, and Taxaceae; high-spine Compositae have spines >1μ; low-spine Compositae have spines <1μ; all other nomenclature follows Munz and Keck (1963)]

Pollen type	Modern pollen (percent)	Fossil pollen (percent)			
		1	2	3	4
Pinus (first count, *N*=200).	72.5	70.5	70.5	63.0	75.0
Abies	36.0	9.0	6.0	2.0	24.0
Picea	0	11.0	9.0	6.0	11.0
TCT	7.0	41.0	39.0	40.0	15.0
Tsuga	1.0	0	0	0	1.0
Pseudotsuga	0	1.0	.5	0	1.0
Arceuthobium	5.0	1.0	.5	1.0	1.0
Quercus	27.0	17.0	12.5	16.0	17.0
Fraxinus	0	0	2.5	1.0	0
Juglans	1.0	0	0	0	0
Alnus	4.0	0	0	0	0
Betula	0	0	0	1.0	0
Cornus	0	0	0	1.0	0
Cyperaceae	1.0	5.0	2.5	3.0	3.0
High-spine Compositae	4.0	1.0	1.0	0	0
Low-spine Compositae	1.0	0	1.0	1.0	1.0
Artemisia	1.0	9.0	7.0	12.0	8.0
Chenopodiaceae plus *Amaranthus*.	1.0	3.0	2.5	2.0	2.0
Sarcobatus	0	0	1.0	1.0	1.0
Ericaceae	2.0	0	0	0	0
Rhamnaceae	3.0	0	1.0	1.0	0
Gramineae	1.0	1.0	8.5	3.0	4.0
Caryophyllaceae	0	0	0	0	1.0
Polygonum, persicaria-type.	0	0	0	1.0	0
Polygonum, californicum-type.	0	0	0	0	1.0
Eriogonum	0	0	.5	1.0	0
Rosaceae	0	0	1.0	0	0
Ranunculaceae	1.0	0	0	0	0
Euphorbia	2.0	0	0	0	0
Malvaceae	0	0	0	0	1.0
Oenothera-type	0	0	0	0	1.0
Unknowns	2.0	1.0	4.0	7.0	7.0
Second sum sample (excluding pine).	100	100	200	100	100

(spruce) pollen. Spruce is not found in the Sierra Nevada today; the nearest recorded locality is on Mount Shasta, more than 250 km northwest of the fossil site (Munz and Keck, 1963; Fowells, 1965; Little, 1971). Spruce pollen is absent not only from all modern and postglacial pollen samples that I have studied from the Sierra Nevada, but also from late glacial samples from Osgood Swamp (Adam, 1967), 37.5 km south of the Tahoe City fossil site and about 100 m higher (fig. 1). However, minor amounts of *Picea* cf. *P. engelmannii* pollen occur regularly in the modern pollen rain at Searles Lake, Calif., which is located about 65 km east of the Sierra Nevada and 450 km southeast of the Tahoe City site (Leopold, 1967, and written commun., 1973). The Mount Shasta spruce population is 700 km to the northwest, but other possible sources for the Searles Lake spruce pollen are located about 450 km to the east and northeast in northern Arizona, south-central Utah, and east-central Nevada (Little, 1971).

I was unable to determine the species of spruce represented in the Tahoe City pollen. However, on the basis of modern distributions of the several North American species of *Picea* (Little, 1971), the most probable species for the spruce in the fossil samples is *P. engelmannii* Parry; the other reasonable possibility is *P. breweriana* S. Watson, which is common in Neogene floras from Nevada (Wolfe, 1969, and oral commun., 1972).

The present southern limit of the distribution of *Picea* in North America appears to be related partly to a requirement for adequate summer rainfall. Wolfe and Leopold (1967) have noted that the southern limit for spruce generally follows the 21°C July mean temperature isotherm, but they further note that the observed exceptions to this rule are a result of low precipitation. Fowells (1965, p. 299) states that for *P. engelmannii*, "Average precipitation exceeds 25 inches annually with only moderate or no seasonal deficiency."

A comparison of the mean monthly precipitation values for U.S. Weather Bureau stations at Tahoe City and Mount Shasta supports this conclusion (fig. 2). Both July and August are very dry months at both stations, but at Tahoe City the dry season includes June and September as well, whereas the Mount Shasta station receives more than 2 cm of rain in each

of those months. This indicates that Engelmann spruce probably cannot tolerate more than a few months of summer drought.

Furthermore, the Sierra Nevada includes a wide range of temperature regimes, which suggests that temperature probably is not the critical factor responsible for the modern absence of spruce from the range. The absence of spruce from the Sierra Nevada is more likely the result of extended summer drought.

If this is so, then the Osgood Swamp pollen record (Adam, 1967) suggests that summer drought prevailed even during late Tioga (Wisconsinan) time and has persisted during the postglacial period. The Tahoe City samples indicate that the summer climate of the Sierra Nevada was different prior to 1.9 m.y. ago, and it is tempting to speculate that the Pacific high-pressure cell must have dominated the summer climate of northern California less than it does now.

The conditions that permitted the survival of spruce in the Sierra Nevada may have persisted over a long period. The K/Ar date provides only a minimum age for the Tahoe City deposits, although the field relations between the dated flow and the underlying sediments suggest that the samples are not very much older. However, the samples could be at least as old as the Verdi flora (about 30 km northeast), which has yielded a K/Ar date of 5.7 m.y. (Evernden and James, 1964) and which contains spruce pollen (H. E. Schorn, oral commun., 1972).

Only four of the fossil samples from Tahoe City contained pollen, and they do not provide a sufficient basis for making a detailed analysis of the paleoclimate or elevation of the site at the time of their deposition. However, the site has been destroyed by borrow operations, and thus the data cannot be duplicated. They are recorded here in the hope that they may be of use to others in a broader context.

ACKNOWLEDGMENTS

Parts of this work were done while the author held a National Science Foundation (NSF) graduate fellowship at the University of Arizona, and other support came from NSF grant GB-1959 to Paul S. Martin. V. C. LaMarche, Jr., P. J. Mehringer, Jr., J. A. Wolfe, and E. B. Leopold made suggestions which improved the manuscript.

REFERENCES CITED

Adam, D. P., 1967, Late-Pleistocene and recent palynology in the central Sierra Nevada, California, *in* Cushing, E. J., and Wright, H. E., Jr., eds., Quaternary paleoecology: New Haven, Yale Univ. Press, p. 275–301.

Birkeland, P. W., 1963, Pleistocene volcanism and deformation of the Truckee area north of Lake Tahoe, California: Geol. Soc. America Bull., v. 74, p. 1453–1464.

Dalrymple, G. B., 1964, Cenozoic chronology of the Sierra Nevada, California: California Univ. Pubs. Geol. Sci., v. 47, p. 1–41.

Evernden, J. F., and James, G. T., 1964, Potassium-argon dates and the Tertiary floras of North America: Am. Jour. Sci., v. 262, no. 8, p. 945–974.

Fowells, H. A., 1965, Silvics of forest trees of the United States: U.S. Dept. Agriculture Handbook 271, 761 p.

Leopold, E. B., 1967, Summary of palynological data from Searles Lake, *in* Pleistocene geology and palynology of Searles Valley, California–Friends of the Pleistocene, Pacific Coast Sec., Mtg., Sept. 23–24, 1967, Guidebook: p. 52–66.

Little, E. L., 1971, Atlas of the United States trees: U.S. Dept. Agriculture Misc. Pub. 1146, 8 p., 200 maps, 9 pl.

Mehringer, P. J., Jr., and Haynes, C. V., Jr., 1965, The pollen evidence for the environment of early man and extinct mammals at the Lehner mammoth site, southeastern Arizona: Am. Antiquity, v. 31, p. 17–23.

Munz, P. A., and Keck, D. D., 1963, A California flora: Berkeley, California Univ. Press, 1681 p.

Russell, R. J., 1947, Sierra climate, *in* Peattie, R., ed., The Sierra Nevada: the range of light: New York, Vanguard Press, p. 323–340.

Storer, T. I., and Usinger, R. L., 1963, Sierra Nevada natural history: Berkeley, California Univ. Press, 374 p.

Wolfe, J. A., 1969, Neogene floristic and vegetational history of the Pacific northwest: Madroño, v. 20, p. 83–110.

Wolfe, J. A., and Leopold, E. B., 1967, Neogene and Early Quaternary vegetation of northwestern North America and northeastern Asia, *in* Hopkins, D. M., ed., The Bering land bridge: Palo Alto, Stanford Univ. Press, p. 193–206.

Jour. Research U.S. Geol. Survey
Vol. 1, No. 6, Nov.-Dec. 1973, p. 695–700

THE LATE CRETACEOUS AMMONITE TRACHYSCAPHITES PULCHERRIMUS (ROEMER) IN NEW JERSEY AND TEXAS

By W. A. COBBAN, Denver, Colo.

Abstract.—*Trachyscaphites pulcherrimus*, described originally by Ferdinand Roemer in 1841 from fragments of nodose ammonites from Germany, is characterized by having five rows of tubercles on each flank of the phragmocone and three to five rows on each side of the body chamber. Weak midventral tubercles are present on some specimens. Ribbing is dense and usually irregular. The species has been recorded from upper Campanian rocks in Germany, Austria, France, Poland, and Russia. Recently a few specimens have been found at the top of the Wenonah Formation of New Jersey and in the Taylor Marl of Texas.

Trachyscaphites pulcherrimus (Roemer) has been known from the Upper Cretaceous of Europe since 1841 where it has served as a guide fossil to rocks of late Campanian age. The species is readily identified by rather dense irregular ribbing and by five rows of tubercles on the flank of the septate coil and three to five rows on each side of the body chamber. Recently several specimens were discovered near Marlboro, Monmouth County, N.J., and near Kimbro, Travis County, Tex. The New Jersey specimens, found by Messrs. John Brzostoski and Richard Heintz, River Plaza, N.J., were made available to me for study through the kind efforts of Mr. Harold Mendryk, Harrison, N.J. These specimens, internal molds of gray very fine grained soft micaceous sandstone, are from the top of the Wenonah Formation according to Mr. Mendryk (written commun., July 17, 1971). The Texas specimens are from hard limestone concretions containing much barite in the Taylor Marl on Cottonwood Creek 1 mile northwest of Kimbro, Travis County. Two of the four Texas specimens were made available for study by Dr. Keith Young, University of Texas, Austin. I greatly appreciate the loans from Mr. Brzostoski and Dr. Young and the donations from Mr. Heintz.

The photographs were made by Robert E. Burkholder, of the U.S. Geological Survey. Specimens that have USNM numbers are in the National Museum of Natural History in Washington, D.C. Plaster casts of all figured specimens are in the National Museum of Natural History and in the Cretaceous collections of the U.S. Geological Survey at the Federal Center, Denver, Colo.

According to Schlüter (1872, p. 86), Roemer (1841, p. 91) based his species on fragments of nodose scaphites. Roemer noted that the species had five rows of tubercles on each side, but his single illustration showed a lateral view of a septate coil having four rows of tubercles on a side. Schlüter accepted Roemer's description, but he assigned Roemer's illustrated specimen to the new species *Scaphites spiniger* Schlüter. Two specimens were illustrated by Schlüter as examples of *S. pulcherrimus*. The larger specimen, 90 mm in length, is preserved in the Geologisch-palaeontologisches Institut und Museum, Bonn, Germany, and a plaster cast (fig. 1*k*, *l*) is in the U.S. Geological Survey's Cretaceous collections at the Federal Center, Denver, Colo. The smaller specimen may have been lost during World War II.

TRACHYSCAPHITES PULCHERRIMUS (ROEMER)

Figures 1 and 2

1841. *Scaphites pulcherrimus* Roemer, p. 91 (not pl. 14, fig. 4).
1866. *Scaphites multinodosus* von Hauer, p. 306, pl. 1, figs. 7, 8.
1872. *Scaphites pulcherrimus* Roemer. Schlüter, p. 85, pl. 26, figs. 1–5.
1893. *Scaphites pulcherrimus* Roemer. De Grossouvre, p. 250, pl. 32, figs. 6, 9a, b [1894].
1916. *Acanthoscaphites pulcherrimus* (Roemer). Nowak, p. 63.
1925. *Scaphites (Acanthoscaphites) pulcherrimus* Roemer. Diener, p. 206.
1927. *Acanthoscaphites pulcherrimus* (Roemer). Reeside, p. 33.
1951. *Acanthoscaphites pulcherrimus* (Roemer). Mikhailov, p. 96, pl. 18, figs. 83, 84.
1959. *Acanthoscaphites pulcherrimus* (Roemer). Naidin and Shimanskii, p. 195, pl. 6, fig. 14.
1964. *Trachyscaphites pulcherrimus* (Roemer). Cobban and Scott, p. E1.
1968. *Scaphites pulcherrimus* Roemer. Arnold, p. 314, text fig. 36.

Schlüter's drawing of the larger specimen is reversed and idealized (Schlüter, 1872, pl. 26, figs. 1–3). It shows a septate coil having numerous rectiradiate ribs and five equal-spaced rows of small tubercles, and a body chamber having fewer ribs, a few conspicuous umbilical tubercles, and three outer rows of tubercles. Tubercles on opposite sides of the midline of the venter are arranged in a zigzag manner. The drawing shows the

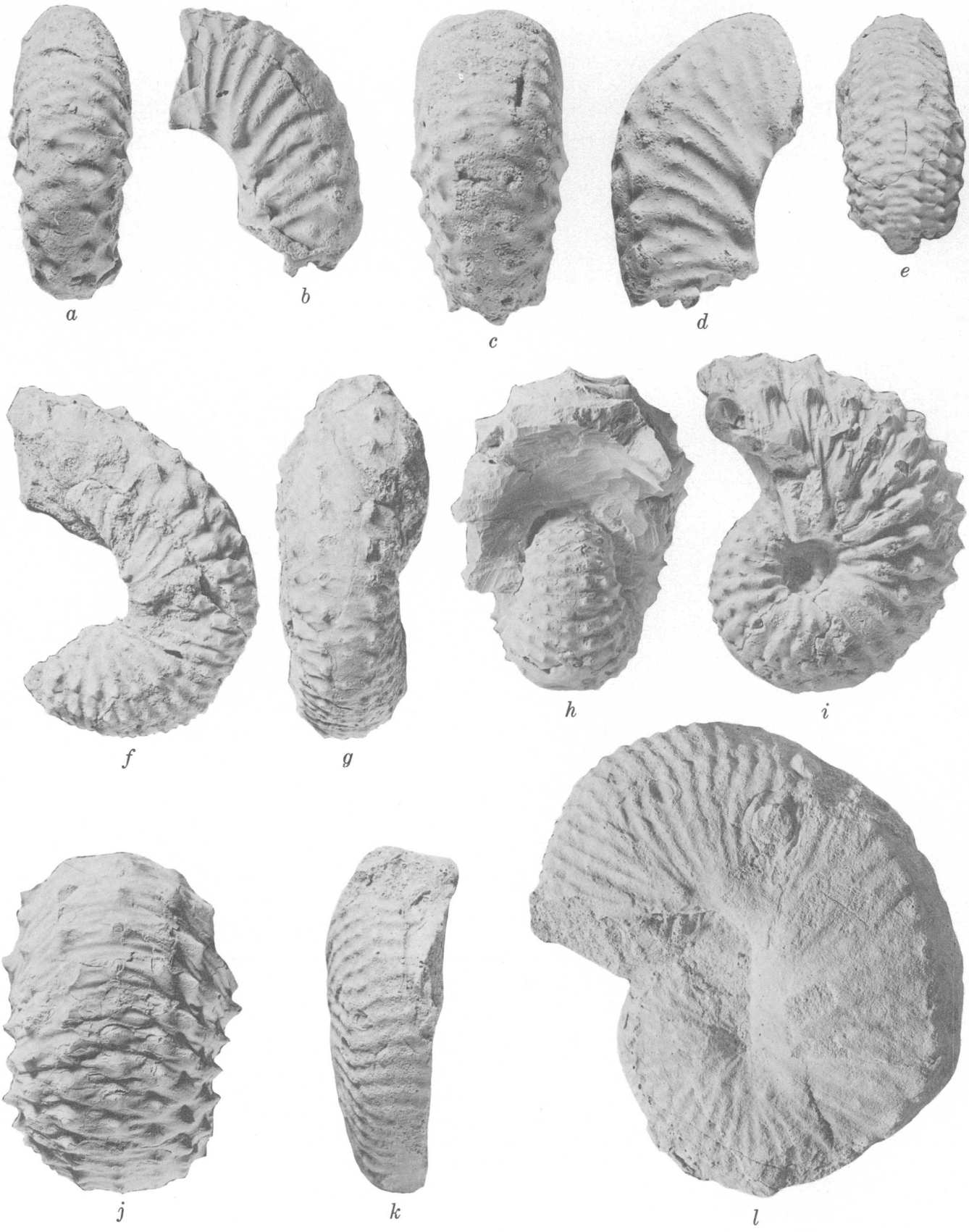

Figure 1.

innermost of the three outer rows of tubercles on the venter extending back to and connecting with the fourth row out from the umbilicus on the septate coil. According to this arrangement, the species could be interpreted as having six rows of tubercles on a side. The plaster cast, however, reveals a rather poorly preserved specimen on which the innermost of the three outer rows of tubercles can be just as well connected to the third row out from the umbilicus on the septate coil. The cast also reveals the presence of a fourth row of very weak tubercles on the younger part of the body chamber. The specimen can be interpreted as a female by its large size, very small umbilicus, and broad body chamber having a slightly convex umbilical wall (Cobban, 1969, p. 10–11). The smaller of Schlüter's specimens is a body chamber that has a concave umbilical wall; it can be interpreted as a male. Schlüter's drawing shows seven or eight umbilical tubercles and three equal-spaced rows of tubercles on the outer third of the flank of which the innermost row is very faint.

De Grossouvre (1893, pl. 32, figs. 9a, b) illustrated a complete specimen assigned to *S. pulcherrimus* from southwestern France (Dordogne). The specimen has a slender body chamber and concave umbilical margin; I interpret this specimen as a very large male. It differs from the specimens figured by Schlüter by having all five rows of tubercles of a side persisting on the body chamber. Tubercles on opposite sides of the middle of the venter have a zigzag arrangement like that of Schlüter's larger specimen.

Frech (1915, p. 556) interpreted *S. pulcherrimus* in a different manner than did Schlüter and de Grossouvre. In the course of analyzing the scaphites of the Upper Cretaceous, Frech defined a "Gruppe des *Sc. pulcherrimus*" characterized by three to four rows of lateral tubercles as well as a midventral row.

Nowak (1916, p. 63) also included within the scope of *S. pulcherrimus* specimens that had midventral tubercles, although he did restrict it to specimens having five rows on a side. He also assigned *pulcherrimus* to his new genus *Acanthoscaphites*.

Mikhailov (1951, p. 96–98, pl. 18, figs. 83, 84) carefully described a nearly complete specimen 72 mm in length from siliceous marls of the Donets region in southern Russia. This specimen differed from those of Schlüter by the five rows of tubercles on the flank of the septate coil persisting onto the older half of the body chamber. Mikhailov described the rows of tubercles as umbilical, umbilicolateral, lateral, ventrolateral, and outer. He noted that only the ventrolateral and outer rows persisted to the aperture. Mikhailov also observed that ribs were thin and tended to occur in bundles separated by furrows, and that the tubercles were confined to the bundles of ribs. Such a rib and tubercle arrangement is well shown on the illustration of the septate coil of the larger specimen of Schlüter (1872, pl. 26, fig. 1). The large size, very small umbilicus, and wide body chamber of Mikhailov's specimen suggests a female. Although the specimen lacked midventral tubercles, Mikhailov assigned it to *Acanthoscaphites*. Mikhailov's terminology of umbilical, umbilicolateral, lateral, and ventrolateral for rows of tubercles will be adopted here, but ventral will be used in place of outer. For further clarity midventral tubercles will be referred to as siphonal tubercles.

The genus *Trachyscaphites* was proposed by Cobban and Scott (1964, p. E6–E7) for scaphites having three to five rows of tubercles on each flank and numerous ribs that weaken on the body chamber and tend to lack differentiation into strong primaries and secondaries as in most groups of scaphites. Cobban and Scott (1964, p. E7) noted that "*Trachyscaphites* differs from *Acanthoscaphites* by its smaller size, whorls wider than high, simpler suture, lack of midventral nodes, and straighter living chamber which has the younger part separated considerably from the chambered whorls," and that *Acanthoscaphites* "Should be restricted to a group of large tightly coiled scaphites in which midventral nodes are ordinarily present. In addition, the suture is highly incised for a scaphite, the ribs are straight, and the nodes are usually present only on the living chamber." Since the publication of Cobban and Scott's paper, a large septate coil of *T. redbirdensis*, the type species of *Trachyscaphites*, has been discovered that has a midventral row of small pointed tubercles (fig. 1*h–j*). Accordingly, the definition of *Trachyscaphites* is herein emended to include specimens with or without midventral tubercles. Inasmuch as *T. pulcherrimus* has whorls higher than wide, the degree of stoutness of whorls is removed from the definition of the genus. *Trachyscaphites* is readily distinguished from typical *Acanthoscaphites*, such as the large specimens illustrated by Nowak (1912, pl. 32), by its peculiar bundling of ribs separated by furrows, and by the three to five rows of lateral tubercles on the septate coil. *Scaphites varians* Lopuski (1911, p. 120, pl. 4, figs. 1–3, text fig. 4), usually assigned to *Acanthoscaphites* (Nowak, 1912, p. 578; Mikhailov, 1951, p. 104; Schmid, 1965), has midventral tubercles as well as three rows of lateral tubercles on the septate coil; perhaps this form should be assigned to *Trachyscaphites*.

Figure 1.—*Trachyscaphites pulcherrimus* (Roemer) (*a–g, k, l*) and *T. redbirdensis* Cobban and Scott (*h–j*), natural size.

a–d. Two views each of the older two-thirds of two body chambers (males) of *T. pulcherrimus* from the Wenonah Formation near Marlboro, N.J. Private collection of John Brzostoski, River Plaza, N.J.

e–g. Three views of part of the phragmocone and part of the body chamber of another specimen, probably a female, from the Wenonah Formation. Private collection of John Brzostoski.

h–j. Three views of the phragmocone and part of the body chamber of an example of *T. redbirdensis* that has siphonal tubercles. From the Red Bird Silty Member of the Pierre Shale at USGS Mesozoic loc. D418, 1½ miles southwest of Newcastle, Wyo. Hypotype USNM 187707.

k, l. Top and side views of plaster cast of the holotype of *T. pulcherrimus*.

Figure 2.

GEOGRAPHIC DISTRIBUTION AND AGE OF TRACHYSCAPHITES PULCHERRIMUS

Trachyscaphites pulcherrimus has been recorded from Germany (Roemer, 1841, p. 91; Schlüter, 1872, p. 85; Arnold, 1968, p. 314), Austria (von Hauer, 1866, p. 306), France (de Grossouvre, 1893, p. 250), Poland (Pożaryski, 1938, p. 18; Pożaryska, 1954, table 1; Błaszkiewicz, 1966, table; Cieśliński and Pożaryski, 1970, p. 212), and Russia (Mikhailov, 1951, p. 96; Naidin and Shimanskii, 1959, p. 195; Naidin, 1969, p. 181). The species seems to be confined to the upper Campanian. Pożaryska (1954, table 1) and Błaszkiewicz (1966, table) record *T. pulcherrimus* in the upper part of the upper Campanian but not at the top.

AMERICAN EXAMPLES OF TRACHYSCAPHITES PULCHERRIMUS

Parts of 10 scaphites from near the top of the Wenonah Formation near Marlboro, N.J., were available for study. All are internal molds, and most are uncrushed. Four are considered males (fig. 1*a–d*; fig. 2*a–f*), and two are considered females (fig. 2*i–k*, *n*, *o*). The others are too incomplete for assignment to either sex.

The nearest complete specimen of the females consists of most of the body chamber and part of the last septate whorl of a specimen 76.5 mm in length (fig. 2*n*, *o*). Ribs are flexuous, prorsiradiate, and tend to occur singularly or in pairs separated by poorly defined furrows. The ribbing weakens a little on the older two-thirds of the body chamber and then becomes strong again on the younger third. Tubercles on the outer septate whorl are small, pointed, nearly equal in size, and arranged in five equally spaced rows. Umbilical tubercles increase greatly in size on the body chamber where they are circular and sharp and six in number. Maximum thickness of the shell is through the umbilical tubercles at the end of the straighter part of the body chamber. The umbilicolateral tubercles, in contrast, decrease in size on the body chamber where they are very small, pointed, and more numerous than the umbilical ones. The lateral tubercles persist across the body chamber maintaining the same size as on the septate whorl. The ventrolateral and ventral tubercles are equal in number, pointed, and increase in size on the body chamber. There are no siphonal tubercles; the middle of the venter is smooth on the body chamber and ribbed on the outer septate whorl. Opposite tubercles of the ventral rows are arranged in a zigzag manner. The suture is moderately complex. This specimen closely resembles the one figured by Mikhailov.

A somewhat poorly preserved septate coil 54 mm in diameter of a large female is of interest by having siphonal tubercles on the last part (fig. 2*i–k*). These tubercles are very small, nodate, and more numerous than the ventral ones. Clearly defined siphonal tubercles are absent on the older part of the whorl where their place is taken by nodose ribs. Another specimen, probably a female, has more conspicuous nodose ribs on the middle of the venter on the younger part of the phragmocone where two occur for each tubercle in a ventral row. (fig. 1*e–g*).

Two of the four male specimens from New Jersey are represented by very well preserved complete body chambers 40 and 50 mm in height. The larger one, which has a compressed section, (fig. 2*d–f*) shows much resemblance to the smaller of Schlüter's specimens. Ribs are prorsiradiate, and umbilical tubercles, which number six, are nodate and equal in size and persist to the aperture. The rest of the ornamentation is different from that on the older half of the body chamber and that on the younger half. Ribs are rather weak and irregular in strength on the older half and strong and regular on the younger half. The older half has very small umbilicolateral and lateral tubercles and strong sharp clavate ventrolateral and ventral tubercles, whereas the younger half lacks umbilicolateral and lateral tubercles and has small nodate ventrolateral and ventral tubercles that persist to the aperture. The younger half has in addition weak nodate siphonal tubercles. On the younger half, the tubercles of each row are equal in numbers and each siphonal, ventral, and ventrolateral tubercle is alined with a rib. Tubercles on opposite sides of the midline of the venter have a zigzag arrangement. The aperture is constricted like that of other scaphites. The smaller specimen (fig. 2*a–c*) is much like the larger except that the cross section is not as compressed and the tubercles are a little stronger and sharper. The other two males (fig. 1*a–d*) consist of the older two-thirds of large stout body chambers that have unusually strong ribs. Umbilicolateral tubercles are missing, and the lateral tubercles are weak. Ventral tubercles have a zigzag arrangement.

Three of the four Texas specimens consist of body chambers with parts of the septate coils attached. The body chambers are slender and have concave umbilical walls which suggest males. The original lengths of these three specimens are estimated as 53, 65, and 68 mm. All five rows of tubercles on the side of the septate coil persist onto the body chamber of

---

Figure 2.–Specimens of *Trachyscaphites pulcherrimus* (Roemer) from New Jersey and Texas, natural size.

a–f. Three views each of two body chambers believed to be males from the Wenonah Formation near Marlboro, N.J. Specimen *a–c*, collected by Richard Heintz, is hypotype USNM 187708; specimen *d–f* is from the private collection of John Brzostoski, River Plaza, N.J.

g. Side view of part of a body chamber from the Wenonah Formation collected by Richard Heintz. Hypotype USNM 187709.

h. Side view of a small laterally compressed adult (male) from the Taylor Marl 1 mile northwest of Kimbro, Tex. Univ. Texas 37972.

i–k. Three views of a stout phragmocone believed to be a female from the Wenonah Formation near Marlboro, N.J. Private collection of John Brzostoski.

l, m. Two views of an unusually large male from the same locality as *h*. Univ. Texas 33433.

n, o. Two views of a slender female from the Wenonah Formation near Marlboro, N.J. Private collection of John Brzostoski.

the largest specimen, although the umbilicolateral and lateral tubercles are weakened there (fig. 2*l*, *m*). Siphonal tubercles are not present on this body chamber, and the tubercles of the ventral rows have a zigzag arrangement. The older part of the body chamber of the intermediate specimen has strong pointed umbilical, ventrolateral, and ventral tubercles, weaker but sharp lateral tubercles, and no umbilicolateral tubercles, whereas the younger part has all five rows of tubercles as well as very small pointed siphonal ones. The smallest specimen has compressed flanks on which are present all five rows of tubercles, although the umbilicolateral ones are barely discernible (fig. 2*h*). The midventral area on the younger part of this body chamber is not preserved. A septate coil 36 mm in diameter with a small part of the body chamber attached represents the fourth Texas specimen. It has a zigzag arrangement of the ventral tubercles and the connecting ribs. The suture is shown on figure 3.

Figure 3.—External suture, × 3, at a diameter of 32.5 mm of *Trachyscaphites pulcherrimus* (Roemer) from the Taylor Marl at USGS Mesozoic loc. 17386 on Cottonwood Creek ½ mile southwest of Manda, Travis County, Tex. Hypotype USNM 187710.

REFERENCES CITED

Arnold, Hellmut, 1968, Das Obercampan des Stemweder Berges und seine Fauna: Bremen Überseemus. Pub., v. 3, ser. A, no. 6, p. 273–342, illus.

Błaszkiewicz, Andrzej, 1966, Uwagi o stratygrafii kampanu i mastrychtu doliny środkowej Wisły [Remarks on the Campanian and Maestrichtian stratigraphy of the middle Vistula valley]: Kwart. Geol., v. 10, no. 4, p. 1060–1071. (Polish, with English summ.)

Cieśliński, Stefan, and Pożaryski, Władysław, 1970, Kreda, *in* Pożaryski, Władysław, ed., Stratygrafia Mezozoiku obrzeżenia Gór Swietokrzyskich [The stratigraphy of the Mesozoic in the margin of the Góry Świętokrzyskie]: [Poland] Inst. Geol. Prace, v. 56, p. 185–231, 5 pls.

Cobban, W. A., 1969, The Late Cretaceous ammonites *Scaphites leei* Reeside and *Scaphites hippocrepis* (DeKay) in the western interior of the United States: U.S. Geol. Survey Prof. Paper 619, 29 p., 5 pls.

Cobban, W. A., and Scott, G. R., 1964, Multinodose scaphitid cephalopods from the lower part of the Pierre Shale and equivalent rocks in the conterminous United States: U.S. Geol. Survey Prof. Paper 483-E, p. E1–E13, pls. 1–4.

Diener, Carl, 1925, Fossilium Catalogus, I, Animalia, pt. 29, Ammonoidea neocretacea: Berlin, W. Junk, 244 p.

Frech, Fritz, 1915, Die Bedeutung von *Scaphites* für die Gliederung der Oberkreide, Pt. 1 *of* Über Scaphites: Centralbl. Mineralogie Jahrg. 1915, p. 553–568.

Grossouvre, Albert de, 1893, Les ammonites de la craie supérieure, Pt. 2, Paléontologie, *of* Recherches sur la craie supérieure: Carte Géol. Détaillée France Mém., 264 p., 39 pls. [1894].

Hauer, F. R. von, 1866, Neue Cephalopoden aus den Gosaugebilden der Alpen: Kaiserlichen Akad. Wiss. Wien Sitzungsber., Math.-Naturw. Kl., v. 53, p. 300–308, 2 pls.

Lopuski, Geslaw, 1911, Przyczynki do znajomosci fauny kredowej gub Lubelskiej [Contribution to the study of the Cretaceous fauna of the Lublin Plateau] [In Polish with French summ.]: Towarzystwo Naukowe Warszawskie Sprawozdania z Posiedzen, Comptes Rendus, v. 4, p. 104–140, 4 pls.

Mikhailov, N. P., 1951, Ammonity werchnego mela yuzhnoj chasti jewropejskoj chasti SSSR i ich stratigraficheskoe znatschenie [The ammonites of the Upper Cretaceous of the southern part of the European part of the USSR and their stratigraphic significance]: Akad. Nauk SSSR Geol. Inst. Trudy, no. 129, Geol. ser. no. 50, 143 p., 19 pls.

Naidin [Najdin], D. P., 1969, Biostratigraphie und Paläogeographie der Oberen Kreide der Russischen Tafel: Geol. Jahrb., v. 87, p. 157–186, illus.

Naidin, D. P., and Shimanskii, V. N., 1959, Golovonogne Molluski *in* Moskvin, M. M., ed., Atlas verkhnemelovoi fauny severnogo Kavkaza i Kryma [Cephalopod Mollusca, *in* Atlas of the Upper Cretaceous fauna of the northern Caucasus and Crimea]: Moscow, Vses. Nauchno-Issled. Inst. Prirod. Gazov Trudy, p. 166–220.

Nowak, Jan, 1912, Die Scaphiten, Pt. 2 *of* Untersuchungen über die Cephalopoden der oberen Kreide in Polen: Acad. Sci. Cracovie Bull. Internat., 1911, ser. B, p. 547–589, pls. 32, 33.

—— 1916, Zur Bedeutung von *Scaphites* für die Gliederung der Oberkreide: K.-k. Geol. Reichsanstalt Verh., Jahrg. 1916, no. 3, p. 55–67.

Pożaryska, Krystyna, 1954, O przewodnich otwornicach z kredy górnej Polski środkowej [The Upper Cretaceous index foraminifers from central Poland]: Acta Geol. Polonica, v. 4, no. 2, p. 249–276, illus. (English summ., p. 62–72).

Pożaryski, Władysław, 1938, Stratygrafia Senonu w Przełomie Wisły między Rachowem i Puławami [Senonian stratigraphy in the breach of the Wisla River between Rachow and Pulawy in central Poland]: Poland, Inst. Géol. Bull. 6, 94 p. [German summ.]

Reeside, J. B., Jr., 1927, The scaphites, an Upper Cretaceous ammonite group: U.S. Geol. Survey Prof. Paper 150-B, p. 21–40.

Roemer, F. A., 1841, Die Versteinerungen des norddeutschen Kreidegebirges: Hannover, Germany, 145 p., 16 pls.

Schlüter, Clemens, 1871–72, 1876, Cephalopoden der oberen deutschen Kreide: Palaeontographica, 1871–72, v. 21, p. 1–120, pls. 1–35; 1876, v. 24, p. 121–264, pls. 36–55.

Schmid, Friedrich, 1965, *Acanthoscaphites tridens varians* (Lopuski 1911) aus dem Maastricht von Hemmoor (Niederelbe) in nordwest-Deutschland: Geol. Jahrb., v. 83, p. 681–692, pls. 62, 63.

Jour. Research U.S. Geol. Survey
Vol. 1, No. 6, Nov.-Dec. 1973, p. 701—707

DETERMINATION OF THE ASSOCIATION AND DISSOCIATION OF HUMIC ACID FRACTIONS BY SMALL ANGLE X-RAY SCATTERING

By R. L. WERSHAW and D. J. PINCKNEY,
Lakewood, Colo.

Abstract.—A procedure has been devised for the fractionation of humic acid samples from different environments. This procedure involves fractionation of the sample by adsorption chromatography on a Sephadex G-50 column followed by chromatography on either a G-25 or a G-100 column. The fractions of the solutions are then examined by small angle X-ray scattering. Three different types of behavior have been detected among the humic acid fractions: (1) Some fractions show very little change in aggregation at pH values above 3.5. (2) One fraction forms aggregates at pH values above and below pH 7, but at pH 7 it is completely dissociated. (3) In some fractions the degree of aggregation decreases with increasing pH. However, even at pH values as high as 11.5 some large particles are still present. These differences in association behavior are due to the interaction of different attractive and repulsive forces. In many aggregating systems only one type of attractive force is dominant; however in humic acid systems hydrogen bonding, π bonding between planar aromatic moieties, and other coulombic interactions apparently all play a role in the formation of molecular aggregates.

A number of different procedures have been used in attempts to determine the molecular weights or molecular sizes of humic acid particles in solution. Most of the classical methods of molecular weight determinations have been tried, but there is little overall agreement between the various measurements.

Scheffer and Ulrich (1960), Schnitzer and Desjardins (1962), Wershaw and Burcar (1967), and others have reviewed the literature on molecular weight determinations of humic acids. In general, they have found that measurements which are dependent upon changes in the colligative properties of thermodynamic systems yield lower molecular weights than other methods. Most of these measurements have been on unfractionated humic acids, although a few have been made on partially fractionated samples. A comparison of the results of various procedures, which might then permit us to account for the differences in apparent molecular weight from one method to another, would require a detailed knowledge of the molecular weight distribution of the particles in the solutions; unfortunately these data are not available. Some workers have attempted to measure the molecular distribution by gel-permeation chromatography. However, as we have shown (Wershaw and Pinckney, 1973), these results are at best highly questionable.

In theory it should be possible to directly measure the distribution of particle sizes in polydisperse systems by low angle X-ray scattering or ultracentrifugation. Unfortunately, in actual practice the necessary detailed information on the physical and chemical properties of all the particles in the system is generally not available (See Beeman and others, 1957; Schachman, 1959). However, the range of particle sizes can be readily evaluated, and as we shall demonstrate, this information alone can give us a valuable insight into the chemistry of the system.

Flaig and Beutelspacher (1968), Stevenson, Van Winkle, and Martin (1953), and Piret and others (1960) have studied unfractionated humic acid salt solutions by ultracentrifugation. All these authors found that the solutions were polydisperse, and they reported sedimentation average molecular weights (Z average molecular weights). Piret and others (1960) found that 90 percent by weight of the humic acid particles had molecular weights less than 3×10^5.

Wershaw and others (1967), using low-angle X-ray scattering, were the first to measure some of the particle sizes in an unfractionated sodium humate solution; after this work Lindqvist (1970) found that acid hydrolysis of a chernozem sodium humate that contained a number of different size particles in solution yielded a monodisperse system in which all the particles had radii of gyration between 17 and 19 A. Others (Wershaw and others, 1967, 1970; Wershaw and Pinckney, 1971) have extended their work to measurements of particle sizes in different sodium humate fractions. They have shown that one of the sodium humate fractions isolated by gel-permeation chromatography forms molecular aggregates in solution which disaggregate at approximately pH 7; above and below this pH the molecules aggregate. In this paper we shall discuss the other types of aggregates that are found in solutions of sodium humate fractions.

All molecular weight measurement procedures when applied to polydisperse systems, such as humic acid salt solutions, yield results which are functions of the molecular weight distribution of the particles in the system. Those methods which are dependent on colligative properties will give number average molecular weights, methods such as viscosity measurements will give weight average molecular weights, and still others such as ultracentrifugation give so-called Z average molecular weights. The weight average molecular weights will be more influenced by the higher weight particles than by the lower weight particles. This effect will be even more pronounced in the Z average determinations. Comparisons of molecular determinations from one author to another and from one method to another are further complicated by the fact that the molecular weight distribution in a polyelectrolyte system in which molecular association is taking place is generally a function of the pH, the ionic strength, and the concentration of the solution (Wershaw and Pinckney, 1971).

EXPERIMENTAL PROCEDURE

The sodium humate samples were isolated from soils and natural waters. These isolates were then fractionated on Sephadex G-50[1] columns and refractionated into subfractions on Sephadex G-25 or G-100 (see Wershaw and Pinckney (1973) for a detailed description of the isolation and fractionation procedures used for the various samples). The low angle X-ray scattering measurements were made by use of the procedure outlined by Wershaw and others (1967). In our present study we were mainly interested in the smaller particles present in the various fractions, and therefore we used a 150-μm entrance slit and a 300-μm receiving slit for most of the measurements. Where measurements of the larger particles in a system were desired, an 80-μm entrance slit and a 200-μm receiving slit were used. Solutions of 0.5 percent (weight/volume) concentration of each of the fractions were prepared in various buffers (table 1). The solutions were put into a 1-mm-diameter, thin-walled quartz capillary tube for the low angle X-ray scattering measurements. The measurements of scattered intensity versus scattering angle were made on a Kratky low angle X-ray scattering goniometer. Partial monochromatization of the X-radiation was achieved by using a nickel filter and proportional detector coupled to a pulse height analyzer. The experimental data were smoothed by use of a sliding five point least-squares fit of the curve to a third degree polynomial, and the collimation effects were eliminated by a computer program developed by Lake (1967); weighting functions for our goniometer configurations were evaluated by the computer program of Buchanan and Hendricks (1967).

[1] Sephadex is a registered trademark of Pharmacia Fine Chemicals, Inc. Use of the term in this paper is for descriptive purposes only and does not constitute an endorsement of the product by the U.S. Geological Survey.

Table 1.—*Composition of buffer solutions for particle-size measurements*

[Data from Weast (1965)]

pH	0.1 M KH_2PO_4 (ml)	0.1 M $KHC_8H_4O_4$ (ml)	0.05 M Na_2PO_4 (ml)	0.1 M HCl (ml)	0.1 M NaOH (ml)
3.5	...	50	...	8.2	....
5.0	...	50	...	...	23.9
7.0	50	...	...	...	29.1
8.0	50	...	...	...	46.1
11.0	...	...	50	...	4.1

DISCUSSION OF RESULTS

The scattered intensity as a function of scattering angle that is measured in a low angle X-ray scattering experiment is normally analyzed by the method of Guinier (see Guinier and Fournet, 1955). Guinier has shown that for an ensemble of randomly oriented, identical scattering particles in which there is no long range order, the scattered intensity, $I(h)$, may be represented to a close approximation by the equation

$$I(h) = I_e(h)Nn^2e^{-h^2R^2/3}, \quad (1)$$

where $I_e(h)$ is the scattered intensity that would result if a single electron were substituted for one of the scattering particles, N is the total number of particles in the ensemble, n is the number of electrons per particle, R is the radius of gyration of one of the particles, and $h = \frac{2\pi \sin 2\theta}{\lambda}$, where 2θ is the scattering angle and λ is the wavelength of the impinging X-radiation. This equation may be written as

$$\ln I(h) = \frac{-h^2R^2}{3} + \text{constant}. \quad (2)$$

The radius of gyration of the particle, which is defined as the root mean square distance of the electrons in the particle from the center of charge, is a useful general parameter of comparative molecular or particle size.

From equation 2 it is seen that the radius of gyration may be easily calculated from the slope of a plot of $\ln I$ versus h^2; this is the so-called Guinier plot or curve. In a system in which all the scattering particles are of equal size the Guinier plot will be a straight line.

In a polydisperse system the Guinier plot, which is actually a summation of many Guinier plots, is no longer a straight line, but is concave up. If there are only a few widely different sizes of particles in the system it may be possible to discern discrete straight-line segments of the curve, and these may be used to calculate radii of gyration of the different particle sizes. In the general case, a Guinier plot of a polydisperse system of particles of uniform electron density will yield only the range of particle sizes present in the system, not the distribution of sizes (see Kratky, 1963). However, as we shall show, this

information on the range of particle sizes is very useful in giving some insight into the chemical and physical properties of a polydisperse system.

In a system in which changes in the distribution of particle sizes can be brought about by altering one of the chemical or physical properties of the system, such as pH or ionic strength, then the change in distribution will be reflected in a change in the shape of the Guinier plot. If the polydispersity of the system is increased the plot will become more concave; if it is decreased the plot will flatten out and approach a straight line.

Solutions of sodium humate fractions and subfractions that we have examined by low angle X-ray scattering are polydisperse under most circumstances, and therefore the Guinier plots of these systems are commonly concave. However, pH changes alter the Guinier plots of different subfractions in three different ways. In the first group (group I) the concavity of the Guinier plots changes very little with changes in pH. In the second group (group II) the concavity decreases with increasing pH from 3.5 to 7; at pH 7 the plots are virtually straight, and then at pH values greater than 7 the concavity increases again. In the third group (group III) the concavity continually decreases with increasing pH. At pH values of about 10 some of the plots are almost straight.

There are some variations in behavior within each of the three different groups in our classification of the Guinier plots of sodium humate subfractions. These differences are most apparent in group III, and therefore we shall discuss it first. Group III may be divided into two subgroups: one in which there is a continual decrease in particle size with increasing pH; and one in which after reaching a minimum size with increasing pH, a further increase in pH causes some reaggregation. This reaggregation is evidenced by an increase in slope at low angles. The higher angle parts of the curves are virtually straight. Subfraction 3B (fig. 1) (see Wershaw and Pinckney, 1973, especially fig. 2, for identification of subfractions) is typical of the first subgroup and subfraction 4A (fig. 2) of the second subgroup; examples of the various groups will be discussed below.

In figure 1 we see that the curves for pH values greater than 3.5 are straight lines with equivalent slopes (R = 8.1 A) over practically the entire range of h values measured, and only at very low h values do the curves exhibit a slight concavity. This very low angle region was examined in more detail with an 80-μm entrance slit (fig. 3), and the following radii of gyration were measured: pH 3.5, 56.8 A; pH 5, 47.4 A; pH 7, 45.9 A; pH 8, 26.5 A; at pH 9.7 the particles were too small to give appreciable scattering with this slit system.

The Guinier curve of the Florida subfraction 4B (fig. 4) at pH 3.5 has a straight segment with a slope corresponding to a radius of gyration of 14.4 A. At smaller h values than shown in the figure the curve is concave up; this segment is due to particles with radii of gyration larger than 14.4 A. At pH 5 the radius of gyration determined from the straight segment of the curve is 8.9 A. The low angle end of the curve has much less curvature than the pH 3.5 curve. At pH 7, pH 8, and pH 9.4 the plots are virtually straight over the entire range of h values measured; however, the pH 7 curve gives a radius of gyration of 6.6 A, while at pH 8 the radius is 8.1 A and at pH 9.4 it is 8.4 A. Some of the increase in size from pH 7 to pH 9.4 may be due to changes in shape or degree of hydration of the particles in solution; however, as the volume of the 6.6-A particle is approximately half of that of the 8.4-A particle, an 8.4-A particle may simply be an aggregate of two 6.6-A particles.

In subfraction 4A (fig. 5) at pH values of about 3.5 a straight-line portion of the curve at very small angles (h^2 values from 2 to 7 $(A^{-1})^2$ has a slope corresponding to a radius of gyration of about 67 A. At even smaller angles the slope of the curve is still higher, corresponding to particles with radii of gyration larger than 67 A. At larger angles the scattered intensity of the pH 3.5 solution drops off very rapidly, the Guinier plot having a slope corresponding to a radius of gyration of about 16 to 17 A at h^2 values greater than 80×10^{-4}. The solutions of higher pH all exhibit much greater scattered intensities and lower slopes of the Guinier curves over most of the region examined. It is only at very low angles that scattered intensity from the pH 3.5 solution approaches that of the other solutions. This indicates that most of the particles in the pH 3.5 solution are greater than 67 A in radius of gyration, whereas in the higher pH solutions practically all the particles are much smaller than this. At pH 8 and pH 9.4 there appears to be some increase in the degree of aggregation. This increase may also be seen on the data measured at higher angles with the 150-μm front slit (see fig. 2).

In general all the subfractions of fraction 1 from the samples that we have studied fit into group I. In this group at pH values of 3.5 and below a marked increase in aggregation and particle size is detected; however, above pH 3.5 all the curves of a particular subfraction have virtually the same shape (see figs. 6 and 7), indicating that the distribution of particle sizes in these subfractions changes very little with increasing pH.

Several explanations could be proposed for the changes in the slope of the Guinier plots of the sodium humate subfractions that we have classified into groups II and III. These would include folding and unfolding of polymer chains, changes in the hydration of the molecules, and changes in the degree of aggregation of the molecules in solution. Although the first two possibilities may take some part in the observed flattening of the Guinier curves of the third group of subfractions, most of the change is apparently due to changes in degree of aggregation of the particles in solution. This explanation is preferred for three reasons: (1) the wide range of particle sizes that was detected, (2) the predominance of very large particles and the initiation of precipitation at low pH, and (3) the disappearance, at the higher pH values, of the very large particles which predominate at pH 3.5.

Although there is still insufficient evidence to assign mechanisms to the aggregation reactions of humic acid salts in

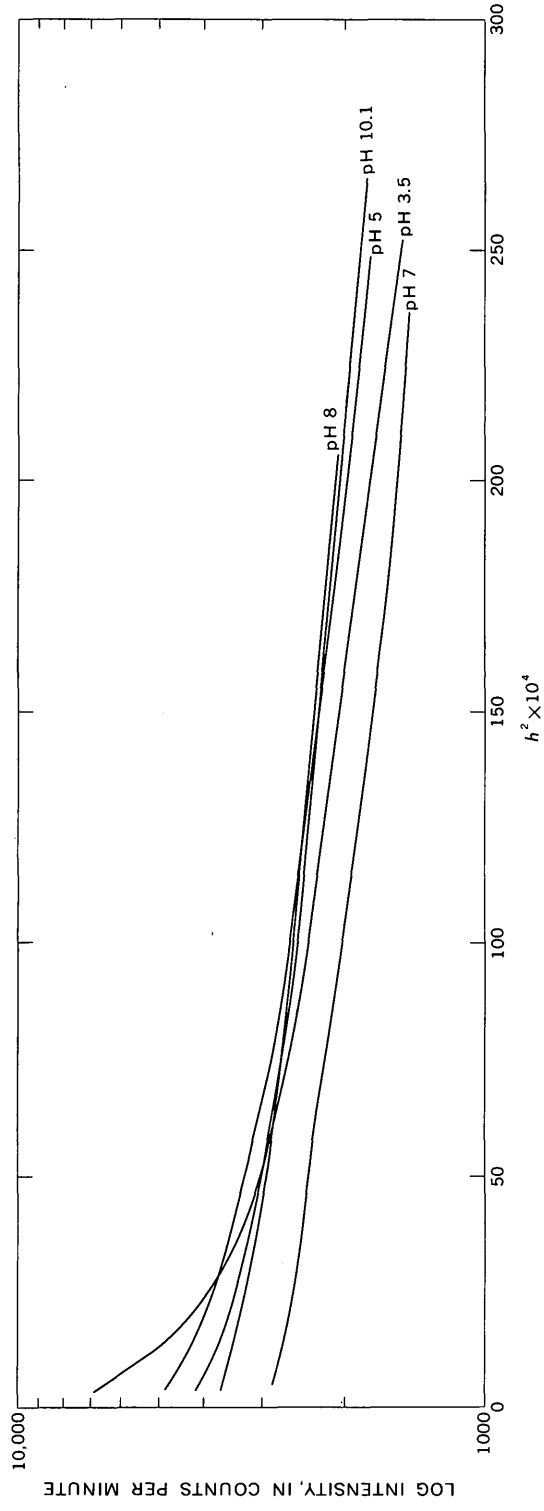

Figure 1.—Guinier plots of New Mexico subfraction 3B with 150-μm entrance slit.

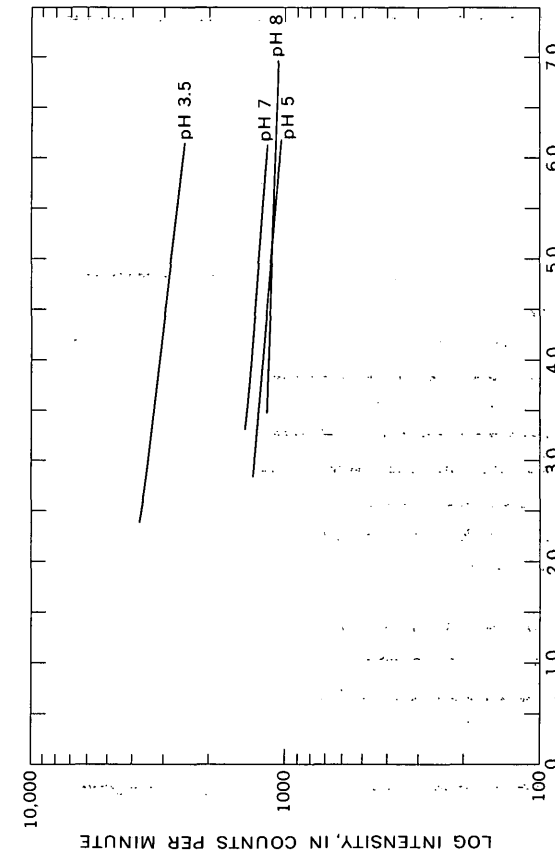

Figure 3.—Guinier plots of New Mexico subfraction 3B with 80-μm entrance slit.

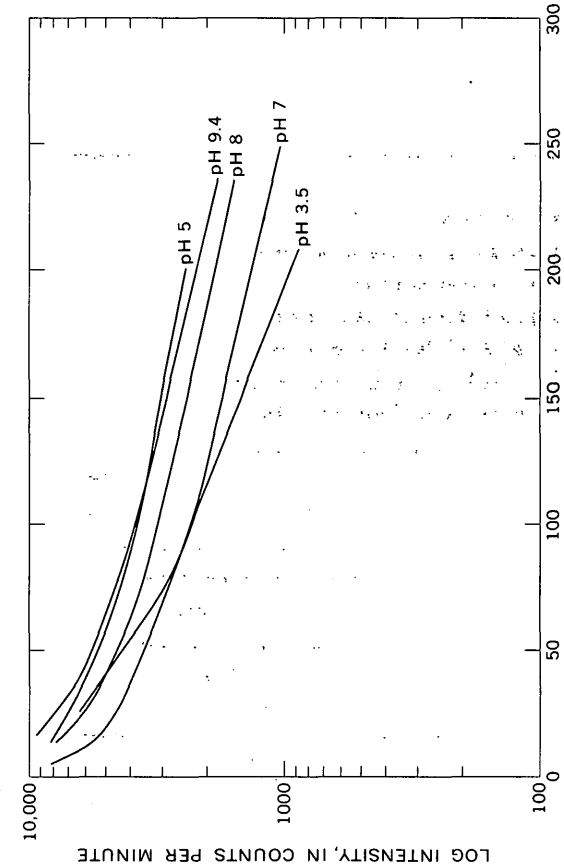

Figure 2.—Guinier plots of New Mexico subfraction 4A with 150-μm entrance slit.

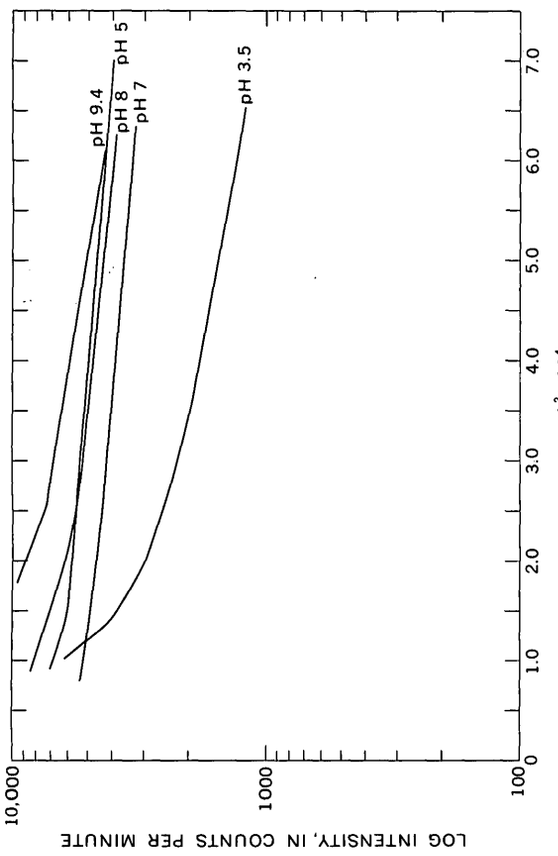

Figure 5.—Guinier plots of New Mexico subfraction 4A with 80-μm entrance slit.

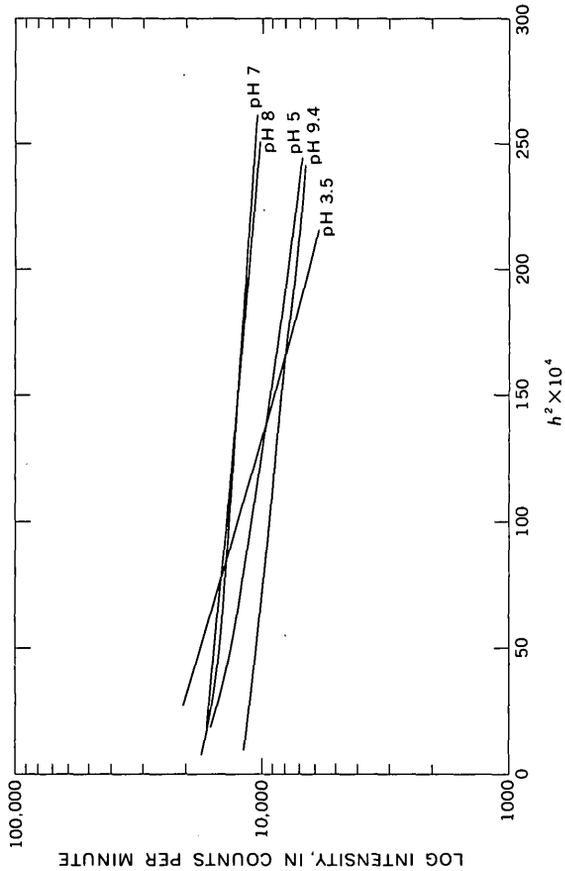

Figure 4.—Guinier plots of Florida subfraction 4B with 150-μm entrance slit.

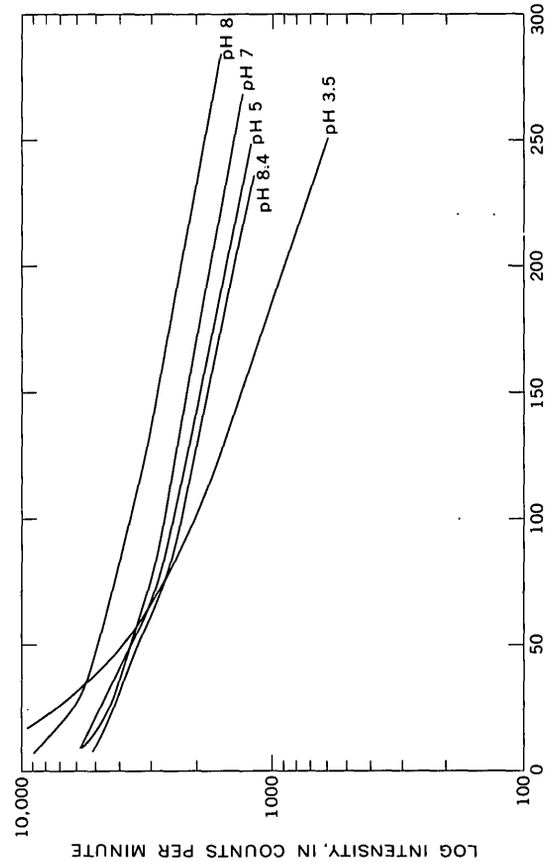

Figure 7.—Guinier plots of Florida subfraction 1B with 150-μm entrance slit.

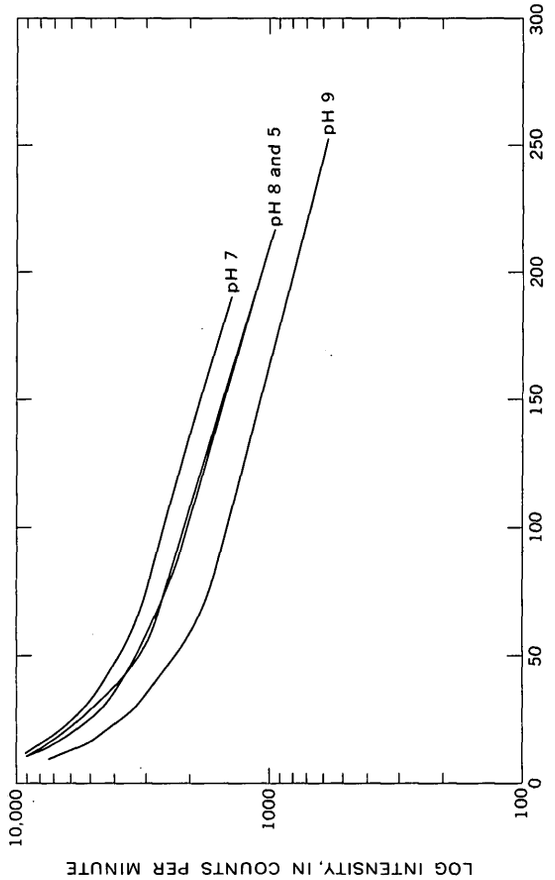

Figure 6.—Guinier plots of Flordia subfraction 1A with 150-μm entrance slit.

solution, it is worthwhile to discuss several of the more likely possibilities. The mechanism or mechanisms that bring about the aggregation and disaggregation of humic acid particles will be determined by charge distribution and functional-group distribution on the exposed surfaces of the particles. A number of workers (see Wershaw and Pinckney, 1973, for references) have shown that humic acids contain abundant acid, phenol, and quinone and similar functional groups. These groups will normally participate in both intermolecular and intramolecular hydrogen bonding (Pauling, 1960).

In addition to hydrogen bonding, bonding due to coulombic attraction of charged particles will also take place in solutions of humic acid salts. In solutions, molecules of polyelectrolytes, such as the salts of humic acid, interact both with other solute molecules and with solvent molecules. These interactions are generally due to coulombic forces acting between charged sites on the molecules. Attractive forces between oppositely charged sites on the polyelectrolyte molecules or between shared counter ions and polyelectrolyte molecules will tend to cause aggregation of the polyelectrolyte molecules. This tendency to form aggregates will be opposed by the attractive forces between the polyelectrolyte molecules and the solvent molecules.

The charged sites on a polyelectrolyte molecule may arise in several different ways. Ionic compounds will dissociate in solution, producing molecules with charged sites. These charged sites may also result from charge-transfer reactions such as the transfer of an electron from a carbanion or a radical anion to another molecule (Szwarc, 1972a).

It is reasonable to assume that charge-transfer reactions between free radicals are important in the aggregation of humic acid salts in light of the high concentrations of free radicals that have been detected both in soils and humic acid preparations. Steelink and Tollin (1967) have shown that free radicals are present both in soils and in humic acid preparations. We have found very high free-radical concentrations in some of the sodium humate fractions that we have isolated, both in the solid phase and in solution. The free radicals detected in soils and humic acids may arise from the reduction of a diamagnetic molecule by a solvated electron (Kemp and Stone, 1962), enzymatic reactions, or photolysis (Commoner, 1961).

Szwarc (1970, 1972b) has reviewed the reactions of radical anions in solution with especial emphasis on electron-transfer processes. Several different types of electron-transfer reactions can lead to aggregation of the radicals. Disproportionate reactions may lead to the formation of dianions:

$$2\,B^{-} = B^{2-} + B.$$

The conversion of two mononegative ions into a dinegative ion and an uncharged species is facilitated by the aggregation of the dinegative ions with cations. Cations may be shared between both mononegative and polynegative anions, yielding aggregates in which the cations act as bridges between the anions. Adams, Staples, and Swzarc (1970), for example, have found evidence suggesting that in durosemiquinone systems triple ions of the type DQ, Na^{+}, DQ^{-} and DQ, $2Na^{+}$, DQ^{-} are formed. Triple ions are also formed between sodium ions and *p*-benzosemiquinone and purazine (Atherton, 1971). The formation of π-bonded charge-transfer complexes of aromatic molecules is common in solution (Effenberger and others, 1971); in some of these complexes a metal cation is sandwiched between two planar aromatic groups.

Further aggregation or polymerization can take place both in hydrogen-bonded and free-radical systems. One type of aggregation that has been intensively studied is that which takes place in the so-called living polymer systems (Szwarc, 1970). These are polymers which do not terminate, but which are able to continually add monomers to their terminal groups. Because the addition of the monomers is reversible, the living polymers may also disaggregate under suitable conditions. Thus a solution of living polymers eventually reaches a state of equilibrium.

Dipole-dipole interaction between the solvent and the polyelectrolyte molecules will cause solvent molecules to be attracted to the polyelectrolyte molecules. The cloud of solvent molecules around two polyelectrolyte molecules will interfere with their approaching each other to form a dimer. The amount of aggregation that takes place between polyelectrolyte molecules in solution will therefore be a function of the relative strengths of the solvent-solute interactions and the solute-solute interactions.

The fact that humic acid salts form molecular aggregates profoundly affects their behavior in natural water systems. One would expect them to behave like proteins and nucleic acids in living systems. Thus the enormous amount of work that has been done by those studying living systems should provide us with guidelines for study of organic polyelectrolytes in natural water systems.

SUMMARY

Fractions and subfractions of humic acid salts form molecular aggregates in solution, and the degree of aggregation is a function of both pH and concentration. Three different types of aggregation have been detected: (1) increased aggregation below pH 3.5 with little disaggregation above pH 3.5, (2) disaggregation up to pH 7 and then reaggregation above pH 7, and (3) a continual decrease in aggregation with increasing pH.

The changes in degree of aggregation of humic acid salts in solution probably reflect the interaction of several different bonding mechanisms. There are not yet enough data however, to elucidate the mechanisms of the interactions. An elucidation of the mechanisms of aggregation of humic acid salts should lead to greater understanding of the behavior of humic substances in natural water systems.

REFERENCES CITED

Adams, R. F., Staples, T. L., and Szwarc, Michael, 1970, ESR studies of electron-transfer reactions in the durosemiquinone system. Formation of the intermediate complex: Chemistry Physics Letters, v. 5, no. 8, p. 474–476.

Atherton, N. M., 1971, Recent magnetic resonance studies of ion-pairs—The complexes of O-dimesitoyl benzene and alkali metals: Internat. Cong. of Pure and Applied Chemistry, 23d, Boston, 1971, v. 4, p. 469–483.

Beeman, W. W., Kaesberg, P., Anderegg, J. W., and Webb, M. B., 1957, Size of particles and lattice defects, *in* Handbuch der Physik, v. 32: Berlin, Germany, Springer Verlag, p. 321–442.

Buchanan, M. G., and Hendricks, R. W., 1967, Program weight—A Fortran IV program for evaluation of weighting functions used in small-angle X-ray scattering: U.S. Atomic Energy Comm., Oak Ridge Natl. Lab. TM-1950, 54 p.

Commoner, Barry, 1961, Electron spin resonance studies of biochemical and biological systems: Acad. Royale Belgique Mem., Cl. Sci., v. 33, no. 3, p. 114–161.

Effenberger, Franz, Nagel, Klaus, and Agster, Wolfgang, 1971, Nucleophilic aromatic substitution—A new synthetic route to biphenyls: Angew. Chemie, internat. ed., v. 10, no. 8, p. 566–567.

Flaig, W. A. J., and Beutelspacher, H., 1968, Investigation of humic acids with the analytical ultracentrifuge, *in* Isotopes and radiation in soil organic-matter studies: Vienna, Internat. Atomic Energy Agency, p. 23–30.

Guinier, A., and Fournet, G., 1955, Small-angle scattering of X-rays: New York, John Wiley and Sons, Inc., 268 p.

Kemp, T. J., and Stone, J. J., 1962, Spectroscopic and kinetic aspects of reduction by solvated electrons: Advances in Chemical Physics, v. 4, p. 365–381.

Kratky, O., 1963, X-ray small angle scattering with substances of biological interest in diluted solutions: Prog. in Biophysics, v. 13, p. 107.

Lake, J. A., 1967, An iterative method of slit correcting small angle X-ray data: Acta Cryst., v. 23, p. 191–194.

Lindqvist, Ingvar, 1970, A small angle X-ray scattering study of sodium humate solutions: Acta Chemica Scandinavica, v. 24, p. 3068–3069.

Pauling, Linus, 1960, The nature of the chemical bond: Ithaca, N.Y., Cornell Univ. Press, 644 p.

Piret, E. L., White, R. G., Walther, H. C., Jr., and Madden, A. J., Jr., 1960, Some physico-chemical properties of peat humic acid: Royal Dublin Soc. Sci. Proc., ser. A, v. 1, p. 69–79.

Schachman, H. K., 1959, Ultracentrifugation in biochemistry: New York, Academic Press, 272 p.

Scheffer, Fritz, and Ulrich, Bernhard, 1960, Lehrbuch der Agrikulturchemie und Bodenkunde, III. Teil, Humus und Humusdungung, v. I: Stuttgart, Germany, F. Enke, 266 p.

Schnitzer, Morris, and Desjardins, J. G., 1962, Molecular and equivalent weights of the organic matter of a podzol: Soil Sci. Soc. America Proc., v. 26, p. 362–365.

Steelink, Cornelius, and Tollin, Gordon, 1967, Free radicals in soil: Soil Biochemistry, v. 1, p. 147–169.

Stevenson, F. J., Van Winkle, Q., and Martin, W. P., 1953, Physico-chemical investigations of clay-adsorbed organic colloids: Soil Sci. Soc. America Proc., v. 17, p. 31–34.

Szwarc, Michael, 1970, Studies of ions and ion pairs: Science, v. 170, p. 23–31.

——1972a, Radical anions and carbanions as donors in electron-transfer processes: Accounts Chem. Research, v. 5, p. 169–176.

——1972b, Concept of ion pairs, *in* Szwarc, Michael, ed., Ions and ion pairs in organic reactions, v. 1: New York, John Wiley and Sons, Inc., 399 p.

Weast, R. C., ed., 1965, Handbook of chemistry and physics: Cleveland, The Chemical Rubber Co., 1713 p.

Wershaw, R. L., and Burcar, P. J., 1967, Physical-chemical properties of naturally occurring polyelectrolytes—I. Sodium humate: Am. Water Resources Conf., 3d, San Francisco, Calif., Nov. 8–10, 1967, Proc., p. 351–364.

Wershaw, R. L., Burcar, P. J., Sutula, C. L., and Wiginton, B. J., 1967, Sodium humate solution studied with small-angle X-ray scattering: Science, v. 157, no. 3795, p. 1429–1431.

Wershaw, R. L., Heller, S. J., and Pinckney, D. J., 1970, Measurement of the molecular size of a sodium humate fraction: Advances X-ray Analysis, v. 13, p. 609–617.

Wershaw, R. L., and Pinckney, D. J., 1971, Association and dissociation of a humic acid fraction as a function of pH, *in* Geological Survey Research 1971: U.S. Geol. Survey Prof. Paper 750-D, p. D216–D218.

——1973, The fractionation of humic acids from natural water systems: U.S. Geol. Survey Jour. Research, v. 1, no. 3, p. 361–366.

Jour. Research U.S. Geol. Survey
Vol. 1, No. 6, Nov.-Dec. 1973, p. 709—717

FLUORESCENT SPECTROSCOPY, A TECHNIQUE FOR CHARACTERIZING SURFACE FILMS

By MARVIN C. GOLDBERG and DAVID H. DEVONALD III, Lakewood, Colo.

Abstract.—A relationship is established between fluorescent spectra obtained by using a light path through the liquid solution and the fluorescent spectra obtained by a direct reading of surface reflection (remote sensing). A brief review of quantum fundamentals provides the necessary information to conclude that "see-through" and reflectance spectra are identical in wavelength response. Many floating films contain fluorescent materials; thus fluorescent spectroscopic techniques were used to obtain the fluorescent spectra of lube oil, crude oil, and lignosulfonic acid in an effort to detect, identify, and quantify these representative fluorescent materials in water solutions. For each material tested the emission maximum was established. The emission maximum was then held constant while the absorption spectrum was recorded and the absorption maximum established. The complete spectral curves are presented.

The interface between surface-water bodies and the gaseous atmosphere generally contains partially miscible floating films. These films are part of the water-quality regime; they change the evaporation kinetics and take part in the chemical hydrodynamics of dissolved and suspended material transport. The materials that comprise the films react by mechanisms such as solubilization, solution, sorption, and ion exchange. Consequently, surface films can be one of the major regulatory parameters of water quality in a hydrologic system. It is necessary to understand the mechanistic reactions of the films and to relate these data to the economics and feasability of water use and reuse (Goldberg and others, 1973; Goldberg and Weiner, 1972).

Most of the literature available concerning surface films describes the areal extent and the thickness of these films (see for example, Goolsby, 1971; Klemas, 1971; Chandler, 1971; and Measures and Bristow, 1971). Some attempts have been made to correlate surface films with undesirable ecological manifestations (Zobell, 1971; Duce and others, 1972). Yet, there remains the important aspect of correlating surface films with other water-quality variables to gain a more complete understanding of hydrologic systems.

This report establishes the background for choice of methods, techniques, and the application of specific optical phenomena that are best adapted to the study of surface films. Data are herein found that relate only to fluorescent spectroscopy using "through-the-solution" light paths. A strong case, however, is presented for the use of this method for recording fluorescent "see-through" response and correlating it with that obtained by fluorescence recorded from surface reflection.

This report also presents the fluorescent spectra of a few common materials that form surface films.

In recent years most of the surface-film data available were collected for purposes of describing oil spills. It is the common practice of investigators in this field to describe floating films by areal extent, thickness, and composition.

When referring to units of measurement for surface films it should be realized that an immiscible liquid can be described in concentration units. The criterion used to label a liquid system as an emulsion or an immiscible film is the same criterion for application of concentration units to discuss the amount of material A present in material B in two-component immiscible liquid systems. As long as an emulsion exists, concentration units can be used. Because see-through techniques are used, the Beer-Lambert relationship is presented wherein the luminosity of the solutions is discussed as the component variables—extinction coefficient, light path, and solution concentration. For this reason we discuss the standard and unknown solutions in terms of concentrations.

A remote laser fluorosensor (see Stoertz and others, 1969) can be used to trace industrial effluents and urban-runoff effluents in concentration ranges from 0.5 to 100 mg/l. The fluorescent-sensing technique will easily adapt to remote use (Weinman, NASA, written commun., 1972) with distances ranging from 20 to 2,000 feet from the sample. A boat or truck-mounted unit, and conceivably an aircraft-mounted unit could be used to rapidly scan large water areas.

FLUORESCENCE

Three components of the fluorescent effect that can be measured are: the wavelength maxima of emission, the wavelength maxima of absorption, and the fluorescent decay time. If all three are known it may be possible to identify unknown compounds. In this study only the emission and absorption were measured. The decay time can be measured with a rapidly pulsed excitation source and a synchronized fast-response detector.

Each one of the three components of the fluorescent effect characterizes the compound under observation (Parker, 1968).

Theory

From a quantum-mechanical standpoint, the solution of the Schroedinger equation yields eigenvalues that describe the energy state of an atom or molecule (Herzberg, 1945, 1950; Becker, 1969). Thus, a simplistic definition of fluorescence is given in figure 1 by plotting interatomic distance versus molecular energy eigenvalues.

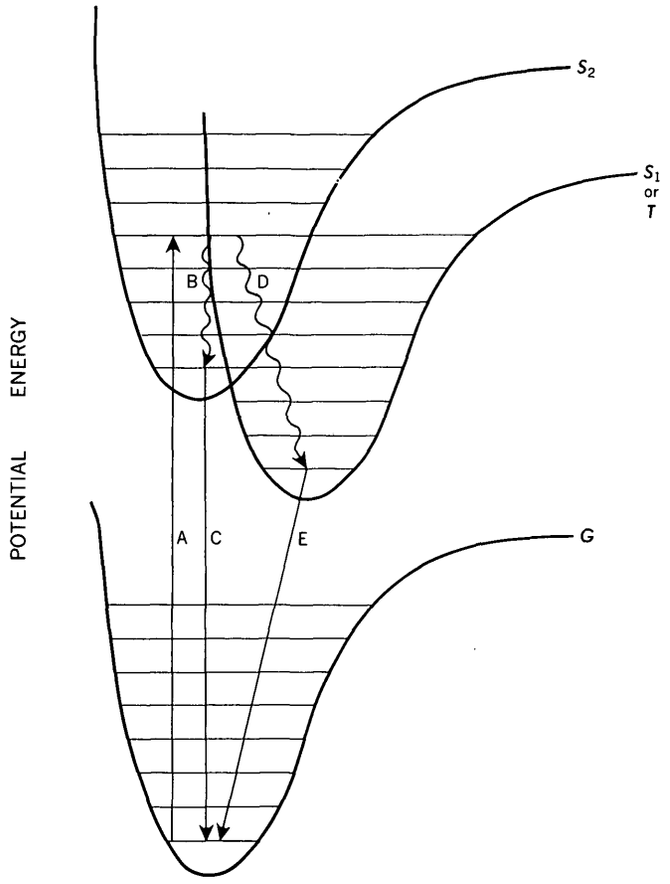

Figure 1.—Energy-level diagram depicting some typical quantum-mechanical analogies to illustrate fluorescence and phosphorescence. A, incident light absorption; B, radiationless transition to ground state of S_2 electronic level; C, fluorescent emission; D, intersystem crossing; E, phosphorescent emission; S_1, singlet excited electronic state one (T, symmetry configuration); S_2, singlet excited state two; and G, ground state.

Figure 1 diagrammatically illustrates a light photon (A) activating the ground-electronic state of an atom or molecule. The photon energizes the molecule to an excited electronic state. This excitation is instantaneous. The process of losing the excitation energy can take place in several ways. A radiationless process can occur to lower the energy level to the vibrational ground state (B) of electronic level S_2. The sequential photon emission (C) that takes place as the energy is further lowered from the ground vibrational level of electronic state S_2 to the ground state G is called fluorescence. A time delay may be evidenced between molecular energy stimulation and light emission, caused by the time it takes for a radiationless transition (B). If this time delay is lengthened by a process such as intersystem crossing (D) then the decay process is known as phosphorescence (E). The definitive difference between fluorescence and phosphorescence is the length of time between photon stimulation and photon emission. It is usually accepted as a definition that elapsed times of 10^{-9} seconds or greater categorize the phenomena as phosphorescence.

Fluorescence is a short, time-differential effect and phosphorescence a long, time-differential effect when measured from the time of the original light quantum absorption. The original absorption is usually 10^{-15} seconds duration. Fluorescence is described by the relationship

$$I = I_0 e^{-t/\tau}, \tag{1}$$

where I = fluorescent intensity at time t,
I_0 = maximum fluorescent intensity during excitation,
t = time elapsed since removing the source of excitation, and
τ = average lifetime of the excited state.

τ is defined as the time for the fluorescent intensity to fall to $1/e$ of its initial value. It ranges in value from 10^{-10} to 10^{-5} seconds for some selected condensed ring molecules. τ can be approximated by the formula $1/\tau \approx 10^4 \cdot \epsilon$ max (Parker, 1968) where ϵ is the molecular extinction coefficient defined as

$$\log_{10} I_0/I = \epsilon c d,$$

where ϵ = the molecular extinction coefficient,
c = concentration of the water solution, and
d = optical path through the solution.

When this formula is used, the radiation lifetime can be approximated. If ϵ max is about 10^5, then the radiation lifetime is in the order of 10^{-9} seconds. To measure radiation lifetimes would necessitate a pulsed light source in the order of a nanosecond and a fast time readout. Such measurements can be obtained remotely by use of a pulsed laser such as a doubled YAG (yttrium, aluminum, garnet) and a high-speed, dual-trace oscilloscope to record the return signal. (Some comprehensive references on fluorescence are: Phillips, 1969; Guilbault, 1967; Udenfried, 1962; Berlman, 1965.)

Detection of fluorescent materials depends upon the quantum yield of fluorescence (ϕ). The ϕ is equal to (number of quanta emitted)/(number of quanta absorbed) or more appropriately:

$$I = I_0 \epsilon c d \text{ and } \phi = \frac{I}{I_0 \epsilon c d}. \quad (2)$$

Quantum efficiencies as measured by Weber and Teale (1957) are given in table 1 for selected fluorescent compounds.

Table 1.—*Quantum efficiencies (ϕ) of selected fluorescent compounds in water solution*

[Values from Weber and Teale (1957)]

Solute	Solvent	ϕ
Fluorescein	Water at pH 7	0.65
1 Amino-napthalene 3:6:8-sulfonate.	Water	.15
9 Amino-acridine	do	.98
Uranyl acetate	do	.04
Indole	do	.45
Skatole	do	.42

Measurement of oil in water

Goolsby (1971) has measured oil in environmental surface waters. Klemas (1971) reports fluorescence maxima in oils excited by ultraviolet radiation. The results of some work done by Klemas are shown in figure 2. The spectra are of diesel oil, quinine sulfate, and natural crude oil.

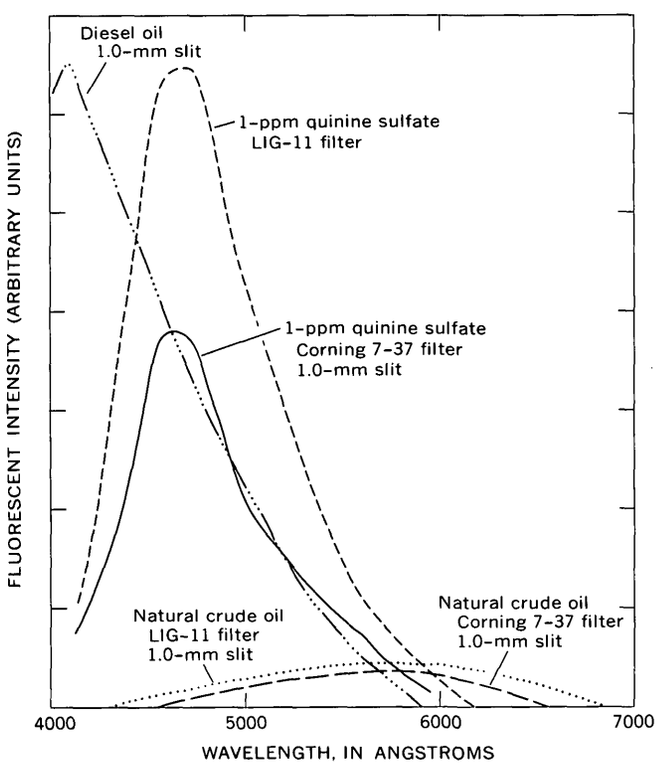

Figure 2.—Fluorescent spectra of diesel oil, quinine sulfate, and natural crude oil (after Klemas, 1971).

EQUIPMENT

All the measurements reported in the following section were made in our laboratory on an Aminco Bowman SPF spectrophotofluorometer.[1] This instrument has two single monochromators, one for the excitation source and one for scanning the fluorescent return signal (Udenfried, 1962). (See fig. 3.)

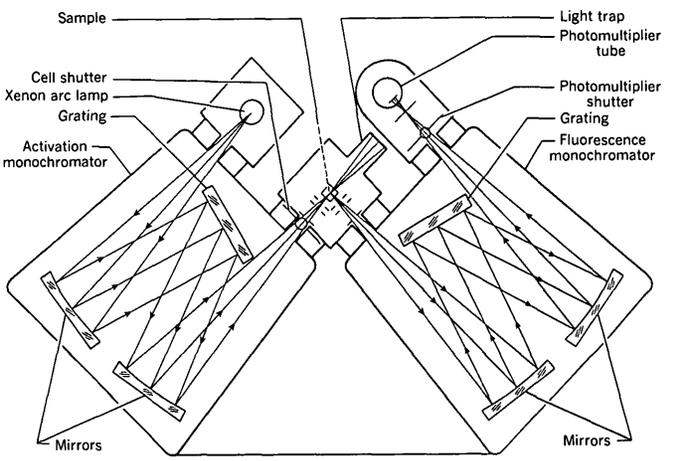

Figure 3.—Optical system of the Aminco Bowman spectrophotofluorometer.

OPTICAL SYSTEM

This double monochromator system allows a choice of excitation frequencies between 200 and 800 nanometers and a complete scan of fluorescent emission frequencies between 200 and 800 nm.

The light source is a xenon flash lamp. For purposes of broadband excitation it is sufficient. To achieve greater sensitivity a laser source should be substituted. This latter source is monochromatic. Usually there is an easily determined optimum wavelength for the fluorescent effect, as was illustrated in figure 1. In most instances a laser can be chosen that will furnish discrete light frequencies closely matching this optimum wavelength.

Measurements

A sample of crude oil donated by The Refinery Co., Denver, Colo., labeled as a crude oil from Colorado fields, was used to obtain standard fluorescent emission spectra (see fig. 4). Spectra from the above reference sample are representative of an oil film and indicate the complexity of fluorescent response from mixtures of petroleum hydrocarbons.

The fluorescent emission spectrum was scanned at several excitation frequencies in order to find the optimum excitation

[1] The use of named products in this report is for identification only and does not imply endorsement by the U.S. Geological Survey.

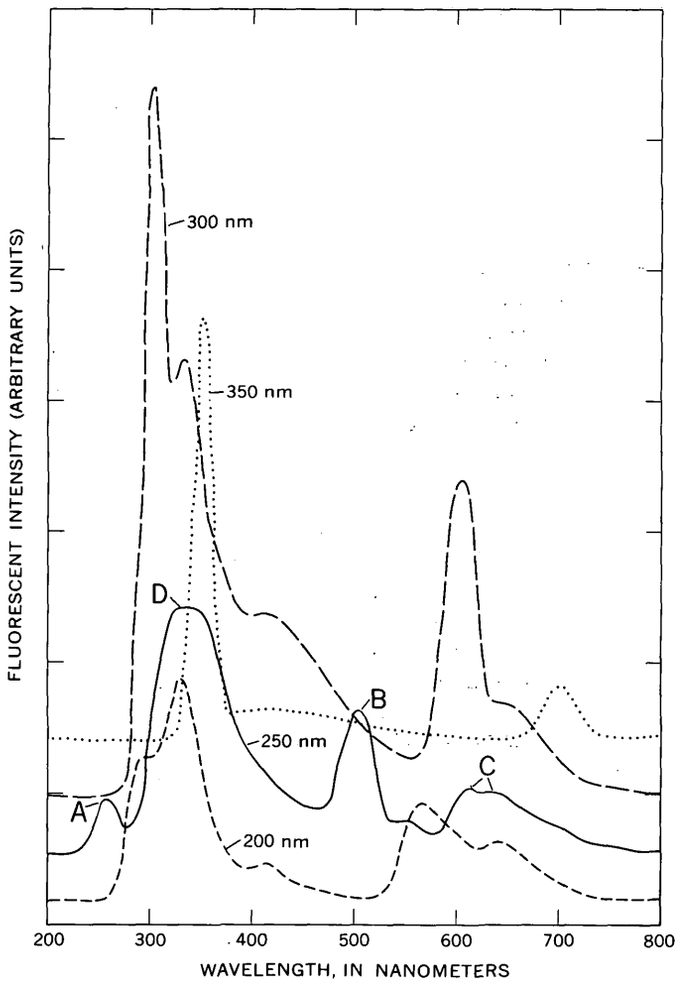

Figure 4.—Fluorescent emission of a crude-oil sample at excitation wavelengths of 200, 250, 300, and 350 nm. The peaks on the 250-nm excitation wavelength (solid line) are as follows: A, Tyndall and Rayleigh scattering; B, second order Tyndall and Rayleigh scattering; C, second order fluorescent scattering; D, fluorescent emission.

energy. Excitation frequencies evaluated were 200, 250, 300, and 350 nm. The fluorescent peak center shifts as follows:

Excitation frequency (nm)	*Fluorescent peak center (nm)*
200	330
250	340
300	340
350	...

Because the fluorescent peak center of interest responds at about 340 nm, the optimum excitation frequency must be less than 340 nm. The optimum excitation frequency was determined to be 250 nm. Most of the fluorescent emission data were recorded at this wavelength.

The solid line on figure 4 is a fluorescent spectrum of crude oil taken at excitation wavelength of 250 nm. As both fluorescence and scattering take place when the incident radiation impinges upon the sample, there will be fluorescent radiation at the same wavelength as the excitation wavelength and scattered radiation at its multiples. Note the Tyndall and Rayleigh scattering peak (A) at the fluorescent emission frequency of 250 nm and again at 500 nm. The peak (B) at 500 nm is a second order Rayleigh and Tyndall scattering, and the peak (C) from 600 to 700 nm is the second order fluorescent scatter. The peak of the oil fluorescent emission (D) occurs between 300 and 400 nm.

If the emission frequency maximum is held constant while the absorption frequency is scanned, the absorption maximum is obtained. This measurement indicates the frequencies of greatest light absorption, and is another of the three information factors that tend to pinpoint the identity from the luminous activity of the solute.

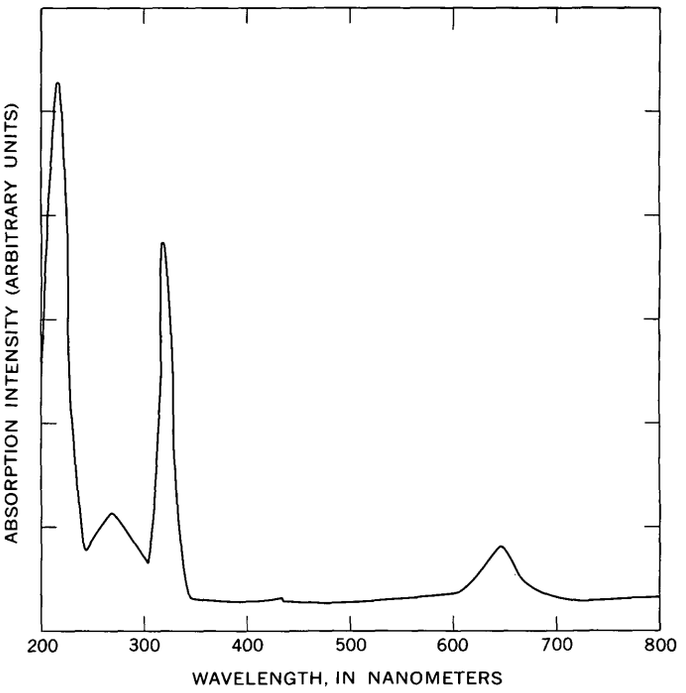

Figure 5.—Crude-oil absorption spectrum; emission wavelength set at 324 nm.

Figure 5 is an absorption spectrum of crude oil taken at emission frequency of 324 nm. The absorption maximum is 220 nm.

Another scattering effect that can appear in these samples is Raman scattering (Parker, 1959); it is a weak scattering effect that shows up at frequencies below the excitation frequency and is usually manifested as a Stokes effect. The anti-Stokes line also occurs but is hard to observe because it is three orders of magnitude less responsive than the Stokes line.[2] Unlike

[2] A Stokes line is a line that occurs below the excitation frequency. The terminology emanates from Stokes law of fluorescence; namely, scattered radiation never has a higher frequency than the excitation radiation.

Tyndall or Rayleigh scattering, the Raman scattered light is manifested by a frequency shift that is characteristic of the scattering molecule. Indeed, the frequency shift for a given molecule is independent of the frequency of the incident light.

Raman scattering from water results in a return signal that may complicate the fluorescent spectrum; thus, it must be considered in interpretation of fluorescent spectra.

Raman return signals usually are three to eight orders of magnitude below the energy of the incident light. When water is exposed to an excitation wavelength of 250 nm, the Raman shift is about 20 nm. Figure 6 is a graph of Raman shift versus excitation frequency for water. For organic compounds the Raman return signal occurs at a lesser wavelength displacement than for water. A few typical examples are listed in table 2.

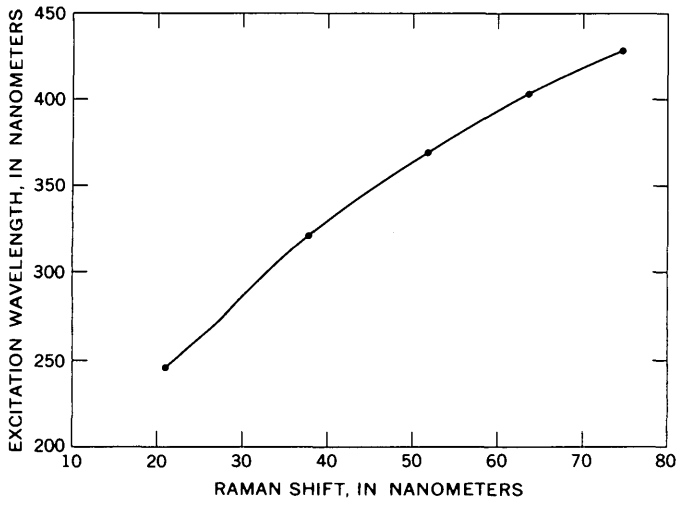

Figure 6.—Raman scatter as a function of excitation wavelength for water.

The fluorescent peaks are quantitatively related to concentration as shown by equation 2. Figure 7 is an illustration of spectra taken of three aqueous concentrations of the crude oil from Colorado fields. Integration of the area under the fluorescent peaks yields a linear calibration curve (see fig. 8). The concentration ranged over less than one order of magnitude.

A second oil sample was similarly calibrated. This sample was a government-specified, low-viscosity lube oil.[3] It should have similar characteristics to the crude oil standard. Density of the crude oil was 0.88 and density of the lube oil was 1.018.

Figure 9 is an illustration of the emission spectra of lube oil and crude oil from Colorado fields. The fluorescent response is greater for the lube oil; also, the peak is sharper and more symmetrical. A peak center occurs at 350 nm. Compounds giving similar fluorescent responses are anisole and tryptophan among others.

[3]Designated as: Lube oil I.C.E.; subzero Mil L-102958; Federal stock No. 9150-242-7603; batch, 3424; quality, S-5; density, 1.018.

Table 2.—*Most prominent Raman bands*
[Parker, 1968]

	Excitation wavelength (nm)				
	248	313	365	405	436
Water	271	350	416	469	511
Ethanol	267	344	409	459	500
Cyclohexane	267	344	408	458	499
Carbon tetrachloride	...	320	375	418	450
Chloroform	...	346	410	461	502

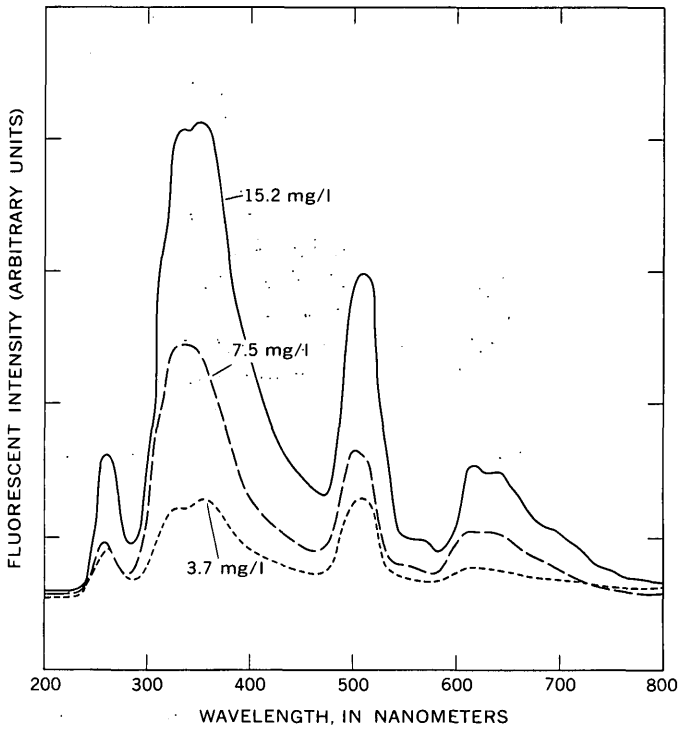

Figure 7.—Emission spectra of crude oil in concentrations of 3.7, 7.5, and 15.2 mg/l. The excitation wavelength was 250 nm.

Because these fluorescent compounds are chemically very similar, the lube oil and crude oil wavelengths of maximum fluorescent emission are also similar as illustrated in figure 9. The emission and absorption maxima are as follows:

	Emission maxima (nm)	*Absorption maxima (nm)*
Lube oil	348	228–292
Crude oil	300, 320	220

Figure 10 is a scan of the absorption of the two materials. This illustrates the broad absorption band for lube oil and the more narrow but more intense absorption band found in crude oil.

Environmental films

The Houston Ship Channel is one of many loading and pumping dock areas where one finds surface films. Samples of water were collected from the Houston Ship Channel by the

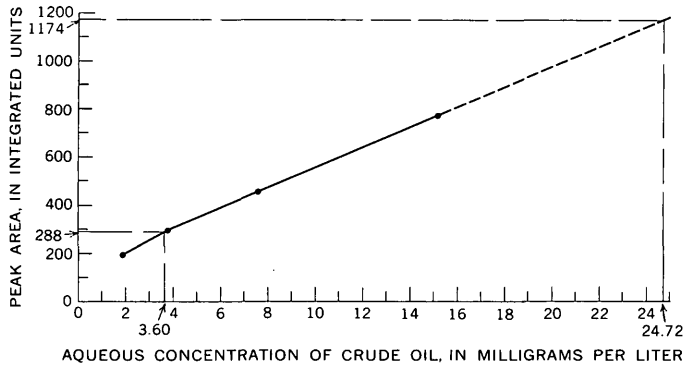

Figure 8.—Integrated peak area as a function of aqueous concentration of crude oil.

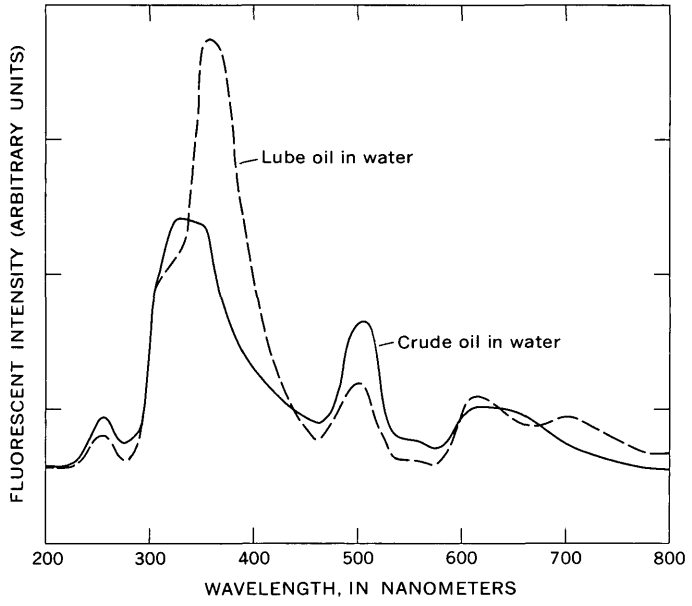

Figure 9.—Emission spectra of lube oil and crude oil. The excitation wavelength was 250 nm.

Texas subdistrict personnel, U.S. Geological Survey, and shipped to M. C. Goldberg at the Federal Center, Denver, Colo. Fluorescent spectra were taken of the untreated samples. Figure 11 is typical of the emission spectra obtained from these samples.

Two facts are evident from figure 11. A fluorescent-response peak area ranging from 325 to 400 nm exists, and a further area either of fluorescent or phosphorescent response shows up from 400 to 470 nm. Without further information, such as fluorescent decay time and (or) specific chemical identification via other methods, it is not possible to determine the chemical composition of the fluorescing compounds. It is possible to bracket the fluorescent response from certain known materials such as lube oil or crude oil samples. Within these narrow comparison limits, fluorescent emissions can be interpreted. These limits broaden as the data concerning the

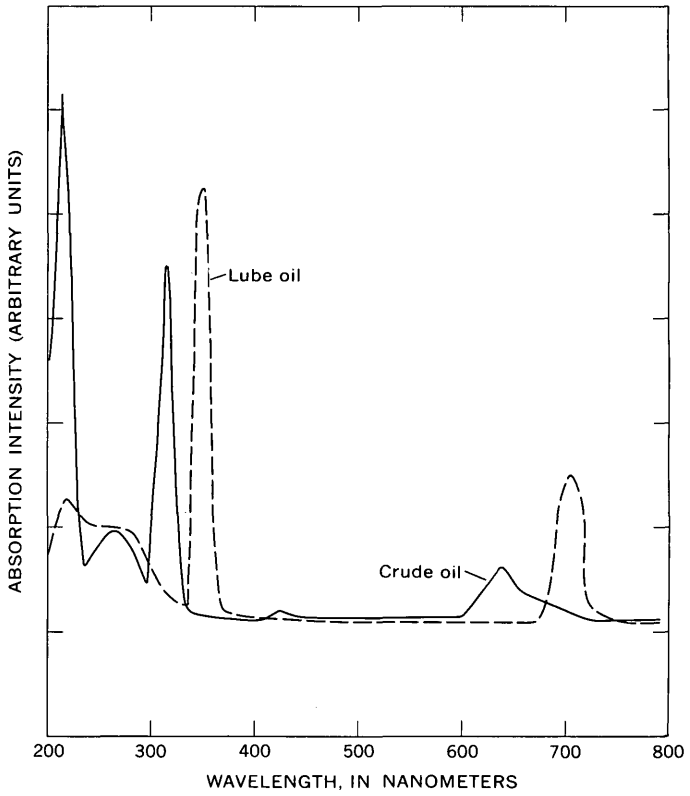

Figure 10.—Absorption maxima of crude oil and lube oil.

fluorescent compounds are increased. Many analytical procedures rely on the high sensitivity of fluorescence, but measurements are made only after a specific chemical separation insures that one is measuring the fluorescence from a pure compound.

Figure 12 illustrates the absorption spectrum of water taken from the Houston Ship Channel; emission and absorption maxima are shown in the tabulation below. As the fluorescent emission seemed to peak at 360 nm and then again at 495 nm the scan was run at 350 nm. A sharp absorption peak is present at 235 nm and a medium broad peak at 296 nm.

	Emission maxima (nm)	*Absorption maxima (nm)*
Water from Houston Ship Channel.	360(b), 400(b)	235(s), 296(b)

A comparison of the spectral fluorescent emission response from the two oil references and the Houston Ship Channel sample 3 is shown in figure 13. The fluorescent response of the Houston Ship Channel sample 3 begins at 320 nm, but the fluorescent response of both the crude and lube oils starts at 245 nm. The ship channel sample has a primary peak center at 360 nm and a secondary peak center at 400 nm. If the total peak area from the ship channel sample spectrum that lies within the crude oil reference wavelengths were considered to be oil, and the intensity of response between the Colorado

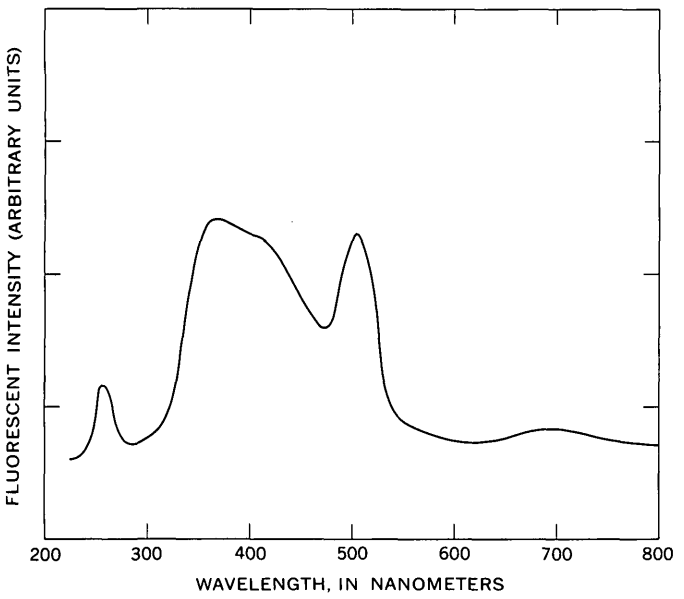

Figure 11.—Fluorescent emission spectrum of the Houston Ship Channel sample 3. The excitation wavelength was 250 nm.

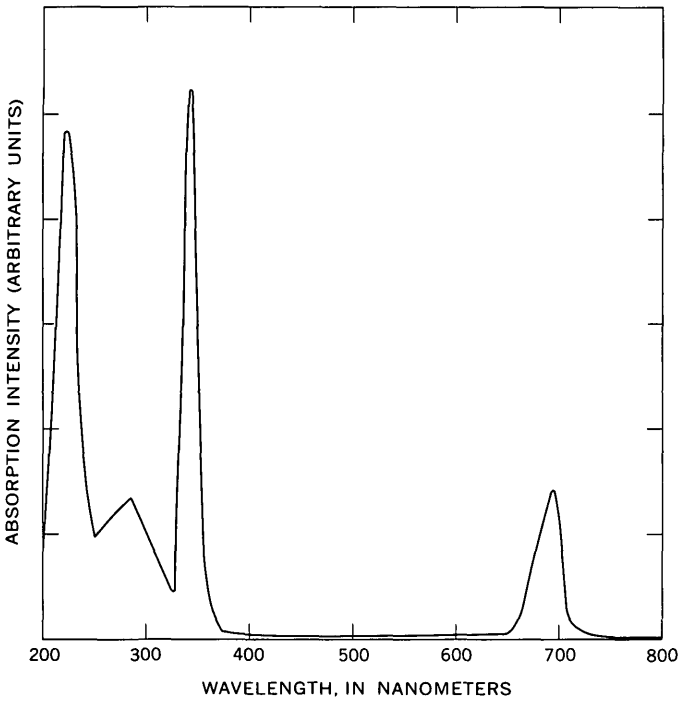

Figure 12.—The absorption spectrum of water from the Houston Ship Channel. The frequency of emission was set at 350 nm while the excitation frequency was scanned.

crude oil reference and the ship channel sample were equal, then there would be 3.6 mg/l of oil in the ship channel sample. This figure is not accurate but represents the type of data to be obtained from more refined fluorescent measurements. If the presence of oil could be confirmed by ground truth, that is, chemical laboratory analysis, then with some further

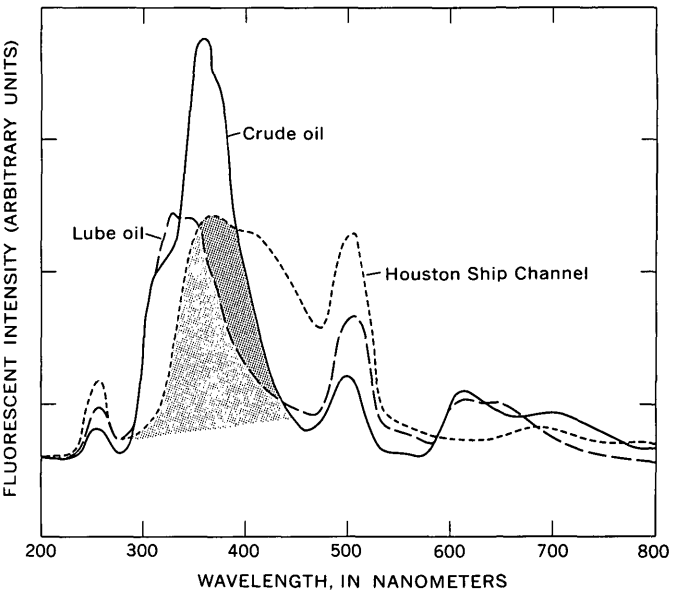

Figure 13. Fluorescent emission spectra of crude oil, lube oil, and Houston Ship Channel sample 3. The excitation wavelength was 250 nm.

chemical work such as liquid chromatography or thin-layer separations supported by infrared, ultraviolet, and mass-spectrometric identification, this type of spectral curve can be qualitatively and quantitatively complete (Guilbault, 1967; and Berlman, 1965).

Lignosulfonic acid

A characteristic material released from paper-pulp plants into holding ponds or water courses is lignosulfonic acid. This material has a natural fluorescence and seems suited as a tracer for waste discharge from paper-pulp plants.

Figure 14 is a set of concentration-dependent spectra illustrating the fluorescent response of this material. The fluorescent emission peak centers at 380 nm. Measures and Bristow (1971) report the limiting fluorescent sensitivity for calcium lignosulfonate (CA-L) at 0.5 mg/l. Thruston (1970) has shown in some streams a Ca-L background of 1–2 mg/l.

The absorption spectrum of lignosulfonic acid is given in figure 15; emission and absorption maxima are shown in the tabulation below.

	Emission maxima (nm)	*Absorption maxima (nm)*
Ligno-sulfonic acid.	380 (b)	287 (s), 245 (s), 325 (b)

It is apparent that from 220 nm to 320 nm, very strong absorption takes place. Such broadband excitation facilitates the use of broadband light sources.

DISCUSSION AND CONCLUSIONS

This study shows that the compounds chosen for investigation can be characterized by fluorescent emission and absorp-

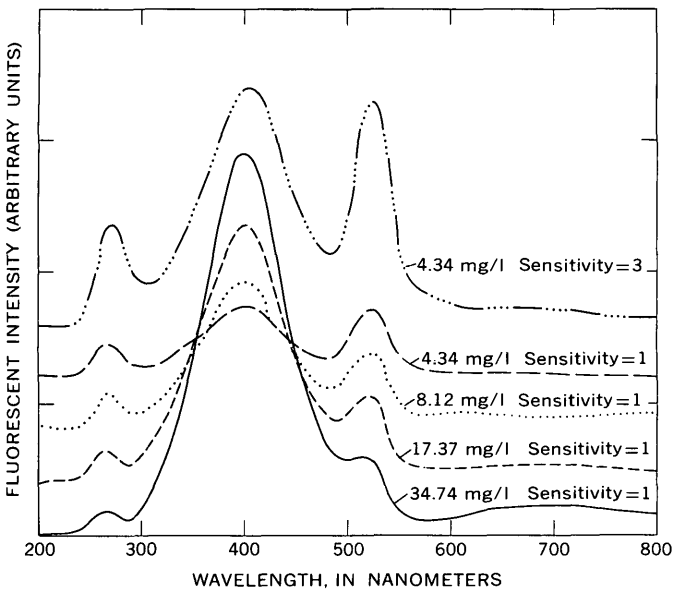

Figure 14.—Fluorescent emission spectra of lignosulfonic acid at different concentrations. The excitation wavelength was 250 nm.

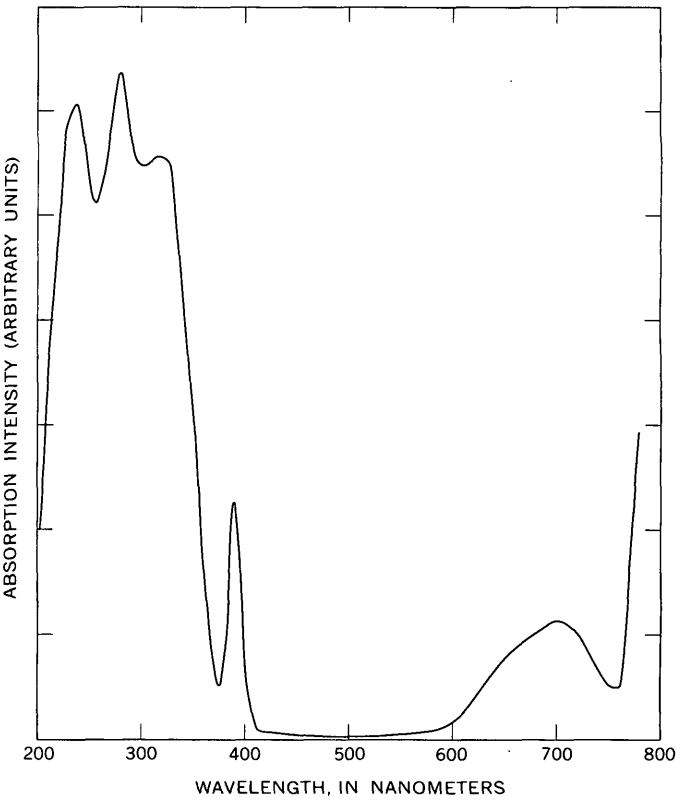

Figure 15.—Absorption spectrum of lignosulfonic acid. The emission wavelength was set at 395 nm.

tion spectroscopy. The following specific data were obtained for lube oil, crude oil, and lignosulfonic acid: The excitation frequency best suited to stimulate fluorescent emission from these materials was 250 nm. The emission maximum for lignosulfonic acid is 380 nm; absorption maxima occurred at 287, 245, and 325 nm. The crude oil emission maxima were at 300 and 320 nm; the absorption maximum occurred at 220 nm. The lube oil emission maximum differed from the crude oil maximum and was a single value occurring at 348 nm, but the absorption maximum was broader; it was displayed at 228–292 nm.

At the concentrations studied the emission curves yield a linear response to the concentration of the fluorescent material as long as the concentration did not differ by more than a factor of 10.

A sample taken from the Houston Ship Channel was analyzed. This sample exhibited a fluorescent response similar to that of the two oil standards but also exhibited additional fluorescent response from 300 to 400 nm, a longer wavelength response than from the oil samples. Very possibly this spectral curve would be unique when compared to that of other samples.

As was pointed out, the fluorescent emission is the result of a light photon returning to the ground state, but not immediately and not from the same energy level as the initial photon stimulation. The intermediate energy exchange that takes place, such as intersystem crossing, is independent of the surroundings. An emulsion or a surface film will react to light in an identical manner. Thus "through-the-solution" fluorescence is a valid method of simulating reflectance fluorescence.

Fluorescent spectroscopy is one method for characterizing materials that are known to be the main components of surface films. These films occur both on fresh water and salt water; however, with a high-powered light source and a sensitive detection system, component characterization such as that reported in this article may be applied to in situ samples regardless of location.

The information contained herein points out the usefulness of fluorescent spectroscopy as a tool to study and characterize the types of materials that comprise surface films.

REFERENCES CITED

Becker, R. S., 1969, Theory and interpretation of fluorescence and phosphorescence: New York, Wiley Interscience, 283 p.

Berlman, I. B., 1965, Handbook of fluorescence spectra of aromatic molecules: New York, Academic Press, 258 p.

Chandler, P. B., 1971, Oil pollution surveillance: Joint Conf. on Sensing of Environmental Pollutants, Palo Alto, Calif., Nov. 8–10, Paper 71-1073, 8 p.

Duce, R. A., Quinn, J. G., Olney, C. E., Piotrowicz, S. R., Ray, B. J., and Wade, T. L., 1972, Enrichment of heavy metals and organic compounds in the surface microlayer of Narragansett Bay, Rhode Island: Science, v. 176, p. 161–163.

Goldberg, M. C., DeLong, L. L., and Sinclair, Mark, 1973, Extraction and concentration of organic solutes from water: Anal. Chem., v. 45, no. 1, p. 89–92.

Goldberg, M. C., and Weiner, E. R., 1972, Applications of spectroscopy to remote determination of water quality: Nat. Oceanic and

Atmospheric Adm. and U.S. Naval Research Lab. 4th Ann. Earth Resources program rev., Manned Spacecraft Center, Houston, Tex., v. III, p. 81–11 to 81–14.

Goolsby, A. D., 1971, Water pollution detection by reflectance measurements: Joint Conf. on Sensing of Environmental Pollutants, Palo Alto, Calif., Nov. 8–10, Paper 71-1069, 6 p.

Guilbault, G. G., 1967, Fluorescence, theory, instrumentation and practice: New York, Marcel Dekker, Inc., 697 p.

Herzberg, Gerhard, 1939, Molecular spectra and molecular structure, I. Spectra of diatomic molecules: Princeton, N.J., D. Van Nostrand and Co., Inc., 1st ed., 658 p.

——1945, Molecular spectra and molecular structure, II. Infrared and Raman spectra of polyatomic molecules: Princeton, N.J., D. Van Nostrand Co., Inc., 632 p.

Klemas, Vytautas, 1971, Detecting oil on water—a comparison of known techniques: Joint Conf. on Sensing of Environmental Pollutants, Palo Alto, Calif., Nov. 8–10, Paper 71-1068, 6 p.

Measures, R. M., and Bristow, M., 1971, The development of a laser fluoresensor for remote environmental probing: Joint Conf. on Sensing of Environmental Pollutants, Palo Alto, Calif., Nov. 8–10, 7 p.

Parker, C. A., 1959, Raman spectra in spectrofluorimetry: Analyst, v. 84, p. 446.

——1968, Photoluminescence of solutions with applications to photochemistry and analytical chemistry: New York, Elsevier Publishing Co.

Phillips, R. E., 1969, Fluorometry in research and industry: Am. Lab., v. 10, p. 8–12.

Stoertz, G. E., Hemphill, W. R., and Markle, D. H., 1970, Remote analysis of fluorescence by a fraunhofer line discriminator: Marine Technology Soc., 6th Ann. Conf. and Exposition, Washington, D.C., June 29–July 1, 1970, v. 2, p. 1017–1040 [Preprints].

Thruston, A. D., Jr., 1970, A fluorometric method for the determination of liquid sulfonates in natural waters: Water Pollution Control Federation Jour., v. 42, p. 1551–1555.

Udenfried, Sidney, 1962, Fluorescence assay in biology and medicine: New York, Academic Press, 517 p.

Weber, G., and Teale, F. W. J., 1957, Determination of the absolute quantum yield of fluorescent solutions: Faraday Soc., Trans., v. 53, p. 646.

Zobell, C. E., 1971, The occurrence, effects and fate of oil polluting the sea: Internat. Air-Water Pollution, v. 7, p. 173–197.

Jour. Research U.S. Geol. Survey
Vol. 1, No. 6, Nov.-Dec. 1973, p. 719—723

PROBLEMS OF UNDERGROUND STORAGE OF WASTES

By RAYMOND L. NACE, Raleigh, N.C.

Abstract.—Problems of underground storage of waste involve geology in its broadest sense, including hydrology, geochemistry, and geophysics. Wastes may be solid, liquid, or gaseous, and they may be chemically toxic or noxious, esthetically offensive, or radioactive. Some wastes require only temporary containment, whereas others must be isolated for indefinitely long periods. The means and locale for emplacement underground depend upon many governing geological factors, including the physical, chemical, hydrological, and hydraulic properties of the host formation. These must be studied relative to the physical, chemical, and thermal properties of the waste and of potential interactions between the waste and the host formation. Thorough knowledge is essential because lack of it may lead to undesirable or disastrous environmental consequences. Escape of waste may contaminate the surface or near-surface environment; it may destroy the usefulness or accessibility of resources such as ground water, petroleum, and minerals. Effective management of underground waste requires adaptation of current technology and development of new technology.

Increasing stringency of governmental regulation of pollution by discharge of industrial, sewage, and other wastes into surface waters in the United States has caused many producers of pollutants to consider underground disposal or storage. The thesis is that underground injection of wastes would be cheaper than treatment required for discharge at the land surface. A half century of experience in oil fields, where brine (produced along with petroleum) is injected underground to avoid contamination of surface waters and fresh ground waters, has led to optimism that injection may be feasible for some industrial wastes and treated sewage. Many thousands of brine-injection wells are in use at present. In addition, thousands of injection wells are used to repressure oil-producing reservoirs.

For many years hydrogeologists have called attention to the tremendous amount of water stored in aquifers, but in the United States ground water has received little attention in regional water-resources planning. A common point of view is that ground water is available for individual, local, and small-community use, but has no significance in regional water-resources development. Ironically, the great capacity of geological formations for liquid storage now is being cited as an argument favoring their use for waste storage. At the same time, planners are awakening to the potential benefits of joint management of ground water and surface water as a single resource.

A quality of human nature is to seize upon each supposedly new alternative solution of a problem as though it were a panacea. But subsurface waste disposal is no panacea, as has been ably explained by Piper (1969). Moreover, the practice is not new. The cesspool and the septic tank, which have been used for centuries, are underground disposal devices.

Literature on underground waste injection in the United States is fairly abundant, but most of it is conjectural, some is misleading, and some is downright erroneous. A symposium on underground waste management was staged in Houston, Tex., during December 6–9, 1971. This should place the problem in perspective. Beyond that, it seems important to have an international forum, where experiences and ideas of workers from various countries may be exchanged. It would be timely for an international organization to sponsor a symposium on the topic. Meantime, one or more international organizing seminars might be useful.

Acknowledgments.—I wish to acknowledge gratefully the careful and constructive reviews of the manuscript of this article by Paul H. Jones, Francis A. Kohout, Robert Schneider, and Leonard A. Wood.

HISTORICAL NOTE

The oil industry was one of the first to generate and dispose of large volumes of waste liquid—to be specific, brine, a byproduct of petroleum production. Early in this century brine was disposed of simply by dumping it on the ground or into seepage pits. This became unacceptable because of infiltration and runoff into streams, and during the past 50 years many thousands of brine disposal systems have been installed, chiefly so-called reverse wells for underground injection of brine.[1]

Underground injection received little attention in other industries until about 20 years ago, when the atomic energy industry began a serious search for means and places to get rid of dangerous radioactive liquid wastes. The search was unsuccessful because no responsible geologist was willing to

[1] A commonly accepted definition of a water well is a hole in the ground from which water is sought or obtained. The term "reverse well" may be appropriate for a ground-water recharge hole, but it is inappropriate for a disposal structure.

say that dangerous liquid waste, injected in any given formation, would remain there for the necessary period of 600 to 1,000 years.

Underground injection of other types of wastes received little consideration by industry before about 1950. However, the number of underground waste injection systems in the conterminous United States has increased from about six in 1953, to 35 in 1963, and about 150 in 1969 (Cleary, 1969). No doubt many disposal operations exist that have not been reported or canvassed.

PREVIOUS EXPERIENCE

As previously noted, the petroleum industry has acquired a great deal of experience during the past 50 years in underground injection of waste brine solutions. The supposition is common that this wealth of experience should be applicable to the construction and operation of structures for disposal of industrial wastes. While some of the experience is applicable, the problem of industrial waste disposal is vastly different from that of brine disposal.

In some oil-field operations, water-injection holes serve to repressure the oil reservoir and thus to prolong or increase oil production. Pretreatment of injection water is common, and this practice generally raises no serious problems. The brine commonly returns to the formation from which it came; pore space having lowered pressure is available; and the brine is chemically compatible with the host formation and its contained fluids. In other operations the brine returns, not to the original host formation, but to some more shallow zone which has the capacity to accept the waste. The more shallow zone may be lithologically similar to the host zone, and no serious problem arises of chemical compatibility with the formation or its contained native liquid. Where incompatibility arises, injection may be accomplished anyway by exerting high pressures upon the relatively low volumes generally involved in any one operation.

Oil-field practices have caused countless problems, many of which have not received wide publicity. Many abandoned oil wells have not been effectively plugged, and pressure in the salaquifer has caused brine to leak out at the surface. In other abandoned wells the casing has deteriorated and brine finds its way to the land surface, into phreatic aquifers, and thence into surface streams, causing salinity problems. In extensive areas in the southern midcontinent, both underground and at the surface, waters are too saline for ordinary use. This natural condition has been aggravated by human activity, but the extent of the aggravation has not been determined.

Much oil-field experience is inapplicable to the problem of industrial wastes. Except for the uncertainty of control, the disposal of industrial wastes poses wholly different problems. These problems stem from the facts that (1) industrial plant sites have not been chosen with the feasibility in mind of underground waste disposal; (2) the properties of waste materials cover a wide range, and their physical, chemical, thermal, and radioactive properties are foreign to oil-field experience; and (3) the volumes of waste injected into a single well may be many times greater than in a brine-disposal well. The problem at hand, therefore, is new and requires the development of a wholly new technology.

CLASSIFICATION OF WASTES

Industrial and other wastes may occur in any of the three phases of matter: solid, liquid, or gaseous. Some wastes are mixtures of phases or mixtures of differing wastes in a single phase. The variety of materials in each phase is bewildering. In terms of their character the wastes may be esthetically offensive, biologically noxious or toxic, or dangerously radioactive.

These wastes may be so varied in their chemical, physical, and radiometric properties that it is not possible to classify them by simple groups. Waste effluent from a single industrial plant may contain more than 100 different chemical compounds. The liquids may include alkali, acid, chromate, nitrate, phosphate, and sulfite solutions, various organic materials such as alcohol, ketone, phenol, cyanide, and chlorinated hydrocarbon (Cleary, 1969, p. A-2). Some radioactive wastes have noxious or toxic characteristics in addition to radioactivity.

SPECIFIC PROBLEMS

Any proposed or actual waste-injection operation will entail many problems. Some of these problems will require virtually complete knowledge of the geology, hydrology, geochemistry, and seismicity of the disposal site and surrounding area. Disposal would require so much expense for site study, testing, and monitoring that, in many areas, it would be cheaper to treat the waste for surface disposal than to meet reasonable requirements for safe underground injection.

Salaquifers

In U.S. Geological Survey usage, water is classed as saline if it contains 1,000 mg/l or more of dissolved solids. Higher concentrations are used at some places for domestic and stock-water supply, and also for irrigation where less mineralized water is not available. Saline water may be used for industrial cooling also.

Traditionally, saline ground water has been considered as a nuisance, which in some places it will always be. For that reason, some advocates of underground injection of wastes have assumed that all salaquifers are potential zones for injection. The premise is that the native water is useless and that no harm will be done. This is erroneous. With advances in desalting technology, saline water becomes a resource. Kohout and others (1970) described a variety of ways in which saline water and salaquifers may be used directly and indirectly.

The total volume of saline ground water exceeds by many

times that of fresh water in the United States. This probably is true also of much of the world land area. Feth and others (1965) showed that waters containing 1,000 mg/l or more of dissolved solids underlie much of the United States. The depth to saline water is less than 150 m in somewhat more than one-third of the United States. The use of salaquifers as waste sinks, therefore, must be evaluated relative to other possible uses.

Underground storage capacity

At 15 percent porosity, a mass of 1 km^3 of rock or sediment could contain 150×10^6 m^3 of liquid. Such examples have been cited as evidence that the potential for underground injection is immense. However, all rock pores beneath the earth's unsaturated zone (zone above the water table) are saturated with fluid, either gaseous or liquid. This fluid must be displaced or compressed to provide room for injected liquid. Several ways in which additional space could be created are pressure-compression of the native fluid, hydraulic uplift of the overburden, and hydraulic fracturing.

For practical purposes, water is incompressible and little storage space could be created by compression in a salaquifer unless the contained volume of liquid is very large.

In some aquifers the weight of overburden is sustained partly by grain-to-grain contact of rock minerals and partly by hydraulic forces. Increase of hydraulic pressure in some circumstances theoretically could expand the aquifer and raise the overburden. Where the waste-injection zone is at considerable depth—on the order of thousands of meters—the required injection pressure would be very high.

Hydraulic fracturing is a technique developed in the petroleum-production industry to facilitate flow of oil from the reservoir rocks into wells. For waste disposal a modified technique may be used to accomplish the reverse process—flow of waste from an injection well into the host rock. We do not have space here to describe the technique in detail. In some geological situations it is feasible. De Laguna (1970) has described the method in detail for one set of circumstances dealing with radioactive liquid waste.

Existing stress underground can be very important to the success of waste injection. A well about 3,600 m deep, extending to the basement rock, was drilled a few miles from Denver, Colo., for the purpose of injecting noxious liquid waste in a geologic environment where it presumably could do no harm. Inasmuch as the rock is dense and very low in permeability, waste was injected at very high pressure. Within a few months after injection began, a series of mild to moderate earthquakes shook the Denver area. The possibility of a relation between the quakes and the waste injection occurred to one geologist (Evans, 1966). Study of seismic records and injection rates showed an apparent correlation. Subsequent study has confirmed this (Raleigh, 1972), although direct proof of a relation has not been established. Use of the injection well has ceased and the earthquakes have not recurred.

Chemical compatibility

Chemical compatibility of the waste liquid with the host rock and native water is an important aspect of subsurface storage. Chemical reactions may yield precipitates, clogging the openings in the host rock. The heat of reactions may also produce adverse changes in the rock. Reactions and changes in some rocks produce an increase in pore volume, further complicating the situation. Some reactions produce gases which could be noxious or inflammable. Gases are much more mobile than water, and their escape from the storage reservoir is more likely. Entrained gases in the injected fluid will drastically reduce permeability, causing higher pressures or decreased flow.

Detention time

Detention time in the waste-injection zone is an important criterion of the feasibility of injection. In the operation described by de Laguna, liquid waste is mixed with clay and cement to form a slurry. After injection the slurry solidifies in the fractures created at depths which are on the order of 100 m or more beneath the land surface. The waste will remain motionless and will not enter the surface environment until erosion exposes it thousands or millions of years in the future.

Most ground water, including that in many salaquifers, is in motion. Liquid wastes that remain liquid are potentially mobile in ground-water systems. Motion in an aquifer implies that the liquid is discharging by seepage or through springs at outcrops or by leaking into other formations. Injection of foreign fluid might accelerate motion; the waste might then migrate to locations where it is undesirable, leak into other geological formations, or appear at the land surface.

Ground-water movement in general is very slow. In highly permeable aquifers, such as clean gravel, the rates of movement may reach as much as 15 or 18 m day^{-1}. In material with only slight permeability the rate may be only a few centimeters per year. In clay, motion may be nil because molecular forces binding water to the clay may be stronger than gravitational and (or) hydraulic forces. On the other hand, osmotic forces may cause liquid to move through clay beds that separate aquifers in which the differences in salinity are large (Jones, 1969, p. 3, 63).

Presumably, some waste injection zones will be at considerable depth, where formations are virtually impermeable. Injection there can be accomplished only by hydraulic fracturing. The fluid presumably would move only so long as pressure and more liquid continued to be applied. However, some risks are involved. If fractures formed vertically rather than horizontally, liquid might migrate upward into locations

where it is undesirable. Liquid might migrate upward also if it reached a permeable fault zone, or if movement occurred along a fault.

Contamination or denial of resources

The possibility that fresh ground water and surface water may be inadvertently contaminated by waste-injection operations is obvious. As is well known, few if any confined (artesian) aquifers are absolutely confined. Upward leakage through confining beds may be extremely small per unit area, but total leakage through a large area can be significant. Where the confining bed is very thick, a given molecule of liquid might require hundreds or thousands of years to pass through. On the other hand, waste liquid might react with the confining bed either to make it even less permeable or to make it more so. If the latter occurs, waste might migrate into bodies of fresh ground water or even reach the land surface.

Many useful mineral deposits remain undiscovered. Contamination of the lithosphere may deny access to such deposits. From geologic evidence it is certain that readily available mineral deposits form only a small fraction of 1 percent of the earth's crust. Projections indicate that the demand for primary minerals will increase fourfold by the year 2000. Many secondary minerals are already in short supply, and the average grade of ore mined diminishes with time.

It is therefore important to explore thoroughly each proposed injection site, if that has not been done already, in order to avoid contamination of resources or denial of access to resources.

MONITORING

The geology, hydrology, meteorology, and other aspects of the environment at an injection site must be thoroughly known and understood; in addition, it is necessary to monitor the effects of disposal operations. Advance knowledge helps prediction, and perhaps even control, of the behavior of wastes underground. It is not possible to obtain information on all important parameters of the underground environment in advance. Therefore, results of injection may not conform to predictions. Monitoring is necessary to observe actual behavior of waste in storage underground.

Monitoring may be simple under some circumstances and very complicated under others. Monitoring should always be done in the injection well. Generally, the sealed annular space between the well casing and the injection tubing is filled with an innocuous fluid that counteracts upward pressure against the seal in the lower part of the hole. Monitoring of the pressure and fluid quality in the annular space permits detection of leakage of waste from the injection tubing or through a ruptured seal. Injection pressure and the integrity of injection mechanisms must also be monitored. Case histories are on record where injection mechanisms failed, thus permitting thousands of gallons of waste liquid to discharge at the land surface where they could not be contained or recovered. Dikes around an injection well are advisable to retain wastes in the event of an accident; also storage facilities should be provided to contain wastes when injection mechanisms fail.

The nature of injected waste also must be monitored because it is commonly variable and may change drastically with changes in processes that produce the waste. Changes in the physical, chemical, and thermal properties of the waste may have a strong bearing on the feasibility of continued injection.

Monitor wells should be installed in the host formation and adjoining formations to determine the paths and rates of waste movement, reactions with the rock, and properties of residual fluids. Hydraulic phenomena must also be monitored. The hydraulic gradients in a natural aquifer may be markedly altered by the stress of waste injection.

CONCLUSIONS

Some "authorities" have hailed the idea of underground waste management as a virtual panacea for industrial waste problems. Others believe that underground injection is, at best, an interim measure that can be used only as a stopgap pending development of technology that will permit treatment of wastes so that they may be discharged safely at the land surface.

The weight of evidence seems to favor a view that, in some circumstances, waste may be disposed of safely underground. To use a simple example, treated sewage effluent discharged into a salaquifer may have better quality than the native water in the aquifer. Most wastes and problems of waste management, however, are much more complex than the example. It seems unlikely that large volumes of noxious or toxic wastes can be stored safely underground as a general practice. In many situations complete treatment and renovation of waste for surface discharge must be accomplished.

Statements about general practice, however, should not be construed to exclude consideration of underground waste storage in some areas. Data from exploration deep underground in petroleum-bearing provinces, for example, show that fluids, including saline aqueous solutions, have been held naturally in subsurface storage for millions of years. Artificially injected natural gas has been stored routinely underground in geological formations for many years with only a few reported instances of escape.

Evidently, if underground waste storage is to become predictably safe as well as technically feasible, new technology must be developed, including new kinds of appraisals of subsurface environments. Hydrologic, geochemical, and geophysical parameters must be appraised and tested; methods, devices, and procedures for testing and monitoring effects of underground emplacement must be developed. Legal and economic factors also must be considered in studies of the problem. Specific problems will require specific answers for specific instances.

REFERENCES CITED

Cleary, E. J., 1969, Public policy, legislative and legal aspects, pt. 1 *of* Perspective on the regulation of underground injection of wastewaters: Cincinnati, Ohio River Valley Water Sanitation Comm., 19 p.

de Laguna, Wallace, 1970, Radioactive waste disposal by hydraulic fracturing: Indus. Water Eng., Oct. 1970, p. 32–37.

Evans, D. M., 1966, The Denver area earthquakes and the Rocky Mountain Arsenal disposal well: Mtn. Geologist, v. 3, no. 1, p. 23–36.

Feth, J. H., and others, 1965, Preliminary map of the conterminous United States showing depth to and quality of shallowest ground water containing more than 1,000 parts per million dissolved solids: U.S. Geol. Survey Hydrol. Inv. Atlas HA-199.

Jones, P. H., 1969, Hydrology of Neogene deposits in the northern Gulf of Mexico basin: Louisiana Water Resources Research Inst. Bull. GT-2, 105 p.

Kohout, F. A., ed., 1970, Saline water, a valuable resource: Water Resources Research, v. 6, no. 5, p. 1441–1531. [Series of 16 papers reprinted as a special symposium volume]

Piper, A. M., 1969, Disposal of liquid wastes by injection underground–neither myth nor millennium: U.S. Geol. Survey Circ. 631, 15 p.

Raleigh, C. B., 1972, Earthquakes and fluid injection, *in* Cook, T. D., ed., Underground waste management and environmental implications: Am. Assoc. Petroleum Geologists Mem. 18, p. 273–279.

Jour. Research U.S. Geol. Survey
Vol. 1, No. 6, Nov.-Dec. 1973, p. 725–734

EFFECTS OF MIGRATORY WATERFOWL ON WATER QUALITY AT THE MONTEZUMA NATIONAL WILDLIFE REFUGE, SENECA COUNTY, NEW YORK

By MARK R. HAVE, Albany, N.Y.

Work done in cooperation with the Bureau of Sport Fisheries and Wildlife of the U.S. Fish and Wildlife Service

Abstract.—This study was done in response to the shellfish industry's concern that bacteria in effluent from the national wildlife refuges along the northeast coast of the United States may be adversely affecting the harvest of shellfish. A line graph shows inconsistent relationships between bird population at the Montezuma refuge and total coliform, fecal coliform, and fecal *Streptococci* counts. *Salmonella* were found in only one of 17 samples of water taken within the refuge. Counts of nonpathogenic bacteria in the two major streams flowing into the refuge, Black Brook and White Brook, were greater than they were in water flowing out of the refuge. Specific conductance of water flowing out of the refuge was less than that of water flowing into the refuge, although the effluent had higher concentrations of phosphorus and nitrogen than the influent. A settling-pond effect in the quiet water of the refuge may help explain the improvement in the quality of the water leaving the refuge. The study shows how its quality changes both chemically and biologically as water flows through the refuge. Further study is needed, however, to determine the effects that a similar effluent would have on a coastal habitat of shellfish.

The shellfish industry is concerned that effluent at national wildlife refuges along the northeast coast of the United States may be detrimental to shellfish in this area. Shellfish taken from a polluted marine environment can be contaminated with pathogenic as well as nonpathogenic bacteria. These organisms can be present in the product when it reaches the consumer; therefore, the risk of disease is present, especially in shellfish that are eaten raw or after being only briefly cooked (E. B. Pike and A. L. H. Gameson, written commun., Sept. 1969).

Moran, Van Houweling, and Ellis (1965) found *Salmonella* in feces from domestic ducks and geese, but apparently few, if any, similar studies have been done with wild ducks and geese. Therefore, the U.S. Geological Survey, in cooperation with the Bureau of Sport Fisheries and Wildlife of the U.S. Fish and Wildlife Service, monitored the quality of influent and effluent at the Montezuma National Wildlife Refuge in Seneca County, N.Y., to determine the effects of migratory waterfowl on the quality of effluent at wildlife refuges. It is beyond the scope of this study to predict the effect of effluent from a wildlife refuge on the harvest of shellfish. To be able to do this, one would need to determine the effect of wind, streamflow, and tides on the distribution of pollutants in the habitat of shellfish. The Montezuma National Wildlife Refuge study was made strictly to determine how water quality changes when water flows through a wildlife refuge.

The refuge lies 32 miles west of Syracuse, N.Y., at the north end of Cayuga Lake in Seneca County. The refuge headquarters is 4 miles northeast of Seneca Falls on New York State Route 5 and U.S. Route 20 (fig. 1). The refuge provides a typical marsh-type environment with controlled inlets and outlets.

Acknowledgment.—Much helpful data on bird population and water management were furnished by Martin S. Phillips, refuge manager at the Montezuma National Wildlife Refuge.

THE REFUGE AREA

Montezuma National Wildlife Refuge consists of 6,344 acres of cattail marshes, timbered impoundments, and cultivated fields. Originally, the refuge area was a great marsh, where, according to Jesuit missionaries, clouds of wild ducks and geese obscured the sun (U.S. Dept. Interior, 1969). An attempt to use the marshland for cultivation and the construction of the New York State Barge Canal largely drained the marshland. The refuge, established in 1938 to restore the former marshland, serves as an important resting place for birds on their migrations during spring and fall (Murphy, 1968, p. 276).

INHABITANTS

The varied habitat of the refuge provides homes for numerous birds, mammals, and fish of many species. About 270 species of birds have been observed on the refuge. Blue-winged teal, mallard ducks, and wood ducks are the most abundant nesting waterfowl. There is also a variety of herons, shore birds, terns, and songbirds. Population of waterfowl is

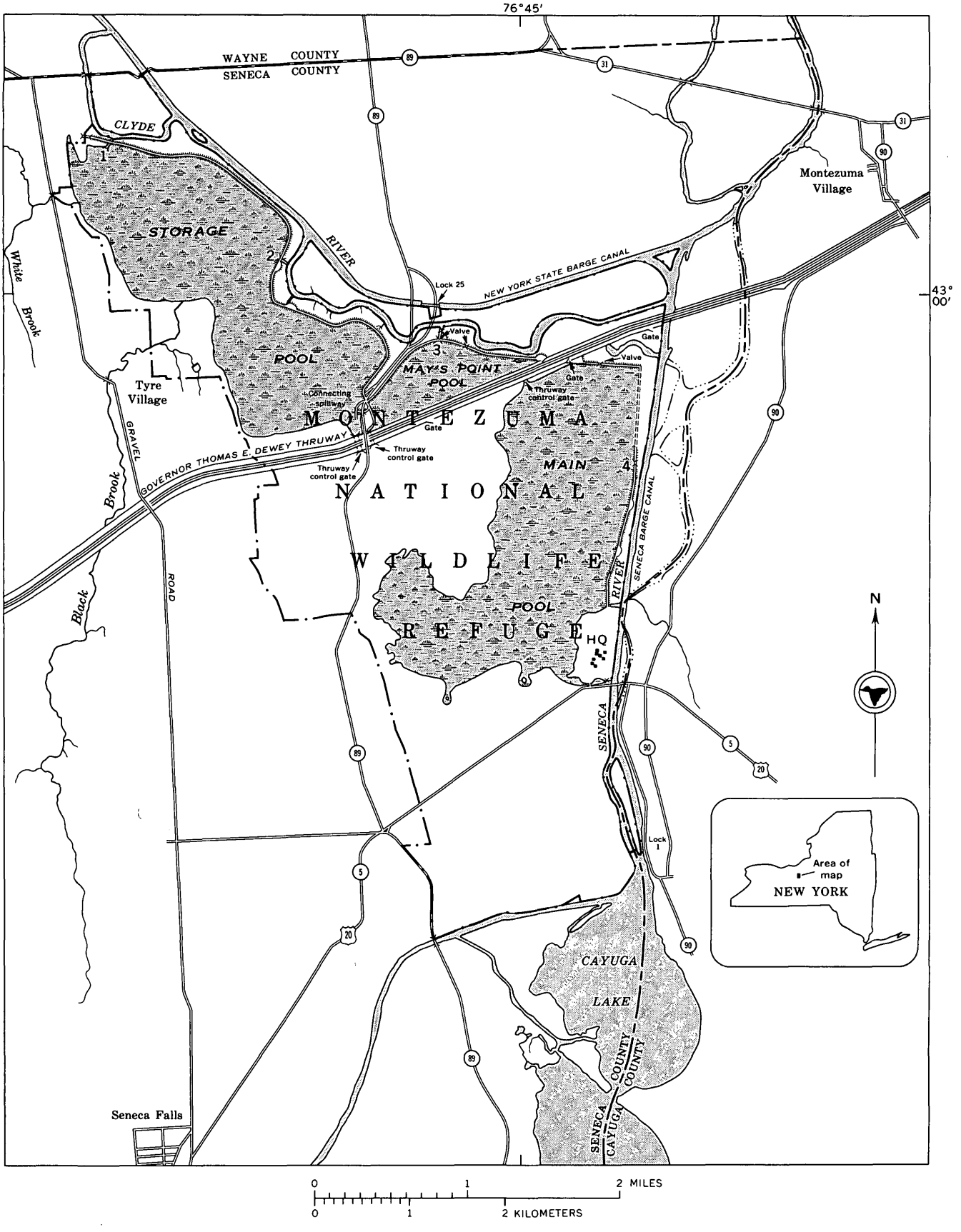
76°45'
WAYNE COUNTY
SENECA COUNTY
CLYDE
STORAGE
POOL
RIVER
NEW YORK STATE BARGE CANAL
Lock 25
Montezuma Village
43° 00'
White Brook
Tyre Village
GRAVEL ROAD
Black Brook
GOVERNOR THOMAS E. DEWEY THRUWAY
Connecting spillway
Thruway control gate
Valve
Gate
MAY'S POINT POOL
MONTEZUMA
NATIONAL
WILDLIFE
REFUGE
MAIN POOL
HQ
SENECA RIVER
SENECA BARGE CANAL
Lock 1
CAYUGA LAKE
SENECA COUNTY
CAYUGA COUNTY
Seneca Falls
N
Area of map
NEW YORK
0 1 2 MILES
0 1 2 KILOMETERS

Figure 1

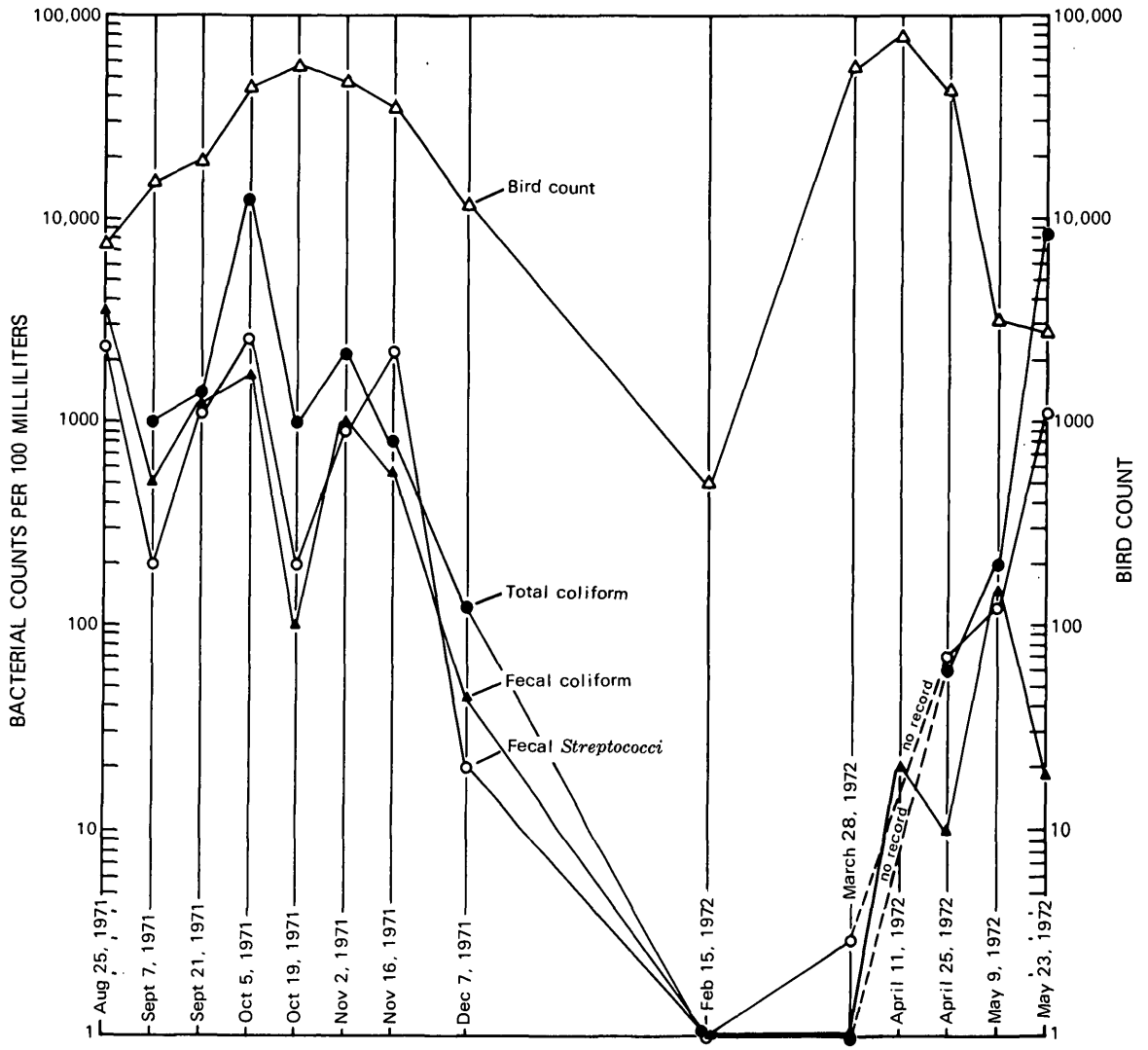

Figure 2.—Bacterial counts at Seneca spillway, Montezuma National Wildlife Refuge, near Seneca Falls, N.Y., and bird counts at the refuge. Birds are counted once a week at the refuge (not necessarily on the same day that bacteria are counted), and that count is used as the bird population for the entire week.

greatest during spring and fall migrations. (See fig. 2.) Peak counts of 70,000 geese in April and 100,000 ducks in October have been noted (U.S. Dept. Interior, 1969).

Deer and woodchucks are commonly seen on the refuge. Woodchucks are abundant and, during spring, are a nuisance along the dikes where they burrow. The marshland is an excellent habitat for muskrats. When properly managed, the activities of the muskrats help maintain marsh vegetation for use by waterfowl. The population of muskrats is controlled by trappers, who harvest between 1,000 and 8,000 annually.

Figure 1.—Montezuma National Wildlife Refuge. Dot-dash line is refuge boundary. Sampling sites within the refuge are: 1, White Brook spillway; 2, Black Brook spillway; 3, Mays Point spillway; and 4, Seneca spillway. (Modification of operating map, Montezuma National Wildlife Refuge, Seneca County, N.Y., U.S. Dept. Interior, Bureau of Sport Fisheries and Wildlife, drawing 5R-N.Y.-234-407, June 13, 1966.)

Warmwater fish are plentiful in the Clyde and the Seneca Rivers and in Cayuga Lake. Popular species include brown bullhead, northern pike, and walleye (U.S. Dept. Interior, 1969).

HYDROLOGY OF THE REFUGE

Water flowing into the refuge

The major flow into the refuge is by means of Black Brook and White Brook, which flow into the west side of Storage Pool (fig. 1). The two streams are 4.6 and 2.3 miles long and have drainage areas of 20 and 7 sq mi, respectively. They meander between long parallel ridges and through cultivated fields and pastureland. There are a few houses along each stream.

The chemical qualities of Black Brook and White Brook are similar. Both streams have a calcium bicarbonate sulfate type

water. This reflects the Camillus Shale of the Salina Group in the area. The Camillus Shale belongs to the Upper Silurian Series of rocks and has an average thickness of about 525 feet. The shale contains beds of limestone, salt, and gypsum (L. J. Crain, written commun., 1969).

For this study, discharge was measured routinely only at Black Brook, the larger of the two streams. Measured discharge ranged from 0.96 cfs on October 19, 1971, to 32 cfs on April 11, 1972. On May 9, 1972, after many days of rain, flow was estimated to be 97 cfs.

Water in the refuge

The refuge has three major pools—Storage Pool, Mays Point Pool, and Main Pool. All the pools are surrounded by earthen dikes. Water in Mays Point Pool and Main Pool is obtained mainly by diverting water in Storage Pool through connecting outlets and inlets. Water levels in Storage Pool and Mays Point Pool are controlled by spillways regulating flow into the Clyde River, which is part of the New York State Barge Canal. The water level in Main Pool is controlled at its outlet, Seneca spillway, which empties into the Seneca River. The Seneca River merges with the New York State Barge Canal at the northeast corner of the refuge.

The water is a mixed type dominated by calcium, sodium, bicarbonate, sulfate, and chloride ions (U.S. Geol. Survey, unpub. data, 1971). These ions reflect swamp and lake deposits in the refuge and surrounding area. The deposits are mainly composed of silt and clay but contain peak, muck, and marl (L. J. Crain, written commun., 1969).

SAMPLING SITES AND SAMPLING FREQUENCY

Water samples for both chemical analysis and bacterial counts were collected from three primary sites—Seneca spillway, Black Brook at the gravel road, and White Brook at the gravel road (fig. 1). In general, samples were collected biweekly from August 25 through December 7, 1971, and from March 28 through May 23, 1972. Samples were also taken on February 15 and 16, 1972. Water samples for only bacterial counts were collected on April 25, 1971, at two secondary sites—Black Brook spillway and White Brook spillway—during the peak of spring runoff and the spring migration of waterfowl. Mays Point spillway was considered as a secondary sampling site, but it was not flowing at the time the other two secondary sites were sampled. Black Brook spillway was sampled again on May 9, 1972.

PARAMETERS DETERMINED

Parameters determined at the sampling sites included air and water temperatures, sampling depth, specific conductance, pH, alkalinity (reported as carbonate and bicarbonate), dissolved oxygen and percent saturation of dissolved oxygen, total coliform, fecal coliform, fecal *Streptococci*, and *Salmonella*. Discharge and gage height (stage) were determined in the field at Black Brook and at Seneca spillway. Parameters determined in the laboratory included ammonia as N (nitrogen), organic N, nitrate as N, nitrite as N, total N, phosphorus, total solids (dissolved plus undissolved) and fixed solids (residue after ignition at 600°C, Celsius, for 5 minutes), and TOC (total organic carbon).

ANALYTICAL PROCEDURES

Specific conductance, pH, alkalinity, and air and water temperatures were determined by the methods of the American Public Health Association and others (1971, p. 323, 276, 52, and 348) and Brown, Skougstad, and Fishman (1970). Dissolved-oxygen concentration was determined by a dissolved-oxygen meter. Dissolved-oxygen concentration and water temperature were used in the calculation of percent saturation of dissolved oxygen (Am. Public Health Assoc. and others, 1971, p. 480). Samples were taken near the surface, so the sampling depth was assumed to be 0.1 foot. All samples were unfiltered.

Discharge at Black Brook was measured with a current meter. Gage height was determined by measuring the distance from a reference point on the bridge to the water surface.

Discharge at Seneca spillway was calculated by the discharge equation for a contracted weir. Gage height was read from the staff gage at the spillway.

Phosphorus and total and fixed solids were collected and determined by the methods of the American Public Health Association and others (1971, p. 526 and 535) and Brown, Skougstad, and Fishman (1970).

Samples for the determination of ammonia as N, nitrate as N, and nitrite as N were collected by the method of Brown, Skougstad, and Fishman (1970, p. 17). The parameters were determined on a Technicon autoanalyzer.[1,2] The digestion and the distillation steps of the Kjeldahl method, described by Brown, Skougstad, and Fishman (1970, p. 122), were used for determining organic nitrogen. The distillate was then analyzed on the autoanalyzer. Total N was calculated by adding the concentrations of the different forms of N.

Total organic carbon was determined by the method of Goerlitz and Brown (1972, p. 4).

Total coliform, fecal coliform, and fecal *Streptococci* were determined by the membrane-filter technique described by the American Public Health Association and others (1971, p. 679, 684, and 690) and by Slack and others (1970). These parameters were determined in triplicate and were averaged for presentation in table 1.

Qualitative tests described by the American Public Health Association and others (1971, p. 698) were modified to

[1]The use of named products in this report is for identification purposes only and does not imply endorsement by the U.S. Geological Survey.

[2]Technicon Corporation, Tarrytown, N.Y., 1969, Technicon industrial method, 19-69W, 33-69W, and 35-69W.

determine whether *Salmonella* were present. At each sampling site, two 1-liter samples of water were collected and were immediately filtered through separate sterile 0.45-μm filters. One filter was placed into a vial containing a solution of tetrathionate broth, and the other was placed into a vial containing selenite broth. After the vials of broth were incubated for 24 hours at 35°C, plates of brilliant green agar, bismuth sulfite agar, and "Salmonella Shigella" agar were streaked with selenite and tetrathionate cultures. These plates were then incubated for 24 hours at 35°C. After the vials were incubated for an additional 24-hour period at 35°C, fresh plates were streaked and incubated as before. The plates were inspected for characteristic *Salmonella* colonies, and suspected colonies were restreaked onto fresh plates to purify the culture. The purified cultures were then streaked onto slants of TSA (tryptic soy agar), incubated at 35°C for 24 hours, and maintained at refrigerator temperature until final confirmation could be made.

Preparation for the confirmation tests was begun by further purifying the refrigerated cultures. This was done by streaking the slant cultures onto TSA plates and restreaking the plate cultures onto new TSA plates until pure cultures were obtained. The latest plate cultures were then streaked onto fresh TSA slants. All these transfers were incubated at 35°C.

The fresh TSA slant cultures were then streaked onto slants of urea, phenylalanine, lysine iron, and TSI (triple sugar iron) agars. Presence of *Salmonella* was indicated if the TSI test was positive and the others were negative.

The TSA slant cultures were then subjected to one more confirmation test, an agglutination test with Salmonella O antiserum poly A-1. If this test was positive, the culture was then considered to be *Salmonella*.

RESULTS AND DISCUSSION

Table 1 shows monthly counts of total coliform, fecal coliform, and fecal *Streptococci* for all the sampling sites. During the migration months of October, November, and March, 80 percent of the bacterial counts at Black Brook and White Brook were higher than those at Seneca spillway. During April, another migration month, bacterial counts at Black Brook and White Brook were higher than at any of the three spillways.

Table 1.—*Comparative bacteria counts at primary and secondary sampling sites*

[Where two dates are shown, the result is the average of the two]

Sampling site	Sampling date	Total coliform (per 100 ml)	Fecal coliform (per 100 ml)	Fecal *Streptococci* (per 100 ml)
Seneca spillway	8-25-71	(1)	3,600	2,400
	9-7, 9-21-71	1,000	900	700
	10-5, 10-19-71	7,000	940	1,400
	11-2, 11-16-71	1,400	780	1,600
	12-7-71	130	45	20
	2-15-72	<1	<1	<1
	3-28-72	<1	<1	[2]3
	4-11, 4-25-72	160	110	140
	5-9, 5-23-72	4,400	90	670
White Brook	8-26-71	11,000	690	1,200
	9-8, 9-22-71	6,400	3,500	2,800
	10-6, 10-20-71	14,000	2,200	3,400
	11-3, 11-17-71	3,400	640	3,600
	12-8-71	2,700	650	4,800
	2-16-72	3,200	490	([3])
	3-29-72	43	20	70
	4-12, 4-26-72	1,600	89	190
	5-10, 5-24-72	2,500	1,400	1,200
Black Brook	8-26-71	45,000	24,000	13,500
	9-8, 9-21-71	61,000	5,000	76,000
	10-5, 10-19-71	5,000	230	560
	11-2, 11-16-71	2,100	270	1,900
	12-7-71	10,000	2,700	40,000
	2-15-72	1,000	290	8,700
	3-28-72	440	56	130
	4-11, 4-25-72	870	92	720
	5-9, 5-23-72	1,800	640	1,600
Black Brook spillway	4-25-72	140	10	60
	5-9-72	53	34	12
White Brook spillway	4-25-72	760	24	75

[1] Total coliform too numerous to count.
[2] Estimated.
[3] No data.

Many factors—such as sunlight, temperature, amount of organic matter, and the presence of other microorganisms—affect the concentration and the type of bacteria in water. In a literature search of the effects of various environmental factors on bacteria, Rudolfs, Falk, and Ragotzkie (1950) found much contradictory evidence. But, as a general rule, fecal coliform and fecal *Streptococci* counts reflect the degree of fecal pollution.

The generally higher counts of bacteria at White Brook and Black Brook than at Seneca spillway are probably due to wastes of farm animals and various wild animals, septic tanks, or sewage draining into the streams. In the refuge, where water is moving relatively slowly, a settling-pond effect is probably pronounced. This tends to settle bacteria, especially those that are adsorbed to particulate matter. Also, the water within the refuge may support various forms of predatory microorganisms (Salle, 1961, p. 547).

From August 25 to December 7, 1971, there was no discharge at Seneca spillway. Thus, there was very little water movement through the refuge. On December 7, 1971, the discharge at the spillway was estimated to be only 0.3 cfs. A study by Geldreich and Kenner (1969) reports that various genera of enteric bacteria in water die off at an exponential rate. This suggests that in a slowly flowing body of water there would be fewer bacteria surviving at a point downstream than at the point of entry.

During fall migration (1971), only a few birds were concentrated around the Seneca spillway area of Main Pool; therefore, high bacterial counts at the spillway were probably not the result of the corresponding bird counts. The lack of correlation between bird population and bacterial count is illustrated in figure 2.

During spring migration (1972), ducks used all pools in the refuge, but their greatest concentration (50 percent of the ducks) was at Storage Pool. Geese concentrated on Main Pool until the ice thawed on April 10; afterward, two-thirds of the geese concentrated on Storage Pool (M. S. Phillips, written commun., 1972). The lowest bacterial counts in Main Pool for the period of study occurred during the period of ice covered, when the droppings could not fall into the water and when water temperature was lowest. Because death rate for bacteria depends on temperature, the die-off rate would be greatest during the period of ice cover.

The relatively high total coliform counts on October 5 and May 23 are unexplained, but they may be due to an aftergrowth (Van Donsel and others, 1967). A nonrandom sample is another possibility for the high counts.

Qualitative tests confirmed *Salmonella* in only one of 45 samples collected from August 1971 through May 1972 at the five stations sampled. This sample, taken at Seneca spillway on September 22, 1971, was the only confirmation out of 17 samples taken from the refuge itself. One cannot assume from this single result that more *Salmonella* can be found at Seneca spillway than at any of the other sites. Geldreich (1966), in a comprehensive study of fecal coliform in the environment, pointed out that the presence of fecal coliform is indicative of the possible presence of pathogenic organisms such as *Salmonella*. It would seem to follow that the higher the fecal coliform count the higher the probability of finding pathogens. However, studies by Gallagher and Spino (1968) have shown that this assumption is questionable and that further study of the correlation is needed.

During fall migration, a fresh fecal sample taken among a flock of geese on the ground near the refuge headquarters and a water sample taken among a flock of geese that was concentrated near the middle of Main Pool were tested for *Salmonella*. None was found in either sample.

As shown in tables 2, 3, and 4, concentrations of total and fixed solids were higher in Black Brook and White Brook than they were at Seneca spillway; but the percentage of organic solids (table 5) was higher at Seneca spillway than at the other two sites. This relatively high percentage can be expected in the marsh-type water typical of the Montezuma National Wildlife Refuge.

The lower specific conductances at Seneca spillway than at White Brook or Black Brook could be the result of certain dissolved constituents, such as calcium, carbonate, and sulfate, precipitating out of solution. This precipitation could be due to the higher pH values (resulting from photosynthesis) in the refuge as compared with the values of Black Brook and White Brook. By this process, the ratio of organic solids to inorganic solids would increase. Also, the high concentrations of algae in the refuge remove various ions from the water.

Specific conductance at Seneca spillway was noticeably higher during November, December, and February than during the other months. This supports the possibility that photosynthesis plays an important role in controlling the concentration of dissolved salts in spring and summer. The specific conductance was higher at Seneca spillway than at both Black Brook and White Brook for the months of December and February.

Specific conductance and concentrations of total and fixed solids are inversely related to the discharge in Black Brook. This is due to a dilution effect during high flows. Although discharge was not measured at White Brook, the dilution effect was observed there during corresponding sampling periods. This does not mean, though, that more total solids are being carried by Black Brook into Storage pool during periods of high concentrations of total solids than during periods of low concentrations. For example, T/d (tons per day) calculated by the formula

$$T/d = mg/l \times cfs \times 0.0027$$

for October 5, 1971, when discharge was 1.4 cfs and total-solids concentration was 1,440 mg/l, would equal 5.4. For March 28, 1972, when discharge was 29 and total-solids concentration was 388 mg/l, T/d would equal 30.

Table 2 shows that concentrations of nitrogen and phosphorus at Seneca spillway are generally higher than at Black Brook

(table 3) and White Brook (table 4), particularly from August to November. Similar to bacterial counts, nutrient levels do not seem to be affected by bird population but, rather, reflect conditions in the marsh. For example, bluegreen algae, which were found at the refuge, characteristically fix atmospheric nitrogen as well as different forms of nitrogen in the water. The high concentrations of plant and animal life in the refuge corresponded to the high concentrations of phosphorus. Continuous availability of phosphorus for microbiological growth is probably accomplished by various forms of mechanical mixing of the bottom nutrients with the water. Wave action, diving birds, and carp, which stir up the bottom sediments in search of food, are the primary means of mechanical mixing in the refuge. Table 2 shows phosphorus concentrations at their lowest during the period of ice cover, when microbiological activity and mechanical mixing had least effect.

When the water temperatures decline as winter approaches, total nitrogen and total phosphorus concentrations also decline because of the decrease in microbiological activity in the refuge water. Nitrogen and phosphorus concentrations at Seneca spillway are of the same magnitude as those at Black Brook and White Brook during this period of relatively low temperatures, which extends into May.

Nitrogen and phosphorus concentrations at Black Brook increase substantially after heavy rains (table 3). For example, on September 8, 1971, discharge was 1.9 cfs, and total nitrogen and total phosphorus concentrations were 1.3 and 0.08 mg/l, respectively. On September 21, 1971, discharge was 15 cfs after a night of rain. Total nitrogen concentration was 3.7 mg/l, and total phosphorus concentration was 0.29 mg/l. The higher concentrations on September 21 probably resulted from nitrogen and phosphorus fertilizers and livestock wastes washed from the soil. Also, the larger amounts of suspended sediment stirred up from the river bottom by the faster, more turbulent flows caused by the rainfall would add more bottom nutrients to the water layer above (Greeson, 1971).

The result of photosynthesis at Seneca spillway shows up in values of pH and percent saturations of dissolved oxygen (table 2). The low percent saturations in February and March at Seneca spillway occurred while there was still much ice cover. The ice layer acted as a shield between the water and the atmospheric source of oxygen. Oxygen was utilized by respiratory processes of the biota and by oxidation of decaying materials.

FURTHER WORK NEEDED

In order to determine the effects of concentrations of parameters listed in tables 1 and 2 on water in a shellfish habitat, one would have to do a coastal water-quality study. Under the National Shellfish Sanitation Program, an industry-State-Federal cooperative program which is administered jointly by the Food and Drug Administration and State shellfish control agencies, sanitary surveys are made of each shellfish habitat before the State approves the habitat as a source of shellfish for market or for use in a controlled purification or relaying operation. The sanitary quality of each area is reappraised at least biennially (U.S. Dept. Health, Education, and Welfare, 1965, p. 10).

The purpose of the sanitary survey is to identify and evaluate factors influencing the sanitary quality of a shellfish habitat. The factors include: sources of pollution, potential or actual; volume of dilution water; effects of currents, winds, and tides in disseminating pollution throughout the growing area; bacterial quality of water and bottom sediments; die-off of polluting bacteria in the tributaries and the estuary; bottom configuration; and salinity and turbidity of the water.

A study in which data of the type obtained at the Montezuma National Wildlife Refuge is used in conjunction with a sanitary survey would be necessary to determine whether effluent from a coastal wildlife refuge adversely affects shellfish habitats.

CONCLUSIONS

The concentration of bacteria in water leaving the Montezuma National Wildlife Refuge is generally lower than that in the two largest inflowing streams (Black Brook and White Brook). This is probably due to settling of the bacteria in the quiet water of the refuge and to the die-off of bacteria between the point of entry and the sampling points. Predatory microorganisms may also influence the bacterial concentrations. *Salmonella* were detected in only one of 17 samples of water taken within the refuge.

Water leaving the refuge has lower specific conductance and generally higher dissolved-oxygen content than water flowing into the refuge. These two parameters suggest that the net effect of the refuge is to improve the quality of water that flows through it.

Table 2.—*Water-quality data for Seneca spillway at the Montezuma National Wildlife Refuge near Seneca Falls, N.Y.*

[DO, dissolved oxygen; TOC, total organic carbon]

Date	8-25-71	9-7-71	9-21-71	10-5-71	10-19-71	11-2-71	11-16-71	12-7-71	2-15-72	3-28-72	4-11-72	4-25-72	5-9-72	5-23-72
Time	1400	1500	1530	1330	1130	1100	1300	1300	1400	1345	1130	1200	0855	1130
Air temperature °C	17	29	19	21	16	21	5	6	4	1	7	3.5	7	25
Water temperature °C	17	24	20	20	16	17	5	0	2	3.5	5	10	9	24
Gage height ft	.97	1.08	1.28	1.40	1.50	1.60	1.66	2.77	[1]2.98	2.06	1.90	1.85	1.27	1.35
Discharge cfs	.0	.0	.0	.0	.0	.0	.0	[1].3	[1]1.3	1.6	11	12	[1]12	8.3
Sampling depth ft	.1	.1	.1	.1	.1	.1	.1	.1	.1	.1	.1	.1	.1	.1
Specific conductance (μmhos/cm at 25° C)	545	557	594	637	602	633	667	753	838	398	350	413	507	541
pH	8.9	9.1	9.2	7.8	9.3	8.5	8.1	8.1	7.4	6.9	7.1	7.4	7.6	8.1
Carbonate mg/l	8	13	16	0	16	6	0	0	0	0	0	0	0	0
Bicarbonate mg/l	110	139	136	158	146	156	174	189	213	107	84	78	109	139
DO mg/l	11	10	15	12	14	12	11	.....	8.2	12	13	13	11	9.8
DO (percent saturation)	112	117	159	128	136	120	86	.....	62	87	105	115	93	115
Ammonia as N mg/l	3.4	1.5	.26	2.0	.29	1.8	1.3	.11	1.0	.5	.27	.10	.15	.02
Organic N mg/l	12	5.4	4.5	5.7	4.4	6.9	5.3	1.8	1.7	1.6	2.0	2.2	1.5	2.9
Nitrate as N mg/l	.2	.0	.1	.1	.0	.0	.1	.0	.2	.1	.1	.0	.1	.0
Nitrite as N mg/l	.02	.01	.02	.01	.01	.01	.01	.01	.01	.01	.01	.00	.00	.01
Total N mg/l	16	6.9	4.9	7.8	4.7	8.7	6.7	1.9	2.9	2.2	2.4	2.3	1.8	2.9
Phosphorus mg/l	.47	.16	.27	.33	.22	.37	.31	.07	.03	.09	.13	.12	.14	.20
Total solids mg/l	452	332	500	515	555	530	505	564	637	282	249	331	389	449
Fixed solids mg/l	311	314	362	374	382	138	385	433	526	227	178	222	288	314
TOC mg/l	13	59	51	58	33	34	34	24	20	12	21	32	35	43
Total coliform (colonies/100 ml)	.....	[1]1,000	[1]1,000	13,000	1,000	2,100	800	130	<1	<1	.....	60	200	8,600
Fecal coliform (colonies/100 ml)	3,600	[1]500	1,300	1,800	100	1,000	560	45	<1	<1	20	10	160	19
Fecal *Streptococci* (colonies/100 ml)	2,400	200	1,200	2,700	200	920	2,200	20	<1	[1]3	.....	70	140	1,200
Remarks	Overcast; total coliform too numerous to count.	Partly cloudy.	Clear.	Partly cloudy.	Clear.	Cloudy and windy.	Overcast and windy.	Overcast; pool mostly ice covered.	Overcast and windy; pool ice covered.	Overcast and windy; pool ice covered.	Overcast.	Clear.	Overcast, windy, and rainy.	Clear.

[1] Estimated.

Table 3.—*Water-quality data for Black Brook at Tyre, N.Y.*

Date	8-26-71	9-8-71	9-21-71	10-5-71	10-19-71	11-2-71	11-16-71	12-7-71	2-15-72	3-28-72	4-11-72	4-25-72	5-9-72	5-23-72
Time	1030	1000	0845	0815	0800	0740	0900	0845	0900	0930	1000	0800	1530	0845
Air temperature °C	20	31	16	14	4	17	5	4	4	−1	8	2	9	17.5
Water temperature °C	16	25	17	15	10	12	6	1	0	1	5	7	8.5	15.5
Gage height ft	.18	.16	.57	.14	.14	.19	.32	2.48	[1]1.97	1.51	.94	.00	2.75	.48
Discharge cfs	2.1	1.9	15	1.4	.96	1.4	4.0	.....	.....	29	32	31	[1]97	8.9
Sampling depth ft	.1	.1	.1	.1	.1	.1	.1	.1	.1	.1	.1	.1	.1	.1
Specific conductance (μmhos/cm at 25° C)	1,200	1,240	816	1,420	1,680	1,610	1,360	345	643	505	570	557	318	913
pH	8.0	8.3	7.9	7.8	8.2	7.9	8.0	7.5	7.6	7.5	7.7	7.8	7.6	8.2
Carbonate mg/l	0	0	0	0	0	0	0	0	0	0	0	0	0	0
Bicarbonate mg/l	269	272	187	374	312	310	302	89	132	142	154	162	122	278
DO mg/l	9.7	8.5	8.0	8.4	9.8	8.5	11	.....	13	14	11	12	11	10
DO (percent saturation)	98	101	82	82	87	79	90	.....	86	98	88	102	94	101
Ammonia as N mg/l	.31	.12	.32	.15	.13	.15	.49	.37	.80	.32	.26	.12	.20	.01
Organic N mg/l	1.4	.88	2.6	.60	.48	.48	1.1	1.2	1.1	.88	1.1	1.1	1.2	1.1
Nitrate as N mg/l	.5	.3	.7	.3	.1	.0	.6	1.0	1.0	.2	.3	.2	.3	.3
Nitrite as N mg/l	.03	.01	.06	.01	.01	.00	.06	.03	.02	.01	.01	.01	.01	.02
Total N mg/l	2.2	1.3	3.7	1.1	.72	.63	2.2	2.6	2.9	1.4	1.7	1.4	1.5	1.4
Phosphorus mg/l	.06	.08	.29	.04	.03	.03	.06	.28	.12	.10	.07	.12	.16	.06
Total solids mg/l	1,220	1,090	683	1,440	1,670	1,440	1,110	370	467	388	418	468	284	790
Fixed solids mg/l	1,050	880	557	1,250	1,410	1,260	924	272	387	310	322	330	219	580
TOC mg/l	14	13	22	3	1	6	11	22	13	16	13	20	19	18
Total coliform (colonies/100 ml)	45,000	[1]1,700	[1]120,000	4,200	5,700	3,300	850	10,000	1,000	440	.....	870	1,300	2,200
Fecal coliform (colonies/100 ml)	24,000	1,300	9,400	250	220	240	300	2,700	290	56	100	83	730	550
Fecal *Streptococci* (colonies/100 ml)	14,000	1,600	[1]150,000	890	240	1,000	2,800	[1]40,000	8,700	130	.....	720	2,000	1,100
Remarks	Cloudy.	Partly cloudy.	Partly cloudy.	Partly cloudy.	Clear.	Intermittent rain.	Overcast and windy.	Overcast.	Overcast; ice on bottom of stream channel.	Partly cloudy and windy.	Overcast.	Clear.	Overcast and rainy.	Clear.

[1] Estimated.

Table 4.—*Water-quality data for White Brook near Tyre, N.Y.*

Date		8-26-71	9-8-71	9-22-71	10-6-71	10-20-71	11-3-71	11-17-71	12-8-71	2-16-72	3-29-72	4-12-72	4-26-72	5-10-72	5-24-72
Time		0915	1430	0800	0830	0800	0800	0745	0745	0815	0735	0930	0700	0930	0800
Air temperature	°C	18	31	8	13	11	10	3	4	−5	.5	9	.5	8	17
Water temperature	°C	16	25	12	14	11	12	5	3	0	0	5.5	4	8	15
Sampling depth	ft	.1	.1	.1	.1	.1	.1	.1	.1	.1	.1	.1	.1	.1	.1
Specific conductance (μmhos/cm at 25°C)		1,100	1,010	890	1,600	1,440	1,380	1,140	654	775	781	754	876	568	1,120
pH		8.2	8.5	8.1	7.9	8.1	8.0	8.0	7.7	7.6	7.8	8.1	8.0	7.9	8.1
Carbonate	mg/l	0	8	0	0	0	0	0	0	0	0	0	0	0	0
Bicarbonate	mg/l	230	282	318	310	350	400	345	221	191	239	232	265	215	320
DO	mg/l	8.6	8.2	9.8	7.6	6.2	8.0	11	.....	14	13	12	13	11	8.4
DO (percent saturation)		87	98	91	73	56	74	88	.....	93	90	92	98	96	82
Ammonia as N	mg/l	.16	.13	.11	.21	.24	.15	.11	.07	.20	.09	.29	.04	.05	.01
Organic N	mg/l	1.1	.90	.83	.55	.56	.64	.42	.61	.88	.48	.38	.49	.52	.41
Nitrate as N	mg/l	.2	.1	.3	.2	.1	.1	.2	1.1	1.1	.6	.5	.4	.6	.2
Nitrite as N	mg/l	.02	.01	.01	.01	.01	.00	.01	.01	.02	.01	.00	.00	.01	.00
Total N	mg/l	1.5	1.1	1.2	.97	.91	.89	.74	1.8	2.2	1.2	1.2	.93	1.2	.62
Phosphorus	mg/l	.10	.12	.10	.08	.11	.09	.06	.08	.07	.03	.12	.11	.07	.03
Total solids	mg/l	1,130	856	676	1,220	1,340	1,140	898	474	555	550	523	714	392	922
Fixed solids	mg/l	970	708	558	1,040	1,090	956	750	380	459	448	446	522	310	730
TOC	mg/l	77	13	8	4	3	3	6	9	9	5	5	18	4	7
Total coliform (colonies/100 ml)		11,000	[1]7,200	12,000	14,000	13,000	6,100	800	2,700	3,200	[1]43	.....	1,600	940	4,100
Fecal coliform (colonies/100 ml)		690	[1]4,000	3,000	1,300	3,000	1,000	280	650	490	20	110	68	160	2,600
Fecal *Streptococci* (colonies/100 ml)		1,200	2,400	3,300	2,700	4,200	4,500	2,800	4,800	.....	70	.....	190	540	1,900
Remarks		Overcast.	Partly cloudy.	Partly cloudy.	Cloudy.	Clear windy.	Cloudy.	Overcast.	Overcast.	Partly cloudy and snowy; stream partly ice covered.	Clear.	Partly cloudy.	Clear.	Partly cloudy.	Clear.

[1] Estimated.

Table 5.—*Summary of data collected at Seneca spillway, Black Brook, and White Brook*

[TOC, total organic carbon; TC, total coliform; FC, fecal coliform; FS, fecal *Streptococci*; DO, dissolved oxygen]

Parameter	Seneca spillway				Black Brook				White Brook			
	Maximum	Minimum	Mean ($\bar{x}$)	Standard deviation (σ)	Maximum	Minimum	Mean ($\bar{x}$)	Standard deviation (σ)	Maximum	Minimum	Mean ($\bar{x}$)	Standard deviation (σ)
Discharge cfs	12	0.0	3.3	0.08	97	0.96	19	1.0				
Specific conductance (μmhos/cm at 25°C)	838	350	574	.03	1,680	318	941	.83	1,600	568	1,000	22
pH	9.3	6.9	8.1	.00	8.3	7.5	7.8	.22	8.5	7.6	8.0	.00
Carbonate mg/l	16	0	4	.83	0	0	0	.00	8	0	0	2.2
Bicarbonate mg/l	213	78	138	1.7	374	89	222	.83	400	191	280	.55
DO mg/l	15	8.2	12	.17	14	8.0	10	.14	14	6.2	10	.23
DO (percent saturation)	159	62	110	1.4	102	79	91	1.4	98	56	86	.00
Ammonia as N mg/l	3.4	.02	.91	.01	.80	.01	.27	.01	.29	.01	.13	.01
Organic N mg/l	12	1.5	4.1	.14	2.6	.48	1.1	.05	1.1	.38	.63	.01
Nitrate plus nitrite as N (mg/l)	.2	.0	.1	.00	1.0	.0	.4	.07	1.1	.1	.4	.02
Phosphorus mg/l	.47	.07	.21	.09	.29	.03	.11	.06	.12	.03	.08	.01
Total solids mg/l	637	249	449	1.1	1,670	284	845	2.2	1,340	392	814	1.7
Fixed solids mg/l	526	138	318	.06	1,410	219	696	.73	1,090	310	669	.28
Organic solids percent	74	6	29	1.4	30	12	20	1.4	27	14	18	.00
TOC mg/l	59	12	34	1.9	22	1	14	.62	77	3	12	.79
TC/100 ml	13,000	<1	2,300	120	120,000	435	15,000	24,000	14,000	43	5,900	4.9
FC/100 ml	3,600	<1	650	3.9	24,000	56	2,900	110	4,000	20	1,200	160
FS/100 ml	2,400	<1	860	21	150,000	130	17,000	340	4,800	70	2,400	120

Explanation of symbols:

$$\bar{x} = \frac{\Sigma x_i}{n} \qquad \sigma = \sqrt{\frac{\Sigma x^2}{n-1}}$$

x_i = individual observation

n = total number of observations $\quad x = x_i - \bar{x}$

HAVE

REFERENCES CITED

American Public Health Association, American Water Works Association, and Water Pollution Control Federation, 1971, Standard methods for the examination of water and wastewater (13th ed.): New York, Am. Public Health Assoc. 874 p.

Brown, E. M., Skougstad, M. W., and Fishman, M. J., 1970, Methods for collection and analysis of water samples for dissolved minerals and gases: U.S. Geol. Survey Techniques Water-Resources Inv., book 5, chap. A1, 160 p.

Gallagher, T. P., and Spino, D. F., 1968, The significance of numbers of coliform bacteria as an indicator of enteric pathogens, *in* Water research: New York, Pergamon Press, v. 2, p. 169–175.

Geldreich, E. E., 1966, Sanitary significance of fecal coliforms in the environment: Federal Water Pollution Control Adm., Pub. WP-20-3, 122 p.

Geldreich, E. E., and Kenner, B. A., 1969, Concepts of fecal *Streptococci* in stream pollution: Water Pollution Control Federation Jour., v. 41, no. 8, pt. 2, p. R336–R352.

Goerlitz, D. F., and Brown, E. M., 1972, Methods for analysis of organic substances in water: U.S. Geol. Survey Techniques Water-Resources Inv., book 5, chap. A3, 40 p.

Greeson, P. E., 1971, Limnology of Oneida Lake with emphasis on factors contributing to algal blooms: U.S. Geol. Survey open-file rept., 185 p.

Moran, A. B., Van Houweling, C. D., and Ellis, E. M., 1965, The results of typing *Salmonella* from animal sources in the United States, *in* Natl. Conf. on Salmonellosis, 1964, Proc.: U.S. Public Health Service Pub. 1262. p. 33–37.

Murphy, Robert, 1968, Wild sanctuaries: New York, E. P. Dutton and Co., Inc., 288 p.

Rudolfs, W., Falk, L. L., and Ragotzkie, R. A., 1950, Literature review on the occurrence and survival of enteric, pathogenic, and relative organisms in soil, water, sewage and sludges, and on vegetation. I. Bacterial and virus diseases: Sewage and Indus. Wastes, v. 22, p. 1261–1281.

Salle, A. J., 1961, Fundamental principles of bacteriology (5th ed.): New York, McGraw-Hill, Inc., 812 p.

Slack, K. V., Biesecker, J. E., Greeson, P. E., Kolipinski, M. C., and Lipscomb, R. G., 1970, Selected procedures for biological and microbiological investigations: U.S. Geol. Survey open-file rept., 68 p.

U.S. Department of Health, Education, and Welfare, 1965, National shellfish sanitation program manual of operations. Pt. 1, Sanitation of shellfish growing areas: U.S. Dept. Health, Education, and Welfare, 32 p.

U.S. Department of the Interior, 1969, Montezuma National Wildlife Refuge: U.S. Dept. Interior, Fish and Wildlife Service, Bureau of Sport Fisheries and Wildlife Refuge Leaflet 38-R3.

Van Donsel, D. J., Geldreich, E. E., and Norman, A. C., 1967, Seasonal variations in survival of indicator bacteria in soil and their contribution to stormwater pollution: Federal Water Pollution Control Adm., 23 p.

Jour. Research U.S. Geol. Survey
Vol. 1, No. 6, Nov.-Dec. 1973, p. 735–744

FLOW CHARACTERISTICS OF A SUBSURFACE-CONTROLLED RECHARGE BASIN ON LONG ISLAND, NEW YORK

By ROBERT C. PRILL and DONALD B. AARONSON, Mineola, N.Y.

Abstract.—Ponding studies at the Woodbury recharge basin on Long Island, N.Y., show that the principal zones controlling infiltration are a surface-loam stratum and an intermediate gravelly, sandy loam stratum. The saturated hydraulic conductivities of these strata are 0.90 and 0.1 ft per day, respectively. The surface loam acts as the principal zone controlling infiltration until a perched ground-water mound develops above the intermediate gravelly, sandy loam and extends to the bottom of the surface loam; then the intermediate gravelly, sandy loam becomes the principal infiltration controlling zone. Infiltration rates at 15.6°Celsius are 1.4 ft per day when the surface loam is acting as the principal controlling zone and 0.5 ft per day when the intermediate gravelly, sandy loam is acting as the principal controlling zone. Projections of the probable infiltration rates associated with both the partial and the complete removal of the surface-loam stratum show that if recharge continues for several days total infiltration would not be greatly different whether or not the loam stratum is completely removed. The principal advantage of completely removing the surface-loam stratum is the resulting greater infiltration capacity during the early stages of ponding. This advantage is offset by potential problems associated with more intensive clogging of the subsurface controlling zone.

Recharge of ground-water reservoirs with storm runoff and highly treated domestic and industrial effluent is receiving increasing emphasis on Long Island, N.Y. Parker, Cohen, and Foxworthy (1967, p. 208) estimated that recharge of storm runoff through basins on Long Island amounted to 100 mgd in 1966. Accordingly, a major concern to Long Island water managers in selection of sites and design of recharge basins is forecasting the infiltration capacity of a basin. Among other things, such forecasting requires a quantitative description of the hydraulic properties of the materials in the unsaturated zone. Consequently, an artificial-recharge project on Long Island is presently concerned with developing such quantitative descriptions and using the data to develop and apply methods for predicting flow characteristics at basins. Study sites at which flow patterns can be evaluated quantitatively can supply valuable data for testing methods of predicting flow characteristics. More than 2,000 recharge basins are used on Long Island to collect storm runoff. Because the unsaturated zones at these basins include a wide range of lithologic conditions, the basins provide an extensive choice of sites for study. As part of the research project, seven basins on Long Island are being studied.

This report describes the flow characteristics at the Woodbury recharge basin, where infiltration rates are primarily subsurface controlled. The principal zones limiting infiltration are evaluated from test data, and the probable infiltration rates associated with alternative designs of the basin are projected to illustrate how information concerning the flow characteristics at a test site can be generalized for selecting basin design.

SITE CHARACTERISTICS

The Woodbury basin is operated by the Nassau County Department of Public Works for the collection of storm runoff. The basin is in the northeastern part of Nassau County, Long Island, N.Y., and is excavated in the Ronkonkoma terminal moraine of Pleistocene age. The basin has both a lower level and a bench level (fig. 1). However, during the 2 years in which infiltration characteristics have been studied, the level of storm runoff in the basin has never risen to the bench level.

As shown by the cross section in figure 2, the thickness of the unsaturated zone below the basin floor is about 60 feet. The principal strata in the unsaturated zone underlying the basin are a surface loam, an upper sand and gravel, an intermediate gravelly, sandy loam, and a lower sand and gravel (materials are described in this paper according to soil-survey nomenclature (Soil Survey Staff, 1951)).

FIELD MEASUREMENTS

Measurements at the Woodbury site include basin stage, temperature of the water in the basin, moisture content of materials in the unsaturated zone, water-table elevation, precipitation, and pressure head at the upper boundary of the intermediate gravelly, sandy loam stratum. Moisture content, water-table elevation, and pressure-head measurements are made at selected time intervals, generally during storms. Basin stage and temperature of the water are recorded continuously. Zero basin stage is taken as the average elevation of the lower level. Because of minor surface relief, there is a pronounced

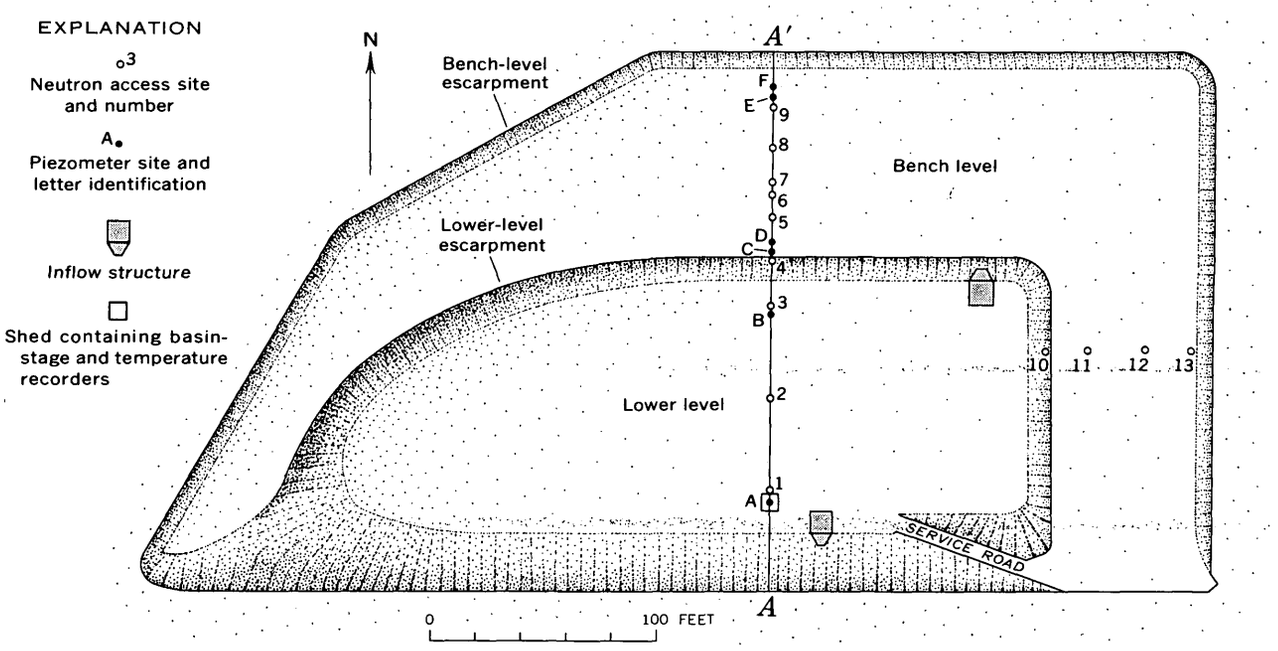

Figure 1.—Plan view of Woodbury recharge basin, showing location of instruments and structures.

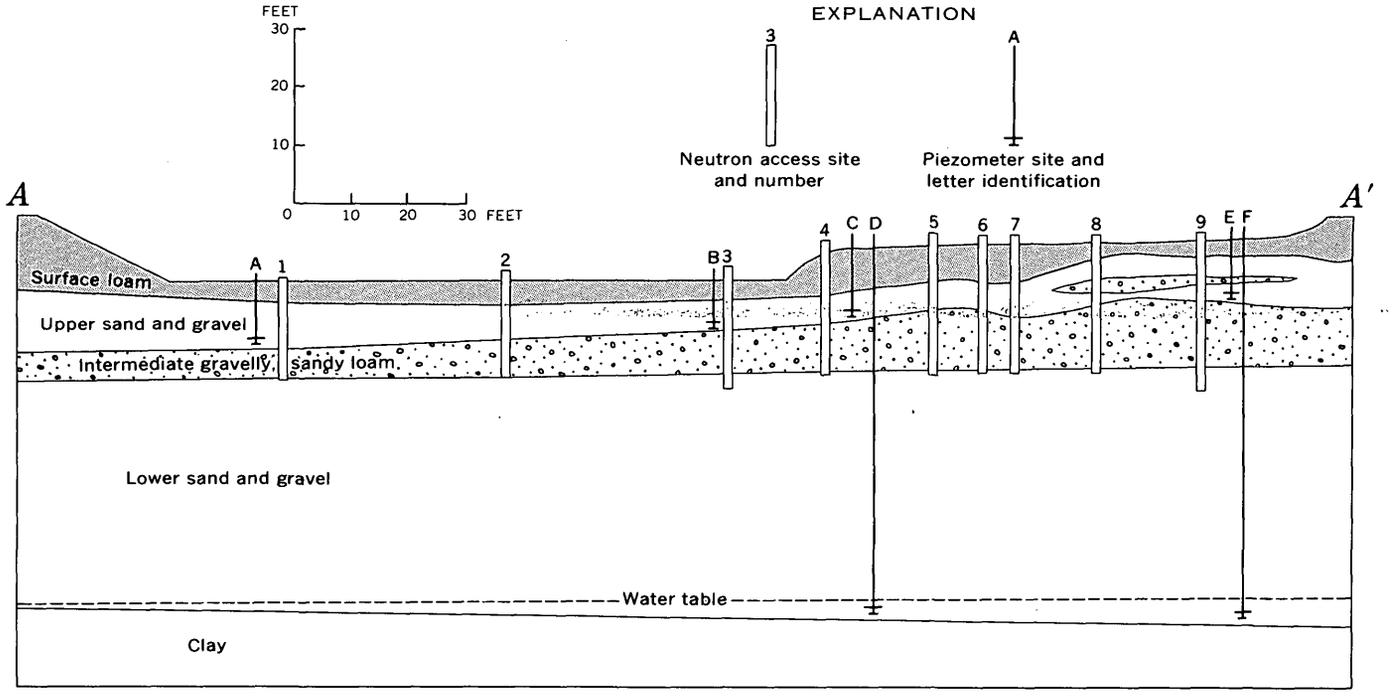

Figure 2.—Cross section of Woodbury recharge basin, showing lithology and positions of instrumentation.

increase in the flooded area as the basin stage rises from 0 to 0.15 foot.

Locations of the measuring sites are shown in figure 1. All the sites are located on a north-south traverse except for several neutron access sites used to measure moisture content by the neutron method.

The access tubing used to measure moisture content is aluminum pipe with a 2-inch outside diameter and a $^1/_{16}$-inch wall thickness. Moisture content is measured with a continuous-logging nuclear meter (Prill and Meyer, 1968) at a logging speed of 2.5 fpm.

TEST RESULTS

Three storms that occurred in September 1971, October 1971, and February 1972 were studied. Approximate inflows to the basin during the storms were 105,000 cu ft, 42,000 cu ft, and 30,000 cu ft, respectively. These inflows are equal to volumes of water having depths of 3.5 feet, 1.4 feet, and 1 foot, respectively, over an adjusted uniform basin floor having an area of 30,000 sq ft.

September 1971 storm

Water from the September storm was retained in the basin for 2.9 days. Inflow to the basin occurred intermittently and only during the first 1.6 days of ponding. Most of the data presented for this storm represent measurements after inflow ceased.

Basin stage and temperature of water in the basin after inflow ceased are shown in figure 3. The basin stage at the time inflow ceased was 0.86 foot. On the basis of basin-stage and temperature records for other storms, the volume of water that had infiltrated before this time is estimated to be 2.6 feet. The rate of decline in basin stage reflects the infiltration rate between 1.6 and 2.9 days after the start of ponding. There was a gradual decrease in the rate as the basin stage declined from 0.86 to 0.15 foot. The rate was 0.70 ft per day when the stage was at 0.75 foot and 0.65 ft per day when the stage was at 0.25 foot. As the basin stage declined below 0.15 foot, there was a gradual increase in infiltration rate. This increase was probably related to the decrease in flooded area that occurs as the basin stage drops below 0.15 foot.

Moisture logs at neutron access site 3, in the north-central part of the basin, are shown in figure 4. Because there was no inflow to the basin during the month preceding the September storm, the log showing conditions before the storm provides approximations of the soil-moisture content at various depths after complete or nearly complete field drainage. The log 1.7 days after the start of ponding shows moisture contents when the basin stage was 0.8 foot. The logs 7.5 and 10.5 days after the start of ponding show moisture contents 4.6 and 7.6 days after the end of ponding in the basin.

Pressure heads at the upper boundary of the intermediate gravelly, sandy loam stratum at piezometer B for the period from 0 to 8 days after the start of storm are shown in figure 5.

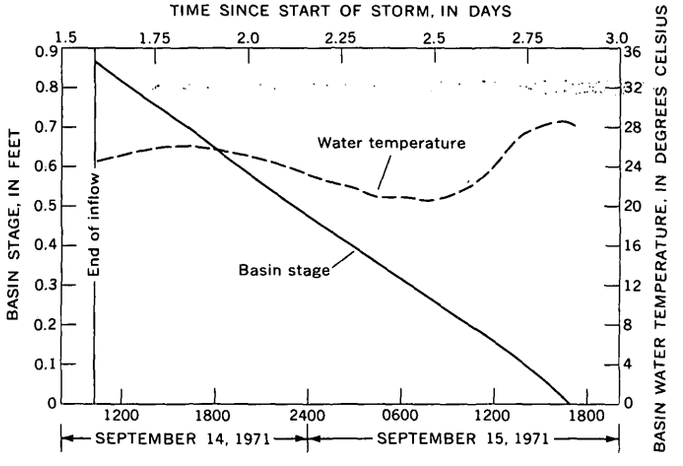

Figure 3.—Basin stage and water temperature during the September 1971 storm.

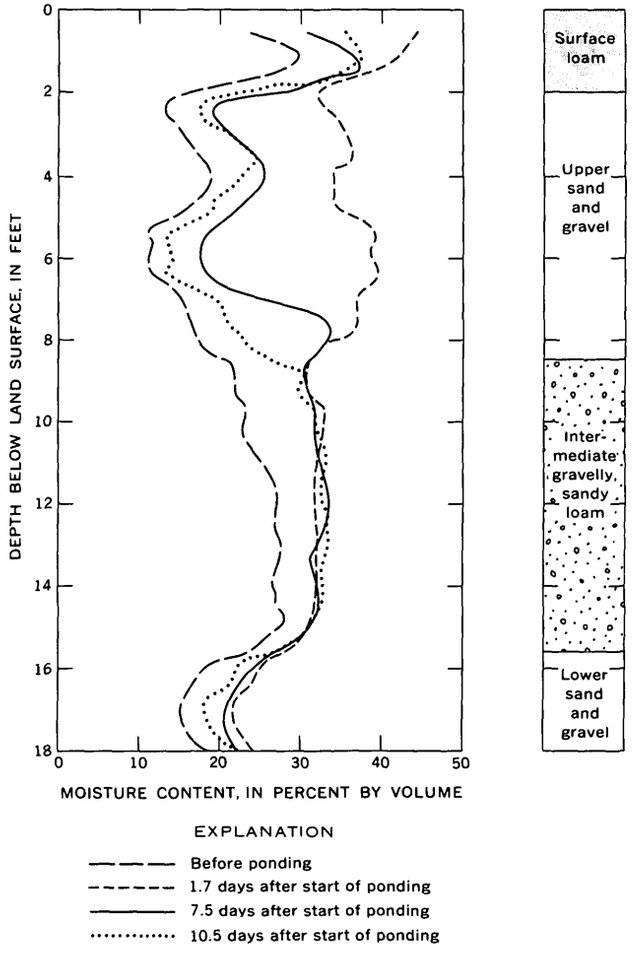

Figure 4.—Logs showing soil-moisture content at neutron access site 3 before ponding caused by September 1971 storm and after start of ponding.

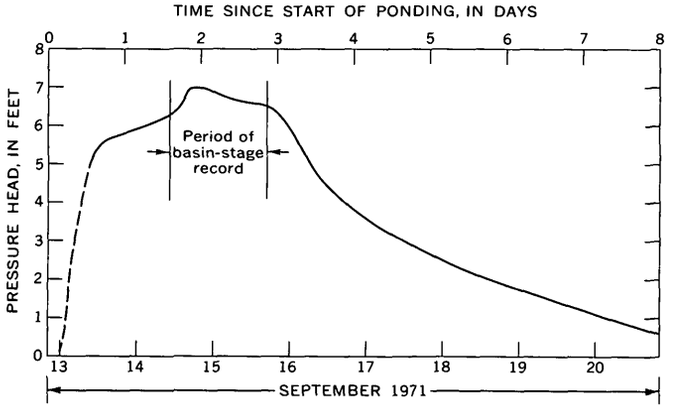

Figure 5.—Pressure head at upper boundary of intermediate gravelly, sandy loam stratum at piezometer B. Dashed where inferred.

Piezometer B is only 4 feet from neutron access site 3. Moisture logs at this sight (fig. 4) and head measurements in the piezometers show that the intermediate gravelly, sandy loam stratum was unsaturated before the storm. Thus, at the start of the storm, the pressure head at the upper boundary of this stratum was negative. The pressure-head data shown in figure 5 reflect a perched ground-water mound in the upper sand and gravel that develops rapidly during ponding and dissipates slowly after ponding.

Lateral spreading of the perched mound north and east of the basin 2.7 days after the start of ponding is projected in figure 6 on the basis of neutron moisture measurements. The lateral extent of the mound at this time was 60 feet east and 45 feet north of the basin. Neutron moisture measurements show that further lateral movement of the mound was insignificant.

Water-table measurements at piezometer D, 13 feet north of the basin, are shown in figure 7 for the period 1 to 10 days after the start of ponding. The first evidence of a rise in the water table at this point was noted about 1 day after the basin had drained. The water table rose 2 feet during the following week.

October 1971 storm

Water from the October storm was retained in the basin for nearly 1 day. Total inflow into the basin was 1.4 feet. Most of the inflow (1.1 feet) was from a storm of high intensity and short duration. As shown in figure 8, inflow from this storm ended 0.3 day after the start of ponding. Total infiltration up to this time is estimated to be 0.4 foot. There was no inflow to the basin between 0.3 and 0.7 day after the start of ponding. The rate of decline in basin stage during this period shows that the infiltration rate gradually decreased with time from 1.44 ft per day when the basin stage was at 0.5 foot to 1.30 ft per day when the stage was at 0.2 foot.

A storm of low intensity occurred 0.7 day after the start of ponding. Inflow from this storm continued through much of

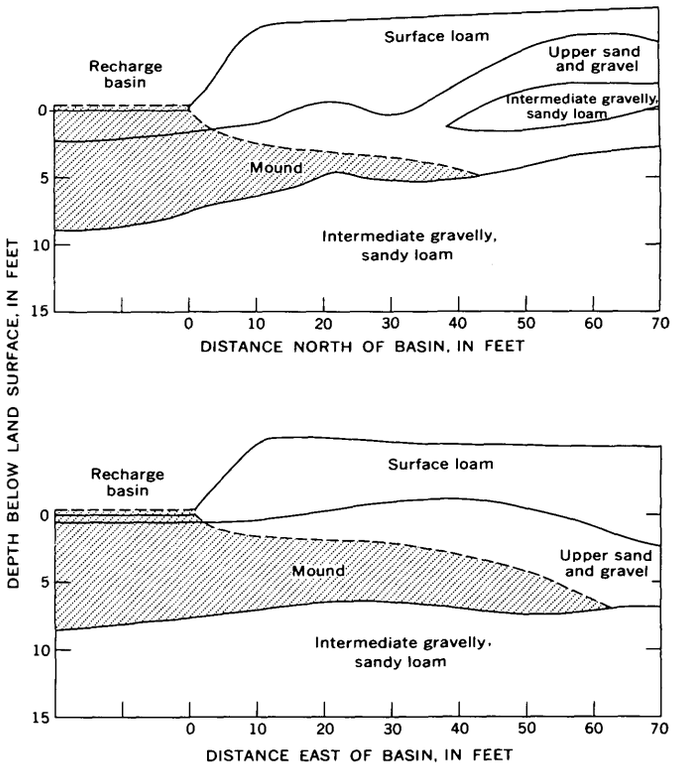

Figure 6.—Perched ground-water mound north (top) and east (bottom) of recharge basin 2.7 days after start of ponding.

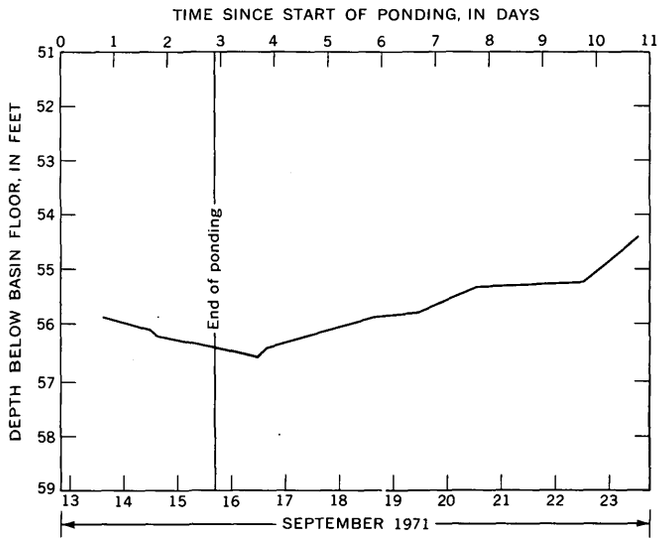

Figure 7.—Water table at piezometer D during the September 1971 storm.

the remaining period of record and prevented any further measurements of infiltration rate.

February 1972 storm

Water from the February storm was retained in the basin for nearly 1 day. Inflow of approximately 1 foot resulted from a

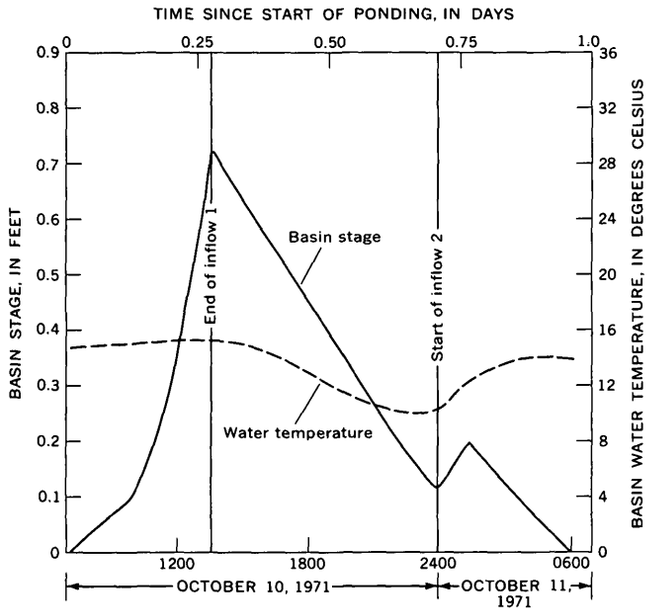

Figure 8.—Basin stage and water temperature during the October 1971 storm.

storm of high intensity and short duration. As shown in figure 9, inflow to the basin ended 0.25 day after the start of the storm. Total infiltration during the first 0.25 day of the storm is estimated to be 0.3 foot. As in the October storm, the infiltration rate decreased gradually with time. The rate was 1.02 ft per day when the stage was 0.5 foot and 0.92 ft per day when the stage was 0.2 foot. Although the storm occurred in midwinter, the materials in the unsaturated zone were not frozen because the weather before the storm was exceptionally mild.

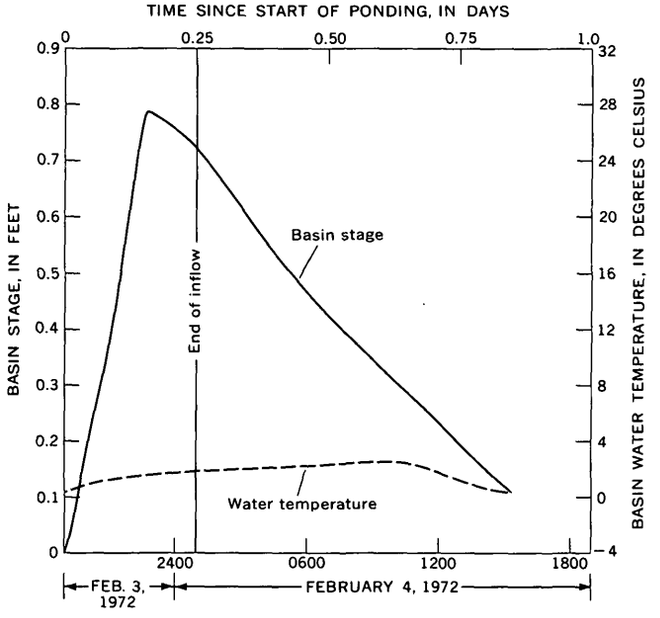

Figure 9.—Basin stage and water temperature during the February 1972 storm.

ZONES LIMITING INFILTRATION

The rate of decline in basin stage during periods when there was no inflow into the basin represents the infiltration rate. Because of differences in storm patterns, the periods for which the basin stage records could be used for determining infiltration rates were different for each of the three storms. The periods used to determine infiltration rates, as measured from the time ponding started, were from 1.6 to 2.9 days, 0.3 to 0.7 day, and 0.25 to 0.85 day for the September 1971, October 1971, and February 1972 storms, respectively. During these periods, total infiltration increased from 2.6 to 3.46 feet, 0.4 to 1.0 foot, and 0.3 to 1.0 foot, respectively.

Infiltration rates measured for the October and the February storms were markedly higher than those measured for the September storm. After adjustments were made for water temperature (Lohman and others, 1972), the average rate was 1.4 ft per day for the October and the February storms and 0.5 ft per day for the September storm. Adjusted rates are compared for the three storms in table 1 at times when the basin stage was at 0.5 foot and at 0.2 foot. As discussed later in the report, the difference in rates was largely related to changes in the hydrologic controls of the system. The higher rates for the October and the February storms, when total infiltration was less than 1 foot, reflect the intake capacity of the basin when the surface-loam stratum was acting as the principal limiting zone. The lower rates measured during the September storm, when total infiltration was between 2.60 and 3.64 feet, reflect the intake capacity of the basin when the intermediate gravelly, sandy loam stratum was acting as the principal limiting zone.

Surface-loam stratum as the principal limiting zone

During ponding, the surface-loam stratum is the principal zone limiting infiltration until the top of the perched ground-water mound that develops above the intermediate gravelly, sandy loam has extended to the bottom of the surface loam (fig. 2). Until this time, the infiltration rate will depend on the hydraulic conductivity of the surface-loam stratum and the pressure head that develops at the upper and the lower boundaries of the stratum. The pressure head that develops at the upper boundary will be positive and equivalent to the basin stage. The pressure head at the lower boundary will be negative because the hydraulic conductivity of the upper sand and gravel is many times higher than the infiltration rate. Thus, flow in the sand and gravel (above the perched mound) will be unsaturated flow and under negative pressure. Negative pressures will be small. Laboratory measurements of the relationship between unsaturated flow rates and negative pressures for the sand and gravel show that rates of 10 feet and 1 ft per day are associated with pressure heads of −0.30 and −0.57 foot of water, respectively. On the basis of these values and an assumed infiltration rate of 1.4 ft per day, the maximum pressure head that could occur at the lower

Table 1.—*Comparison of infiltration rates for basin stages of 0.2 and 0.5 foot during storms of September and October 1971 and February 1972*

Storm	Time since start of ponding (days)	Basin stage (feet)	Total infiltration (feet)	Infiltration rate (ft per day)	Water temperature (°C)	Infiltration rate adusted to 15.6°C (60°F)
September	2.6	0.2	3.3	0.63	24	0.51
	2.1	.5	3.0	.66	24	.54
October	.6	.2	.9	1.30	14	1.32
	.4	.5	.6	1.44	14	1.46
February	.7	.2	.8	.92	2	1.36
	.4	.5	.5	1.02	2	1.51

boundary of the surface-loam is about −0.5 foot. As illustrated in figure 10, the negative head at the lower boundary of the surface-loam stratum will change only slightly until the perched mound has reached the lower boundary.

The perched mound is unlikely to reach the lower boundary of the surface-loam stratum until total infiltration exceeds 1 foot, as available storage space in the upper sand and gravel is at least 1.2 feet. Thus, the infiltration rates measured during the October and the February storms should reflect the intake capacity of the basin when the surface-loam stratum is acting as the principal zone limiting infiltration.

During both the October and the February storms, the infiltration rate decreased as basin stage decreased. (See figs. 8 and 9 and table 1.) This decrease in rate was probably related to the decrease in hydraulic gradient across the loam stratum as the basin stage declined. For instance, the decrease in infiltration rate associated with a decline in basin stage from 0.5 to 0.2 foot was about 10 percent during both storms. On the basis of the probable pressure-head distribution across the loam stratum (fig. 10), a decrease of 0.3 foot in basin stage would result in a nearly 12 percent decrease in the hydraulic gradient across the stratum. That the observed changes are similar to computed changes is evidence of the approximate correctness of the model chosen. Hence, further utilization of the model for predictive purposes seems justified.

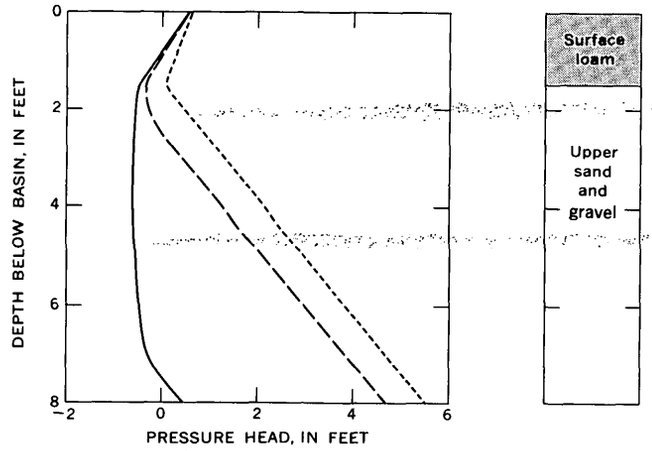

Figure 10.—Pressure head below basin when top of perched mound is in the upper sand and gravel stratum and basin stage is 0.5 foot.

Test data for the October and the February storms indicate that the average vertical hydraulic conductivity of the surface-loam stratum was nearly 0.8 ft per day at 15.6°C (Celsius) or 60°F. This value is based on computations using Darcy's law, which, for vertical flow, can be expressed as

$$Q = K\left(\frac{dh}{dl} + 1\right),$$

where

Q = flux,
K = vertical hydraulic conductivity,
dl = thickness of the surface-loam stratum, and
dh = change in pressure head from the lower boundary to the upper boundary of the surface-loam stratum.

Because most if not all the flow through the surface-loam stratum is probably vertical, or nearly so, the infiltration rate represents the flux through the stratum. When the basin stage during the October storm was 0.5 foot, the infiltration rate was 1.44 ft per day, and the water temperature was 14°C (table 1). Thus, Q was 1.44 feet per day, and the pressure head at the upper boundary of the surface stratum was 0.5 foot. The pressure head at the lower boundary was about −0.5 foot, as illustrated in figure 10. Thus, dh was 1.0 foot. The average thickness of the surface-loam stratum is 1.5 feet.

The computation of vertical hydraulic conductivity of the surface-loam stratum using the preceding values is as follows:

$$K = \frac{Q}{\frac{dh}{dl} + 1} = \frac{1.44 \text{ ft per day}}{\frac{1 \text{ ft}}{1.5 \text{ ft}} + 1} = 0.86 \text{ ft per day at } 14°\text{C}.$$

By correcting for viscosity, the vertical hydraulic conductivity at 15.6°C (60°F) is 0.90 ft per day.

Intermediate gravelly, sandy loam stratum as the principal limiting zone

When the perched ground-water mound rises above the lower boundary of the surface-loam stratum, the intermediate gravelly, sandy loam stratum becomes the principal zone

controlling infiltration. The infiltration rate of about 0.7 ft per day observed between 1.6 and 2.9 days after the start of the September storm (fig. 3) reflects the intake capacity of the basin after the perched mound coincides with the basin stage. The nature of the pressure-head distribution below the basin during this period is shown in figure 11 for stages of 0.7 and 0.1 foot. Each of the pressure-head profiles is an extrapolation based on measured and inferred pressure heads at the lithologic boundaries. The value at the upper boundary of the surface loam is equal to basin stage. The value at the lower boundary (computed by Darcy's law) is the pressure head required to move water vertically through the surface loam at a rate of 0.7 ft per day. The pressure head at the upper boundary of the intermediate gravelly, sandy loam was determined from field measurements (fig. 5). The pressure head at the lower boundary of this stratum is negative, as flow through the lower sand and gravel is unsaturated flow.

The intermediate gravelly, sandy loam, the only stratum in which the hydraulic gradient is greater than 1 (fig. 11), is the principal zone limiting infiltration. Because the hydraulic gradient across this zone decreases by only a few percent as the basin stage decreases from 0.7 to 0.1 foot, very little change in infiltration rate would be expected when the change in basin stage is less than 1 foot. This condition explains the nearly constant infiltration rate during the September storm.

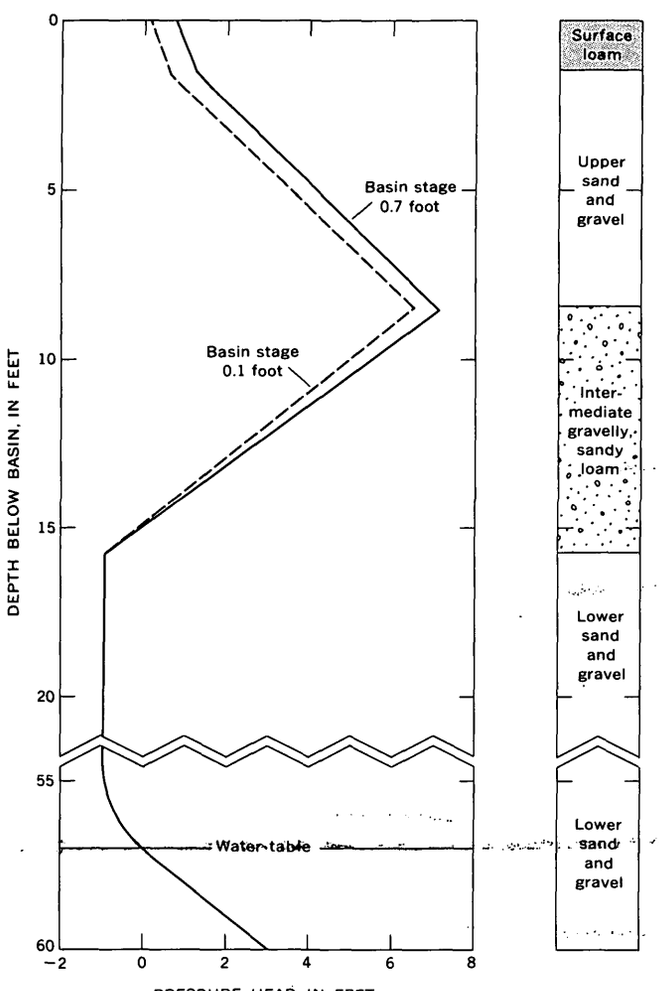

Figure 11.—Pressure head below basin when top of perched mound is coincident with basin stage.

The average hydraulic conductivity of the intermediate gravelly, sandy loam seems to be slightly less than 0.1 ft per day, on the basis of analysis of storage and pressure-head changes shown in figures 4 and 5, respectively. The data in these figures were obtained in the north-central part of the basin. After the end of infiltration, the perched ground water at this location would be almost horizontal. Thus, the flux across the gravelly, sandy loam may be approximated by multiplying the short-term specific yield of the upper sand and gravel (about 0.15, from the neutron logs shown in figure 4) by the rate of water-level decline.

At 5.8 days after the start of ponding (2.9 days after the end of infiltration), the rate of decline in pressure head at the upper boundary of the intermediate gravelly, sandy loam stratum was 0.8 ft per day. Multiplying this rate by 0.15 gives a value for the upper limit of flux (Q) through the confining zone of 0.12 ft per day. At this time, the pressure head at the upper boundary of the zone was 2.0 feet. Laboratory measurements of the relationship of hydraulic conductivity and pressure head indicate that at the above flux the pressure head at the lower boundary of the zone was about −1 foot. Thus the change in pressure head from the lower boundary to the upper boundary of the unit (dh) was 3 feet. The thickness of the unit (dl) is 8 feet. The temperature of the water was about 25°C. Assuming steady state, it follows from Darcy's law that

$$K = \frac{Q}{\frac{dh}{dl} + 1} = \frac{0.12 \text{ ft per day}}{\frac{3 \text{ ft}}{8 \text{ ft}} + 1} = 0.09 \text{ ft per day at } 25°\text{C}.$$

The upper limit of hydraulic conductivity of 0.1 foot per day for the intermediate gravelly, sandy loam stratum is considerably less than that computed for the surface-loam stratum, which, when adjusted to 25°C, is 1.1 feet per day. The lower hydraulic conductivity largely reflects the greater heterogenity of the intermediate gravelly, sandy loam stratum, which produced lower porosities.

EFFECT OF MOUNDING OF THE WATER TABLE ON INFILTRATION CAPACITY

Mounding of the regional water table did not affect the infiltration capacity of the basin during the three storms. Even if the ponding were of long duration, the infiltration rate would probably be unaffected by such mounding. In order to have any noticeable affect on the infiltration capacity of the basin, the mound would have to rise to near the lower boundary of the intermediate gravelly, sandy loam stratum. The large unsaturated thickness of the lower sand and gravel stratum, about 40 feet, and the small rise in the water table during the September storm (fig. 7) would seem to rule out

mounding of the regional water table as a factor controlling the infiltration rate of the basin.

COMPARISON OF ALTERNATIVE BASIN DESIGNS

Part of the potential storage capacity of recharge basins is above ground and is represented by the volume of the basin. The remainder is underground and is represented mainly by unsaturated voids in the materials underlying the basin. Because the quantity of water that can be taken into underground storage over a given period of time depends on infiltration capacity, each site, ideally, would be designed in a manner that will maximize infiltration and storage and minimize costs of construction and maintenance.

In the discussion that follows, the probable infiltration rates associated with two designs at the Woodbury site are considered to illustrate how test data of the type presented in this report might be used to evaluate different basin designs.

Alternative basin designs at the Woodbury site could involve excavating the basin into either the surface loam or the upper sand and gravel strata. Because the intermediate gravelly, sandy loam stratum is 22 to 30 feet below the land surface, excavation into this stratum is not practical.

Of two designs that might be considered, one would involve partial removal and the other complete removal of the surface-loam stratum. Cross sections of the two designs are identified in figure 12 as designs A and B. The design configuration is that of an inverted truncated pyramid. The volume of materials required to be excavated is the same for the two designs. Because a large land area is required for design A, the land-acquisition cost would be higher. However, this higher cost would be offset somewhat by the higher cost of excavating and installing inflow facilities for design B.

If water were added at a rate that would maintain a volume of about 60,000 cu ft in the basins, the water level in the basins would be as shown in figure 12. The anticipated quantity of water that would be taken into storage below the basins at 15.6°C (60°F) is shown in figure 13.

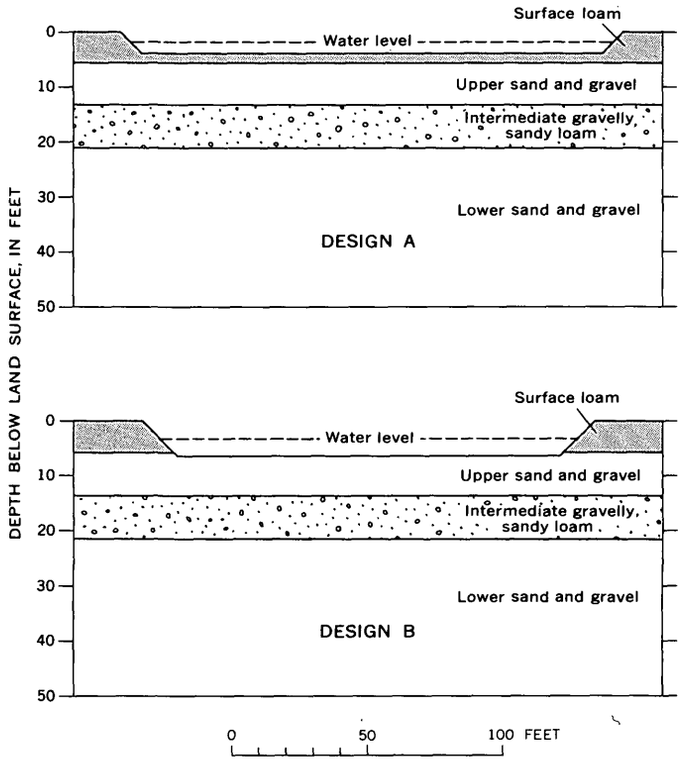

Figure 12.—Two designs for recharge basins at the Woodbury site.

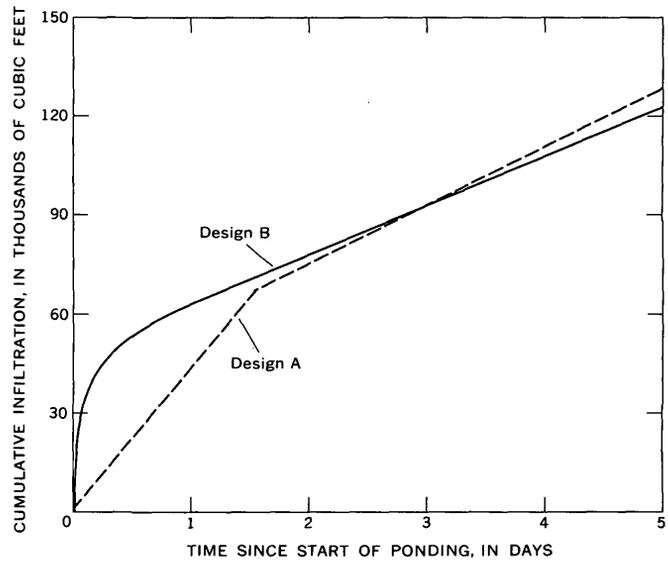

Figure 13.—Projected cumulative infiltration for two designs (fig. 12) of recharge basins at the Woodbury site.

The infiltration rate at basin B would be very high at the beginning of ponding because of the high hydraulic conductivity of the upper sand and gravel. A perched-water mound would develop rapidly above the intermediate gravelly, sandy loam stratum, and within a few hours the infiltration rate would decrease. Lateral spreading of the mound would continue for a short period. The infiltration rate would decrease at a decreasing rate during this period, after which a nearly steady-state infiltration rate would be obtained.

During the early stages of ponding, the infiltration rate at basin A would be controlled by the surface-loam stratum. The initial rate would be considerably less than at basin B but several times higher than if the rate were controlled by the intermediate gravelly, sandy loam stratum. Because a much longer time would be required for the development of the mound above the intermediate gravelly, sandy loam stratum, this stratum would not be fully effective as a controlling zone until cumulative infiltration was about 65,000 cu ft.

When the intermediate gravelly, sandy loam is fully effective as a limiting zone, the pressure head at the upper boundary of

this stratum in the area immediately below the basin is similar for the two designs. Therefore, the quantity of water that would infiltrate during a given time would be directly related to the basin area. Because the basin area would be about 32,000 sq ft at basin A, as compared with 24,000 sq ft at basin B, a larger quantity would infiltrate at basin A. After about 3 days, cumulative infiltration at basin A would exceed that at basin B.

The principal advantage gained by completely removing the surface-loam stratum is that of increasing the quantity of water taken into underground storage during the early stages of ponding. After a few days of continued ponding, the quantity taken into underground storage would not be greatly different whether the stratum were completely removed or only partly removed.

The importance of the added storage capacity in the initial stages of ponding can be evaluated as illustrated in figure 14. Here the storage capacities of the two designs are compared with maximum expected runoff for 50- and 100-year intervals. Storage capacity is equal to the volume of the basin available for water storage (130,000 cu ft) plus cumulative infiltration taken from figure 13. Maximum expected runoff is equal to $IDAP$, where I and D are rain intensity and rain duration, respectively, A is the drainage area served by the recharge basin, and P is the runoff-rainfall ratio characterizing the area. Maximum expected runoffs for 50- and 100-year intervals pertain to a drainage area of 15 acres with a runoff-rainfall ratio of 0.40. Rain intensity and rain duration are obtained from precipitation-intensity data for New York City (Miller and Frederick, 1969).

As shown in figure 13, both recharge-basin designs would have sufficient storage capacity to contain the maximum expected runoff for a 50-year interval. Design B would also have sufficient storage capacity to contain the maximum expected runoff for a 100-year interval. However, the storage capacity of design A would be only marginally adequate for a 100-year interval.

The advantage of increasing underground storage during the early stages of ponding should be weighed against the likelihood that clogging of the intermediate gravelly, sandy loam stratum would be accelerated as a result of the complete stripping of the surface-loam stratum. Studies by Berend, Rebhun, and Kahana (1967) and Thomas (1968) show that when water containing particulate matter is applied over coarse-textured media the particulate matter is only partly filtered as it moves through the media. If a fine-textured stratum occurs below the coarse-textured media, a considerable amount of the particulate matter is removed near the upper boundary of the fine-textured stratum. In contrast, if water is applied over a medium or fine-textured material, much of the particulate matter is removed near the surface. The finer textured media not only acts as a more effective filter but also lowers the infiltration rate. At lower infiltration rates, more time is allowed for the settling of particulate matter from water in the reservoir.

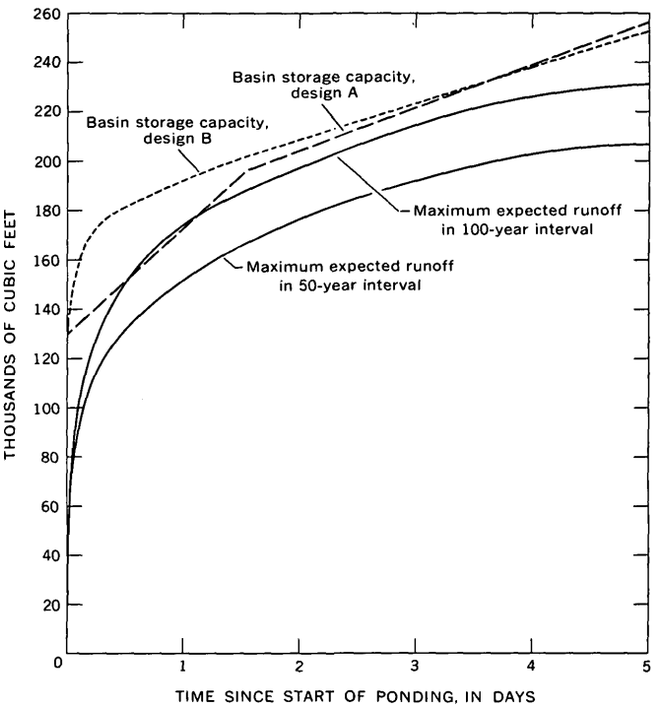

Figure 14.—Comparison between storage capacities of two recharge basin designs (fig. 12) and maximum expected runoffs for 50- and 100-year intervals.

When clogging occurs at or near the land surface, several procedures for restoring the intake capacity of the basin can be used. Among them are surface stripping, raking, and initiating vegetal growth. When clogging occurs at depth, restoring the intake capacity may not be feasible. In essence, clogging at depth may be irreversible.

SUMMARY

The principal zones limiting infiltration at the Woodbury recharge basin are a surface loam, with an average thickness of 1.5 feet, and an intermediate gravelly sandy loam, with an average thickness of 8 feet. These strata are separated by a sand and gravel stratum with a thickness of about 7 feet. The hydraulic conductivities of the limiting zones, computed from field and laboratory data, were 0.90 ft per day for the surface loam and 0.10 ft per day for the intermediate gravelly, sandy loam. The surface stratum acts as the principal zone limiting infiltration until a perched-ground-water mound develops above the intermediate gravelly, sandy loam stratum and extends to near the bottom of the surface loam. Then the intermediate gravelly, sandy loam becomes the principal limiting zone. Infiltration rates at 15.6°C were about 1.4 ft per day, when the surface loam was the principal limiting zone and 0.5 ft per day, when the intermediate gravelly, sandy loam was the principal limiting zone.

The design of a subsurface-controlled recharge basin, ideally, would provide maximum infiltration and storage at minimum

costs of construction and maintenance. Design selection requires predictions of the infiltration rates that will occur if successive layers of material below the land surface are removed.

In this report, probable infiltration rates associated with two designs of the Woodbury recharge basin are projected from the interpretation of field-test data. In one design the surface-loam stratum is completely removed, and in the other the stratum is only partly removed. The projections illustrate how information concerning the flow characteristics associated with known inputs might be generalized for selecting a basin design.

Projection of infiltration rates showed that if ponding continued for several days total infiltration for the two designs would not be greatly different. The principal advantage in completely removing the surface stratum is a greater infiltration capacity during the early stages of ponding. This advantage would have to be weighed against problems that are likely to occur from clogging. Complete removal of the surface stratum is likely to result in more intensive clogging of the subsurface controlling zone. If the surface stratum is only partly removed, clogging is likely to be largely a surface phenomenon. Restoration of the infiltration capacity is much more readily achieved under this condition.

REFERENCES CITED

Berend, J. E., Rebhun, M., and Kahana, Yona, 1967, Use of storm runoff for artificial recharge: Am. Soc. Agr. Engineers Trans., v. 10, no. 5, p. 678–684.

Lohman, S. W., and others, 1972, Definitions of selected ground-water terms—revisions and conceptual refinements: U.S. Geol. Survey Water-Supply Paper 1988, 21 p.

Miller, J. F., and Frederick, R. H., 1969, The precipitation regime of Long Island, New York: U.S. Geol. Survey Prof. Paper 627-A, 21 p.

Parker, G. G., Cohen, Philip, and Foxworthy, B. L., 1967, Artificial recharge and its role in scientific water management, with emphasis on Long Island, New York, *in* Marino, M. A., ed., Symposium on ground-water hydrology, San Francisco, Calif., Nov. 6–8, 1967, Proc.: Urbana, Ill., The Am. Water Resources Assoc. Proc., ser. 4, p. 193–213.

Prill, R. C., and Meyer, W. R., 1968, Neutron moisture measurements by continuous- and point-logging procedures, *in* Geological Survey Research 1968: U.S. Geol. Survey Prof. Paper 600-B, p. B226–230.

Soil Survey Staff, 1951, Soil survey manual: U.S. Dept. Agriculture Handb. 18, 501 p.

Thomas, R. L., 1968, Coarse filter media for artificial recharge: Illinois State Water Survey, Urbana, Rept. Inv. 60, 23 p.

ANNUAL INDEX TO VOLUME 1

Journal of Research of the U.S. Geological Survey

[Issue number precedes colon; page number follows colon]

SUBJECT INDEX

AUTHOR INDEX

RECENT PUBLICATIONS OF THE U.S. GEOLOGICAL SURVEY

(Books may be ordered from the Superintendent of Documents, Government Printing Office, Washington, DC 20402, to whom remittances should be sent by check or money order. Give title, series number, stock number (shown in parentheses in this list), and catalog number [shown in brackets])

Professional Papers

562-K. An experimental study of heavy-mineral segregation under alluvial-flow conditions, by L. L. Brady and H. E. Jobson. 1973. p. K1–K38. 85¢. (2401-00294) [I 19:16:562-K]

712-B. Geohydrology of the eastern part of Pahute Mesa, Nevada Test Site, Nye County, Nev., by R. K. Blankennagel and J. E. Weir, Jr. 1973. p. B1–B35; plates in pocket. $1.75. (2401-00303) [I 19:16:712-B]

716-E. Distribution, thickness, and lithology of Paleocene rocks in Pakistan, by C. R. Meissner, Jr., and Habib-ur Rahman. 1973. p. E1–E6; plates in pocket. $1.25. (2401-00341) [I 19:16:716-E]

726-D. Geophysical studies in the Yuma area, Arizona and California, by R. E. Mattick, F. H. Olmsted, and A. A. R. Zohdy. 1973. p. D1–D36; plates in pocket. $1.75. (2401-00327) [I 19:16:726-D]

748. Structural geology of the Santa Rita Mountains, southeast of Tucson, Ariz., by Harald Drewes. 1972 (1973). 35 p.; plates in pocket. $2.15. (2401-00239) [I 19:16:748]

751-B. Design and operation of the artificial-recharge plant at Bay Park, N. Y., by Ellis Koch, A. A. Giaimo, and D. J. Sulam. 1973. p. B1–B14; plate in pocket. 95¢. (2401-00321) [I 19:16:751-B]

752. Igneous rocks and related mineral deposits of the Barker quadrangle, Little Belt Mountains, Mont., by I. J. Witkind. 1973. 58 p. $1. (2401-00312) [I 19:16:752]

756. Middle Jurassic (Bajocian) ammonites from eastern Oregon, by R. W. Imlay. 1973. 100 p.; 47 plates showing fossils. $2.75. (2401-02208) [I 19:16:756]

770. Palynology of the Upper Campanian (Cretaceous) Judith River Formation, north-central Montana, by B. D. Tschudy. 1973. 42 p.; 11 plates showing fossils. $1.25. (2401-00291) [I 19:16:770]

776. Stratigraphy and geologic history of the Montana Group and equivalent rocks, Montana, Wyoming, and North and South Dakota, by J. R. Gill and W. A. Cobban. 1973. 37 p. 85¢. (2401-00342) [I 19:16:776]

791. Oligocene molluscan biostratigraphy and paleontology of the lower part of the type Temblor Formation, Calif., by W. O. Addicott. 1973. 48 p.; 9 plates showing fossils. $1.25. (2401-00284) [I 19:16:791]

798-A. Geochemistry and potassium-argon ages of plutonic rocks in the Battle Mountain mining district, Lander County, Nev., by T. G. Theodore, M. L. Silberman, and D. W. Blake. 1973. p. A1–A24. 65¢. (2401-00333) [I 19:16:798-A]

809-A. Recognition of natural brine by electrical soundings near the Salt Fork of the Brazos River, Kent and Stonewall Counties, Tex., by A. A. R. Zohdy and D. B. Jackson. 1973. p. A1–A14. 40¢. (2401-02373) [I 19:16:809-A]

820. United States mineral resources, by D. A. Brobst and W. P. Pratt, Editors. 1973. 722 p. $9.15. (2401-00307) [I 19:16:820] (Reprinted.)

841. Crystallization history of lunar feldspathic basalt 14310, by O. B. James. 1973. 29 p. 70¢. (2401-00361) [I 19:16:841]

Bulletins

1292. The geologic story of Mount Rainier, by D. R. Crandell. 1969. 43 p. 85¢. (2401-0197) [I 19:3:1292] (Reprinted 1973.)

1303. Chemical analysis of thermal water in Yellowstone National Park, Wyo., 1960–65, by J. J. Rowe, R. O. Fournier, and G. W. Morey. 1973. 31 p. 35¢. (2401-02367) [I 19:3:1303]

1372-E. Stratigraphic divisions and geologic history of the Laney Member of the Green River Formation in the Washakie Basin in southwestern Wyoming, by H. W. Roehler. 1973. p. E1–E28. 35¢. (2401-00282) [I 19:3:1372-E]

1372-H. Lower and middle Tertiary stratigraphic units of the San Emigdio and western Tehachapi Mountains, Calif., by T. H. Nilsen, T. W. Dibblee, Jr., and W. O. Addicott. 1973. p. H1–H23. 35¢. (2401-00343) [I 19:3:1372-H]

1372-J. Stratigraphic terminology of the Dakota Sandstone and Mancos Shale, west-central New Mexico, by E. R. Landis, C. H. Dane, and W. A. Cobban. 1973. p. J1–J44. 45¢. (2401-00364) [I 19:3:1372-J]

Water-Supply Papers

2018. Ground water in the Eugene-Springfield area, southern Willamette Valley, Oreg., by F. J. Frank. 1973. 65 p.; plates in pocket. $2.75. (2401-00277) [I 19:13:2018]

2028. A national study of the streamflow data-collection program, by M. A. Benson, and R. W. Carter. 1973. 44 p. 45¢. (2401-02372) [I 19:13:2028]